THE GEOLOGY AND GEOCHEMISTRY OF THE LUMWANA BASEMENT HOSTED COPPER-COBALT (URANIUM) DEPOSITS, NW ZAMBIA

A thesis presented for the degree of
Doctor of Philosophy

By Robin Bernau

School of Ocean and Earth Science
Faculty of Science
University of Southampton
August 2007

UNIVERSITY OF SOUTHAMPTON

ABSTRACT

FACULTY OF SCIENCE

SCHOOL OF OCEAN & EARTH SCIENCE

Doctor of Philosophy

THE GEOLOGY AND GEOCHEMISTRY OF THE LUMWANA BASEMENT HOSTED COPPER-COBALT (URANIUM) DEPOSITS, NW ZAMBIA

By Robin Bernau

The Lumwana Cu±Co deposits Malundwe and Chimiwungo are examples of pre-Katangan mineralized basement that are located in the Domes Region of the Lufilian Arc, an arcuate North neo-Proterozoic fold belt, which hosts the Zambian and Congolese deposits that make up the Central African Copperbelt. The Lumwana deposits are situated within the Mwombezhi Dome; a Mesoproterozoic basement inlier consisting of highly sheared amphibolite grade schist to gneiss units that host the Cu±Co mineralization. Kinematic indicators such as s-c fabrics and pressure shadows on porphyroblasts suggest a top to the North shear sense. Peak metamorphism of 750ºC ± 25ºC and 13 ± 1 Kb indicated by whiteschist assemblages occurred during the Lufilian Orogeny at ~530Ma, with burial depths of ~50km. A major decollement separates the high pressure mineral assemblages of the basement from the lower pressure mineral assemblages of the overlying Katangan Supergroup. The age range and lithologies of the pre-Katangan basement of the Domes Region is similar to the pre-Katangan basement of the Kafue Anticline, which underlies the neo-Proterozoic Zambian Copperbelt deposits situated 220km to the SW.

The origin of the protolith to the mineralization is ambiguous at Lumwana with transitional contacts from unmineralized quartz-feldspar±phlogopite basement gneiss to Cu±Co mineralized quartz-phlogopite-muscovite-kyanite-sulphide Ore Schist. The transitional contacts and structural controls on mineralization has led to the hypothesis that these deposits represent metasomatically altered, mineralized and sheared basement, rather than mineralized neo-Proterozoic sediments with amphibolite grade metamorphism. This hypothesis is supported by petrographic analysis, stable isotope analysis ($\delta^{34}S$), whole rock geochemistry, and electron microprobe analysis of ore and host rock assemblages. The transitional contacts observed at Lumwana are due to an alteration event associated with mineralization that removed feldspar from ore horizons resulting in depleted Na and Ca and relatively higher Al components. Sulphides are deformed by the S1 fabric and overprinted by kyanite which formed at peak metamorphism. This indicates that copper was introduced to the basement either syn or pre-peak metamorphism. Post S1 metamorphism with associated quartz-muscovite alteration has remobilized sulphides into low strain zones and pressure shadows around porphyroblasts. $\delta^{34}S_{SULPHIDES}$ give values of +2.3 to +18.5‰ that fall within the range of values observed in the Copperbelt of -17 to +23‰. The mechanism of ore formation at Lumwana was dominated by thermochemical sulphate reduction (TSR), indicated by the relatively heavy $\delta^{34}S$ values and the absence of the light bacteriogenic $\delta^{34}S$ values observed in the Copperbelt. Electron microprobe data of muscovite, phlogopite and chlorite show little variation between early and late mineral phases indicating that metamorphic homogenization of silicate assemblages occurred.

The Lumwana deposits are large mineralized shear zones within the pre-Katangan basement. Various styles of basement mineralization are also observed in the Kafue Anticline and the structural controls on mineralization and lithological similarities to the Lumwana deposits suggests that pre-Katangan basement is a viable source for the Cu-Co budget of the Central African Copperbelt and that basement structures had a key role in its formation.

TABLE OF CONTENTS

LIST OF FIGURES

LIST OF FIGURES

LIST OF FIGURES

LIST OF TABLES

Acknowledgments

Firstly thanks must go to my supervisors, Dr Stephen Roberts and the late Bruce Nisbet, for their advice throughout the project and their invaluable criticisms and comments during the preparation of this thesis. Thanks must also go to Adrian Boyce for his advice concerning stable isotope work.

The Natural Environment Research Council (NERC) funded the majority of the author's studies. In addition, Equinox Minerals Ltd provided financial and logistical support during field work in Zambia. Stable isotope work was carried out using the facilities at the Scottish Universities Environmental Research Centre, East Kilbride, and electron microprobe work was conducted at the Natural History Museum, London, with training provided by Alison McDonald and John Spratt respectively.

Support and advice from the following is acknowledged during time spent in Africa: Mike Richards, Gregg Winch and Noel McNee, (Equinox Minerals Ltd).

The following people have also offered advice during the completion of the studies in the UK: Dr Andy Barker, Dr Damon Teagle and Dr Jim Andrews. Practical support at the University of Southampton from Bob Jones, Jon Ford, Dr Richard Pearce, Kate Davies and Barry Marsh is also acknowledged.

Finally, thanks must go to friends and family for their support throughout the last four years, in particular Gemma for her constant support.

CHAPTER 1: INTRODUCTION

1.1 Rationale

The neo-Proterozoic Katangan Central African Copperbelt that straddles the border between Zambia and the Democratic Republic of Congo is host to one of the world's greatest concentrations of stratiform copper-cobalt mineralization (Cailteux *et al.* 2005). The Lumwana Prospect is a small settlement with the largest known Zambian copper resource outside of the Zambian Copperbelt and ranks as Africa's largest copper mine (Equinox Annual Report 2005). Understanding the mechanism and timing of ore formation and associated wallrock alteration of the Lumwana deposits has implications for the role of pre-Katangan basement in the genesis of the Zambian Copperbelt whose origins have been debated for an excess of 6 decades (Darnley 1960; Whyte & Green 1971; Garlick 1972; Annels 1974; Van Eden 1974; Binda 1975; Annels *et al.* 1983; Sweeney *et al.* 1986, 1991; Sweeney & Binda 1989, 1994; Molak 1995; McGowan *et al.* 2003, 2005; Cailteux *et al.* 2005; Greyling *et al.* 2005; Sutton & Maynard 2005).

Sediment-hosted copper deposits include some of the richest copper concentrations in the world and commonly have metal associations with cobalt and silver, and more minor occurrences of zinc, gold, lead and iron (Kirkham 1989). The age of mineralization ranges from Proterozoic to younger, located in intracontinental and continental margin settings, in predominantly rift controlled environments, commonly within fault-controlled sedimentary basins (Gustafson & Williams 1981). These deposits are commonly hosted in shales, sandstones, and carbonates, within reduced horizons near to oxidation-reduction boundaries, which are typically underlain by red-bed sandstones containing evaporitic sequences. The sulphide mineralogy typically consists of chalcopyrite, chalcocite and bornite with pyrite outside of the ore zones (Binda 1995). Many stratiform copper deposits show a close association with sulphate minerals gypsum and anhydrite including the Zambian Copperbelt, the Polish Kupferchiefer and Redstone River. Sulphate minerals provide a major source of sulphur as well as potential fluid pathways through dissolution. This suggests that the sulphur bearing fluid is subsequently reduced and the sulphur is later fixed as sulphide minerals. Notable exceptions to the association of stratiform copper deposits and sulphate

mineralization include the American deposits, White Pine, Nacimiento and Spar Lake, as well as the deposits in the Democratic Republic of Congo (Gustafson & Williams 1981).

The Lumwana deposits Malundwe and Chimiwungo are hosted by highly sheared amphibolite grade schist to gneiss units of the Mwombezhi Dome, a basement complex antiformal thrust stack that consists of tectonically interleaved slices of Mesoproterozoic basement and Katangan Supergroup rocks, which are separated from the overlying Katangan Supergroup sedimentary rocks by a major décollement (Cosi *et al.* 1992; John *et al.* 2004). Talc-kyanite (whiteschist) assemblages in the Mwombezhi Dome basement indicate peak metamorphism of 750ºC ± 25ºC and 13 ± 1 kb corresponding to burial depths of approximately 50 km (Cosi *et al.* 1992; John *et al.* 2004). The origin of the protolith to the mineralization is ambiguous at Lumwana with transitional contacts from unmineralized quartz-feldspar±phlogopite basement gneiss to Cu±Co mineralized quartz-phlogopite-muscovite-kyanite-sulphide "Ore Schist". The transitional contacts and structural controls on mineralization observed in core has led to the hypothesis that the Lumwana deposits are examples of metasomatically altered, mineralized and foliated basement, rather than mineralized neo-Proterozoic sedimentary rocks overprinted with amphibolite grade metamorphism. This hypothesis is tested through petrographic analysis, stable isotope analysis ($\delta^{34}S$), whole rock geochemistry, and electron microprobe analysis of ore and host rock assemblages, which are examined in detail in this thesis.

In contrast to the Lumwana deposits the majority of the Copperbelt mineralization is hosted by the Lower Roan sedimentary rock sequences of the Katangan Supergroup (Mendelsohn 1961) that unconformably overlie a composite Palaeoproterozoic basement of deformed, metamorphosed, granitic rocks and metavolcano-sedimentary sequences (Cailteux *et al.* 1994; Rainaud *et al.* 2005). Metamorphism in the Zambian Copperbelt is predominantly greenschist facies, except at Luanshya, where epidote-amphibolite facies assemblages are recognised (Mendelsohn 1961). The

CHAPTER 1: INTRODUCTION

Congolese Copperbelt has been subject to lower metamorphic grade from greenschist to prehnite-pumpellyte facies (Selley *et al.* 2005).

The Palaeoproterozoic basement that underlies the Zambian Copperbelt contains widespread copper mineralization in a diverse range of rock types (Cailteux *et al.* 2005; Mendelsohn 1961; Pienaar 1961; Wakefield 1978). The majority of the pre-Katangan basement hosted mineralization is associated with veins, shears and other dilatant features, although copper mineralization is also sparsely disseminated in granitoid and meta-sedimentary rocks (Pienaar 1961). Examples of basement hosted mineralization from the Zambian Copperbelt include the Samba deposit granitoids that are host to an estimated 50 million tonnes at 0.7% Cu, the Nchanga Red Granite with an estimated 1.5 million tonnes at 1.5% Cu and the Muva phyllites south of the Nkana basin with a 3.6m wide zone at 3.6 % Cu (Cailteux *et al.* 2005). The copper ore of the basement hosted mineralization is typically of lower grade than that of the overlying Katangan stratiform ore bodies (Pienaar 1961). The mechanisms of pre-Katangan basement mineralization are poorly understood and have been the subject of little scientific enquiry.

The aim of this study is to determine the genesis of mineralization at Lumwana and to further our understanding of basement hosted copper-cobalt deposits. The structural controls on mineralization and lithological similarities between the Mwombezhi Dome and the basement of the Kafue Anticline suggests that pre-Katangan basement is a viable source for the Cu-Co budget of the Central African Copperbelt and that basement structures had a key role in its formation.

1.2 Location of Lumwana deposits and the Central African Copperbelt

The Lumwana tenement is located 220km northwest of the Zambian Copperbelt, and 65km from the provincial capital of Solwezi in the North Western Province of Zambia. The Copperbelt region of Zambia is located north of the capital Lusaka, adjacent to the border with the Democratic Republic of Congo and includes Mufulira, Chingola and Ndola (figure 1.1).

CHAPTER 1: INTRODUCTION

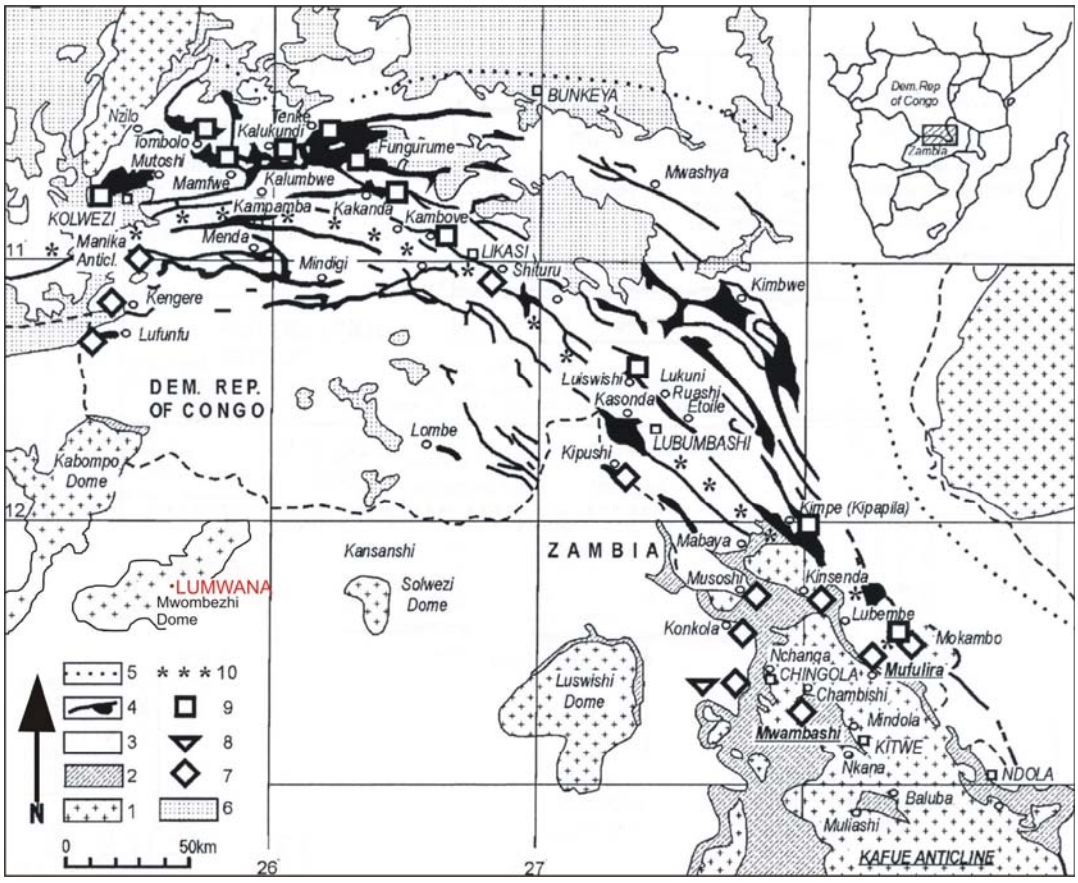

Figure 1.1 Geological map of the Central African Copperbelt. Map symbols: (1) pre-Katangan basement; (2) Roan Group; (3) post-Roan units of Katangan Supergroup; (4) complexes of fragmental rocks; (5) fold-thrust belt boundary; (6) post-Katangan cover; (7) syn-rift Mufulira Formation; (8) base of Petit Conglomerat in Zambia; (9) Fungurume Group foreland succession; (10) Southern Limit of Fungurume Group (after Wendorff 2002, 2005; Porada & Berhorst 2000; Cailteux *et al.* 1994).

This study has concentrated on the Northern lobe of the Mwombezhi Dome within the Domes region of NW Zambia, focusing on the Lumwana deposits Chimiwungo and Malundwe (figure 1.1).

1.3 Exploration history and outline of previous research on the Lumwana deposits

Exploration for mineral resources in the Lumwana region dates back to reconnaissance mapping in the 1930's, which outlined the regional geology of the area but did not reveal the presence of any significant copper, cobalt or uranium mineralization. Stream and soil sediment sampling in the 1960's identified three major copper anomalies that are associated with forest clearings, where the elevated copper content of the soil has stopped tree growth (Benham *et al.* 1976). Since the initial discovery, exploration drilling has been conducted by the Roan Selection Trust (RST), Agip-Cogema

(uranium exploration) and Phelps-Dodge, which identified two targets, Malundwe a copper deposit and Chimiwungo a copper-cobalt deposit. A new "blind" discovery was made by Equinox Minerals LTD in 2004 at Chimiwungo North. A Definitive Feasibility Study was completed in 2005 providing a total measured and inferred resource of 270 million tonnes of ore grading at 0.8% copper.

The mineralization at Malundwe and Chimiwungo have been subject to previous research including a Ph.D. thesis (McGregor 1965) that examined the geology and genesis of the Lumwana deposits which was strongly influenced by the syngenetic theories of Garlick. Dechow & Jensen (1965) examined the $\delta^{34}S$ values of selected sulphides from the Mwombezhi Dome as part of a regional sulphur isotope study on Central African sulphide deposits. Other research includes work which focused on the copper occurrences at Malundwe and Chimiwungo (Benham *et al.* 1976) based on the data collected by RST, and work by Cosi *et al.* (1992) examining the uranium mineralization of the Mwombezhi Dome based on the data collected by the Agip-Cogema joint venture of the 1970's and 1980's. More recently, John *et al.* (2003, 2004) and Johnson and Oliver (2003) have examined the whiteschist from a variety of locations in Zambia and Zimbabwe including from the Mwombezhi Dome that hosts the Malundwe and Chimiwungo deposits.

1.4 Aims & Methods

The principal objectives of this study are:

- To fully understand the geology of the Lumwana deposits, in particular the nature and origin of the Ore Schist that hosts the mineralization.
- To understand the structural, tectonic and metamorphic history of the deposits.
- To determine the sulphide paragenesis including the relationship of Cu-Co mineralization to U mineralization.
- To understand the different styles of alteration and its relationship to the Cu-Co mineralization.

- To characterize the whole rock geochemistry of ore and host rock assemblages.
- To examine the geochemical relationship between silicate and sulphide phases.
- To develop a model for ore genesis.

Fieldwork at Lumwana lasted for 12 weeks and included:

- Logging of boreholes through ore horizons from hanging wall to footwall including very detailed logging of ore sequences.
- Core sampling for:
  - Subsequent geochemical and petrographic analysis.
  - A representative suite of biotite from ore and host rock assemblages to examine variations in geochemical composition.
  - An appropriate set of index minerals to establish P-T conditions and enable mineral geothermometry and barometry.
  - A representative suite of sulphides to enable sulphur isotopic characterisation of sulphides.
  - Mineral geochronometers (mica, zircon, monazite, apatite, uraninite, molybdenite, garnet and titanite) to attempt age dating of key units.
- Synthesis of previous structural data contained in McGregor thesis and from field mapping conducted by Equinox.
- Structural transects for validation of previous field mapping including field sampling for structural interpretation.
- Mine visits to the Zambian Copperbelt deposits Nchanga and Konkola as well as logging of core from Mufulira in order to compare and contrast the styles of mineralization observed at Lumwana and the Copperbelt deposits.

Subsequent laboratory work included:

- Petrographic analysis of sulphide ores and host rock assemblages (including reflected, transmitted light and SEM petrography).
- Whole rock X-Ray fluorescence spectrometry of selected samples for geochemical suite analysis.

CHAPTER 1: INTRODUCTION

- Pilot study of X-Ray fluorescence spectrometry non-destructive core scanner.
- Electron microprobe study at the Natural History Museum, London examining geochemistry of silicate phases and their relationship to the sulphide mineralization.
- Characterisation of sulphur isotopes at the Isotope Community Support Facility, East Kilbride.

CHAPTER 2: REGIONAL GEOLOGY

2.1 Tectonic setting of the Lufilian Arc

The Central African Copperbelt and the Lumwana deposits are situated within the Lufilian Arc, an orogenic Pan-African fold-thrust belt approximately 900km in length that was deformed during the neo-Proterozoic to early Palaeozoic eras. The Lufilian Arc consists of Katangan Supergroup meta-sedimentary rocks that host the Central African Copperbelt deposits and which unconformably overlie a pre-Katangan basement (Mendelsohn 1961) (figure 2.1).

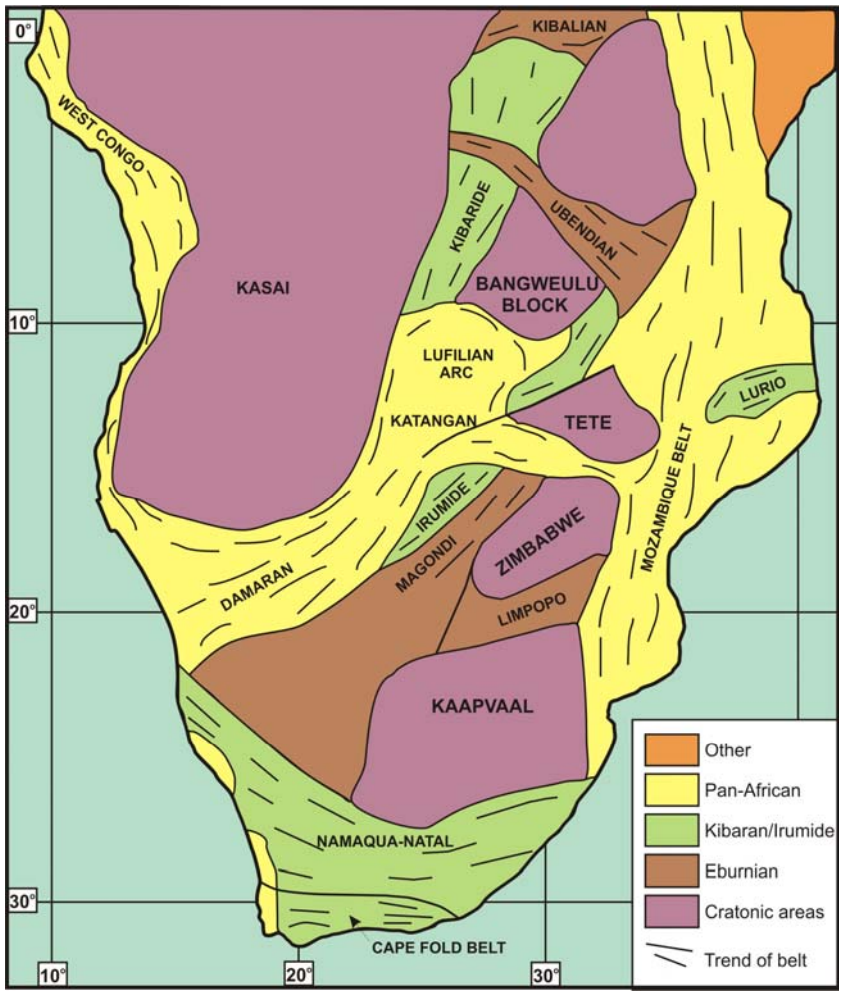

Figure 2.1 Major cratons and fold belts of central and southern Africa (after Duane and Saggerson 1995)

The Lufilian Arc extends northwards into the Democratic Republic of Congo and linking to the southwest with the Damara Belt of Namibia (Cosi *et al.* 1992). The Lufilian Arc is flanked in the northwest by the Neo-Proterozoic and Palaeoproterozoic rocks of the Kasai Shield and the 1.4-1.0 Ga Mesoproterozoic Kibaran Fold Belt (Cahen *et al.* 1984) (figure 2.1 & 2.2).

CHAPTER 2: REGIONAL GEOLOGY

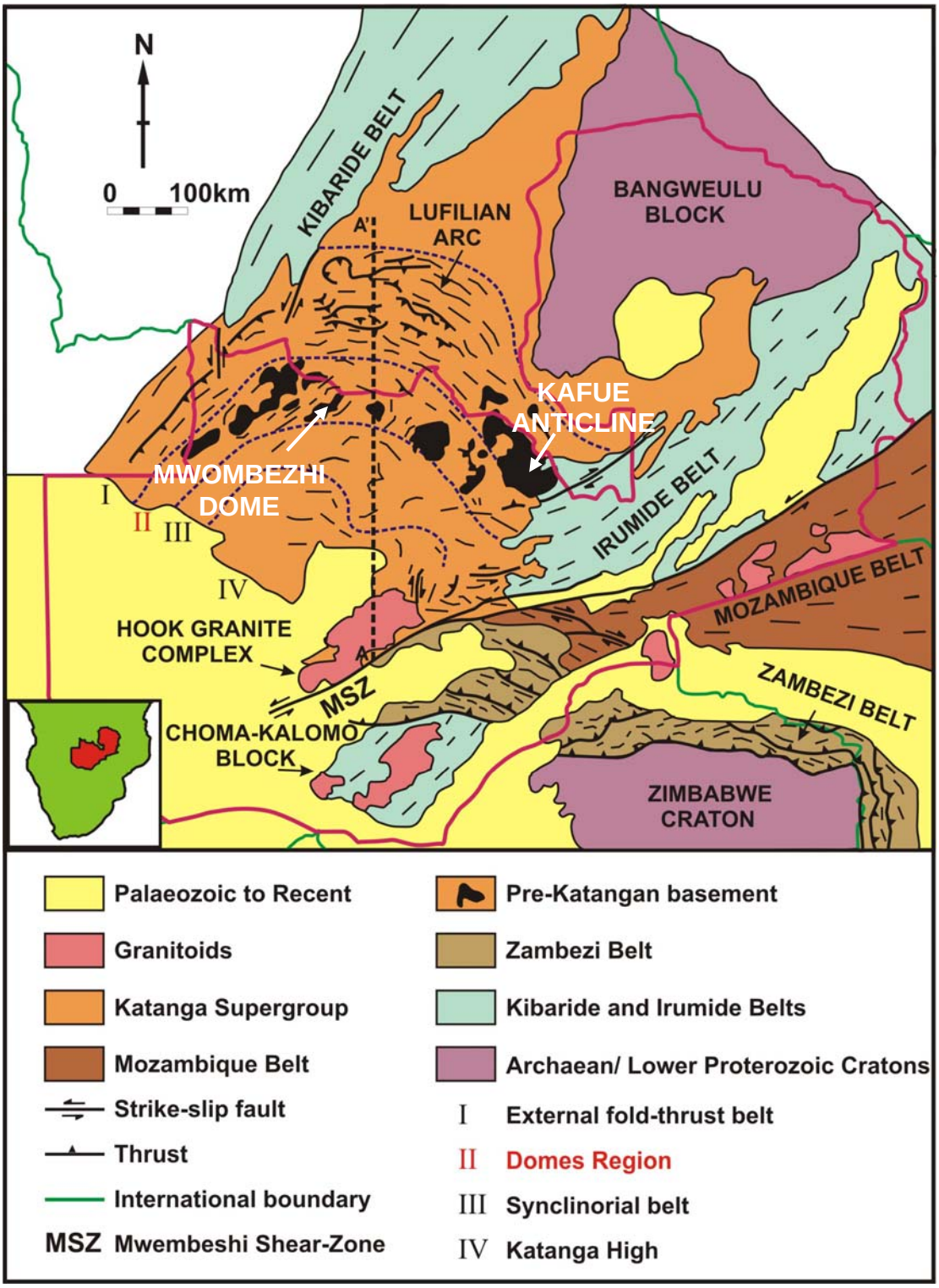

Figure 2.2 Tectonic setting of Zambia and the Lufilian Arc (after Porada 1989; Binda & Porada 1995)

The Lufilian Arc is bordered to the east by the Mesoproterozoic Irumide belt of Kibaran age (Daly *et al.* 1984) and to the south by the Mwembeshi Shear Zone (MSZ). The Mwembeshi Shear Zone has been interpreted as the structure that separates the Kalahari and Congo cratons (Kampunzu &

Cailteux 1997), although this is rejected by Porada & Berhorst (2000) (figures 2.1 & 2.2).

The Lufilian fold belt consists of four distinct, convex-north zones. From north to south these are: I) the External fold and thrust belt that host the Congolese Copperbelt deposits, II) the Domes Region that host the Lumwana deposits, III) the Synclinorial Belt, and IV) the Katanga High (Porada 1989) (figure 2.2 & 2.3).

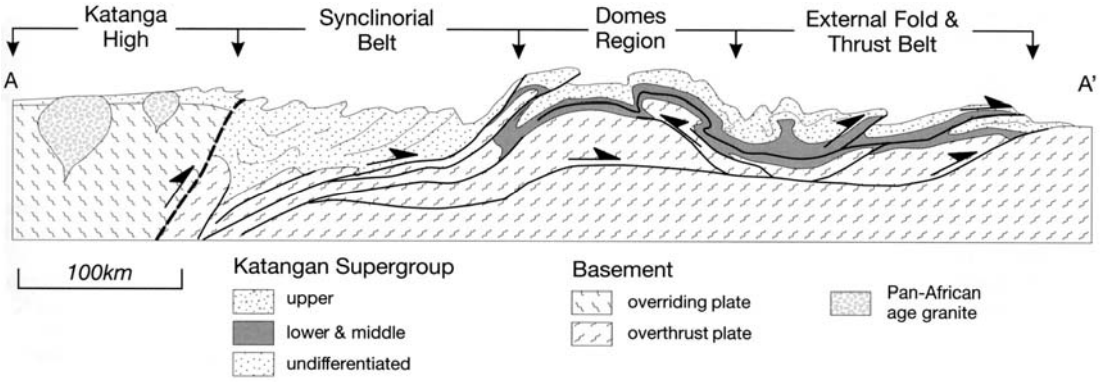

Figure 2.3 Schematic cross section of the Lufilian fold belt (section line shown in 2.2), highlighting the variation in structural style between zones (after Selley *et al.* 2005; Porada 1989)

The External fold and thrust belt is characterized by thin-skinned geometry, with macro-scale fragmentation and thrust repetition of the Katangan Supergroup stratigraphy. Lack of basement in this tectonic zone is commonly considered to reflect widespread decoupling along evaporitic strata at depth, such that lower strata of the Katangan Supergroup were thrust emplaced toward the top of the tectonic pile (Kampunzu and Cailteux 1999; Porada and Berhorst 2000; Jackson *et al.* 2003). Metamorphic grade decreases from greenschist facies at the Zambian Copperbelt to prehnite-pumpellyte facies at the most northern extent of the Congolese Copperbelt (Selley *et al.* 2005).

The basement inliers in the Domes Region are thought to represent antiformal stacks above mid to lower crustal ramps, indicating a thicker skinned deformation than in the External fold and thrust belt (Daly *et al.* 1984). In the Domes Region unconformable relationships between older basement and the younger Katangan Supergroup sedimentary rocks are preserved and metamorphic grade varies from upper greenschist to upper amphibolite facies

(Selley *et al.* 2005). Basement rooted recumbent folds, nappes and juxtaposed thrust blocks of contrasting metamorphic grade have been described (Cosi *et al.* 1992; Binda & Porada 1995; Key *et al.* 2001) (figure 2.3).

Selley *et al.* (2005) suggest that the Domes Region includes the Zambian Copperbelt deposits, with the Kafue Anticline (figure 2.2) representing the most easterly pre-Katangan basement inlier whereas previous authors (Porada 1989; Binda & Porada 1995) consider the Zambian Copperbelt to be the most southerly extent of the external fold-thrust belt. This an interesting point as the transition between these tectonic zones is not well understood, but coincides with a relatively abrupt southward increase in metamorphic grade and change in structural style (Ramsay and Ridgway 1977; Francois and Cailteux 1981; Key *et al.* 2001). Kinematic indicators suggest northwest to northeast directed thrusting during the neo-Proterozoic to Cambrian convergence of the Kalahari and Congo cratons, with displacement vectors radiating perpendicularly with respect to the arcuate trend of the fold belt (Daly 1986; Kampunzu and Cailteux 1999).

The age range and lithological make up of the basement rocks of the Domes Region have a strong similarity with the basement rocks of the Kafue Anticline and have been interpreted to collectively belong to the Lufubu Metamorphic Complex that is interpreted as a Palaeoproterozoic magmatic arc terrane (Rainaud *et al.* 2005).

The Lufubu Metamorphic Complex stretches from northern Namibia to northern Zambia and the Marungu Plateau of the DRC. The Kamanjab-Bangweulu terrane, which collided with the Archaean Tanzanian craton during the 2.0-1.9 Ga Ubendian Orogeny, produced a new composite minicontinental entity, the Kambantan terrane (Rainaud *et al.* 2005). The Kambantan terrane was accreted onto the southern margin of the Congo craton during the Mesoproterozoic Kibaran Orogeny and the outboard side was subject to the 1.05-1.02 Ga Irumide Orogeny, caused by the collision of several terranes with the Congo craton (Rainaud *et al.* 2005).

Subsequently in the Irumide belt, during the sedimentation of the Damara and Katanga Supergroups at 750-730 Ma, a rifted passive margin formed with the opening of an ocean basin which closed during the Pan-African Damaran-Lufilian Orogeny, when the Congo and Kalahari cratons were sutured together (Rainaud *et al.* 2005).

2.2 Evolution of the Pan-African Lufilian Arc-Zambezi Belt orogen

The Lufilian Arc is reported to have formed during the collision of the Angola-Kalahari and Congo-Tanzania Plates and accompanying NE-directed thrusting at 560-550 Ma (Porada & Berhorst 2000) during the assembly of the supercontinent Gondwana between 750 and 500 Ma (Condie 2002). The extent of rifting between the Congo and Kalahari cratons is debatable, however recent evidence (Porada & Berhorst 2000) proposed that rifting started at 880 Ma and separated the Congo-Tanzania plate from the Angola-Kalahari plate, leading to the formation of a passive continental margin on the southern side of the Congo craton. Based on the study of the timing and PT evolution of whiteschist metamorphism in the Lufilian Arc-Zambezi Belt orogen as well as from previous work in the literature John *et al.* (2004) proposed a new model for the pan African mobile belts of central southern Africa (figure 2.4).

Initial rifting took place at 870-880 Ma on the southern edge of the Congo craton (Porada and Berhorst 2000). Rifting was related to the dispersal of Rodinia and led to the formation of an ocean basin (John *et al.* 2003) and the development of a passive continental margin (Porada and Berhorst 2000) (Figure 2.4 A). The extensional regime was followed by compression and during the convergence between the Kalahari and Congo cratons, the ocean basin closed, subducting oceanic lithosphere and forming eclogites at 600 Ma (John *et al.* 2003) (Figure 2.4 B).

CHAPTER 2: REGIONAL GEOLOGY

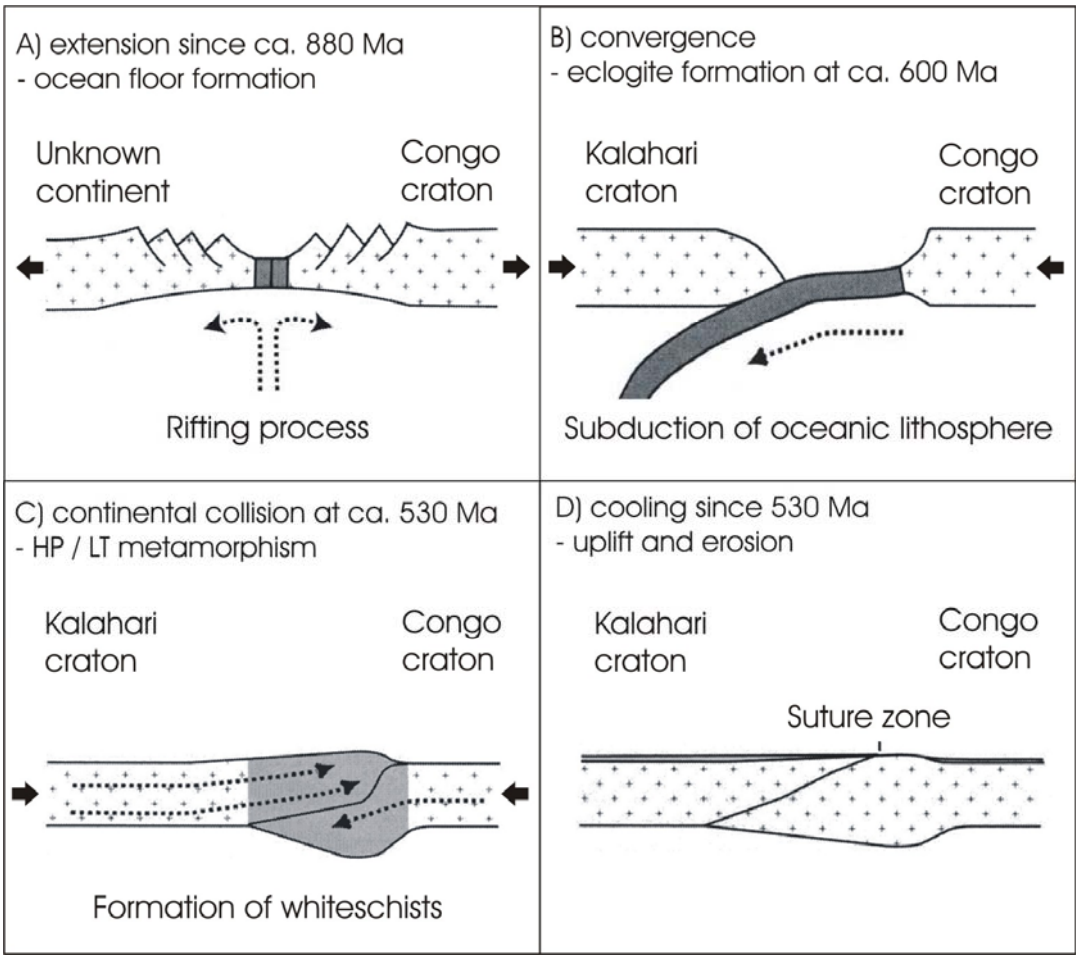

Figure 2.4 Evolution of the Pan-African Lufilian Arc-Zambezi Belt orogen (after John *et al.* 2004)

The final stage of convergence resulted in a continent-continent collision with the Kalahari craton overriding the passive continental margin and colliding with the Congo craton at 530 Ma (Figure 2.4 C). This stage of the pan African evolution is responsible for the formation of the talc-kyanite (whiteschist) assemblages located in the Domes region and Zambezi Belt (figure 2.2). The final collision was followed by rapid erosion, tectonic uplift and cooling (John *et al.* 2004) (figure 2.4 D).

2.3 Geology and geochronology of the Zambian pre-Katangan basement

Pre-Katangan basement is exposed mainly in Zambia and contiguous areas of the Democratic Republic of Congo. In Zambia the basement rocks are exposed in a structural high known as the Kafue Anticline (Garlick 1961). In

the adjacent areas of Katanga, basement exposures are found in the Konkola, Luina and Mokambo Domes (figures 1.1 & 2.2) (Rainaud *et al.* 2005).

The pre-Katangan basement comprises the Lufubu mica schists, quartzites and gneisses with minor metamorphosed carbonates, conglomerates, subgreywackes and arkoses, extensively intruded by granites that constitute up to 50 percent of the basement (Mendelsohn 1961) (figure 2.5).

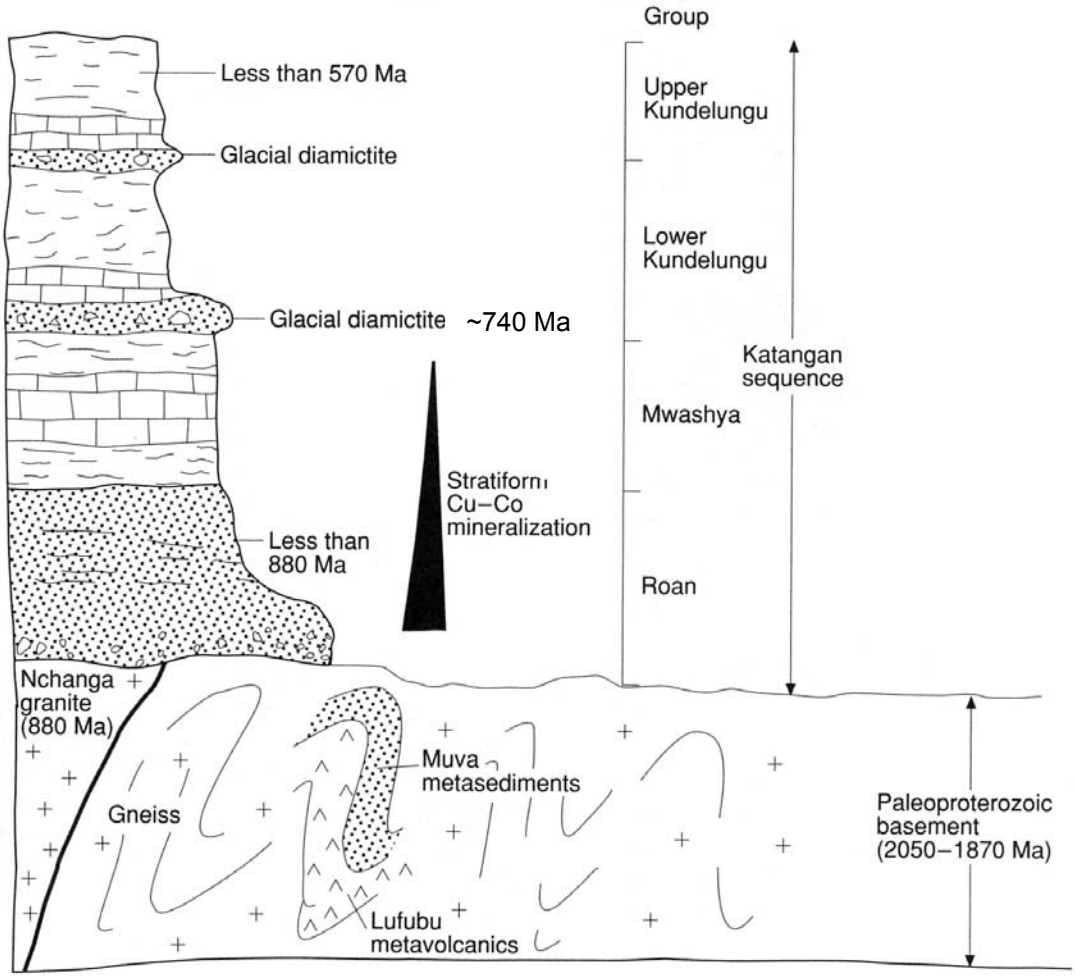

Figure 2.5 Simplified stratigraphic profile through the rocks of the Central African Copperbelt (after Robb 2005; Rainaud *et al.* 2002; Master *et al.* 2002; Key *et al.* 2001)

Rainaud *et al.* (2005) also identify acid intermediate calc-alkaline meta-volcanic rocks within the pre-Katangan basement. In the Copperbelt region, the Lufubu schists and intrusive granitoids are unconformably overlain by the Muva meta-sediments that consist of deformed quartzites, meta-conglomerates and meta-pelitic schists (figure 2.5) (Garlick 1961). The Muva Supergroup of the Kafue Anticline comprises meta-sedimentary packages

strongly deformed during the Mesoproterozoic Irumide Orogeny (De Waele & Fitzsimons 2004).

The pre-Katangan basement of the Domes Region and the Central African Copperbelt is considered part of the Lufubu Metamorphic Complex, a regionally extensive Palaeoproterozoic magmatic arc terrane, which stretches from northern Namibia to northern Zambia and the Marungu plateaux of the DRC (Rainaud *et al.* 2005).

The pre-Katangan basement in Zambia has undergone polyphase deformation and metamorphism as a result of the Ubendian, Kibaran and Lufilian orogenies (Rainaud *et al.* 2005). The metamorphic grade of the pre-Katangan basement varies across the Lufilian orogenic belt from amphibolite facies in the Domes Region (Cosi *et al.* 1992; John *et al.* 2004) to greenschist facies metamorphism in the pre-Katangan basement of the Kafue Anticline (Mendelsohn 1961).

In Zambia and the Democratic Republic of Congo the Lufubu Metamorphic Complex has yielded U-Pb SHRIMP zircon ages of 1980 ± 7 Ma, 1968 ± 9 Ma, 1964 ± 12 Ma and 1874 ± 8 Ma. More evolved granites from the Zambian Copperbelt, the Mufulira Pink Granite and the Chambishi Granite, yield ages of 1994 ± 7 Ma and 1983 ± 8 Ma respectively (Rainaud *et al.* 2005). The Lufubu schists and various granitoids and gneisses that constitute the Lufubu Metamorphic Complex represent a calc-alkaline volcanic arc sequence that formed episodically over a 200 million year period between 2050 and 1850 Ma (Rainaud *et al.* 2005).

The meta-sedimentary sequences that comprise the Muva Supergroup yield Palaeoproterozoic U-Pb SHRIMP detrital zircon ages of 1824 ± 19 Ma to 1882 ± 30 Ma. Age data support derivation from the Ubendian Orogen during, or immediately after Ubendian tectonism, consistent with the Muva Supergroup representing a mollasse-like sequence (De Waele & Fitzsimons 2004).

CHAPTER 2: REGIONAL GEOLOGY

2.4 Mineralization of the pre-Katangan basement

Low grade basement copper mineralization occurs locally in the Lufubu Metamorphic Complex of the Kafue Anticline and is typically associated with veins and intrusive igneous rocks. Pienaar (1961) subdivided basement mineralization into two categories; 1) Mineralized pre-Katangan basement palaeohighs with overlying Katangan orebodies, and 2) pre-Katangan basement mineralization that is not associated with overlying Katangan orebodies (figure 2.6).

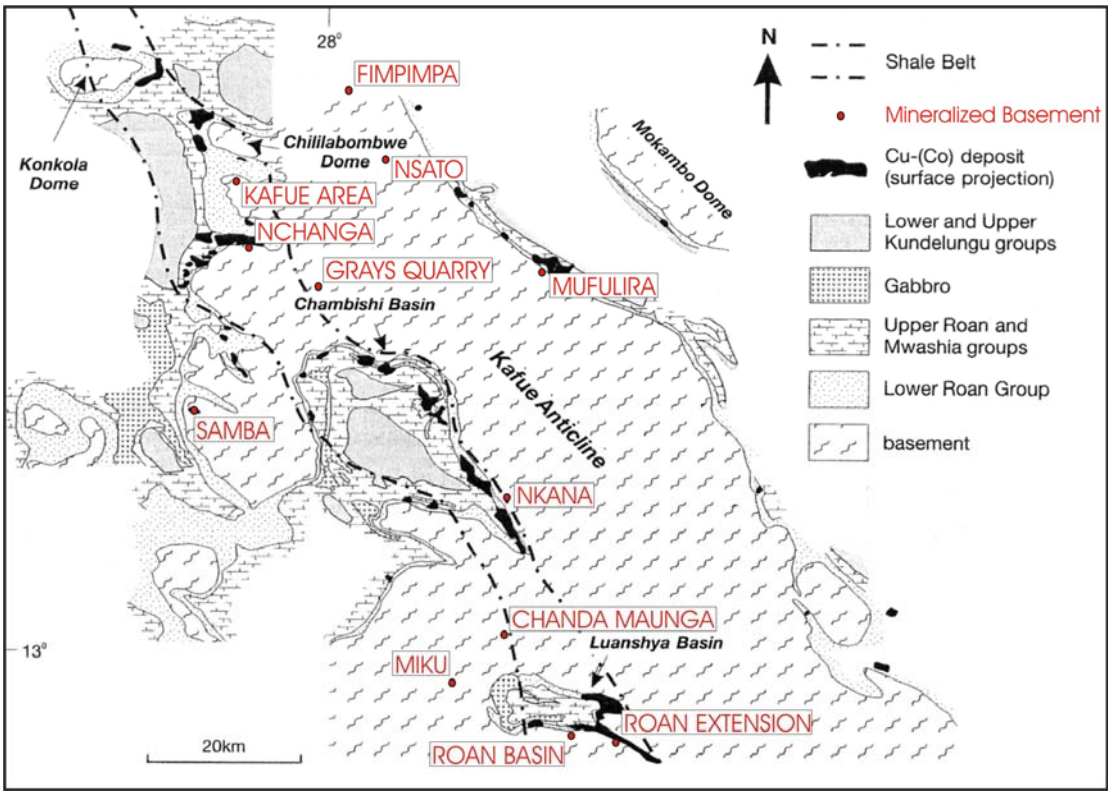

Figure 2.6 Distribution of copper mineralization in the pre-Katangan basement (Pienaar 1961; Selley *et al.* 2005)

Veins are ubiquitous within the basement of the Kafue Anticline and consist of thin and often discontinuous quartz-carbonate, quartz-feldspar and quartz-anhydrite veins as well as quartz veins that vary in thickness from a few centimetres to approximately 30 metres and can have strike lengths in excess of 300 metres (Pienaar 1961). Many veins are devoid of ore minerals but others are erratically mineralized with specularite, tourmaline, pyrite, malachite, chalcopyrite, bornite, chalcocite, pyrrhotite and magnetite as well as rare traces of gold (Pienaar 1961). Locally these minerals can be observed disseminated in the host rocks up to 5 metres from the vein contacts with

associated alteration minerals including fine white mica, chlorite, biotite, and epidote (Pienaar 1961). Copper mineralization is also observed along joints, fractures and shear zones in intrusive igneous rocks such as granite, pegmatite and basic igneous rocks. Locally disseminated mineralization extends up to 2 metres into the host rocks from the intrusive contacts (Pienaar 1961). Copper mineralization associated with overlying Katangan orebodies is observed at Mufulira, Nchanga, Nkana and the Roan Extension (figure 2.6) where mineralization extends downwards into the underlying Lufubu Metamorphic Complex (Pienaar 1961).

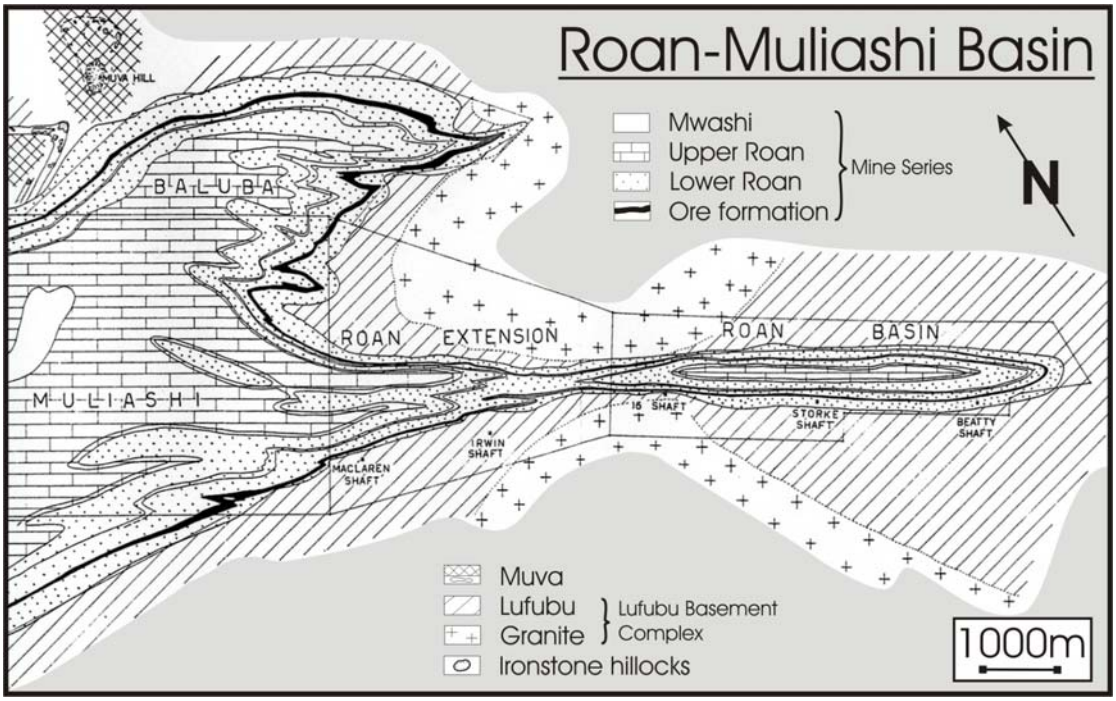

Figure 2.7 Geological map of Roan-Muliashi Basin (modified from Mendelsohn 1961)

In the Roan Extension (figure 2.6 & 2.7) there is a basement palaeo-high that is truncated at the base of the Lower orebody. Where the pre-Katangan basement is overlain by the sedimentary rocks that host the Lower Orebody, sulphide mineralization occurs in the Lufubu schists for approximately 15 metres below the palaeo-surface (figure 2.8).

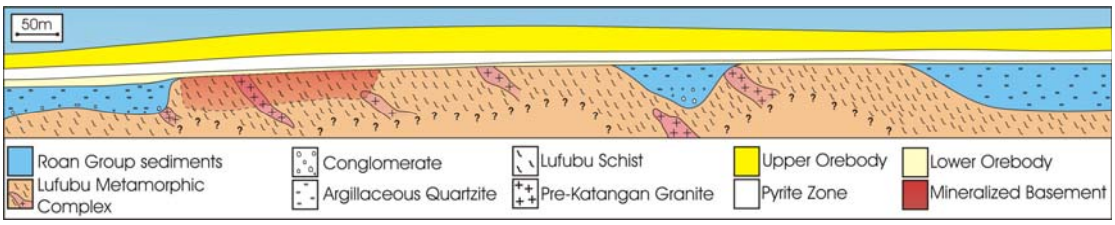

Figure 2.8 Basement mineralization in the Roan Extension (modified Mendelsohn 1961)

CHAPTER 2: REGIONAL GEOLOGY

The mineralization consists of predominantly chalcopyrite, finely disseminated in the biotite schist and scarce in the granite intrusions (Mendelsohn 1961). The overall grade of the mineralized zone is approximately 1% copper (Pienaar 1961).

The basement underlying the Nkana orebody also contains copper sulphides, locally mineralized over 7 metres below the unconformity and grading at 1.5% copper. The ore minerals are chalcopyrite and bornite, essentially the same as the overlying orebody (Pienaar 1961). At Mufulira the Lufubu granites and arenites are mineralized where in contact with the base of the C orebody. The basement mineralization consists of disseminated chalcopyrite and pyrite in sand, pebble, and boulder filled cracks and fissures (Pienaar 1961).

Mineralization of pre-Katangan basement without an association with overlying Copperbelt deposits are observed at Fimpimpa, Nsato, Kafue Area, Roan Area, Nchanga, Greys Quarry, Chanda Maunga, Miku, and Samba (figure 2.6) (Pienaar 1961; Wakefield 1978).

Mineralization Association	**Ore Minerals**	**Gangue Minerals**	**Wall-Rock Alteration**
Intrusive Igneous (granites, pegmatites, basic intrusions)	chalcopyrite, bornite, pyrrhotite, pyrite	quartz, feldspar carbonate anhydrite hematite magnetite tourmaline	sericite chlorite phlogopite epidote
Vein	pyrite, chalcopyrite, bornite, chalcocite, malachite, pyrrhotite, gold (trace)		
Disseminated (up to 5m from vein/igneous contact)			
Shear Zone	chalcopyrite		

Table 2.1 Summary of characteristics of pre-Katangan basement mineralization that is not associated with overlying ore deposits (Summarized from Mendelsohn 1961; Pienaar 1961; Wakefield 1978; McGowan 2003)

In the Roan Basin of the Zambian Copperbelt (figure 2.6 & 2.7), the Lufubu schists are almost universally mineralized with sparsely disseminated pyrite. Occurrences of chalcopyrite and pyrrhotite are observed locally and form coarser concentrations in small irregular discontinuous quartz veins (Mendelsohn 1961).

Intrusive granites of the Roan Basin host veins and pegmatites that are mineralized with pyrite, chalcopyrite and pyrrhotite, or chalcopyrite and minor

bornite. Mineralization extends into the schist wall rock up to 6 metres from the intrusive igneous rocks. Locally, sparse to noticeable disseminated pyrite, chalcopyrite and minor bornite have been described in the granite near to its borders. A 60 metre section intersecting a number of veins was graded at 0.5% copper (Mendelsohn 1961).

Mineralized joints with 15cm alteration zones extend up to 60 metres below the surface of the granite at Nchanga, and in the western part of the mine, vein hosted and disseminated mineralization extends up to 9 metres below the unconformity grading at 0.77% copper (figure 2.6). Thin ore sections separated by barren granite are found well below this depth at Nchanga, and at Mufulira chalcopyrite-anhydrite mineralized fractures have been identified up to 400 metres below the unconformity (Pienaar 1961).

McGowan (2003) described chalcopyrite mineralization within a phlogopite rich fault gouge at Nchanga, associated with an early extensional structure and mineralized thrusts, which deform the Lower Roan units and root into the basement. The association of copper mineralization with basement structures is also observed at Grays Quarry where the Nchanga Red Granite is mineralized with films of pyrite and chalcopyrite in tension fractures below a large thrust fault (Pienaar 1961).

The Kafue Area mineralization (figure 2.6) consists of disseminated chalcopyrite and malachite, hosted by schistose, pebbly and micaceous quartzites. The mineralization occurs in a 9 by 21 metre area that is near to a granite intrusion. Mineralized quartz veins are observed in this area and the richest sections are commonly found proximal to the quartz veins (Pienaar 1961).

Pienaar (1961) describes veins and disseminations of bornite and chalcopyrite in the biotite schists and schistose quartzites of the Nsato Area (figure 2.6). In the Nsato Area copper minerals occur as both isolated grains in the matrices and as veins along joints and planes of schistosity. The extent of the Nsato Area mineralization is unknown.

CHAPTER 2: REGIONAL GEOLOGY

Limited copper occurrences have been identified in the Miku Area and the Chanda Maunga Area of the Kafue Anticline (figure 2.6). In the Miku Area, mineralization consists of disseminated specks and films of malachite, along quartz veins, brecciated zones, and joints in altered quartzites and schists that grade locally up to 0.3% copper with traces of gold (Pienaar 1961). At Chanda Maunga malachite mineralization is hosted by the Muva quartzites along intrusive quartz veins with associated specularite, tourmaline and limonite casts. Mineralization extends only a small distance from the veins into the quartzites with interbedded black phyllite (Pienaar 1961).

At the Fimpimpa Prospect (figure 2.6), copper mineralization occurs along a massive quartz vein in basement schists and gneisses, as well as in a feldspathized quartz diorite. The garnetiferous quartz-mica schists and biotite gneisses are interpreted by Pienaar (1961) as a series of “shear zones.” The structure is described as approximately 8 metres wide, with a westerly strike that can be traced for thousands of metres and mineralized with sporadic malachite, chalcopyrite and bornite. The interpretation that this mineralized structure is a “shear zone” is not qualified by Pienaar (1961) and although the brittle or ductile nature of the structure are not discussed, the term “shear zone” suggests that this structure is a zone of relative displacement. The entire width of the mineralization at the Fimpimpa Prospect contains less than 0.4% copper, although higher grades occur locally (Pienaar 1961).

The feldspathized quartz diorite of the Fimpimpa Prospect is host to fracture bound; vein hosted and disseminated malachite, chalcopyrite and bornite mineralization. The majority of the mineralization is confined to fractures and quartz-calcite veinlets, although minor disseminated mineralization was described in close proximity to these structures (Pienaar 1961).

The Fimpimpa Prospect is host to a copper-bearing quartz vein up to 12 metres thick and that follows the trend of the granite gneiss country rock for more than 150 metres. The full thickness of the vein grades at 0.5% copper although locally grades reach 1.8% copper. The copper mineralization is typically malachite with cores of chalcopyrite and bornite. Hydrothermal

alteration extends up to 2.5 metres from the mineralized veins as thin lenticular fine white mica veinlets with chlorite replacing biotite in the country rock (Pienaar 1961).

The Samba deposit is the largest concentration of copper mineralization in the pre-Katangan basement of the Kafue Anticline. The deposit consists of disseminations, stringers and veinlets of pyrite, chalcopyrite and bornite, hosted by quartz-sericite schists. The mineralized schists have gradational contacts with porphyritic igneous rocks of granodioritic to quartz-monzonitic compositions that have been dated as pre-Katangan to post Lufubu in age (figure 2.9) (Wakefield 1978).

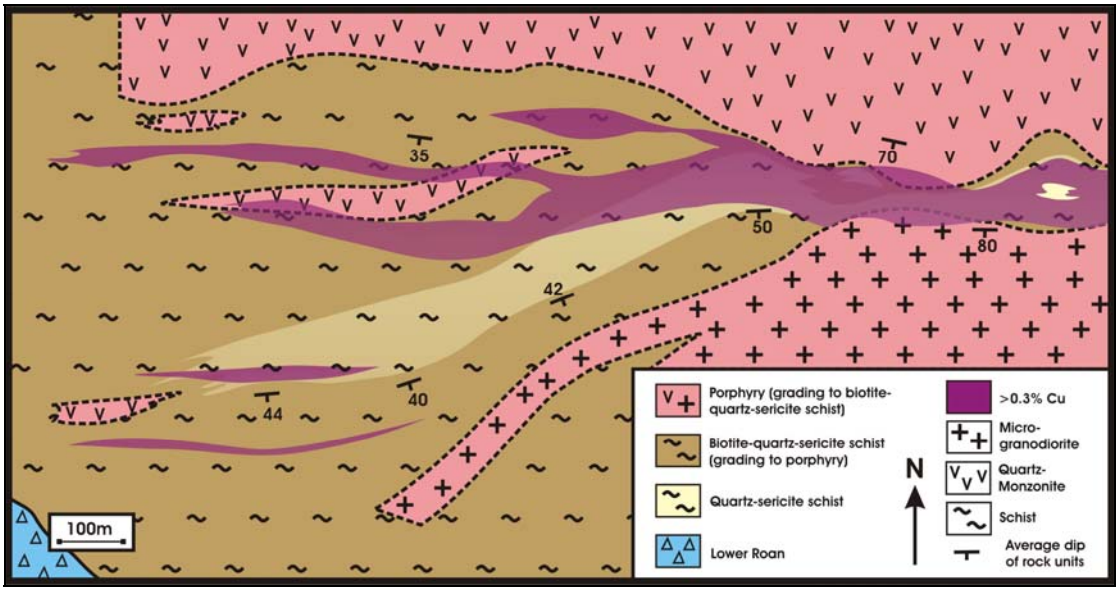

Figure 2.9 Geological plan of the Samba deposit (modified from Wakefield 1978)

Styles of sulphide mineralization at the Samba Porphyry include sub-equidimensional chalcopyrite aggregates disseminated in a poorly foliated or massive host rock known as “bleb” sulphide that is commonly associated with chlorite-bearing schist. With increasing deformation “bleb” sulphide grades into stringer sulphide that consists of fine stringers and disseminations of chalcopyrite and bornite aligned with the foliation, giving the rock a banded appearance in well mineralized zones (Wakefield 1978).

Sulphide minerals are also hosted by quartz-calcite veins that are deformed within the fabric and by undeformed quartz veins that post date the deformation. The sulphide in the late vein hosted mineralization is interpreted

by Wakefield (1978) to have been derived from the adjacent mineralized host rocks.

Bornite and pyrite show an antithetic relationship with pyrite-chalcopyrite forming low grade shoots whereas chalcopyrite and chalcopyrite-bornite form high grade shoots with up to 4% copper. In the east mineralization correlates with the igneous “stratigraphy” but shows no relation to it in the west where a thick unit of typically unmineralized quartz-sericite schist occurs. Thin zones of relatively high-grade mineralization can not be correlated between drill-holes and are separated by zones of poorly mineralized to barren rock (figure 2.9) (Wakefield 1978).

The deformed rocks at Samba are typically L-S tectonites that have been deformed during two main deformation events. During the first phase of deformation, a penetrative cleavage and lineation developed that is defined by the parallel orientation of sericite. The second phase of deformation developed a steep-dipping crenulation cleavage that is defined by the crenulation and microfolding of the penetrative cleavage and by the recrystallization of sericite. The second phase of deformation is only observed in the sericite schist units (Wakefield 1978).

All of the igneous rocks of the Samba Porphyry deposit are pervasively sericitised with fine plagioclase crystals in the matrix altering to fine grains of sericite. However, the plagioclase phenocrysts show a varying degree of sericitisation, which increases in intensity into the mineralized zone and correlates with an increase in the intensity of deformation. Local zones of undeformed and totally sericitised rock are present and indicate that alteration predates deformation (Wakefield 1978).

The gradational contacts between the igneous protolith and the copper mineralized schists suggest that the schists were derived from the igneous protolith through a process of alteration. The process responsible for the alteration of the protolith is ambiguous with possible mechanisms including weathering and hydrothermal alteration.

CHAPTER 2: REGIONAL GEOLOGY

Wakefield (1978) interpreted the host rocks to the Samba deposit to be contiguous with the meta-sedimentary sequences of the Muva Supergroup, although this is disputed by Rainaud *et al.* (2005) who suggest that the host rocks to the Samba deposit form part of the Lufubu Metamorphic Complex. The suggestion that the host rocks to the Samba deposit are part of the Lufubu Metamorphic complex is supported by U-Pb SHRIMP dating of 13 zircons from a sample of meta-volcanic epidotised biotite-muscovite-k-feldspar-quartz schist. The felsic schist yielded a weighted mean age of 1964 ± 12 Ma and is interpreted as the meta-volcanic emplacement age (Rainaud *et al.* 2005).

2.5 Geology and geochronology of the Central African Copperbelt

The neo-Proterozoic Katangan belt is more than 150 km wide and stretches for 700 km from Mwinilunga in the west to Kolwezi in the northwest, to Baluba in the southeast of the belt (Cailteux *et al.* 2005) (figure 1.1).

The copper-cobalt orebodies occur in the Roan Group of the Katangan Supergroup. The Roan Group meta-sedimentary rocks display a regional lateral variation of facies between Zambia-type and Congo-type successions. In Zambia and SE Congo, deposits are mainly hosted in para-autochthonous siliciclastic rocks close to basement terranes deposited in structural basins, separated by basement highs, where the sedimentary rocks rest with an angular unconformity on the granites and schists of the pre-Katangan basement complex (Cailteux *et al.* 1994; Cailteux *et al.* 2005) (figure 2.5).

Although terms applied to sedimentary rocks are used to describe the rocks of the Zambian Copperbelt, the formations are distinctly metamorphic; in particular, the host rocks to the mineralization include mica schists, which may contain carbonates, talc or tremolite (Moine *et al.* 1986). The metamorphic minerals observed include, biotite, sericite, scapolite, tourmaline, chlorite, tremolite-actinolite, epidote and apatite (Mendelsohn 1961).

CHAPTER 2: REGIONAL GEOLOGY

The metamorphic grade across the Copperbelt varies in a northwest to southeast direction from lower greenschist facies at Konkola to upper greenschist to amphibolite facies at Baluba (Hitzman 2000) (figure 1.1). The variation in metamorphic grade across the Copperbelt has been explained by major thrust structures (Hitzman 2000), which have also been recognised within the Domes Region that host the Lumwana Cu-Co deposits (Cosi *et al.* 1992).

In the Zambian Copperbelt the Katangan Supergroup consists of the Upper and Lower Roan Groups overlain by the Mwashia. The Mwashia is overlain by the Kundulungu Series that is subdivided into an upper, middle and lower unit (Mendelsohn 1961; Drysdall *et al.* 1972; Binda & Mulgrew 1974; Fleischer *et al.* 1976).

<table>
<tr><td rowspan="2"></td><td colspan="2">DRC</td><td colspan="4">ZAMBIA</td></tr>
<tr><td colspan="2">Kundulungu Series</td><td colspan="4">Kundulungu Series</td></tr>
<tr><td rowspan="4">KATANGAN SUPERGROUP</td><td rowspan="4">Roan Group</td><td>Mwashya Group</td><td rowspan="4">Roan Group</td><td colspan="3">Mwashia Group</td></tr>
<tr><td rowspan="2">Dipeta Group</td><td>Carbonate Unit</td><td>Upper Roan</td><td rowspan="4">Mine Series</td></tr>
<tr><td>Mixed Unit</td><td rowspan="2">Lower Roan</td></tr>
<tr><td>R.A.T.

(The ‘Roches Argilo-Talqueses’)</td><td>Siliciclastic Unit</td></tr>
<tr><td colspan="6">KIBARAN & PRE-KIBARAN BASEMENT</td></tr>
</table>

Figure 2.10 Simplified lithostratigraphic correlation of the Katangan Supergroup of the Zambian Copperbelt and the DRC (modified after Cailteux *et al.* 1994)

The Upper and Lower Roan in Zambia are collectively known as the Mine Series, ranging in thickness from 800 to 2000 metres, passing upwards from basal continental clastics to accumulations of shallow argillaceous marine

clastics to a mixed carbonate platform sequence consisting mainly of dolomitic units (figure 2.11).

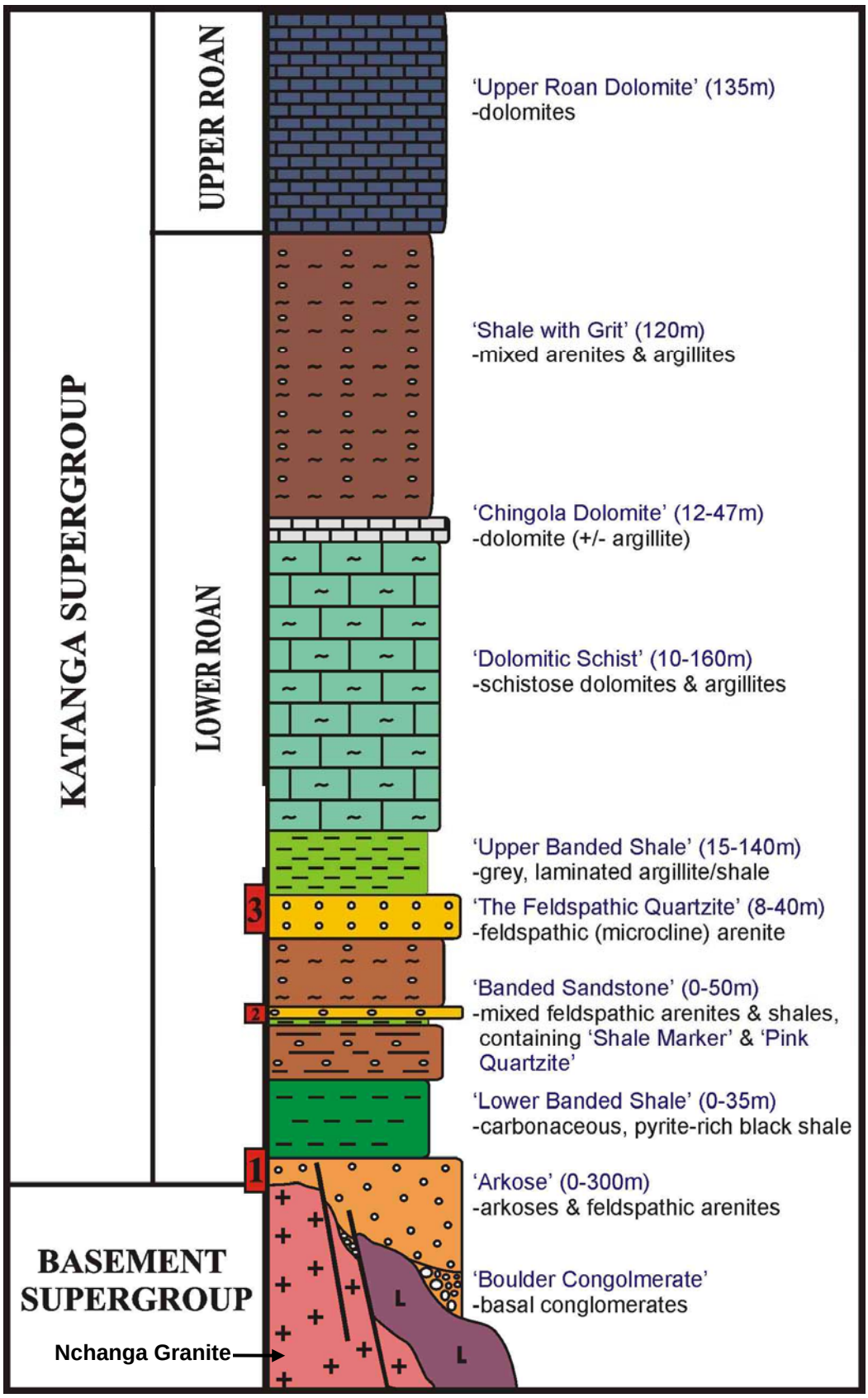

Figure 2.11 Stratigraphy of the Nchanga deposit in the Zambian Copperbelt. 1) A Lower Orebody 2) Intermediate Orebody 3) Upper Orebody (after McGowan 2003)

CHAPTER 2: REGIONAL GEOLOGY

The Lower Roan Group consists of the older Mindola Clastics Formation conformably overlain by the younger Kitwe Formation. The Mindola Clastics Formation comprises texturally immature conglomerates and subarkosic sandstones that were deposited in fluvial, alluvial fan, aeolian and fan delta environments and is characterised by significant lateral and vertical facies variations (Selley *et al.* 2005) (figure 2.12).

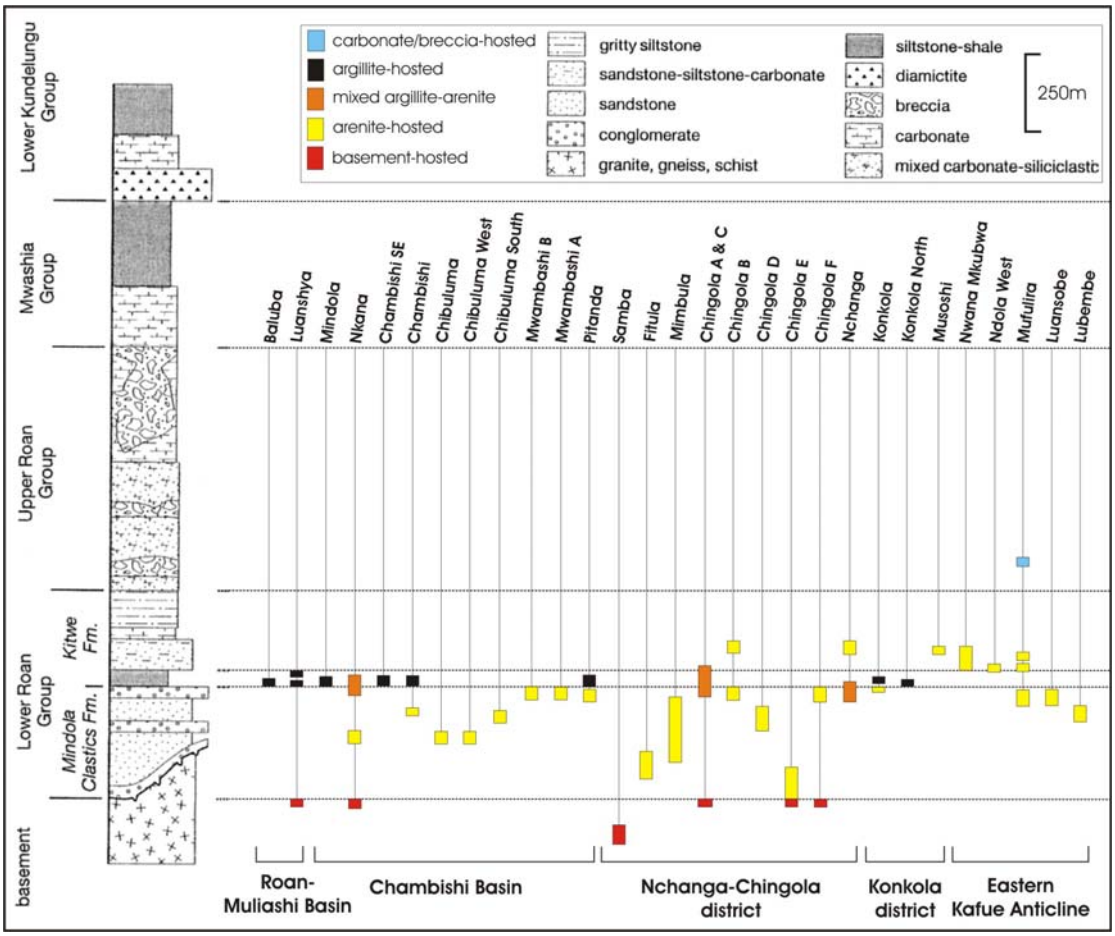

Figure 2.12 Lithostratigraphic distribution of Zambian Copperbelt Cu-(Co) mineralization. Thicknesses of mineralized intersections not to scale due variations in thickness of Lower Roan Group strata (Modified from Selley *et al.* 2005)

The base of the Kitwe Formation is commonly termed the “Ore Shale” and varies from a 20 to 25m finely laminated dolomitic siltstone in the west of the Kafue Anticline to a 1 to 2m dolomitic “Mudseam” to the East of the Kafue Anticline (Binda 1994) (figure 2.12).

At the western margin of the Shale Belt the Copperbelt Orebody Formation is pinched out, where sheared and brecciated dolomites, dolomitic talc-chlorite

schists, and gabbro lie upon Mindola Clastics Formation strata (Binda and Mulgrew 1974; Porada and Berhorst 2000).

The Upper Roan Group is distinguished from the Lower Roan Group by a predominance of carbonate strata and is characterized by laterally extensive upward-fining cycles of sandstone, siltstone, dolomite, algal dolomite on a metre scale. The dolomites commonly contain nodules of talc, quartz and anhydrite, which have been interpreted to represent early diagenetic evaporitic processes in a sabkha environment (Selley *et al.* 2005).

The preserved thickness of the Upper Roan platform carbonate sequence varies from <30 to 800 metres, the changes in thickness often abrupt and associated with breccias, which form both single bodies and multiple stacked bodies which range in thickness from tens of metres to hundreds of metres respectively (Selley *et al.* 2005). In the west of the Zambian Copperbelt the breccias are host to highly altered discontinuous gabbroic bodies >100 metres in length (Annels 1984).

The Mwashia Group was originally defined by Mendelsohn (1961) as a shale dominant sequence overlying the dolomite dominant sequence of the Upper Roan Group. In the DRC, the Mwashya Group comprises of an upper clastic sequence overlying a lower dolomitic sequence that contains volcanic rocks, which are detached from the underlying Upper Roan Group by a polylithic breccia that is interpreted as having a tectonic origin (Cailteux 1994).

The Grand Conglomerate, a sequence of debris flows and diamictites defines the contact between the Mwashia Group and the Kundulungu Group and varies in thickness from ~10 to 100 metres in the Zambian Copperbelt to >1000 metres in the DRC (Binda and Van Eden 1972) (figure 2.5).

The overlying stratigraphy of the Lower Kundulungu Group consists of an upward deepening sequence of carbonates, siltstones and mudstones, 400 to 500 metres thick, which are overlain by the Petit Conglomerate and the

carbonates, siltstones and mudstones of the Upper Kundulungu Group (Selley *et al.* 2005).

In the DRC, dolomites and dolomitic shales (Cailteux *et al.* 1994) define thrust sheets, nappes and klippen that were developed during the Lufilian Orogeny (Demesmaeker *et al.* 1963; Cailteux and Kampunzu 1995; Kampunzu and Cailteux 1999). These structures contain carbonate-dominated megafragments that are hundreds to thousands of metres in length and host the Congo-type mineralization (Francois 1973; Cailteux and Kampunzu 1995; Jackson *et al.* 2003) (figure 2.13).

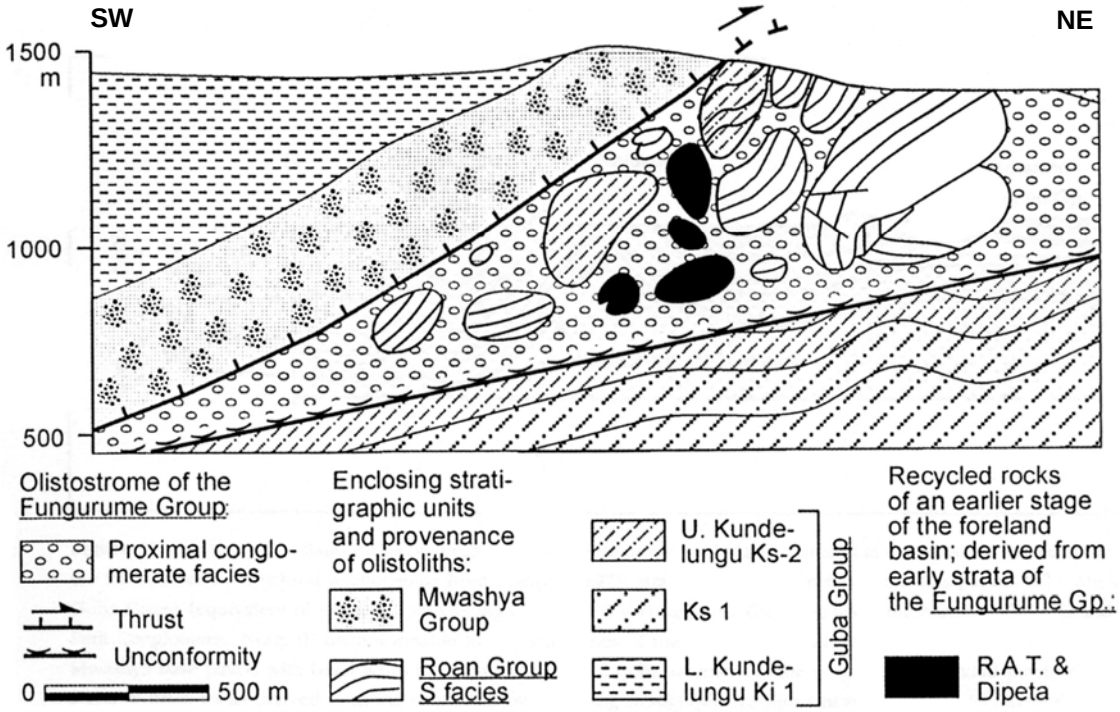

Figure 2.13 Cross-section through Kambove in the DRC suggesting olistostrome origin (after Wendorff 2003).

The origin of the breccias is debatable with theories ranging from a sedimentary olistostrome origin (Porada 1995; Wendorff 1995, 2005) to a tectonic friction breccia origin (Cailteux *et al.* 1994, 1995). It has also been suggested that the breccias represent former evaporitic horizons (Selley *et al.* 2005).

The sedimentary succession of the Katangan Lower Roan sequence can be interpreted on the basis of transgressive and regressive marine phases over a continental pre-Katangan landscape. Early transgression over basement

topography and deposition of footwall siliciclastics was followed by a major northeast directed transgression over the whole of the Copperbelt, resulting in the truncation of basement highs, development of evaporates, and subsequent deposition of the ore-shale horizon in deeper-water facies (Binda & Mulgrew 1974; Diederix 1977).

The Lower Roan Group is the oldest of the Mine Series of the Katangan Supergroup, with a maximum age of 883 ± 10 Ma, constrained by Armstrong *et al.* (2005) using Ion-Microprobe analysis of magmatic zircons in the intruding Nchanga Red Granite. This was supported by further analysis of detrital zircons directly above the unconformity that cluster into 2 populations, one at ~880 Ma and the other at ~2000 Ma that represent the Lufubu Metamorphic Complex and the younger Nchanga Red Granite respectively (Armstrong *et al.* 2005).

The Grand Conglomerate of the Lower Kundulungu Group is correlated globally with the Sturtian diamictites deposited at approximately 740 Ma (Key *et al.* 2001; Bodiselitsch *et al.* 2005) and $^{40}Ar/^{39}Ar$ age data from detrital muscovites provide a maximum age for sedimentation of 573 ± 5 Ma (Master *et al.* 2005). U-Pb SHRIMP dating of detrital zircons from upper Katangan sedimentary rocks yield provenance ages of 2081 ± 28 Ma and 1836 ± 26 Ma, indicating that the sedimentary rocks were derived from the Bangweulu Block and the Lufubu Metamorphic Complex respectively (Master *et al.* 2005).

2.6 Mineralization of the Zambian Copperbelt Deposits

The Zambian Copperbelt differs from most other sediment-hosted stratiform copper deposits in that it lacks significant galena and sphalerite (Gustafson and Williams 1981) and is significantly impoverished in silver and on average, enriched in cobalt (Hitzman *et al.* 2005). The mineralization commonly transgresses or overlaps lithological contacts in both argillite and arenite hosted deposits (Darnley 1960; Annels 1974, 1979; Sweeney *et al.* 1991).

The Copperbelt copper-cobalt orebodies are stratiform with high strike to width ratios, a geometry that is preserved even in areas of pronounced

Lufilian deformation, such as Nkana-Mindola and Luanshya (Mendelsohn 1961). The majority of the copper-cobalt mineralization of the Zambian Copperbelt is confined to the arenites, shales and carbonate rocks of the Mixed and Siliciclastic Units of the Lower Roan Group (McGowan 2003) (figure 2.11) although a 200 metre stratigraphic interval broadly centred on the Copperbelt Orebody Member hosts approximately 70% of the economic mineralization (Selley *et al.* 2005) (figure 2.12).

Several different styles of mineralization can commonly be observed at the deposit scale that either overlap or form spatially distinct zones and include disseminated, pre-folding vein-hosted, post-folding vein-hosted, shear zone hosted and oxidation-supergene mineralization (Selley *et al.* 2005). Hypogene mineralization consists of disseminated, prefolding vein hosted and shear zone hosted chalcocite, bornite, chalcopyrite, pyrite, carrollite and hematite in the absence of copper minerals. Hematite is a common component of unmineralized rocks of the Lower Roan Group and contributes up to 5% of the volume of the Mindola Clastics (after Selley *et al.* 2005).

Styles of Mineralization	**Cu-Co-U bearing mineral assemblages**	**Gangue mineral assemblages**
Hypogene	chalcocite, bornite, chalcopyrite, pyrite, carrollite	k-feldspar, phlogopite, sericite, muscovite, albite, dolomite, calcite, quartz, rutile, anhydrite, pyrite, pyrrhotite and hematite
Supergene	chalcocite, copper carbonate/ sulphate, cuprite, native copper	
Post folding vein-hosted	chalcopyrite, accessory bornite, pitchblende, brannerite, molybdenite	

Table 2.2 Styles of mineralization including ore and gangue mineral assemblages for the Zambian Copperbelt (Summarized from Selley *et al.* 2005)

The primary mineralization is overprinted with secondary chalcocite, copper carbonate, sulphate, cuprite and native copper (after Selley *et al.* 2005) (table 2.2). A progressive change from primary sulphide to secondary sulphide assemblages commonly occurs within 30 to 70 metres of the surface (Mendelsohn 1961) however, chalcocite and malachite extend to greater depths of more than 1km at Konkola and greater than 600 metres at Nchanga (McKinnon and Smit 1961). Post folding vein-hosted mineralization includes chalcopyrite, accessory bornite, pitchblende, brannerite and molybdenite. The uranium mineralization is typically sub economic in the Zambian Copperbelt

with the exception of the Mindola uranium orebody and typically occurs in the late veins and as local disseminations (Selley *et al.* 2005).

The Central African Copperbelt contains significant cobalt concentrations (>0.1 wt % Co) in sulphides carrollite ($Cu(Co,Ni)_2S_4$), linnaeite ($CoCo_2S_4$), cobaltiferous pyrite (FeS_2), and pentlandite ($(Fe,Ni)_9S_8$) that are ubiquitous in the DRC deposits and restricted in the Zambian deposits to a relatively narrow zone between Baluba and Konkola on the western side of the Kafue Anticline (Annels 1974; Fleischer *et al.* 1976; Annels *et al.* 1983).

Many Zambian Cu-Co deposits to the west of the Kafue Anticline exhibit lateral and vertical sulphide zonation over distances of approximately 100 metres to several kilometres from bornite ± chalcocite, through chalcopyrite ± carrollite, to distal pyrite ± pyrrhotite from east to west respectively. A similar vertical zonation is observed with a higher mode of bornite at the base, through chalcopyrite and pyrite at the top (Mendelsohn 1961; Fleischer *et al.* 1976). The distal pyrite coincides mainly with the carbonaceous facies of the Copperbelt Orebody Member and typically extends 8 to 12 kilometres west of the orebodies (Mendelsohn 1961; Fleischer *et al.* 1976).

In the Zambian Copperbelt the host rocks to the mineralization exhibit three main styles of alteration that include calcium-magnesium, potassic and sodic alteration (table 2.3). However, some debate exists over the timing and origin of the alteration (Mendelsohn 1961; Fleischer *et al.* 1976; Sweeney *et al.* 1991; Binda 1995).

Alteration Type	Alteration Minerals	Relation to Ore	Alteration
Calcium-magnesium	Anhydrite, dolomite, calcite & phlogopite	Early – antithetic	Dissolution of evaporitic horizons
Potassic 1	K-feldspar, phlogopite	Syngenetic – intergrown	K-metasomatism
Potassic 2	Sericite-muscovite	Late stage - replacing K-feldspar	Evolution of potassic fluid 1 with lower pH
Sodic	Albite & scapolite	Post dates – replaces K-feldspar and sericite	Fracture facilitated Na alteration

Table 2.3 Summary of alteration styles, minerals and their relation to ore in the Zambian Copperbelt (after Moine *et al*. 1986; Annels 1974, 1989; Warren 1991; van Eden 1974; McGowan *et al.* 2003; Garlick and Fleischer 1972; Sweeney and Binda 1989; Darnley 1960; Richards *et al.* 1988; Selley *et al.* 2005)

Calcium-magnesium alteration is associated with anhydrite, dolomite, calcite and phlogopite and has an antithetic relationship with copper mineralization (Moine *et al*. 1986; Garlick and Fleischer 1972; Sweeney and Binda 1989). Textural evidence indicates that the fluids responsible for calcium-magnesium alteration originated from the dissolution of evaporitic horizons deposited in Sabkha type environments (Annels 1974; Warren 1991; van Eden 1974). Isotopic data of recrystallized anhydrite and dolomite cements supports a dissolved evaporite source with $\delta^{34}S$ values that are compatible with neo-Proterozoic seawater. However, light $\delta^{13}C$ and $\delta^{18}O$ values indicate a possible hydrothermal component (Selley *et al.* 2005).

Potassic alteration is contemporaneous with copper mineralization resulting in intergrowths of k-feldspar and phlogopite with mineralization (Mendelsohn 1961; Darnley 1960; McGowan *et al.* 2003; Sutton & Maynard 2005. A late stage low pH phase of the potassic alteration results in dissolution of k-feldspar and replacement with sericite and muscovite (Selley *et al.* 2005).

A late sodic alteration event post-dates the potassic alteration with albite and scapolite replacing secondary k-feldspar and sericite (Annels 1989; Sweeney and Binda 1989; Darnley 1960; Selley *et al.* 2005). Intense albitization is associated with breccias, fracture zones and veins, which contrasts with the nonfracture related distribution of most secondary k-feldspar (Selley *et al.* 2005). The maximum age of Na alteration is constrained by albitized gabbroic bodies emplaced between 765 and 735 Ma that coupled with the association with fracture-induced permeability indicates that Na alteration occurred during advanced stages of basin maturity (Selley *et al.* 2005).

2.7 Theories of genesis of the Zambian Copperbelt Deposits

Although the Congo-type and Zambian-type deposits show some differences (e.g. clastic vs. carbonate host rocks), they display a large number of similarities, including their location in laterally correlative lithostratigraphic units deposited in supratidal to sabkha-type highly saline environments; similarities of ore textural features predominantly disseminated sulphides closely linked to sedimentary structures, such as laminations and cross-

bedding; identical sulphide paragenesis and zoning of sulphides relating to Eh-pH parameters during ore deposition (Cailteux *et al.* 2005)

The source of the mineralizing fluid, metals and sulphur, as well as the timing, fluid migration and trapping mechanism for metals have been the subject of considerable controversy since the discovery of the Zambian Copperbelt deposits in the late 1920's (Kirkham 1976; Sweeny *et al.* 1991). Early epigenetic theories proposed that the granites, which underlie the mineralized Katangan sedimentary rocks, to be intrusive and the source of mineralizing hydrothermal solutions. This was in part due to the misidentification of scapolite as the contact metamorphic mineral cordierite (Mendelsohn 1957), the presence of copper sulphide veinlets within the Nchanga Red Granite, the association of chalcopyrite and pyrite with crosscutting splays of colourless chlorite, and the presence of mineralized veins within the ore horizons (Gray 1929; Davidson 1931; Jackson 1932). The existence of an unconformity between the basement granites and Katangan meta-sediments was first noted by Schneiderhöhn (1937), and demonstrated by Garlick & Brummer (1951), establishing that a magmatic source is untenable. The recognition of the angular unconformity led to the development of a syngenetic model that has been the most widely accepted for the last sixty years (figure 2.14).

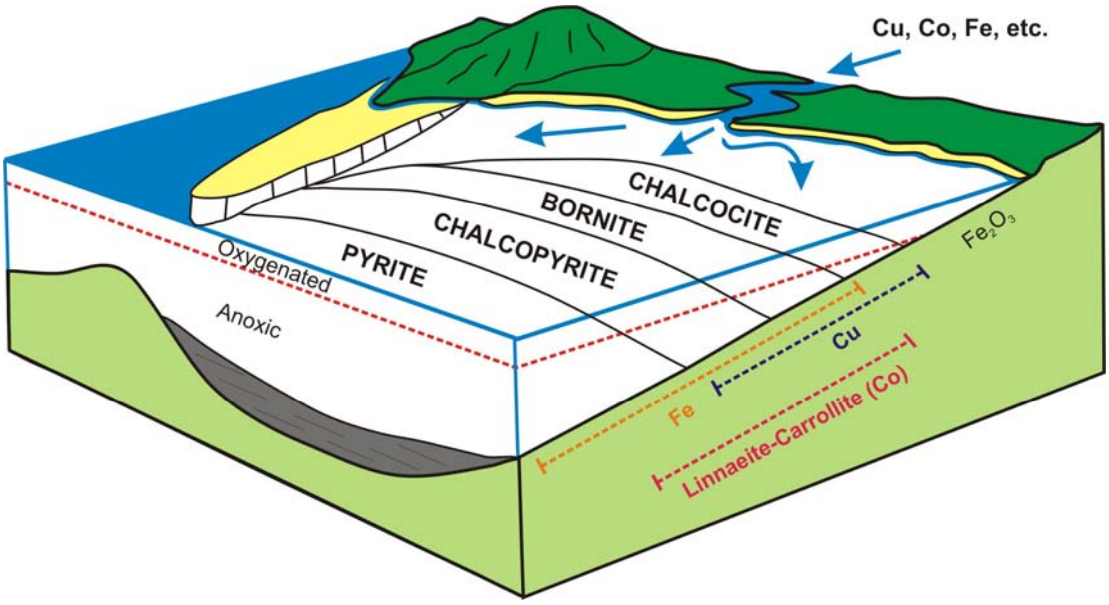

Figure 2.14 Syngenetic model for Zambian Copperbelt mineralization (after Garlick 1961)

The syngenetic model involves the simultaneous input of sediment and dissolved metals from rivers in marginal marine environments. Sulphides precipitated below the oxygenated zone where bacterial activity would result in suitable reducing conditions with precipitation of sulphides in accordance with Schurmann's (1888) "law" of metals solubility, resulting in a series of zones parallel to the palaeo-shoreline.

The copper mineralogy reflects this zoning, with grading from copper-rich species to iron-rich species in an offshore direction. Chalcocite-bornite-chalcopyrite-pyrite zones became fixed during diagenesis, as the fine colloid mixed with sulphides crystallised into grains that reflect the size of the host sediment. This model is also supported by the occurrence of uranium, molybdenum and tungsten minerals in the oxygenated zone closest to the strandline (Sweeney *et al.* 1991) (figure 2.14).

The syngenetic model was extended to a diagenetic model, to take into account the processes that must have occurred following the deposition of the host sediments, but prior to significant compaction. This involves the flow of copper-rich solutions through porous, unconsolidated sediments during diagenesis and the precipitation of sulphides (Sweeney and Binda 1994). This model is supported by the presence of lateral secretion veins that indicate that copper was introduced prior to compaction, as well as evidence that sulphides were remobilised during metamorphism (Garlick 1972). Fluid inclusion data has shown that relatively low (<100 °C) crystallization temperatures of primary syngenetic/early diagenetic versus higher (≤200 °C) crystallization temperatures for late diagenetic sulphides (Cailteux *et al.* 2005).

Exhalative and hydrothermal models have also been suggested, involving the precipitation of sulphides from copper-rich hydrothermal solutions that migrated into cover sequences via deep-basement structures (Sweeney *et al.* 1991). Sources for fluids range from hidden magma chambers at depth (Darnley 1960) to intrusive amphibolite bodies. The relationship of cobaltiferous ore bodies west of the Kafue Anticline and intrusive amphibolite was described by Annels (1974) and led to the suggestion that the two are

genetically related. This is refuted by Cailteux *et al.* (2005) who argue that there is no evidence to support a genetic ore model involving widespread circulation of hydrothermal fluids ascending along rift fractures and deriving metals from deep-seated mafic rocks.

Recent epigenetic models involve the role of migrating; copper-rich basinal brines or metamorphic fluids, being introduced into the Lower Roan during regional Lufilian tectonism. Evidence for this includes the basement and vein hosted mineralization noted by the early epigeneticists (Gray 1929; Davidson 1931; Jackson 1932) and the association of Cu-Co enrichment within shear zones with thrust structures and phyllosilicate development (Molak 1995). Textural evidence from Konkola North suggests that coarse unorientated biotite is coeval with mineralization, but post-dates the fine grained biotite, indicating that mineralization was associated with multiple phases of K-metasomatism over an extended period of time (Sutton & Maynard 2005).

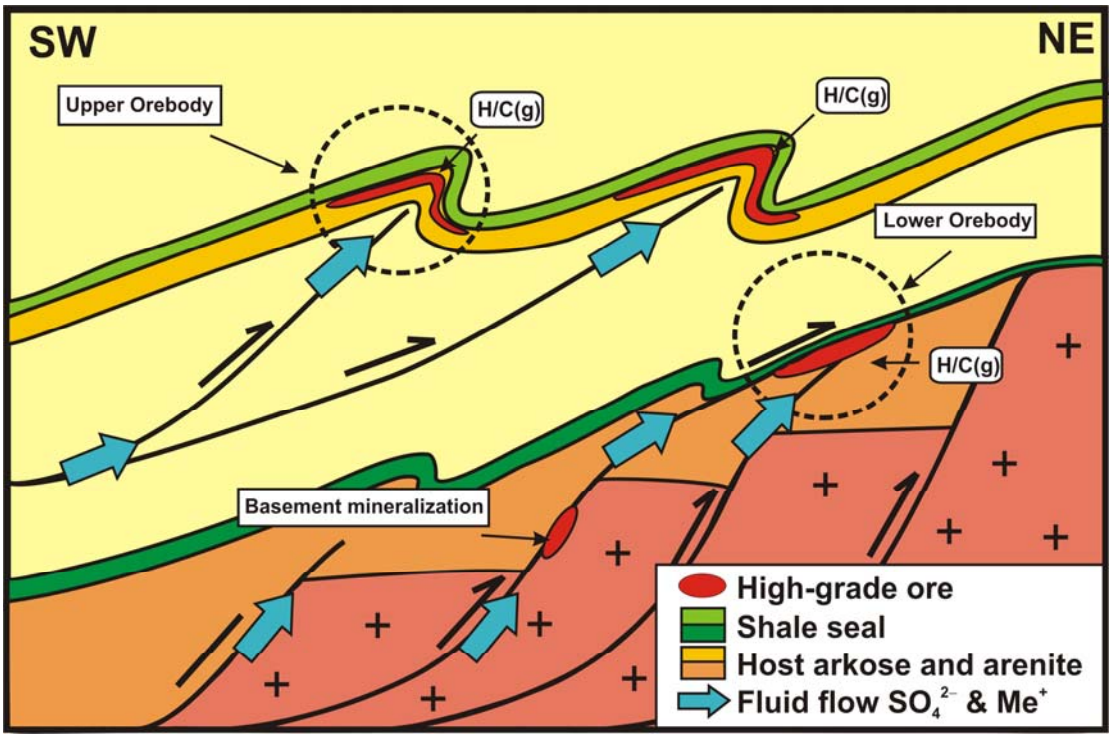

Figure 2.15 Schematic fluid-flow model for mineralization during basin inversion and thrust-fold development of host sequence (after McGowan *et al.* 2003)

McGowan (2003) proposes an epigenetic model where brines generated deep within the host basin were expelled during regional deformation (compression and inversion) towards basin margins. Fluid interaction and dissolution of

continental evaporate sequences would have provided the necessary conditions for both the transport of copper and cobalt as chloride complexes and for the leaching of metals from the basement. During fold-thrust development, oxidising metal-bearing fluids were introduced into fractured and porous quartzo-feldspathic units that were sealed during deformation by overlying shale caps. Precipitation of sulphides occurred through thermochemical reduction of the ore fluid on contact with methane present in the sandstones (figure 2.15).

The epigenetic model is supported by the work of Sutton & Maynard (2005) who suggest a two fluid mixing model for Konkola North based on petrographic and geochemical data and their relationship to basin geometry. This model involves an oxidizing fluid carrying Cu, Ba, K and possibly Co that travelled laterally within the footwall. The fluid was driven from the deep basin to the shallow western flank and into the ore shale by basement highs. A second fluid that is probably reducing and carrying H_2S moves laterally at a stratigraphically higher level than the ore shale. Where the basement topography dropped, the upper fluid moved down stratigraphy and mixed with the ore bearing fluid resulting in Cu-sulphide mineralization and barite precipitation.

Selley *et al.* (2005) suggest that the size, distribution and geometry of the Zambian Copperbelt deposits are controlled by the syn-rift, sub-basin fault architecture, and that the availability of the in situ and mobile reductants is linked to the basin structures. A multistage ore forming event is indicated by the complex textural relationships and geochronological constraints of Cu-Co sulphide phases. The necessity to derive metals from either the local stratigraphy or extra-basinal sources, coupled with the widespread alteration associated the ore forming event, indicates that the mineralization is late diagenetic in origin (Selley *et al.* 2005).

CHAPTER 2: REGIONAL GEOLOGY

2.8 Geology and Mineralization of the Central African Domes Region

The Lumwana deposits are host by the Mwombezhi Dome, one of several basement inliers of early to Mid-Proterozoic age. Similar Eburnian (1800-2000 Ma) basement underlies the late Proterozoic Katangan Supergroup sedimentary rocks that host the majority of the copper-cobalt ores in the Zambian Copperbelt (Unrug 1988). The basement domes are interpreted as antiformal stacks above mid to lower crustal ramps and consist of granite gneiss, migmatites and schist that vary in metamorphic grade from amphibolite facies in the domes region to green schist facies in the Kafue Anticline (Daly *et al.* 1984). The Mwombezhi Dome is located east of the Kabompo Dome and west of the Solwezi and Luswishi domes (Steven and Armstrong 2003) (figure 2.16).

Mineralization within the Domes Region includes the Kalumbila Co-Ni-Cu prospect of the Kabompo Dome (Steven & Armstrong 2003), the Lumwana deposits, Chimiwungo and Malundwe of the Mwombezhi Dome and the vein-hosted Kansanshi Cu deposit to the east of the Solwezi Dome (Broughton *et al.* 2002).

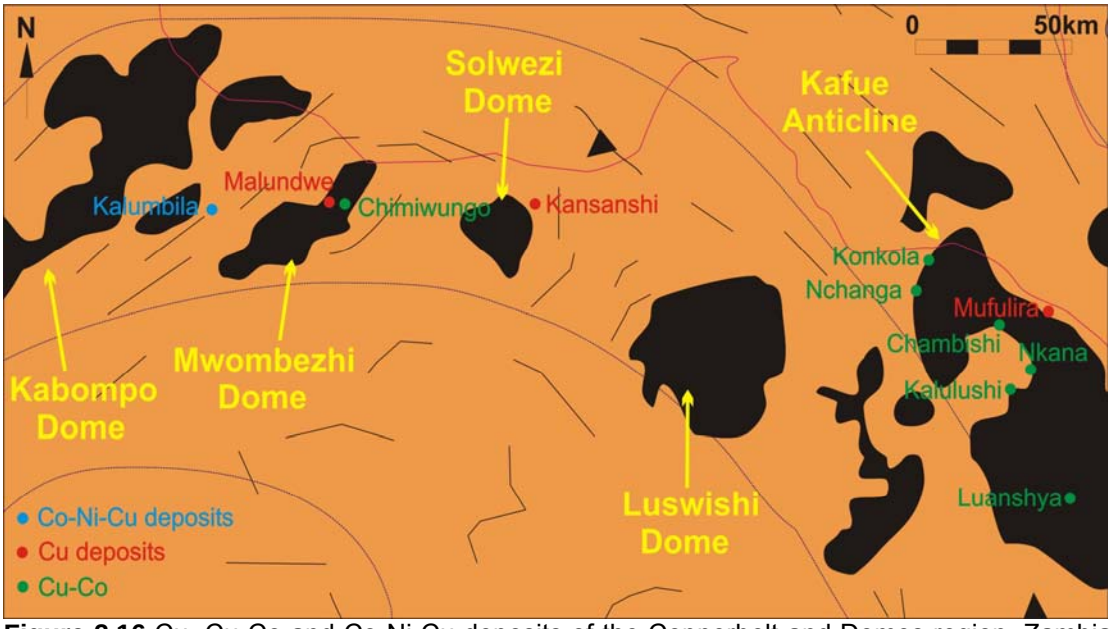

Figure 2.16 Cu, Cu-Co and Co-Ni-Cu deposits of the Copperbelt and Domes region, Zambia (modified after Porada 1989; Binda & Porada 1995).

John *et al.* (2004) determined ages of 1884 ±10 Ma and 1874 ± 9 Ma for the Kabompo and Solwezi Domes respectively with U-Pb_{ZIRCON} SHRIMP technique. The Mwombezhi Dome has been dated by Cosi *et al.* (1992) using a whole rock Rb-Sr technique yielding a younger age of approximately 1.7 Ga. However, the Rb-Sr date of 1.7 Ga is based on a poorly constrained isocron that have been shown to provide younger ages than U-Pb_{ZIRCON} SHRIMP zircon dating technique used for the other basement inliers (Rainaud *et al.* 2005). In addition, the Mwombezhi Dome comprises rocks of similar petrology and metamorphic history to that of the other basement domes suggesting that it is contemporaneous.

The domes comprise granitic gneisses, migmatites, and schists unconformably overlain at their margins by rocks of the neo-Proterozoic Katangan Supergroup. Rocks of the Mesoproterozoic Muva Supergroup are only found along the eastern margin of the Lufilian Arc (Cosi *et al.* 1992). The Katangan Supergroup within and around the domes consist mainly of units of the Lower Roan Group with magnesium-rich quartzite, mica schist, metapelite and amphibolite (John *et al.* 2004). Cosi *et al.* (1992) describe Mg-rich quartzite with hematite rich horizons and 1-5 cm feldspar (microcline or oligoclase) layers and suggest that the protolith was an impure quartzite with dolomitic cement and sedimentary iron formations. The feldspar layers are interpreted as original evaporitic horizons in which chlorine has been replaced by silica and aluminium (Cosi *et al.* 1992). Whiteschists commonly occur close to the contact between the basement and Roan Group and are mainly exposed along the margins of the domes and rarely within the domes (Kabompo and Mwombezhi Dome). The lower units of the Katangan Supergroup and the basement rocks of the domes have poorly defined contacts and are usually interpreted as sheared (John *et al.* 2004).

2.9 Geology of the Mwombezhi Dome

The Mwombezhi Dome Basement Complex that hosts the Lumwana deposits comprises biotite-feldspathic gneiss, hornblende-gneiss, granite gneiss, migmatites and schists (Mulela and Seifert 1998) (figure 2.17). The basement units are intruded by younger granites (Mulela and Seifert 1998) which have

not been dated and are likely to be synchronous with either the 883 ± 10 Ma Nchanga Red Granite (Armstrong *et al.* 2005) located in the Copperbelt or the 559 ± 18 and 566 ± 5 Ma Hook Granite Complex to the south of Mwombezhi Dome located on the northern contact of the Mwembeshi Shear-Zone (figure 2.2) (Hanson *et al.* 1993).

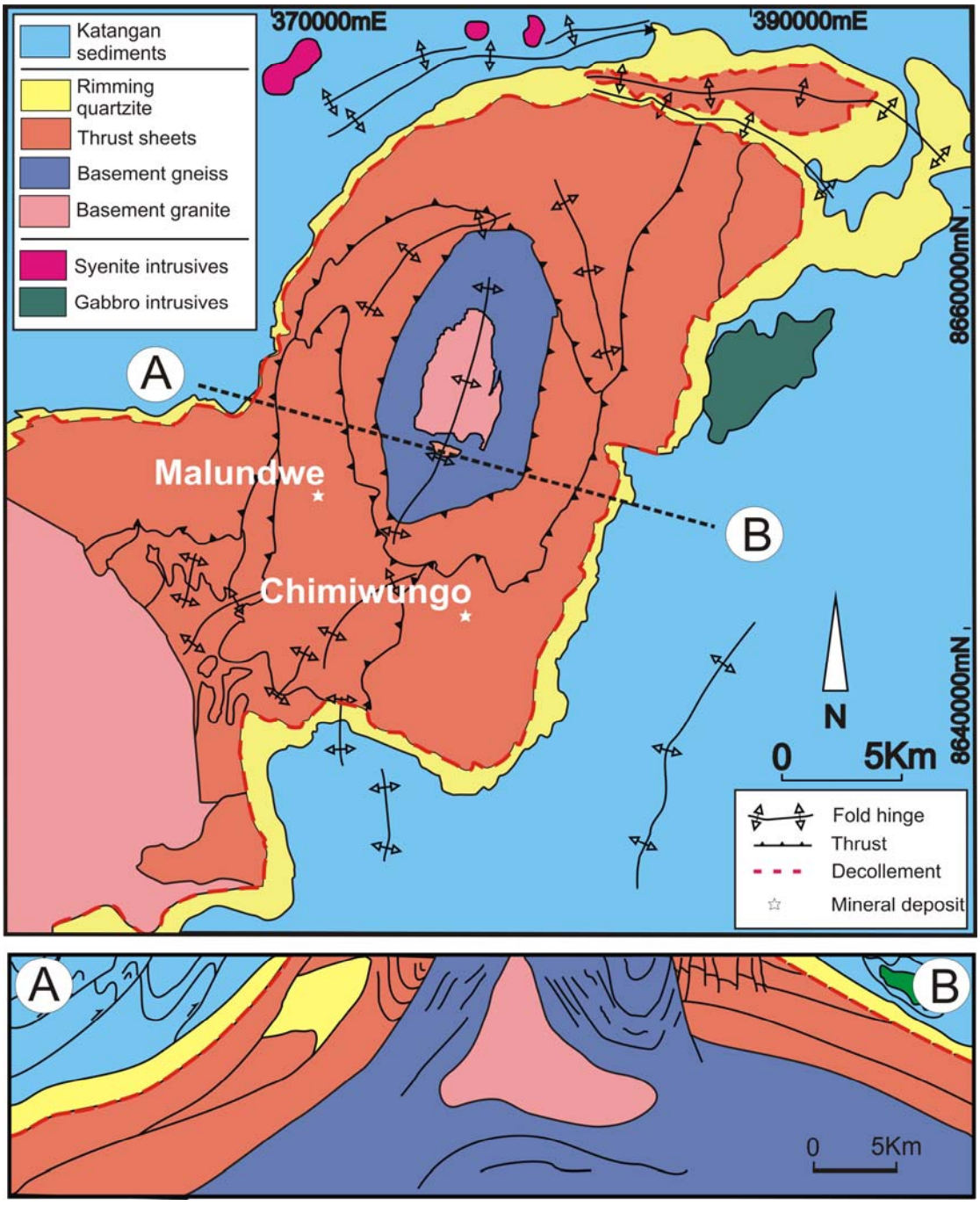

Figure 2.17 Simplified geology of the north-eastern lobe of the Mwombezhi Dome basement complex with schematic cross-section. Thrust sheets, as recognized by Equinox geologists, distinguished by variations in internal tectono-stratigraphy and geophysical characteristics

CHAPTER 2: REGIONAL GEOLOGY

Logging of diamond drill core has revealed that the granites at the core of the north-eastern lobe of the Mwombezhi Dome, exhibit less deformation than the highly deformed granite gneiss units, which host the Chimiwungo and Malundwe deposits. This observation supports the concept that the granites at the core of the north-eastern lobe of the Mwombezhi Dome post date the deformation (figure 2.17).

The Mwombezhi Dome basement complex is separated from the overlying Katangan stratigraphy by a major décollement. The décollement comprises magnesium rich quartzite to muscovite-quartz-talc-kyanite-hematite schist that grades to whiteschist at the contact with the basement units and are collectively known as the “Rimming Quartzite” (figure 2.17). The décollement, shown by the dashed red line separates the Palaeoproterozoic thrust stratigraphy from the overlying thin-skinned tectonic regime of the Katangan sedimentary rocks. The décollement is marked by an L-S tectonite that exhibits an intense north south mineral lineation (figure 2.17).

The “Rimming Quartzite” has been correlated with the Lower Roan lithologies (personal communication, Nisbett 2005), but their protolith is enigmatic as their chemical composition is extremely rare in nature and indicates a metasomatic origin (Johnson & Oliver 2002). The fluids responsible for the metasomatism of the “Rimming Quartzite” are possibly derived from the pore fluids of shallow water sediments, driven off the Congo plate by the over-riding Kalahari plate during continent-continent collision at 530 Ma (John *et al.* 2004).

The whiteschist mineral assemblages observed in the Mwombezhi Dome basement complex and the garnet-hornblende association indicate temperatures of 700° to 750°C, and pressures of 11 to 13kbar, which correlate to burial depths of approximately 50 km (Cosi *et al.* 1992; John *et al.* 2004). Monazites have been dated from assemblages representing peak metamorphism at 524 ± 3 Ma to 532 ± 2 Ma using U-Pb dating (John *et al.* 2004).

CHAPTER 3: GEOLOGY AND MINERALIZATION OF THE LUMWANA DEPOSITS

3.1 Introduction

The Lumwana tenement is a Large Scale Mining License LML-49 that covers 1,355km^2 of the Mwombezhi Dome and includes two major copper deposits, Malundwe and Chimiwungo, as well as numerous exploration prospects. The deposits are low grade Cu ± Co ± U with the largest known Zambian copper resource outside of the Zambian Copperbelt and will rank as Africa's largest copper mine when mining commences in 2007. This chapter provides a detailed description of the geology of the Lumwana deposits, cross-sections constructed across the deposits and macro-scale structural observations made during field mapping and logging of core.

3.1.1 Field area characteristics

The topography of the project area is characterised by gently rolling hills incised by the Lumwana East River and its tributary streams. Elevations in the general vicinity of the Malundwe and Chimiwungo deposits range from approximately 1,270 to 1,410 metres above sea level. The predominant vegetation is miombo woodland with good vegetation cover although wetlands (dambo areas) are common along watercourses (Davis *et al.* 2006) (figure 3.1).

Figure 3.1 Photograph looking to the east of miombo woodland in the Lumwana East River valley (373056E 8646383N)

CHAPTER 3: GEOLOGY AND MINERALIZATION OF THE LUMWANA DEPOSITS

The region has distinct dry (May to October) and wet (November to April) seasons with the majority of the field work conducted during the dry season. Humidity ranges from 45% in the dry season to 90% in the wet season with humidity levels reaching their peak in October at the onset of the wet season. Rainfall mainly occurs in heavy thunderstorms producing typical precipitation events of 20 to 40mm (Davis *et al.* 2006).

The rock units of the Mwombezhi Dome are poorly exposed and outcrops are heavily weathered. The soils of the area are leached of nutrients and locally ferricrete laterite horizons form extensive terraces. The majority of the outcrop comprises a bedded quartzite unit that is resistive to weathering and forms topographic highs. Other rock units are exposed locally in river valleys and a structural traverse was conducted along the Lumwana East River in order to validate existing structural data.

3.1.2 Malundwe and Chimiwungo deposit characteristics

The Lumwana ore bodies are tabular and elongated in a north-south orientation with layer parallel disseminated sulphide zones. The ore bodies have high strike to thickness ratios with thicknesses measured in tens of metres and strike lengths measured in kilometres.

The mineralization is hosted within a thrusted tectono-stratigraphy. The dip and plunge of the ore bodies are parallel to the tectono-stratigraphy and to the foliation (S_1) & stretching lineation (L_1). Ore packages and individual ore schist units pinch and swell forming north-south orientated lenses parallel to the foliation and stretching lineation.

The host rocks to the Lumwana deposits are migmatitic gneisses to amphibolite that grade into kyanite schists. The host rock to the ore bodies are dominated by two mineralogically similar but texturally distinct rock types, a granite to pegmatite gneiss and a banded to augen gneiss that both comprise quartz-feldspar ± biotite/phlogopite ± hematite. The ore bodies comprise muscovite-phlogopite-quartz-kyanite-sulphide schist, although

mineralization can be observed locally within the weakly mineralized intervening gneiss units.

The Malundwe and Chimiwungo deposits are hosted by separate thrust sheets that are identified by their host rock lithologies and geophysical characteristics. In addition to the gneiss and schist units observed at Chimiwungo, the Malundwe footwall also includes units of unmineralized kyanite schist, talc ± epidote ± kyanite schist to quartzite. The kyanite schist to quartzite units are mineralogically similar to the "rimming quartzite" observed at the décollement between the basement rocks and overlying Katangan Supergroup meta-sedimentary rocks. Observation of sedimentary "way up" structures in the footwall quartzite at Malundwe indicates that it forms part of an overturned limb of a recumbent fold (Benham *et al.* 1976; Nisbett *pers comm.* 2004). However, no sedimentary structures were observed during this study. The footwall quartzite overlies emplaced calc-silicates and amphibolites that have been tentatively correlated with the Upper Roan (figure 2.17 & 3.2).

<table>
<tr><th></th><th>MALUNDWE SHEET</th><th>CHIMIWUNGO SHEET</th></tr>
<tr><td>HANGING WALL</td><td>Basement Gneiss</td><td>Basement Gneiss</td></tr>
<tr><td colspan="3">Top D_1 Shear Zone</td></tr>
<tr><td rowspan="5">ORE PACKAGE</td><td rowspan="5">Malundwe Ore Schist</td><td>Upper Ore Schist</td></tr>
<tr><td>Middle Gneiss</td></tr>
<tr><td>Main Ore Schist</td></tr>
<tr><td>Lower Gneiss</td></tr>
<tr><td>Lower Ore Schist</td></tr>
<tr><td rowspan="6">FOOTWALL</td><td>Mottled Schist</td><td rowspan="4">Basement Gneiss & Mottled Schist</td></tr>
<tr><td>Epidote Schist</td></tr>
<tr><td>Mottled Schist</td></tr>
<tr><td>Speckled Schist</td></tr>
<tr><td>Quartzite</td><td rowspan="3">Not Present</td></tr>
<tr><td>Muscovite-Quartz Schist</td></tr>
<tr><td colspan="2">D_1 Thrust</td></tr>
<tr><td>UPPER ROAN</td><td>Carbonates, amphibolites, pelites & gabbros</td></tr>
</table>

Figure 3.2 Simplified stratigraphic comparisons of the Malundwe and Chimiwungo deposits as identified by Equinox geologists, and supported by fieldwork

The Chimiwungo deposit has three main ore horizons separated by intervening internal gneiss units that vary from quartz-feldspar-phlogopite gneiss to garnet-amphibolite. The Malundwe deposit consists of one orebody in the north and two in the south that are separated by an intervening internal gneiss unit. Observed contacts between ore and host rock units are

commonly transitional in nature with an increase in the mode of mica minerals correlating with a decrease in the proportion of feldspar minerals.

The primary sulphide mineralization at Lumwana commonly occurs in mineral pairs of copper sulphides, which exhibit a down section zonation in diamond drill core. The sulphide pairs consist of pyrite (FeS_2) – chalcopyrite ($CuFeS_2$), chalcopyrite – carrollite ($CuCo_2S_4$) (Chimiwungo only) and chalcopyrite-bornite (Cu_5FeS_4). Bornite and chalcopyrite are replaced by minor digenite (Cu_9S_5) chalcocite (Cu_2S) and covellite (CuS). Minor uranium mineralization occurs locally cross-cutting the Cu-Co mineralization. Quartz veins which cross-cut both the mineralization and the barren internal gneiss units are commonly host to pyrite, chalcopyrite and/or bornite. Coarse, elongate, disseminated, aggregates and stringers of sulphide grains are observed parallel to the foliation & stretching lineation. Sulphides were deformed by the S_1 fabric and overprinted by kyanite which formed at peak metamorphism. This indicates that copper was introduced to the basement either syn or pre-peak metamorphism. Sulphides are commonly observed in microstructural dilatant sites such as pressure shadows around porphyroblast grains. This is interpreted as the result of sulphide remobilization during D_{n+1} metamorphism with associated quartz-muscovite alteration.

3.2 Structural geology of the Lumwana area

The general structure of the Mwombezhi Dome has been interpreted by previous authors as either complex recumbent folding of Katangan sediments overlying older basement (Mulela and Seifert 1998) or as an allochthonous nappe complex composed of both basement and cover (Cosi *et al.* 1992) (figure 2.17 and figure 2.3).

McGregor (1965) recognised one pre-Lufilian and three Lufilian deformation events whereas Equinox geologists have recognised a total of 5 Lufilian deformation events (Table 3.1). No pre-Lufilian structures have been identified in the basement gneiss units of the Mwombezhi Dome.

CHAPTER 3: GEOLOGY AND MINERALIZATION OF THE LUMWANA DEPOSITS

Event	Timing	Features
D_1	Early Lufilian	N-S compression resulted in nappe formation, pervasive layer parallel foliation (S_1) and D_1 shear zones with stretching lineation L_1
D_2	Mid Lufilian	E-W compression produced recumbent isoclinal folds with localised fold hinge schistosity (S_2). This event was also responsible for D_2 shear zones and the thrusted tectono-stratigraphy
D_3	Mid Lufilian	NW-SE compression was responsible for listric thin skin thrusting and folding of the Katangan meta-sedimentary cover rocks. D_3 deformation was also responsible for the retrograde metamorphism and the final juxtaposition of the tectono-stratigraphy
D_4	Late Lufilian	NNW-SSE compression produced conical upright open folds that folded the L_1 stretching lineation. D_4 compression was responsible for the development of a local crenulation and fracture cleavage and for the formation of the regional dome antiforms e.g. Mwombezhi Dome
D_5	Post Lufilian	Relaxation and post compression unroofing was responsible for NW-SE & N-S steep brittle normal faults and late felsic anorogenic stocks

Table 3.1 Structural geology of the Mwombezhi Dome (after unpublished Equinox Report)

North - south early Lufilian compression (D_1) in the Mwombezhi Dome produced extensive thrusting, nappe formation, and a pervasive layer parallel foliation (S_1), which generally obliterates bedding. Thrusts trend in a north – south direction at Malundwe but swing to the east south of Lumwana (McGregor 1965).

F_1 fold axial planes were orientated at 160°/ 15° SW and fold hinge lines plunge at 11°/212° (McGregor 1965). D_1 shear zones are host to an intense stretching lineation L_1 (figure 3.3). The stretching lineation (L_1) plunges from 6° towards 180°, which is the approximate dip of the bedding and slightly shallower than the S_1 schistosity. Locally quartz veins form north-south orientated rods.

During the mid-Lufilian, ongoing north - south Lufilian compression was resolved into local east – west compression (D_2) producing recumbent isoclinal folds with localised fold hinge schistosity (S_2). F_2 fold axial planes were overturned and orientated at 170°/44°W. F_2 fold hinge lines plunge at 12°/192° with limbs exhibiting an average dihedral angle of 36° (McGregor 1965). This event is also responsible for D_2 shear zones and the thrusted tectono-stratigraphy.

CHAPTER 3: GEOLOGY AND MINERALIZATION OF THE LUMWANA DEPOSITS

Figure 3.3 Photograph facing west. North-south mineral stretching lineation (L_1) in banded gneiss unit (371791E 8646340N)

Mid-Lufilian NW-SE compression (D_3) is responsible for listric thin skin thrusting and folding of the Katangan meta-sedimentary cover rocks. D_3 deformation is also responsible for the retrograde metamorphism and the final juxtaposition of the tectono-stratigraphy of the basement complex of the Mwombezhi Dome.

Late Lufilian compression rotates from northwest – southeast to north northwest – south southeast (D_4) producing local crenulation and fracture cleavages. D_4 also produced conical upright open folds (F_4) and folded the L_1 stretching lineation and was the last major ductile deformation event of Lufilian Orogeny. This low pressure deformation event has little associated new mineral growth and was responsible for the formation of the regional dome antiforms e.g. Mwombezhi Dome. F_4 fold axial planes are frequently curved orientated between 40° to 120° with a shallow dip to the southwest (figure 3.4) (McGregor 1965).

Post-Lufilian relaxation and post compression unroofing was responsible for NW-SE & N-S steep brittle normal faults and late felsic anorogenic stocks.

CHAPTER 3: GEOLOGY AND MINERALIZATION OF THE LUMWANA DEPOSITS

Figure 3.4 Photograph facing north-west. Complex sheath folds in quartzite demonstrating poly-phase deformation (371294E 8653091N)

In the Mwombezhi dome area, the deformation events D_1 & D_2 produced the regional nappe, with recumbent folding and eastward directed thrusting, due to north – south regional compression being resolved locally into east – west compression. This was interpreted by McGregor (1965) as the result of the central location of the Mwombezhi dome within the Lufilian Arc (McGregor 1965).

The granite basement and Lower Roan Quartzite acted as one competent unit during the deformation phases with a décollement developing at the Lower Roan quartzite - Upper Roan carbonate contact. This situation is also observed in both the Copperbelt and Kabompo Dome (McGregor 1965).

A structural transect across the Malundwe deposit from hanging wall to footwall as well as numerous field excursions validated previous structural data collected by McGregor (1965) and Equinox (figure 3.5 & appendix A4).

CHAPTER 3: GEOLOGY AND MINERALIZATION OF THE LUMWANA DEPOSITS

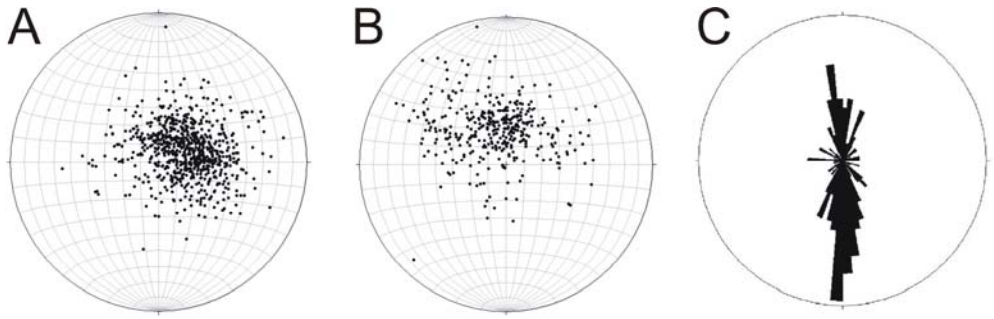

Figure 3.5 Stereographic projections of structural data and rose diagram. A) Malundwe S_1 poles to planes (n=858) B) Chimiwungo S_1 poles to planes (n=632) and C) rose diagram of mineral stretching lineations L_1 recorded from the Mwombezhi Dome (n=206)

Kinematic indicators can be observed in diamond drill core in the host rocks to the mineralization. Shear sense can only be determined in orientated core and where orientated core was examined, kinematic indicators consistently suggest a north-south displacement, typically with top to the north deformation. Examples of kinematic indicators were examined in orientated diamond drill core from Eq-Chi-065 (appendix A2: 377475E 8640150N) including pressure shadows on porphyroblasts, C/S fabrics and asymmetrical extensional shear bands.

From 208.29 to 208.44 meters, Eq-Chi-065 comprises a muscovite-phlogopite-quartz-kyanite-sulphide schist with a 5 cm thick intervening unit with garnet porphyroblast grains. C/S fabrics are observed with sulphides distributed along both C and S planes and garnet porphyroblast grains exhibit sinistral quartz-muscovite-sulphide pressure shadows. In any C/S fabric, S planes represent a penetratively developed strain-sensitive flattening fabric whereas C planes are discrete narrow shear zones which are taken to lie parallel to the flow plane of the progressive deformation (figure 3.6 A) (Hanmer and Passchier 1991).

In addition to garnet, pressure shadows on kyanite porphyroblasts also provide kinematic indicators in the Lumwana deposits and are observed at 233.63 meters in Eq-Chi-065. Poikilolitic kyanite porphyroblast grains in muscovite-phlogopite-quartz-kyanite-sulphide schist exhibit sinistral quartz-muscovite-phlogopite pressure shadows (figure 3.6 B).

CHAPTER 3: GEOLOGY AND MINERALIZATION OF THE LUMWANA DEPOSITS

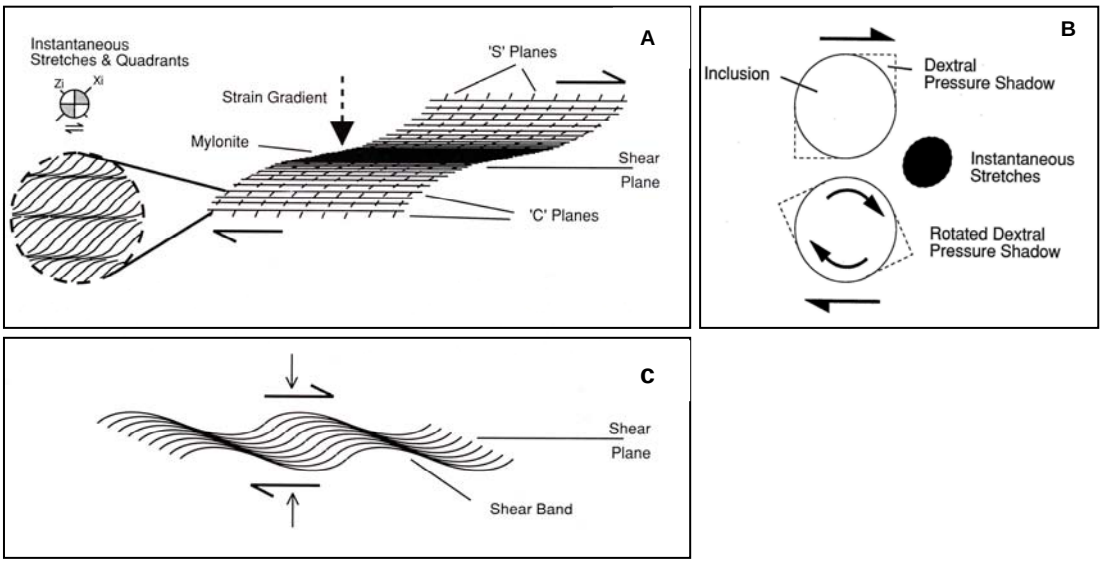

Figure 3.6 Schematic diagrams demonstrating A) C/S fabrics. Cisaillement (C) refers to the shear planes whereas Schistosité (S) refers to the cleavage planes B) Pressure shadows around rigid inclusions C) Asymmetrical extensional shear bands (after Hanmer and Passchier 1991)

Pressure shadows are volumes of material deposited at the contact between the stiff inclusion and its less competent matrix by precipitation from solution. Material may be transported to the site of precipitation by diffuse and/or advective mass transfer (Hanmer and Passchier 1991). Asymmetrical extensional shear bands are common in both mineralized and unmineralized schists at Lumwana and are locally associated with retrograde metamorphic reactions with garnet porphyroblast grains altering to chlorite (figure 3.6 C).

C/S fabrics can be difficult to distinguish from asymmetrical extensional shear bands as geometrically; a mylonitic foliation cut by asymmetrical extensional shear bands bears some resemblance to a C/S fabric (Hanmer and Passchier 1991). All kinematic indicators in Eq-Chi-065 suggest a top to the north deformation direction and are representative of both the Chimiwungo and the Malundwe deposits.

3.3 Geology and mineralization of the Lumwana deposits

The Chimiwungo and Malundwe deposits are large tabular low-grade ore bodies, each approximately 4km in length with a shallow dip to the south and west respectively (figures 3.7 to 3.9).

CHAPTER 3: GEOLOGY AND MINERALIZATION OF THE LUMWANA DEPOSITS

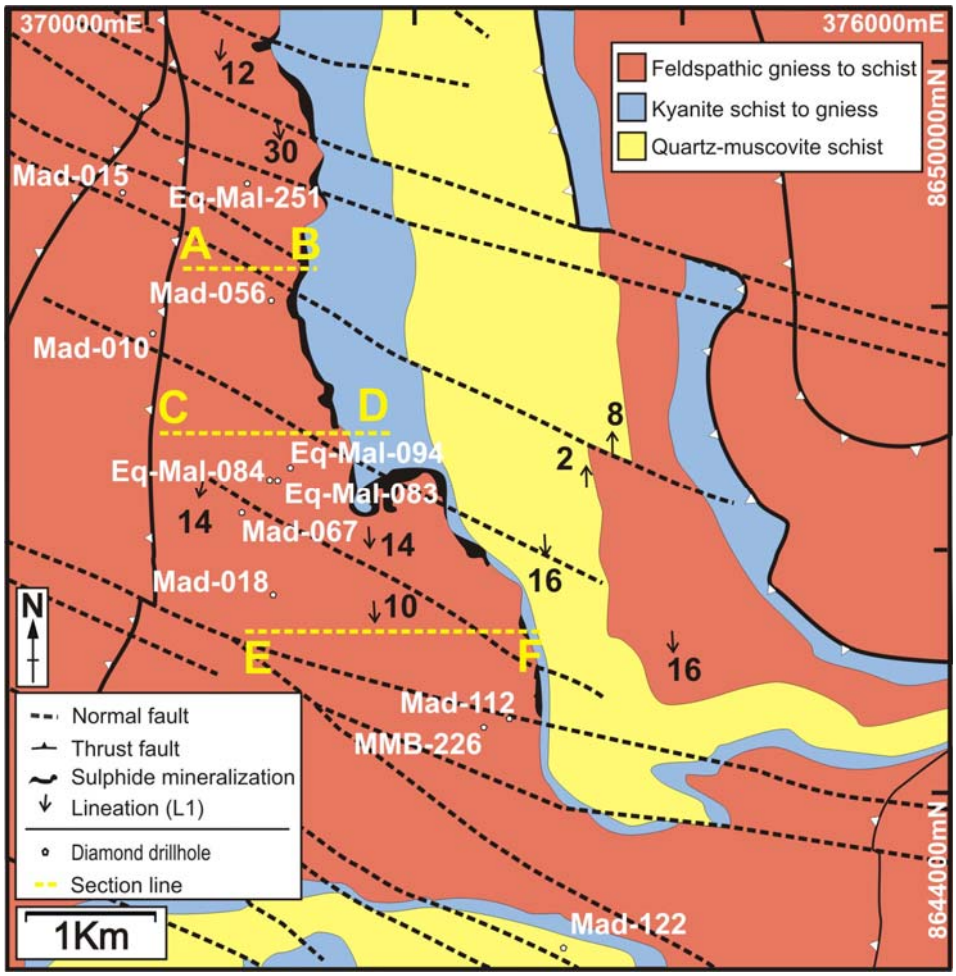

Figure 3.7 Geology of the Malundwe deposit showing locations of logged diamond drill holes

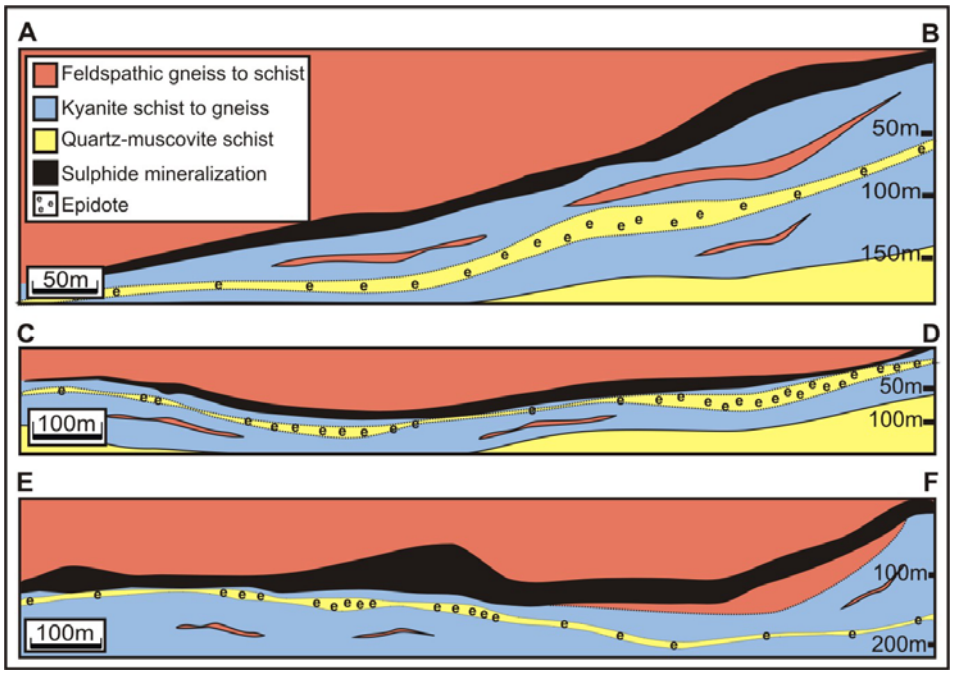

Figure 3.8 Schematic W-E cross-sections with no vertical exaggeration through the Malundwe deposit highlighting the sulphide mineralized zone.

CHAPTER 3: GEOLOGY AND MINERALIZATION OF THE LUMWANA DEPOSITS

The Chimiwungo deposit consists of lenticular horizons of sulphide mineralized kyanite schist that correlate poorly across the deposit. The Chimiwungo deposit pinches out to the west and is down thrown by late normal faults. Kinematic indicators (pressure shadows on porphyroblasts/ S-C fabrics) in the ore suggest a top to the north deformation.

Both deposits can be split into hanging wall, ore schist and footwall units which correlate broadly across the deposits and consist of a range of schist and gneiss units listed in table 3.1, as well as calc-silicates and amphibolites at the base of the Malundwe footwall (figure 3.2 & table 3.2).

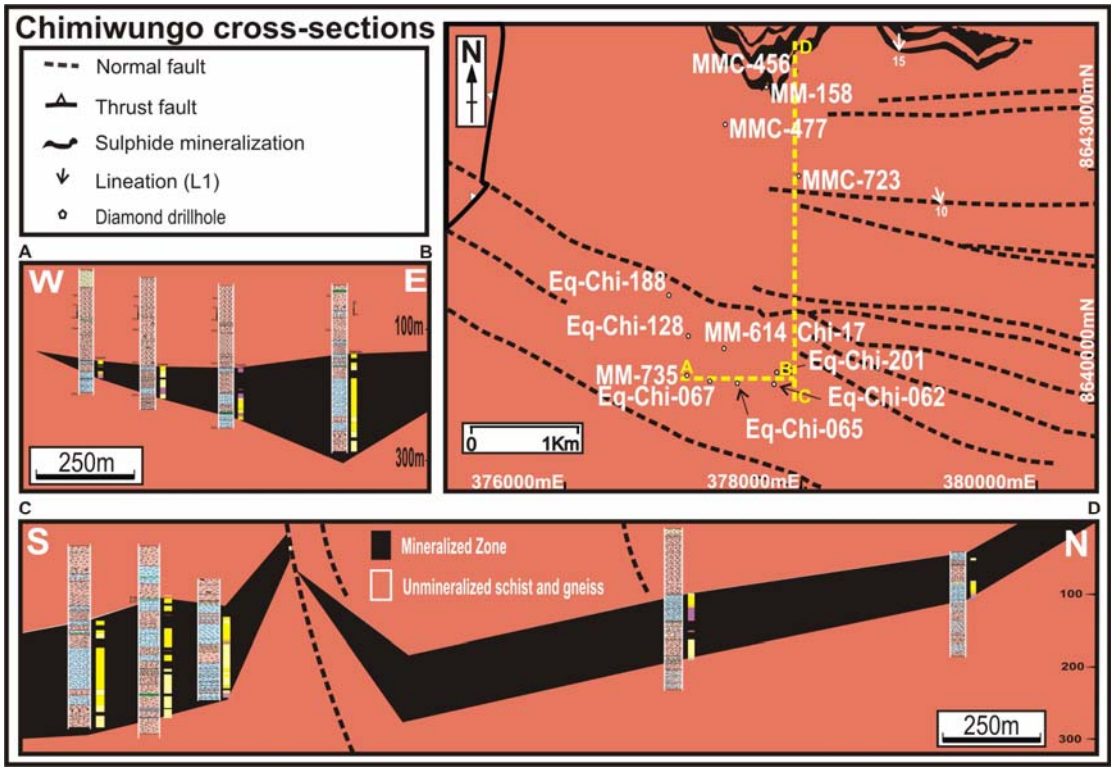

Figure 3.9 Location map of boreholes logged with north-south east-west cross-sections through Chimiwungo deposit highlighting sulphide mineralized zone.

3.3.1 Hanging wall gneiss to schist

At both Malundwe and Chimiwungo the hanging wall units predominantly consist of quartz-feldspar-phlogopite±muscovite±hematite/magnetite granite to pegmatite gneiss and quartz-phlogopite-muscovite-feldspar banded to augen gneiss depending on the crystal/grain size and fabric development respectively (table 3.2 & figures 3.10 and 3.11).

CHAPTER 3: GEOLOGY AND MINERALIZATION OF THE LUMWANA DEPOSITS

	Chimiwungo		Malundwe	
	Schist	**Gneiss**	**Schist**	**Gneiss**
Hanging Wall	**Muscovite-phlogopite-quartz-feldspar** **Muscovite-phlogopite-quartz** **Phlogopite-quartz-scapolite** ***Muscovite-phlogopite-quartz±feldspar ±kyanite*** ***Phlogopite-muscovite-quartz ±feldspar ±kyanite***	**Quartz-feldspar-phlogopite±muscovite ±hematite (granite/pegmatite)** **Quartz-phlogopite-muscovite-feldspar (banded/augen)** ***Quartz-phlogopite-muscovite-feldspar±amphibole (amphibolite)***	**Muscovite-phlogopite-quartz-feldspar** **Phlogopite-quartz** **Phlogopite-quartz-scapolite** ***Phlogopite-muscovite-quartz ±feldspar±kyanite***	**Quartz-feldspar-phlogopite ±muscovite ±hematite (granite /pegmatite)** **Quartz-phlogopite-muscovite-feldspar (banded/augen)** ***Quartz-phlogopite-muscovite-feldspar ±amphibole (amphibolite)***
Ore Package	**Muscovite-phlogopite-quartz-kyanite±sulphide** **Phlogopite-muscovite-quartz-kyanite±sulphide** **Phlogopite-muscovite-quartz-kyanite±garnet± sulphide** ***Muscovite-quartz ±sulphide*** ***Phlogopite-quartz ±sulphide*** ***Phlogopite-muscovite-quartz-kyanite±chlorite ±garnet (mottled schist)***	**Quartz-phlogopite-muscovite-feldspar (banded/augen)** **Quartz-phlogopite-muscovite-feldspar±garnet (banded/augen)** **Quartz-phlogopite-muscovite-feldspar-amphibole±garnet (amphibolite)** **Quartz-feldspar-phlogopite±muscovite (granite/pegmatite)** **Quartz-phlogopite-muscovite-kyanite±sulphide** **Quartz-muscovite-phlogopite-kyanite±sulphide** ***Quartz-feldspar-phlogopite ±muscovite±garnet (granite/pegmatite)*** ***Quartz-muscovite-phlogopite-kyanite±feldspar*** ***Quartz-phlogopite-muscovite-kyanite±feldspar***	**Muscovite-phlogopite-quartz-kyanite±sulphide** **Phlogopite-muscovite-quartz-kyanite±sulphide** ***Phlogopite-muscovite-quartz-kyanite±garnet± sulphide ore schist*** ***Muscovite-quartz±sulphide*** ***Phlogopite-quartz±sulphide***	**Quartz-phlogopite-muscovite-feldspar±sulphide (banded/augen)** **Quartz-phlogopite-muscovite-feldspar±garnet ±sulphide (banded/augen)** **Quartz-phlogopite-feldspar-amphibole ±garnet±sulphide** **Quartz-phlogopite-amphibole±garnet± sulphide** ***Quartz-feldspar-phlogopite ±muscovite ±garnet (granite /pegmatite)***
Footwall	**Phlogopite-muscovite-quartz-kyanite-chlorite ±garnet±hematite (mottled schist)** **Phlogopite-muscovite-quartz-kyanite-chlorite ±garnet±amphibole (mottled schist)** **Phlogopite-muscovite-quartz-feldspar** **Muscovite-phlogopite-quartz-feldspar** **Muscovite-quartz** ***Phlogopite-muscovite-quartz-kyanite±sulphide*** ***Muscovite-quartz-hematite*±kyanite ±talc (whiteschist)**	**Quartz-phlogopite-muscovite-feldspar±garnet (banded/augen)** **Quartz-phlogopite-muscovite-feldspar±amphibole±garnet (amphibolite)** **Quartz-feldspar-phlogopite±muscovite±garnet *(granite*/pegmatite)**	**Phlogopite-muscovite-quartz-kyanite-chlorite ±garnet±hematite (mottled/speckled schist)** **Muscovite-quartz-hematite±kyanite ±talc±garnet (footwall quartzite to whiteschist)** **Muscovite-quartz-epidote (epidote schist)** ***Phlogopite-muscovite-quartz-kyanite-chlorite-epidote***	**Quartz-phlogopite-muscovite-feldspar±garnet (banded/augen)** **Quartz-phlogopite-muscovite-feldspar ±amphibole ±garnet (amphibolite)** **Quartz-feldspar-phlogopite ±muscovite ±garnet *(granite* /pegmatite)** **Quartz-muscovite-hematite (quartzite)**

Table 3.2 Lithological variations of gneiss and schist units in the Lumwana deposits. Bold type denotes a major constituent, normal type represents commonly observed units and italics denote units that are rarely observed. Brackets indicate rock type.

CHAPTER 3: GEOLOGY AND MINERALIZATION OF THE LUMWANA DEPOSITS

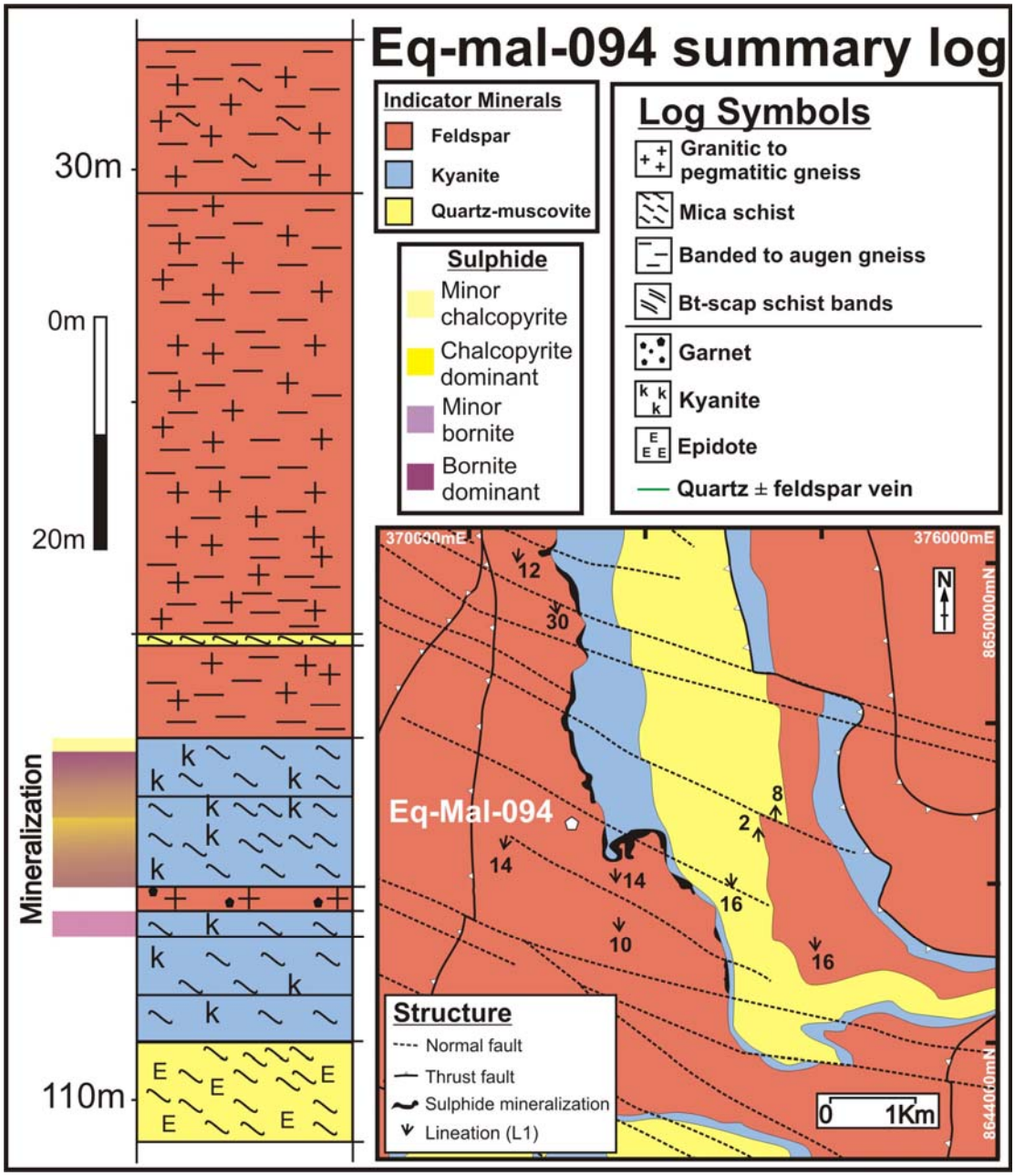

Figure 3.10 Summary log of Eq-Mal-094

The hanging wall banded to augen gneiss units includes rare amphibolite gneiss bands comprising quartz-phlogopite-muscovite-feldspar±amphibole. Occurrences of amphibolite units are uncommon but have been observed at both Malundwe (Eq-Mal-083) and Chimiwungo (Eq-Chi-067). The granitic gneiss end member rock type is a leucocratic although commonly red rock altered (late hematite staining) quartz-feldspar gneiss with minor muscovite and or biotite and varying proportions of euhedral to anhedral magnetite and

hematite crystals. No variation in feldspar composition is associated with the late hematite staining.

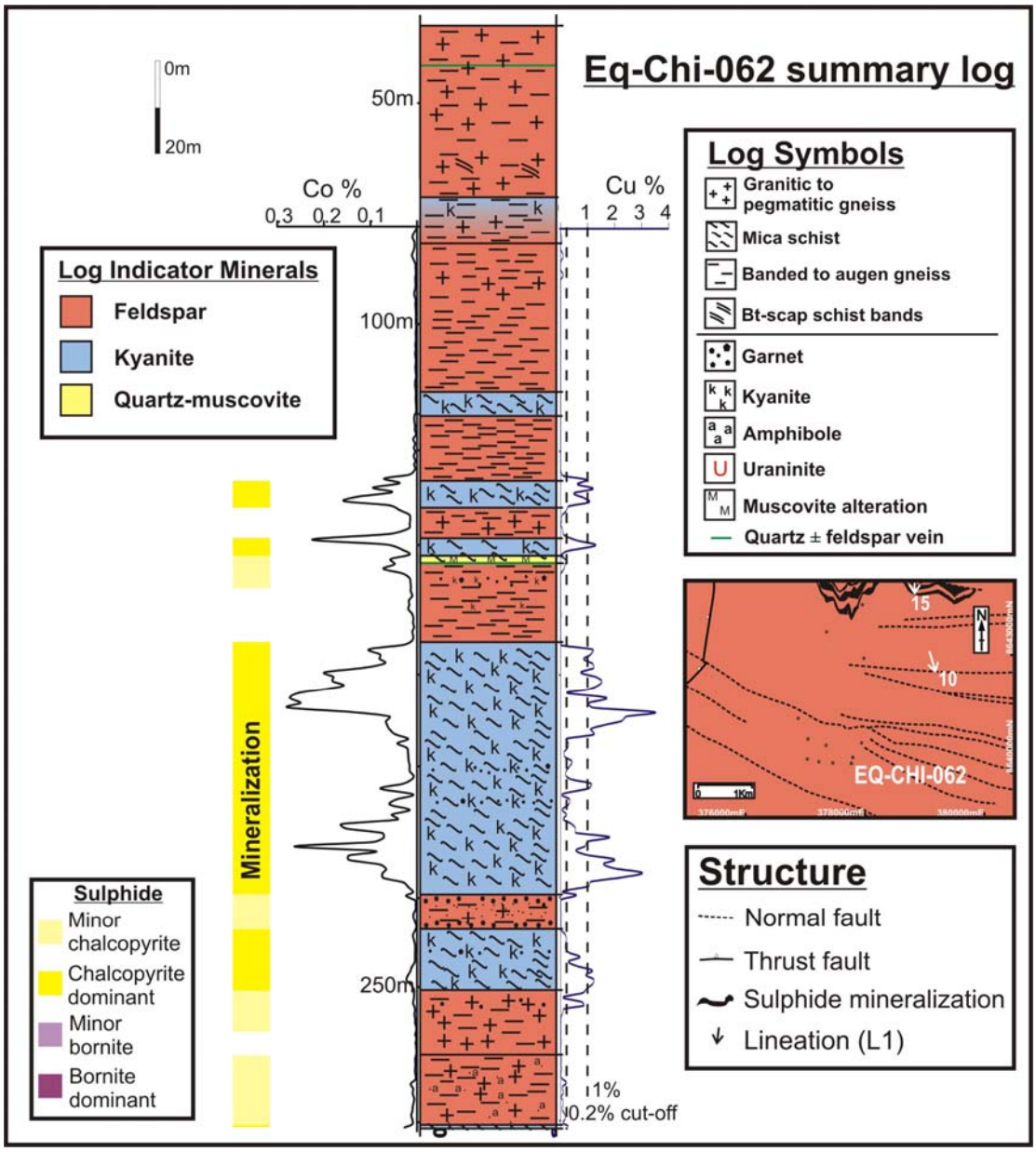

Figure 3.11 Summary log of Eq-Chi-062 with selected assay data

The granite gneiss is typically a fine to medium crystalline rock of granitic composition and has a coarsely spaced foliation defined by the alignment of the biotite (figure 3.12).

Minor patchy muscovite-chlorite alteration with massive to disseminated hematite and magnetite form altered zones can be observed locally in the granite gneiss at Chimiwungo and Malundwe.

CHAPTER 3: GEOLOGY AND MINERALIZATION OF THE LUMWANA DEPOSITS

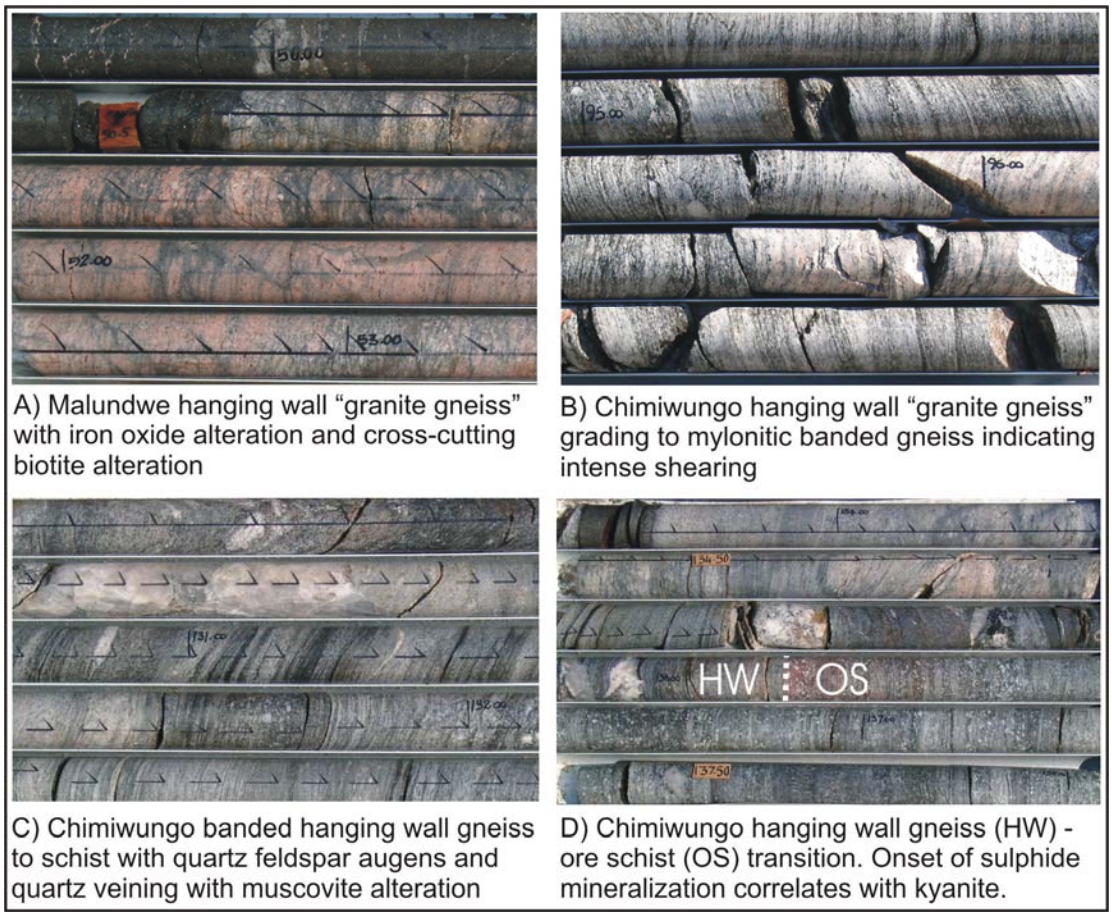

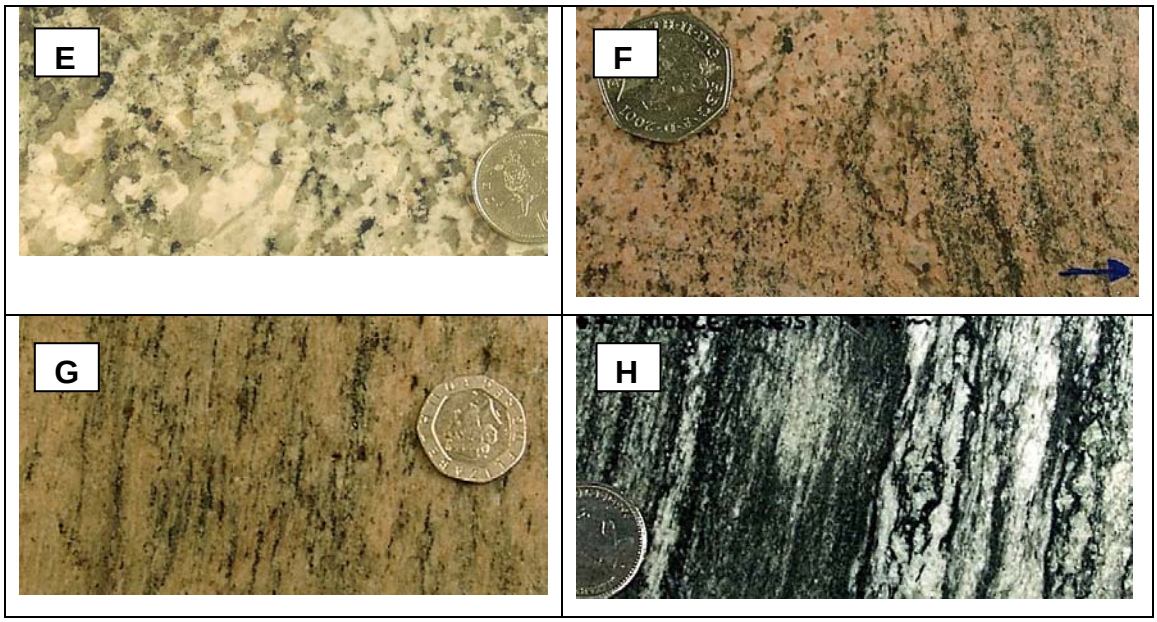

Figure 3.12 Photographs A to H. Selected hanging wall rock types A) core tray (eq-mal-o94) B) core tray (eq-chi-062) C) core tray (eq-chi-062) D) core tray (eq-chi-062) E) granite pegmatite (eq-chi-067) F) granite gneiss with weak foliation (eq-mal-094) G) granite gneiss with increased fabric development (eq-mal-251) H) banded gneiss to schist with quartz-feldspar bands and augens (eq-chi-067)

The altered units either exhibit a more developed fabric with increased foliation or have a vuggy habit with muscovite forming randomly orientated euhedral columnar crystals. The vuggy zones are commonly associated with thick quartz veining on a metre scale and more rarely with massive calcite veins. The columnar muscovite crystals with associated vugs either indicate open fracture fill or suggest that a mineral phase is missing. These zones are only observed in the hanging wall units indicating that the vugs may represent a weathering feature with calcite being removed. The fabric development in the granite gneiss indicates that it was emplaced prior to D_5 and that the undeformed alteration post-dates the deformation.

The granite gneiss exhibits gradational and sharp contacts with internal schist and very fine grained banded mylonite units that range in thickness from sub-metre to tens of metres (figure 3.12 B).

Hanging wall muscovite-phlogopite-quartz-feldspar schist units are common at both deposits associated with increased fabric development and shearing. Where shear zones are more developed a muscovite-phlogopite-quartz schist and a phlogopite-quartz schist are observed, at both Chimiwungo and Malundwe respectively. The schist units lack feldspar and locally exhibit asymmetrical extensional shear bands and mylonite fabrics. Phlogopite-muscovite-quartz±feldspar±kyanite schist are uncommon but can be observed in both deposits, usually in close proximity to the ore horizon. Bands of phlogopite-quartz-scapolite schist clearly cross-cut the granite gneiss; however, layer parallel bands are also observed locally in the banded gneiss units. Texturally late centimetre scale phlogopite shear bands can also be observed locally cross-cutting the granite gneiss fabric. The scapolite alteration may represent a late Na-Cl alteration event.

In contrast to the young porphyritic granites in the core of the dome, the granite gneiss units at Malundwe and Chimiwungo form porphyroblastic augens where there is an increase in mica content and fabric development. The other dominant unit is quartz-biotite-feldspar gneiss ± garnet, amphibole

and muscovite, which exhibits a variable fabric development with augens or bands of quartz and feldspar. The dominant texture in this unit is the banding on either a millimetre or centimetre scale (figure 3.12 B &C).

Quartz veins ± pyrite, hematite and magnetite crosscut and in more schistose units, quartz veins are boudinaged within the fabric. The banded gneiss include coarsely crystalline quartz-feldspar pegmatite units that have associated muscovite, chlorite and hematite/magnetite alteration at the contacts and are interpreted as being the result of interstitial melting (figure 3.12 D).

The main variation between the banded gneiss and the granite gneiss is an increase in the percentage of biotite/phlogopite and an associated fabric development. The hanging wall gneiss units grade into the ore schist in both deposits, although locally the contact can be bounded by quartz veins and quartz-feldspar pegmatite units as well tectonic contacts with the hanging wall gneiss and schist units.

3.3.2 Ore schist units

The Chimiwungo and Malundwe ore packages vary in that the Malundwe ore sheet lacks continuous intervening gneiss units, although minor internal gneiss units are present and the cobaltiferous sulphides (carrollite-bravoite-seigenite) are only present at Chimiwungo. The principal sulphide in the Malundwe ore schist is bornite with varying quantities of chalcopyrite (figure 3.10).

The Chimiwungo ore package can be sub-divided into 3 mineralized ore schist units, each with a characteristic sulphide assemblage, although variations can be observed locally. The upper ore schist consists of pyrite (FeS_2) – chalcopyrite ($CuFeS_2$), whereas the main ore schist is dominated by chalcopyrite – carrollite ($CuCo_2S_4$) and chalcopyrite-bornite (Cu_5FeS_4) towards the base of the unit. The lower ore schist is dominated by a basal bornite zone (±chalcopyrite). The cobalt mineralization is associated with the

copper mineralization at Chimiwungo but is highly variable between ore packages and the peaks in grade are often offset (figure 3.11).

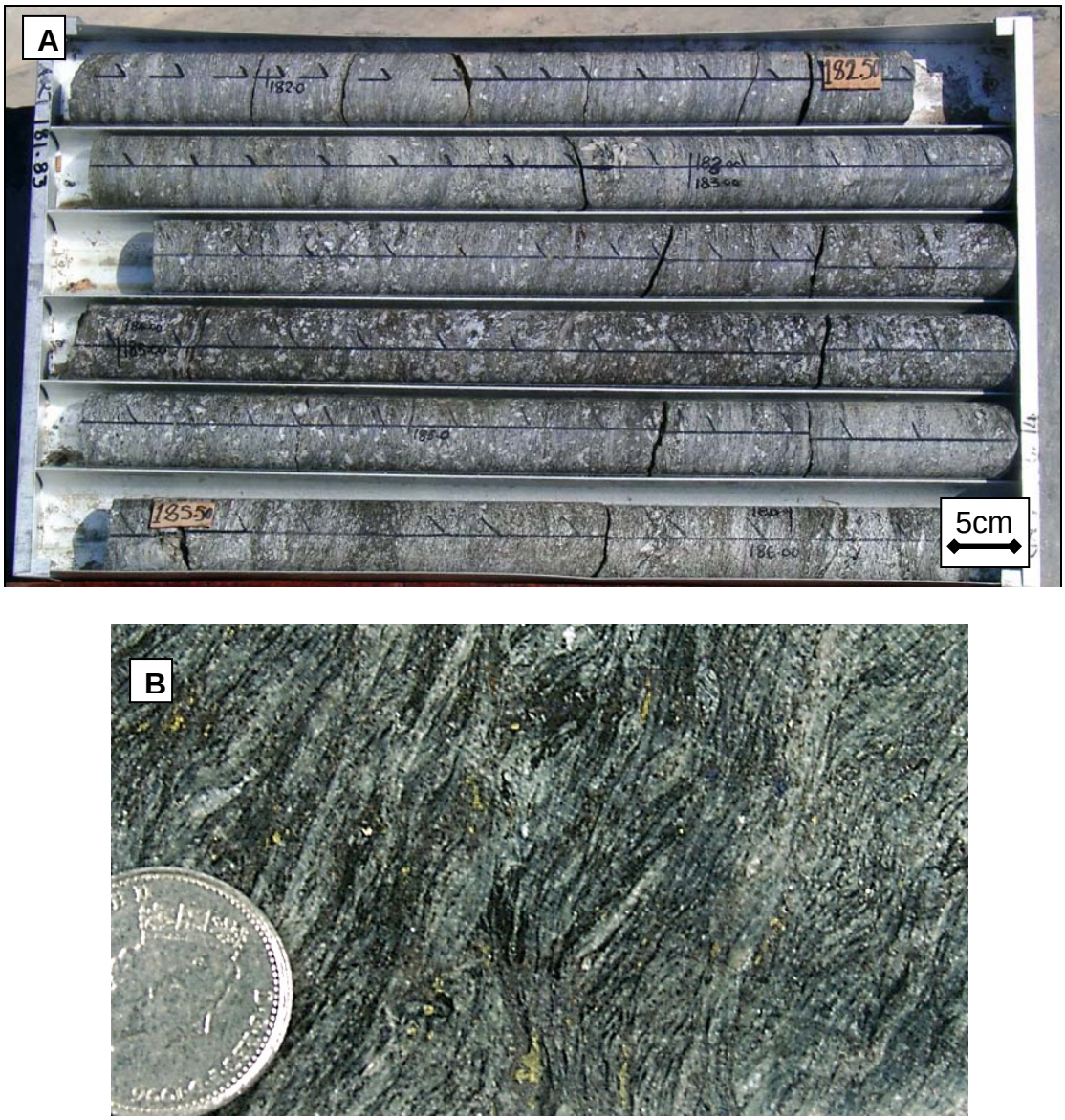

Figure 3.13 Photograph (COS - Eq-Chi-062) A) core tray of Chimiwungo ore schist with darker phlogopite rich zones and lighter zones dominated by muscovite B) Chimiwungo ore schist with asymmetrical extensional shearing developing sigmoid fabric

Although the Chimiwungo and Malundwe ore package differ significantly in terms of sulphide zonation and internal gneiss component, the mineralized ore schist units are very similar in both texture and mineralogy. Both are predominantly muscovite-phlogopite-quartz-kyanite±sulphide schist to phlogopite-muscovite-quartz-kyanite±sulphide schist and commonly exhibit a sigmoid fabric with asymmetrical extensional shear bands and C/S fabrics indicating a top to the north deformation direction (figure 3.13). The mode of

phlogopite and muscovite vary on a metre to centimetre scale and kyanite forms both augen porphyroblasts and porphyroblasts that crosscut the fabric (figure 3.13).

The Chimiwungo upper, main and lower ore schist units vary in thickness of approximately 15m to approximately 80m to approximately 15m respectively. The contacts between ore and host rock packages are often of a transitional nature although well defined contacts are observed locally and are interpreted as of tectonic origin with units separated by thrusts and shear zones. The compositional transition from leucocratic (feldspar-quartz-muscovite-biotite) gneiss to a more biotite rich gneiss with removal of feldspar and increased fabric development is the result of pre/syn metamorphic alteration.

Photographs A to D (figure 3.14) illustrate the transition from hanging wall gneiss to schist. There is a gradual transition from leucocratic (feldspar-quartz-muscovite-phlogopite) banded gneiss to a more phlogopite rich gneiss with removal of feldspar and increased fabric development. The transition is dominated by alteration with the addition of phlogopite. Late high angle fractures with associated quartz, chlorite and calcite alteration cross-cut the fabric and are therefore post-tectonic.

Towards the contact with the ore schist the gneiss comprises banded melanocratic gneiss with leucocratic quartz-feldspar bands in a quartz-biotite-muscovite matrix (figure 3.14 C). This transition is the result of increased alteration and the affect of strain partitioning. A quartz-phlogopite-feldspar-hematite banded augen gneiss on the gneiss-schist boundary can be observed in photograph D, where quartz and feldspar form fine (1-2mm) augens in the fabric, which are concentrated into gneissic bands. The red staining is late remobilized hematite. The transition from hanging wall schist to ore schist is illustrated by photographs E to G. Photograph E shows biotite-quartz-feldspar-kyanite hanging wall schist with kyanite overprinting the feldspar. This is petrographically similar to the ore schist except without sulphide mineralization.

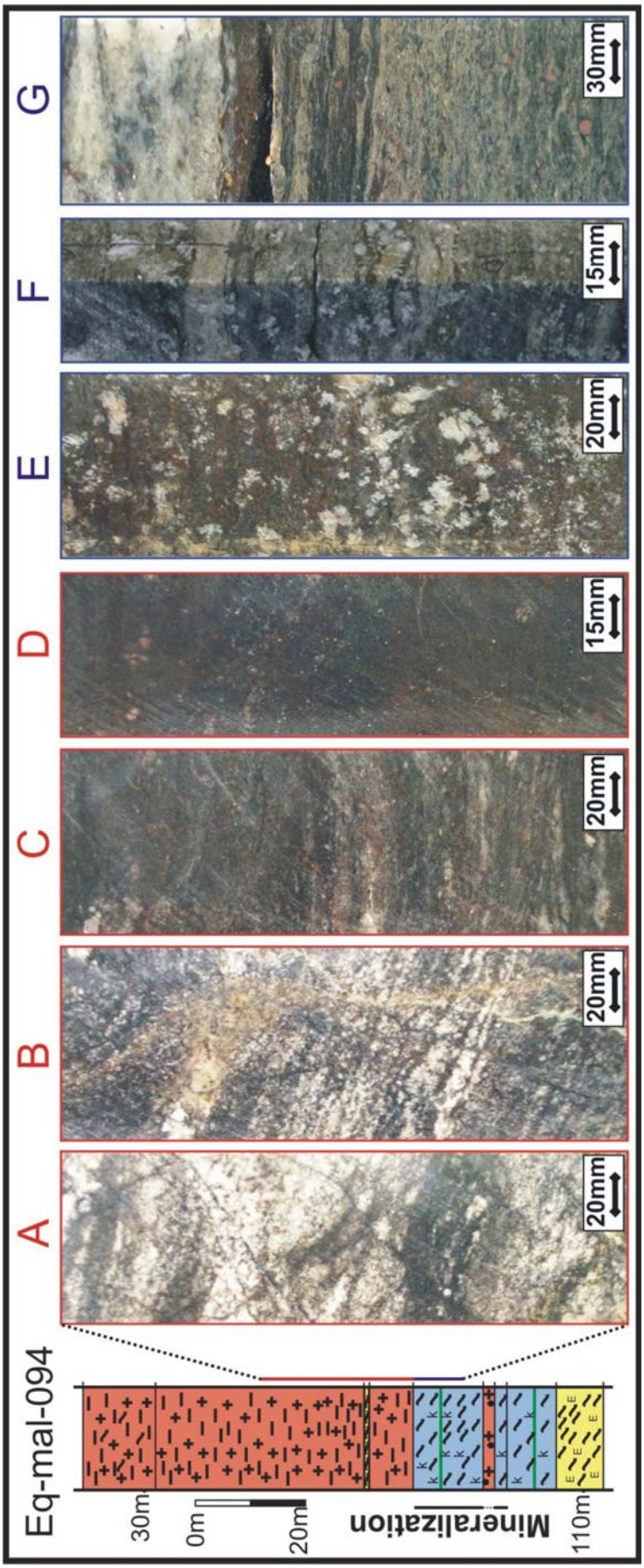

Figure 3.14 Hanging wall gneiss to ore schist transition (Eq-Mal-094)

Photograph F is a classic example of the muscovite-phlogopite-quartz-kyanite-bornite-chalcopyrite±chlorite ore schist. Kyanite overprints the ore that is stretched out within the muscovite-phlogopite-quartz dominated fabric. Photograph G) shows a quartz vein mineralized with bornite-chalcopyrite and with associated chlorite alteration that is destructive to the red garnet and overprinting the ore schist (figure 3.14).

The ore schist varies in copper content from 0 to approximately 5%, the high grade copper hosted in kyanite schist. In these high grade zones, the kyanite porphyroblasts form as augens within the fabric, and quartz-muscovite bands are present. Sulphides form as inclusions within the kyanite, in the pressure shadows of kyanite, along the cleavage of mica minerals and within the quartz bands (figure 3.15).

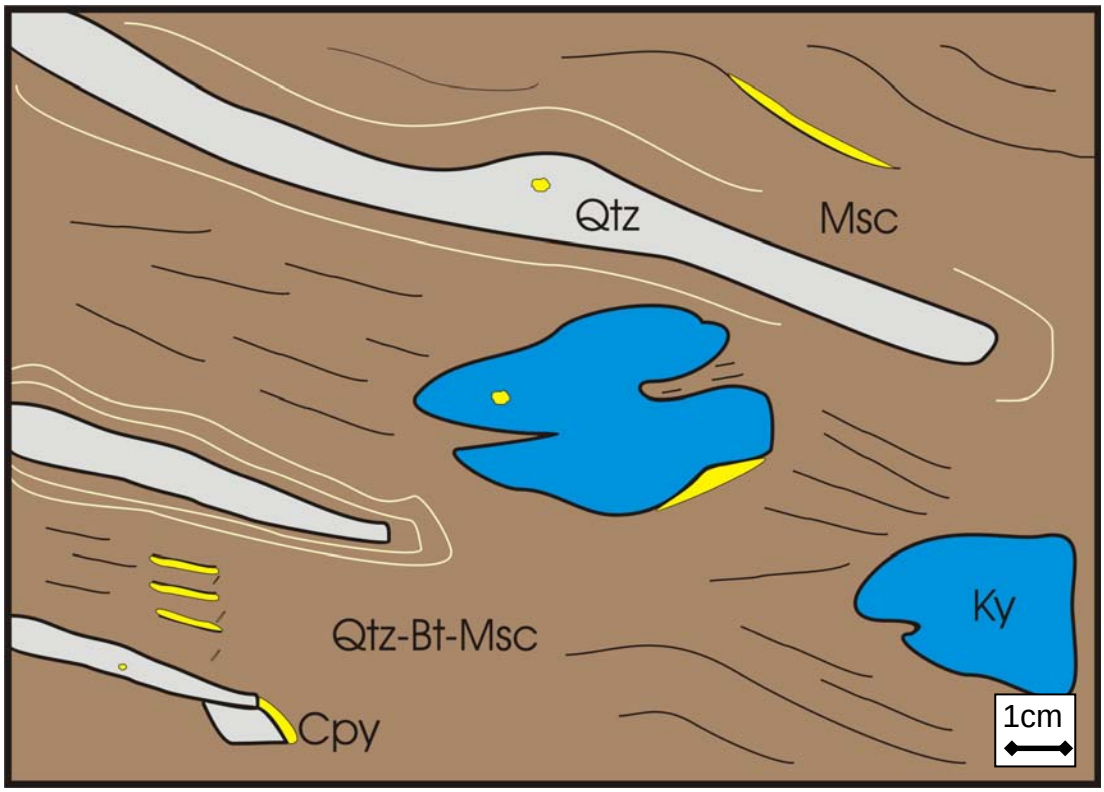

Figure 3.15 Field sketch of ore schist (Eq-Chi-062) Kyanite (Ky) and Chalcopyrite (Cpy) in a quartz-biotite-muscovite (Qtz-Bt-Msc) sigmoid fabric

Quartz veins which cross-cut both the mineralization and the barren intervening gneiss units are commonly host to pyrite, chalcopyrite and/or bornite. Garnet bearing schist units at Chimiwungo and Malundwe are commonly unmineralized although locally phlogopite-muscovite-quartz-

kyanite±garnet±sulphide schist is observed. As a result, when plotted down section, the percentage of copper and cobalt exhibit an antithetic relationship when compared with the occurrence of garnet (figure 3.11). Occurrences of phlogopite-muscovite-quartz±sulphide to muscovite-phlogopite-quartz± sulphide are observed locally at both Chimiwungo and Malundwe.

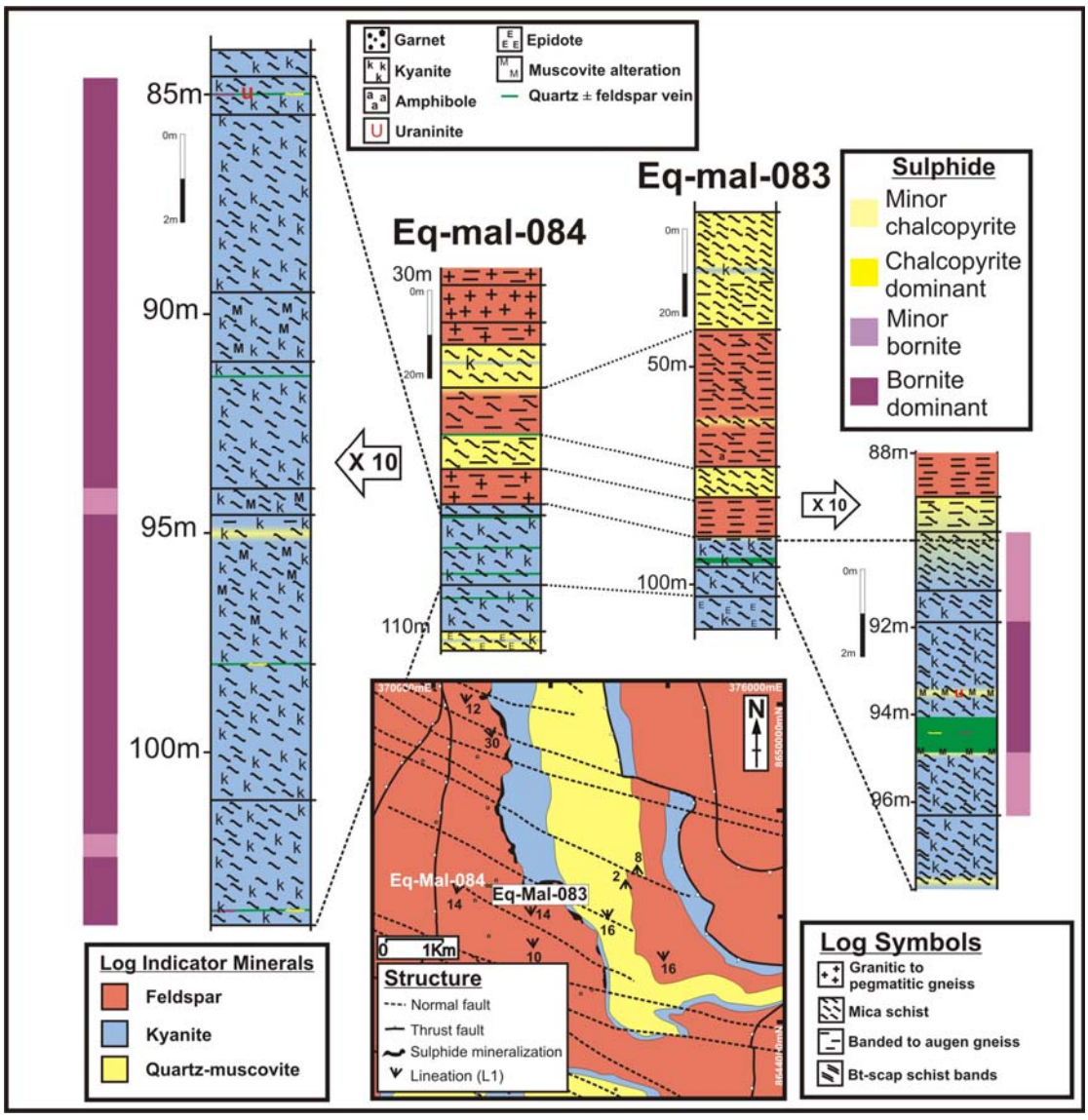

Figure 3.16 Summary and detailed ore zone logs of Eq-Mal-083 and Eq-Mal-084 examining styles of uranium mineralization

In addition to copper and cobalt the Lumwana area is enriched in uranium. Two styles of mineralization have been observed in the Malundwe and Chimiwungo deposits consisting of vein hosted and disseminated uraninite (figure 3.16). Uranium mineralization crosscuts the stratigraphy with occurrences in both footwall and hanging wall units but is commonly located

towards the top of the ore schist. The uranium mineralization commonly occurs with vuggy muscovite alteration and minor molybdenite. Sulphides in proximity to uraninite are often weathered and often occur with traces of malachite. The quartz veining and uraninite weakly effervesced on contact with 10% hydrochloric acid indicating a possible role of carbonates during the uraninite mineralizing process.

3.3.3 Internal gneiss units

Internal gneiss units observed within the Chimiwungo ore package are predominantly quartz-phlogopite-muscovite-feldspar banded to augen gneiss. These intervening gneiss units locally exhibit cataclasite textures suggesting that deformation also occurred above the brittle-ductile transition (figure 3.17).

Figure 3.17 Photograph (Eq-Chi-062) Internal banded gneiss with amphibolite and internal quartz-feldspar pegmatite gneiss units

The banded to augen gneiss can also include garnet and/or amphibole and/or sulphide mineralization. This can also be observed to a lesser degree in the Malundwe deposit (figure 3.18).

CHAPTER 3: GEOLOGY AND MINERALIZATION OF THE LUMWANA DEPOSITS

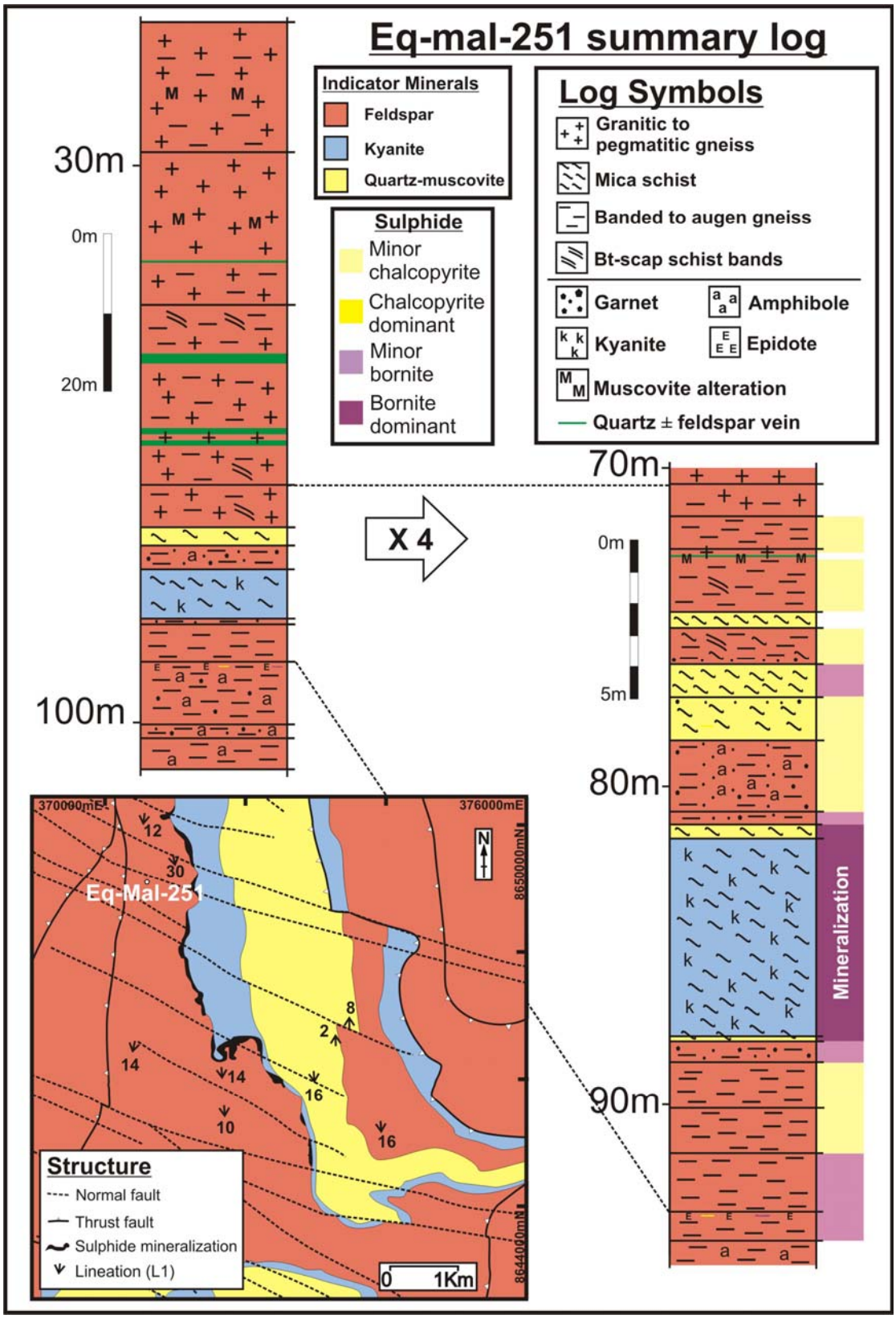

Figure 3.18 Summary and detailed ore package log for Eq-Mal-251 at the northern extent of the Malundwe deposit

Occurrences of quartz-feldspar-phlogopite±muscovite±garnet granite to pegmatite gneiss are wide spread in the Chimiwungo ore package and have also been observed locally at Malundwe. Internal gneiss units that have only been observed at Chimiwungo include quartz-phlogopite-muscovite-kyanite±sulphide gneiss and less commonly quartz-muscovite-phlogopite-kyanite±sulphide gneiss and are the gneissic end members of the ore schist. Kyanite typically exhibits an antithetic relationship with feldspar; however, occurrences of quartz-muscovite-phlogopite-kyanite±feldspar gneiss and quartz-phlogopite-muscovite-kyanite±feldspar gneiss have been observed in the Chimiwungo ore package. Rare occurrences of unmineralized phlogopite-muscovite-quartz-kyanite±chlorite±garnet schist similar to the footwall mottled schist are observed locally at Chimiwungo.

The internal gneiss units vary from the ore schist with a lower mode of sulphides, weaker fabric development and the presence of feldspar. The similarities of the internal gneiss units to the hanging wall and footwall banded gneiss to amphibolite units, coupled with the removal of feldspar in the ore schist indicate that the ore schist is a product of alteration within the banded gneiss units, which has then been the focus of ductile deformation.

3.3.4 Footwall gneiss and schist units

Quartz-phlogopite-muscovite-feldspar±garnet banded to augen gneiss, quartz-phlogopite-muscovite-feldspar±amphibole±garnet amphibolite gneiss and quartz-feldspar-phlogopite±muscovite±garnet granite pegmatites are also major constituents of the Malundwe and Chimiwungo footwall (figure 3.19).

Another major constituent to the Malundwe and Chimiwungo footwall is a phlogopite-muscovite-quartz-kyanite-chlorite±garnet±hematite unit that has a mottled texture due to the coarse poikiloblastic kyanite grains and is known as the mottled schist. The kyanite poikiloblasts vary in size from 1 to 5 cm and contain inclusions of both biotite and quartz and overprint the sigmoidal schist fabric. Typically the chlorite is located both within the fabric as well as partially replacing the kyanite porphyroblasts (figure 3.20).

CHAPTER 3: GEOLOGY AND MINERALIZATION OF THE LUMWANA DEPOSITS

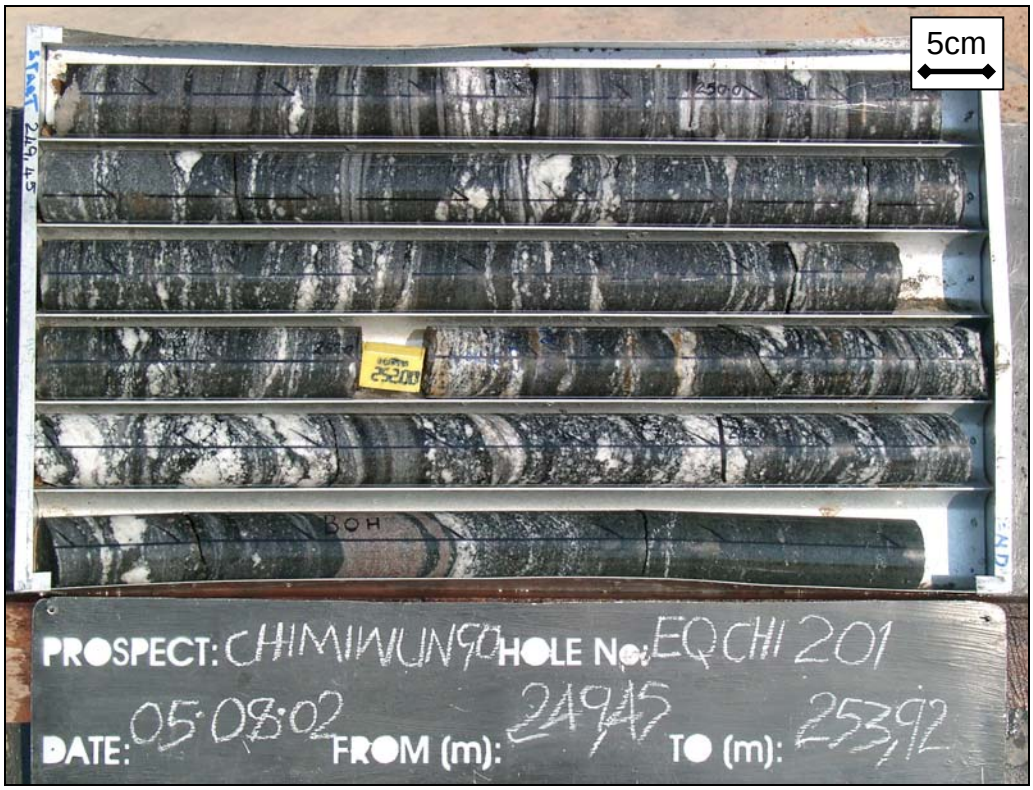

Figure 3.19 Photograph (Eq-Chi-201) Banded gneiss and amphibolite units from the Chimiwungo footwall

Figure 3.20 Photograph (Eq-Mal-094) Banded gneiss and mottled schist units from the Malundwe footwall

CHAPTER 3: GEOLOGY AND MINERALIZATION OF THE LUMWANA DEPOSITS

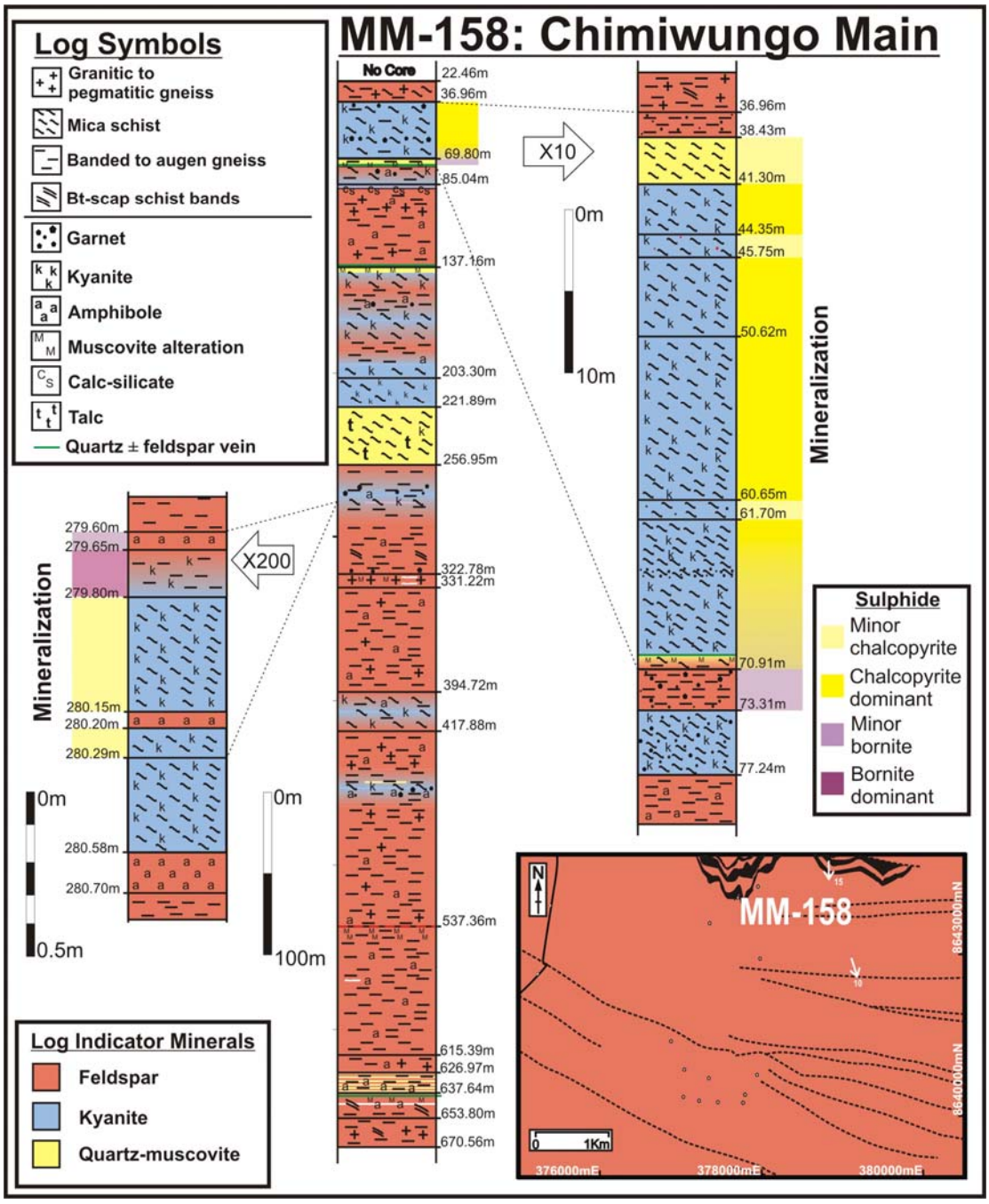

Figure 3.21 Summary and detailed ore schist log of MMB-158 in the north-west of the main Chimiwungo orebody

A variety of footwall kyanite schist with fine kyanite porphyroblasts is known as the speckled schist and has only been observed in the Malundwe footwall. The mottled schist also has variations between the Malundwe and the Chimiwungo footwall as a phlogopite-muscovite-quartz-kyanite-chlorite ±garnet±amphibole mottled schist unit was only observed at Chimiwungo (figure 3.21) whereas a phlogopite-muscovite-quartz-kyanite-chlorite-epidote

mottled schist was only observed locally in the footwall to the Malundwe deposit (e.g. Eq-Mal-084, figure 3.16).

The footwall to the Chimiwungo deposit also includes phlogopite-muscovite-quartz-feldspar schist, muscovite-phlogopite-quartz-feldspar schist, muscovite-quartz schist and a rare phlogopite-muscovite-quartz-kyanite±sulphide schist that are all spatially associated to alteration and shearing (figure 3.21).

A traceable muscovite-quartz-epidote±feldspar schist is present in the Malundwe footwall. The epidote schist is granular, friable and comprises muscovite, quartz and epidote that commonly underlies the mottled schist. The epidote schist is only located under the Malundwe deposit and can vary in position among the footwall units indicating that it is an alteration feature (figure 3.10 & 3.22).

Figure 3.22 Photograph (Eq-Mal-094) Epidote schist from the Malundwe footwall

The absence of epidote schist units at Chimiwungo suggests that they did not have any significant role for the ore fluids responsible for the Cu-Co mineralization. The epidote schist is porous and characteristically includes many cavities and locally forms an aquifer.

The kyanite schist units of the Malundwe footwall exhibit a gradational contact with quartz-muscovite-hematite quartzite and muscovite-quartz-hematite ±kyanite±talc±garnet footwall quartzite to whiteschist. The footwall quartzite varies in thickness and at its maximum thickness it exceeds 150 metres (figure 3.23).

CHAPTER 3: GEOLOGY AND MINERALIZATION OF THE LUMWANA DEPOSITS

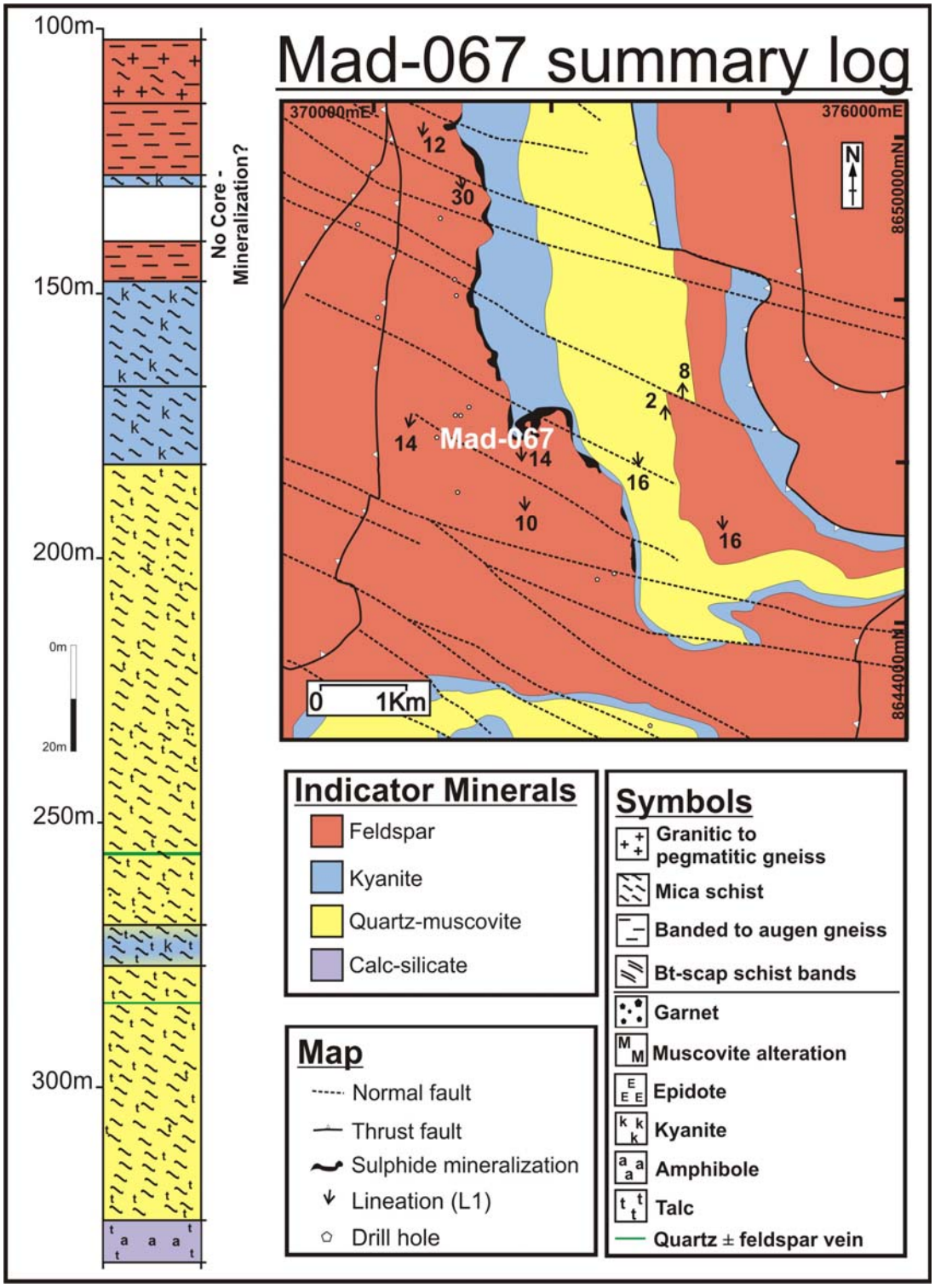

Figure 3.23 Summary and detailed ore schist log of MAD-067 of the Malundwe deposit

The footwall quartzites at Lumwana form the majority of the outcrop in the Mwombezhi dome and have intense north-south stretching lineation and coarse anastomosing fabric on a metre scale (figure 3.24).

CHAPTER 3: GEOLOGY AND MINERALIZATION OF THE LUMWANA DEPOSITS

Figure 3.24 Photograph facing north (Mosa Hill) hematite rich quartzite with a coarse anastomosing fabric (372423E 8646258N)

3.3.5 Lateral continuity

The Chimiwungo deposit can only be broadly sub-divided into hanging wall gneiss, ore schist and footwall gneiss units with the ore schist being further sub-divisable into 3 ore zones separated by internal gneiss units that can be traced across the deposit. In order to examine the lateral variations within these sub-divisions a wedged diamond drill hole Chi-17 was logged and units have been correlated between the wedges (figure 3.25).

Chi-17 is located in the north-east of the Chimiwungo South orebody and comprises hanging wall gneiss, ore schist with intervening internal gneiss and minor footwall gneiss. A second drill-hole (wedge 2) was drilled from the same collar but at a depth of 80 meters. The lateral distances separating the wedges were calculated from the survey data of approximately 0, 5 and 10 metres for depths of 80, 150 and 250 metres respectively. The rock types of Chi-17 have been subdivided by their characteristics and marker horizons into 21 units that correlate between the diamond drill hole wedges.

CHAPTER 3: GEOLOGY AND MINERALIZATION OF THE LUMWANA DEPOSITS

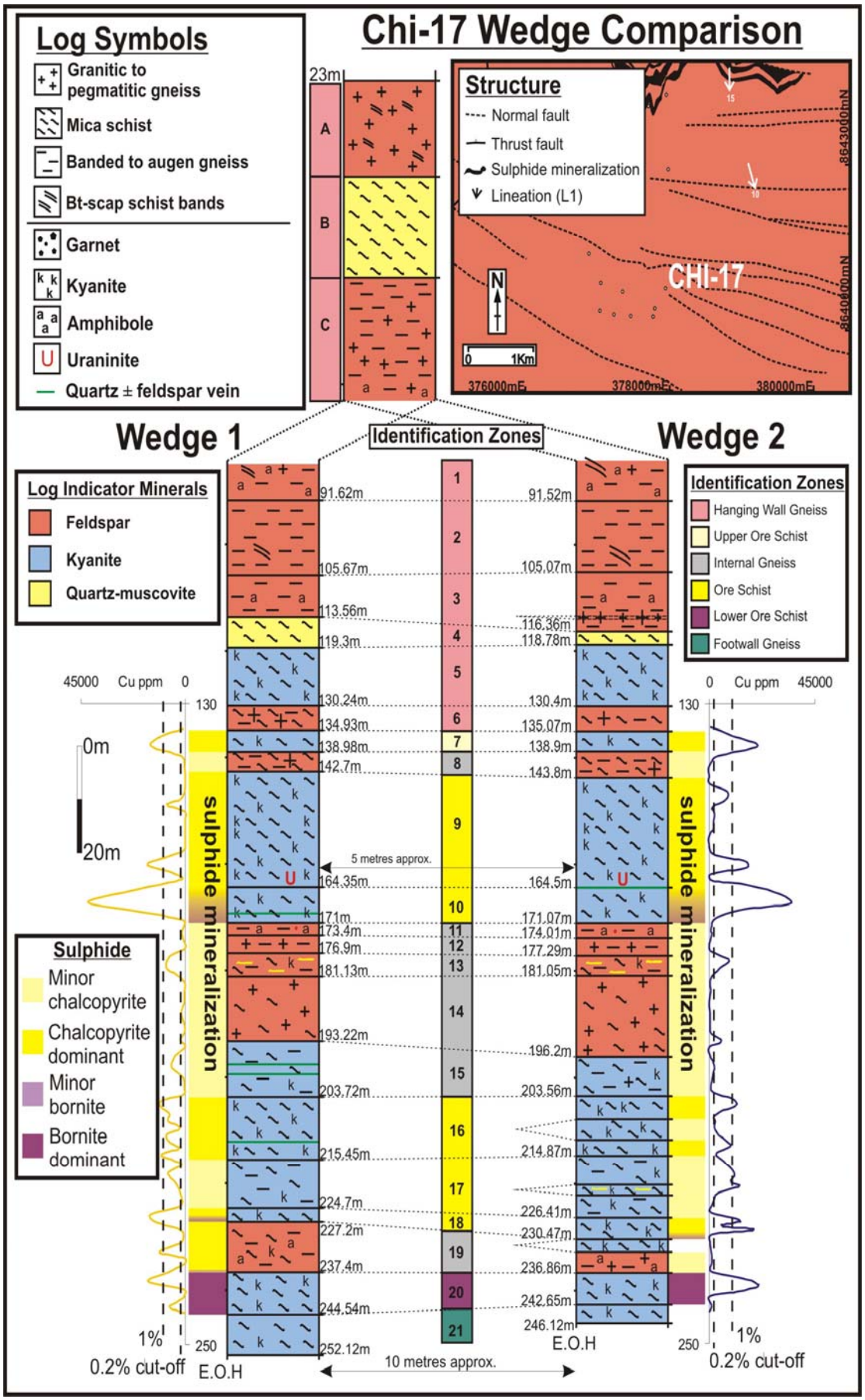

Figure 3.25 Summary log of wedged DDH (Chi-17) with copper assay data

The rock types above the wedge are divisible into 3 units A to C. Units A to C and units 1 to 6 collectively form the hanging wall gneiss. Unit A consists of quartz-feldspar-phlogopite-hematite granite with a weak fabric defined by the alignment of phlogopite. Two alteration styles are present in this unit, a dark grey overprint of fine muscovite and quartz and a pink hematite staining. The fabric is cross-cut by phlogopite-quartz-scapolite schist units (figure 3.25).

Unit B is a phlogopite-muscovite-quartz±feldspar±chlorite schist to mylonite that varies in the mode of phlogopite and muscovite and exhibits a strong planar fabric. Rootless folds of quartz bands and boudinaged quartz-feldspar±gypsum veins are present, cross-cut by late approximately 1mm thick carbonate veinlets.

Unit C consists of banded quartz-muscovite-phlogopite-feldspar gneiss with coarsely spaced fabric very coarse crystalline quartz-feldspar±chlorite pegmatite.

Unit 1 comprises a quartz-feldspar-phlogopite pegmatite with medium to coarse grained banded gneiss that locally grades into amphibolite, and is cross-cut by phlogopite-quartz-scapolite schist. The pegmatite has dark quartz rich bands with fine grained epidote and apatite that correlate in both wedges. The base of the unit is marked by a pegmatite unit with red hematite staining.

Unit 2 includes a medium grained anhedral quartz-phlogopite-feldspar banded gneiss with weak to absent schistosity but a strong gneissose (quartz-feldspar) banding that is cross-cut by bands less than 10mm thick of fine grained epidote and apatite. Minor phlogopite-quartz scapolite schist bands cross-cut the banded gneiss fabric and correlate between wedge 1 and wedge 2. Trace quantities of chalcopyrite and pyrite are associated with coarse magnetite/hematite. It is unlikely that the quartz-feldspar bands correlate between wedges as they are commonly boudinaged and are lenticular in outcrop.

Unit 3 consists predominantly of banded gneiss with amphibolite bands that range from centimetres up to 1.5 metres in thickness. Both wedges contain quartz-feldspar bands and augens that are more frequent and thicker in wedge 1. The larger amphibolite bands appear to correlate between wedges. In wedge 2 there is a 0.5m quartz-feldspar pegmatite unit that possibly correlates with a 20cm unit in wedge 1. Trace sulphide mineralization is associated with chlorite and minor apatite and is more prevalent in wedge 2 than wedge 1. Wedge 1 has minor malachite staining in the amphibolite bands.

Unit 4 is highly foliated to mylonitic and consists of phlogopite-muscovite-quartz schist ± trace sulphide that has transitional contacts with minor quartz-feldspar granitic gneiss units that are interpreted to represent the original protolith. The schist varies from phlogopite rich to muscovite-quartz rich and has a strong planar fabric although local asymmetrical shear bands produce a sigmoid anastomosing fabric. The granite gneiss lacks kinematic indicators and is locally overprinted with a light grey alteration. The intense fabric and presence of sulphides in the schist is similar to the ore schist; however, this unit lacks kyanite is fine grained and probably felsic although mylonitic grain size reduction makes mineralogical observations difficult. Trace pyrite/chalcopyrite can be observed associated with the phlogopite rich schist bands. In wedge 2 only, a quartz vein is observed parallel to the fabric with an apparent thickness of 4cm.

Unit 5 is an unmineralized muscovite-phlogopite-quartz±kyanite±chlorite ±hematite schist similar to unit 4 but marked by the occurrence of fine grained euhedral kyanite crystals that are associated with minor chlorite. Kyanite zones correlate between wedges including the mode and form with fine grained 1-4mm diameter crystals at the top of the unit and coarser grained 2-8mm crystals at the base. In addition, this unit is cross-cut by minor phlogopite-scapolite schist bands that correlate between wedges and late carbonate veinlets. Fine apatite grains form bands in wedge 1 and are disseminated in wedge 2.

Unit 6 exhibits a mylonitic to highly foliated fabric and comprises a phlogopite-muscovite-quartz schist similar to unit 4 with numerous quartz-feldspar pegmatites that are overprinted with phlogopite-muscovite alteration. The alteration coupled with variations in size and mode of the pegmatites make them impossible to correlate between wedges. Feldspar rhombs that exceed 4cm in diameter can be observed in wedge 2 in a band of coarse phlogopite. Late light brown rutile cross-cuts the feldspar rhombs and the phlogopite fabric. Both wedges are cross-cut by numerous late high angle carbonate veinlets.

Unit 7 is the upper most ore schist unit and is marked by the observation of kyanite and sulphide mineralization. Both wedges consist of phlogopite-muscovite-quartz-kyanite-chalcopyrite-pyrrhotite schist that varies texturally from a strongly planar fabric to segregated muscovite-phlogopite and quartz dominant anastomosing bands. The sulphides exhibit two textural styles of mineralization that relate to the deformation of the host rock. Where the ore schist exhibits a planar fabric the sulphides are evenly disseminated and where the fabric has undergone extensional shearing indicated by the anastomosing fabric the sulphide is remobilised along the shear planes. Both wedges exhibit a variable number of silicified zones that range in thickness and are characterised by a decrease in muscovite phlogopite and sulphide, and an increase in the mode of quartz.

Unit 8 consists predominantly of banded gneiss with a varying amount of granite pegmatite and is weakly mineralized with trace quantities of chalcopyrite and pyrrhotite. The banded texture is overprinted with muscovite-phlogopite alteration which is more extensive in wedge 1 than wedge 2. Wedge 2, however, has an increased mode of quartz-feldspar bands and pegmatic granite gneiss units. Wedge 2 includes a quartz-phlogopite-feldspar gneiss with a coarsely spaced fabric defined by quartz-feldspar bands in which phlogopite forms unorientated clusters producing a spotted texture. Both units have a gradational contact with the underlying kyanite schist. The transition initially indicates an increase in shearing with the development of a

strong planar fabric with minor quartz-feldspar bands and augens. The introduction of asymmetrical extensional muscovite shear lenses ± kyanite produces a “zebra texture” that develops into the ore schist of Unit 9.

Units 9 and 10 constitute the main ore schist. Unit 9 is the top unit of the main ore schist and consists mainly of phlogopite-quartz-kyanite schist ± muscovite ± chlorite ± chalcopyrite that varies in copper grade from well mineralized to barren (figure 3.25).

Areas of significant muscovite alteration are observed in unit 9 that are commonly but not exclusively associated with quartz alteration, which develops a segregated texture of phlogopite-quartz-kyanite-chalcopyrite schist cross-cut by sub-parallel anastomosing bands of muscovite-quartz schist ± minor phlogopite. The sub-parallel bands anastomosing bands have a sigmoid form and are interpreted to represent D_2 extensional shear bands. Wedge 2 is significantly more feldspathic than wedge 1 and locally kyanite is observed overgrowing the feldspar-quartz bands augens and boudins. The feldspathic zones in wedge 2 correlate with silicified quartz-phlogopite-muscovite-kyanite-chalcopyrite schist in wedge 1 indicating that silicified areas are altered quartz-feldspar banded gneiss. Traces of pyrite and pyrrhotite are only observed in association with feldspar suggesting that they are paragenetically early and pre-date the alteration of the feldspathic zones.

At the base of unit 9 is a zone of uranium mineralization host by a phlogopite-quartz-kyanite±uraninite schist that correlates from wedge 1 to wedge 2 and exhibits no visible sulphide mineralization. In wedge 1 the uraninite forms 1-4cm grains deformed within the anastomosing fabric whereas in wedge 1 the mineralization is more equigranular and disseminated within the rock. A large quartz-feldspar vein is observed locally in wedge 2 at the contact with unit 10. The lateral distance at this point between the wedges is approximately 5 metres.

Unit 10 forms the base of the main ore schist and has an increased mode of muscovite and the occurrence of bornite. The unit consists of a muscovite-phlogopite-quartz-kyanite-chalcopyrite-bornite schist with an anastomosing fabric defined by quartz-muscovite and muscovite-phlogopite rich bands. This unit has the highest percentage of copper with up to 4 percent copper. The sulphide phases vary down unit from high grade bornite ± chalcopyrite to chalcopyrite-pyrite at the contact with the unit 11 that is marked locally in wedge 1 by a 17cm thick quartz vein. A high angle dolomite-bornite-chalcopyrite vein is observed locally in wedge 1 but not in wedge 2. Unlike the sulphide phases, the silicate assemblages show little variation down unit.

Units 11 to 15 comprise gneiss, amphibolite, schist and pegmatite units that constitute internal waste within the Chimiwungo orebody. Unit 11 consists of a banded quartz-phlogopite-feldspar gneiss with amphibolite bands that include garnet porphyroblast grains. The amphibolite bands are a major constituent of the unit and trace quantities of chalcopyrite are observed locally. A high angle unmineralized dolomite vein with a muscovite alteration halo is observed only in wedge 1.

Unit 12 consists predominantly of quartz-feldspar pegmatite gneiss with minor quartz-phlogopite-feldspar banded gneiss. The pegmatite gneiss units have minor muscovite alteration and a small proportion garnet porphyroblast grains that appear to correlate between the wedges. However, the variations in texture of the banded gneiss units that separate the pegmatite gneiss units suggest that they are lenticular units that do not correlate. Trace chalcopyrite mineralization is observed in wedge 2 only.

The rock types of unit 13 comprise quartz-muscovite-phlogopite-feldspar±garnet banded gneiss that grades into muscovite-phlogopite-quartz±kyanite±chalcopyrite±pyrite±pyrrhotite schist. An anastomosing fabric is present throughout the unit; however; it is more developed around augens of unorientated muscovite-phlogopite-quartz and poikilolitic kyanite. Unit 13 is thinner in wedge 1 than wedge 2 and contains a higher proportion of sulphide

mineralized schist. Wedge 1 also exhibits an increase in the mode of pyrrhotite towards the centre of the unit.

Unit 14 is predominantly a quartz-feldspar±garnet pegmatite approximately 15m thick with muscovite alteration and phlogopite that forms either discrete crystals or unorientated areas. The pegmatite is host to muscovite-phlogopite-quartz±feldspar±chalcopyrite±pyrite schist domains that have well defined upper contacts and gradational lower contacts. The larger schist units may correlate between wedges. Muscovite-quartz alteration is observed at the base of the unit although it is more prevalent in wedge 2.

Unit 15 consists of a quartz-muscovite-phlogopite±feldspar±kyanite ±chalcopyrite±pyrrhotite gneiss to schist and represents a muscovite altered banded gneiss. No internal units correlate between wedges and where kyanite and feldspar are present together the kyanite overprints the feldspar. Wedge 2 is consistently more feldspathic than in wedge 1, which is cross-cut by quartz veins and a dolomite-bornite vein. Exclusive to wedge 2 is 0.5m medium crystalline quartz-muscovite-feldspar-garnet±kyanite±phlogopite ±chalcopyrite leucratic granite gneiss with the traces of chalcopyrite that are spatially associated with phlogopite. In wedge 1 this corresponds to a weakly mineralized quartz-phlogopite-kyanite±chalcopyrite±pyrrhotite gneiss with coarse kyanite.

Units 16 to 18 constitute the lower portion of the Chimiwungo main orebody. A repetition of the sulphide zonation observed in the main ore schist suggests that this orebody either formed in the same mineralizing conditions as the overlying Chimiwungo main orebody or that it was repeated by thrusting.

Unit 16 consists of a phlogopite-muscovite-quartz-kyanite-chalcopyrite schist. The mode of muscovite increases down section as the mode of phlogopite decreases. Unit 16 includes a basal phlogopite rich zone that varies in chalcopyrite content from well mineralized in wedge 2 to only trace amounts in wedge 1. Wedge 2 has a higher proportion of kyanite than wedge 1 and a

central silicified quartz-phlogopite-muscovite-kyanite gneiss unit that is not observed in wedge 1. At the base of the silicified zone are coarse aggregates of kyanite crystals up to 5cm in diameter. Wedge 1 includes a 25cm quartz vein not present in wedge 2.

Unit 17 consists of a phlogopite-quartz±feldspar±kyanite schist to gneiss that represents ore schist overprinting quartz-phlogopite-feldspar banded gneiss with quartz-feldspar pegmatite bands. The degree of overprinting between wedges varies and in wedge 1 kyanite is observed overprinting the quartz-feldspar bands. Wedge 2 includes two boudinaged quartz veins that have muscovite growth in the pressure shadows and a 3cm chalcopyrite-pyrite-pyrrhotite vein deformed within the fabric. After unit 17 no correlations are possible between internal units.

Unit 18 consists of phlogopite-muscovite-quartz-kyanite-chalcopyrite±bornite schist. At the top of the unit the sulphide is chalcopyrite but down section the mode of chalcopyrite decreases and the mode of bornite increases to a basal bornite rich zone.

Unit 19 is the lowest intervening internal gneiss unit and consists of banded gneiss with amphibolite and quartz-feldspar pegmatite bands. Wedge 1 includes ore schist that has overprinted banded gneiss and is moderately mineralized with chalcopyrite and bornite. The sulphides in wedge 1 are spatially distributed in the phlogopite-muscovite rich units. Wedge 2 is poorly mineralized to barren and includes a unit of phlogopite-quartz-kyanite±chlorite schist that is similar to the footwall gneiss. The amphibolite bands are thicker in wedge 2 than in wedge 1 and the quartz-feldspar pegmatite bands only exhibit muscovite alteration in wedge 1.

Unit 20 constitutes the lower ore schist and comprises a phlogopite-quartz-kyanite-bornite±chlorite schist with the bornite concentrated in 10 to 20cm bands. The mode of chlorite increases down unit and muscovite-chlorite are

overprinting the phlogopite schist. Unit 20 has a gradational contact with the underlying footwall gneiss.

Unit 21 is the last unit of Chi-17 and forms the upper most unit if the footwall gneiss and consists of phlogopite-quartz-kyanite-chlorite-muscovite schist. This unit is highly foliated and coarser grained than the ore schist with large kyanite porphyroblasts up to 2cm in diameter being replaced by chlorite and muscovite. The anastomosing fabric is defined by large phlogopite crystals. This unit has been termed the mottled schist due to its large kyanite porphyroblasts.

Observations of Chi-17 have highlighted that if lateral distances are less than 5 metres, variations in texture, composition, alteration and mineralization are minor in the ore and host rocks to the Chimiwungo deposit. Where units are separated by a distance greater than 5 metres it becomes increasingly difficult to correlate with confidence and if lateral distances are greater than 10 metres it is only possible to correlate the orebodies. This demonstrates the heterogeneity of these deposits and supports the lack of petrological correlation between logged diamond drill holes.

The lateral variations in Chi-17 indicate that the Lumwana deposits are lenticular orebodies hosted within a basement gneiss complex. This interpretation is supported by the logging of diamond drill core and by macro-scale field observations.

CHAPTER 4: HOST ROCK AND ORE MINERALOGY

4.1 Introduction

This chapter presents the hand-specimen and micro-scale observations of ore and host rock assemblages in order to identify the relative timing of key events in the geological history of the Lumwana ore deposits. Understanding the textural relationship of ore minerals to micro-structure, metamorphism and hydrothermal alteration of the host rocks is an important part of understanding the origin and history of an ore deposit (Craig & Vaughan 1981).

4.2 Host rock mineralogy

The Lumwana deposits are highly heterogeneous reflecting a complex alteration, deformation and metamorphic history with samples often showing significant variations at the polished thin section scale.

4.2.1 Hanging wall units

Hanging wall gneiss and schist units at Chimiwungo and Malundwe are broadly similar, consisting petrographically of granite gneiss that through increased alteration and foliation alters to augen gneiss, schist and mylonite. The granite gneiss units observed at both Chimiwungo and Malundwe consists of predominantly quartz (~45%), feldspar (~35%), and biotite (~5%) with a dark grey selective alteration commonly observed in hand specimen. The fabric coarsely spaced and defined by quartz bands that vary in thickness across the section from 3-4mm to 100-200µm, separated by interlocking subhedral feldspar (microcline and plagioclase) (figure 4.1.1).

Quartz displays two textures, anhedral coarse areas interlocking with feldspar and subhedral recrystallised bands that exhibit a weakly sigmoidal texture. These are interpreted as primary & secondary textures respectively. The feldspar is dominated by microcline ($KAlSi_3O_8$) and exhibits cross hatched twinning and moderate sericitization. The dark grey alteration observed in hand specimens of granite gneiss and augen gneiss units correspond to the sericitization of feldspar crystals (figure 4.1.2).

Epidote ($Ca_2(Al, Fe)_3(SiO4)_3(OH)$) is not ubiquitous in the hanging wall gneiss units but where present can constitute up to 1% of the sample and form small

(<100µm) anhedral grains that crosscut quartz, biotite and feldspar. Muscovite (~4%) grains form anhedral laths that crosscut both feldspar and quartz (figures 4.1.1 & 4.1.2). The mode of magnetite/hematite varies from less than 1% to 5% of the unit and locally forms large euhedral grains.

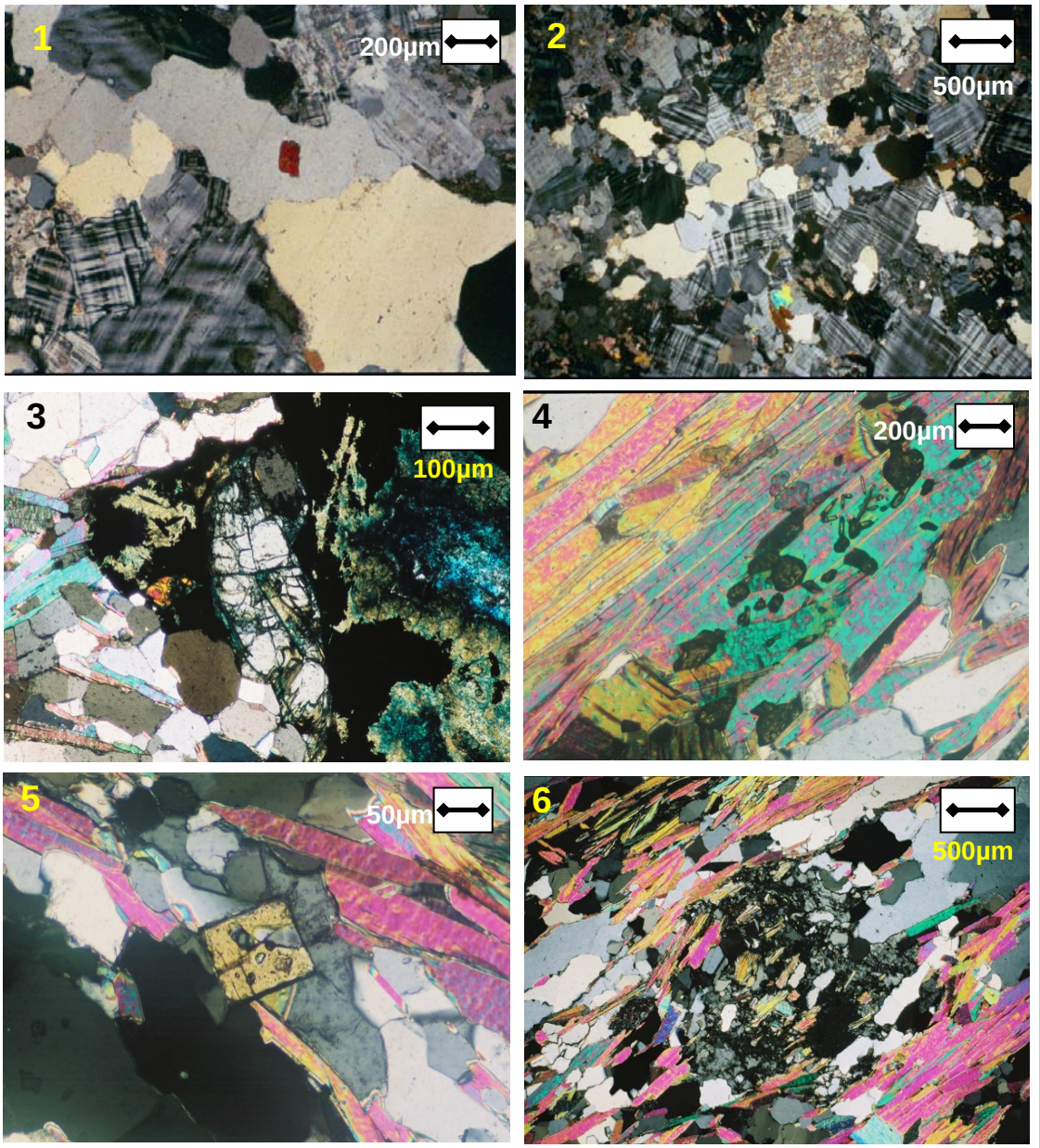

Figure 4.1 Hanging wall transmitted light photomicrographs (cross-polars): 1) (Eq-Mal-094-1b) Red allanite (epidote group) grain overprinting quartz band in granite gneiss with a microcline and quartz dominated matrix **2) (Eq-Mal-094-1b)** Primary anhedral interlocking quartz and feldspar crystals. Feldspar exhibits minor sericitization **3) (Mad-82-2)** Secondary copper minerals rimmed with hematite in hanging wall supergene enrichment zone. Large titanite lozenge and minor epidote are not replaced **4) (Eq-Chi-062-1)** Rutile in biotite band **5) (Eq-Chi-062-1)** Late titanite diamond crosscutting subhedral quartz band **6) (Eq-Chi-062-1)** Kyanite augen altering to quartz and sericite in sheared schist to gneiss. Shearing is indicated by C/S fabric development

The gneiss to schist units of the Chimiwungo and Malundwe hanging wall consist predominantly of quartz (~40%), muscovite (~40%) and biotite (~15%)

and locally exhibit C/S shear fabrics (figure 4.1.6). The quartz forms large elongate aggregates up to 4mm long and 2mm wide in the low strain zones separated by muscovite and lesser amounts of biotite. Kyanite is not observed in the hanging wall at Malundwe, although can be observed locally in the hanging wall schist to gneiss units at Chimiwungo, as augen porphyroblasts retrogressed to sericite in low strain zones.

The more schistose units of the Chimiwungo and Malundwe hanging wall commonly contain rutile (TiO_2) (~1%) grains, which form concentrated bands within the high strain muscovite dominated areas. Locally the fabric is overprinted by bands of rutile indicating that it is texturally late (figure 4.1.4). Titanite ($CaTiSiO_5$) (<1%) ranges in morphology from diamond to lozenge shaped grains that are up to 80μm in diameter (figure 4.1.5).

A hanging wall biotite-quartz schist unit which was observed only at Malundwe consists of biotite (~60%), quartz (~30) and muscovite (~10%). The fabric is dominated by biotite that picks out the schistosity and forms a later crenulation cleavage. The rock has undergone moderate segregation into quartz-mica layers. The quartz form polycrystalline augen structures up to 4mm in length, often rimmed by biotite and minor muscovite. Muscovite grains form more commonly in the pressure shadows of the quartz augens (200μm laths) but is coarser when found associated with biotite (600μm laths). Biotite forms coarse patches that exhibit a decussate texture and are truncated by the quartz augens.

Copper sulphides are not observed in the hanging wall schist and gneiss units at Chimiwungo and Malundwe. However, locally at Malundwe, secondary copper carbonate hydroxides malachite ($Cu_2CO_3(OH)_2$) and azurite ($Cu_3(CO_3)_2(OH)_2$ are observed close to the contact with the ore schist and are interpreted as controlled by the position of the water table. The rock also contains minor K – feldspar (1 large 200μm grain), rare small 10μm epidote grains and lozenge shaped titanite grains (figure 4.1.3).

4.2.2 Ore schist units

The rocks that host the ore typically exhibit a strong S_1 fabric that deforms the sulphides.

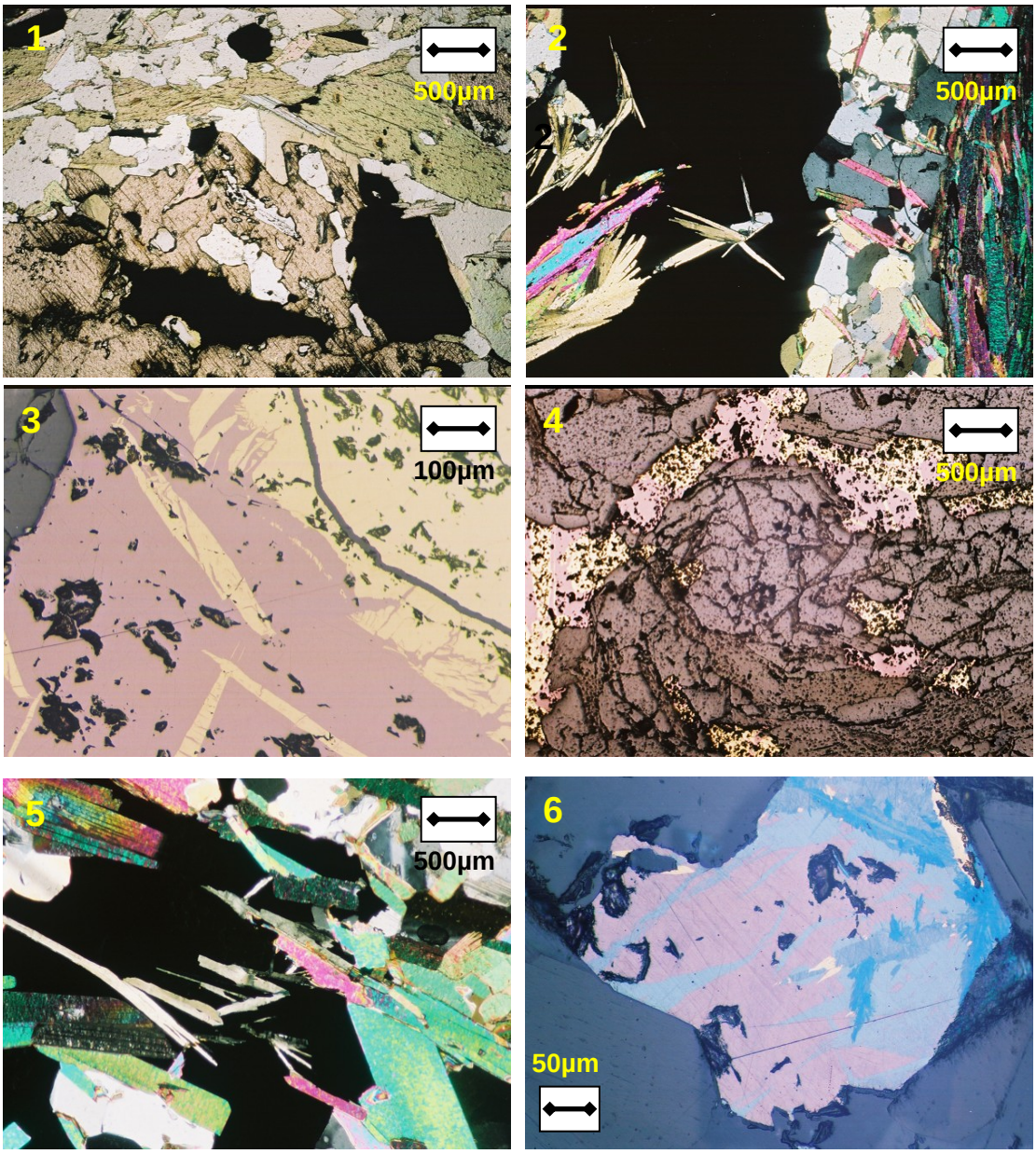

Figure 4.2 Ore schist transmitted and reflected light photomicrographs: 1) (Eq-Chi-062-27) Carrollite mineralization within kyanite and carrollite-chalcopyrite mineralization in kyanite pressure shadow (trans, ppl) **2) (Eq-Chi-062-28)** Thick muscovite band, low strain quartz, ore – crosscut by muscovite band and chlorite (trans, cpl) **3) (Eq-Chi-062-28)** Exsolution textures in bornite and chalcopyrite (ref) **4) (Eq-Chi-062-28)** Bornite-chalcopyrite deformed around quartz augen (ref) **5) (Mad-82-4)** Bornite and chalcopyrite mineralization crosscut by laths of late muscovite and chlorite (trans, cpl) **6) (Mad-82-4)** Bornite, digenite, chalcopyrite and covellite in a quartz matrix (transmitted light=trans, reflected=ref, cross-polars=cpl, plane polars=ppl)

The host rocks to the mineralization at Chimiwungo and Malundwe typically consist of bands of muscovite-biotite-phlogopite of various proportions ±

kyanite, separated by apparent low strain quartz bands. However, it is possible that evidence for strain-induced crystal-plastic was removed by annealing and hence creating apparent low strain.

Figure 4.2 shows 6 photomicrographs of rocks from the Malundwe and Chimiwungo ore schists that exhibit the different textures and mineralogies. Kyanite is observed as augens within the fabric and as porphyroblasts crosscutting the fabric. Retrograde metamorphism is observed with kyanite and garnet breaking down to chlorite and quartz. Sulphides are located as inclusions within kyanite and as pressure shadows around kyanite indicating that they predate peak metamorphism and that they have been remobilized (figure 4.2.1).

An increase in the mode of kyanite corresponds with a reduction in feldspar. The proportion of chlorite varies and is commonly associated with the ore minerals indicating that the ore was in place prior to the retrogressive event. Two distinct types of chlorite are observed, one with decussate texture and berlin blue interference colours the other with fine lath shaped grains that are commonly located where sulphides are crosscut by muscovite. This has been interpreted as the alteration of muscovite to chlorite in the presence of sulphide (figure 4.2.4).

The ore schist is commonly host to pervasive quartz-mica bands that are orientated sub-parallel to S_1 fabric and are associated with asymmetrical extensional shear bands. The quartz-mica bands are interpreted as the result of late retrogressive event S_2. The quartz-mica bands consist of quartz (~40%), biotite (~25%) and muscovite (~35%) with thin quartz bands 200 to 400µm wide separated by muscovite and biotite that dominate the fabric. Small equidimensional and acicular grains of rutile (~1%) are observed that are approximately parallel to the primary foliation direction, but locally crosscut and overprint both the primary and secondary cleavages.

Garnet can be observed locally within ore schist units at both Chimiwungo and Malundwe, often associated with more feldspathic horizons. Although garnet has an antithetic association with the copper grade, locally copper sulphide minerals and garnet are observed together. Plagioclase and quartz are observed locally as inclusions within garnet indicating that they are either pre- or syngenetic with the garnet phases. Two phases of phlogopite are observed with garnet, coarse grains in pressure shadows and late fine grained cross-cutting laths and with no preferred orientation.

A Leo 1450 VP (Carl Ziess SMT limited) Scanning Electron Microscope with a PGT light element EDS detector from the National Oceanographic Centre, Southampton were used to identify unknown minerals in thin section.

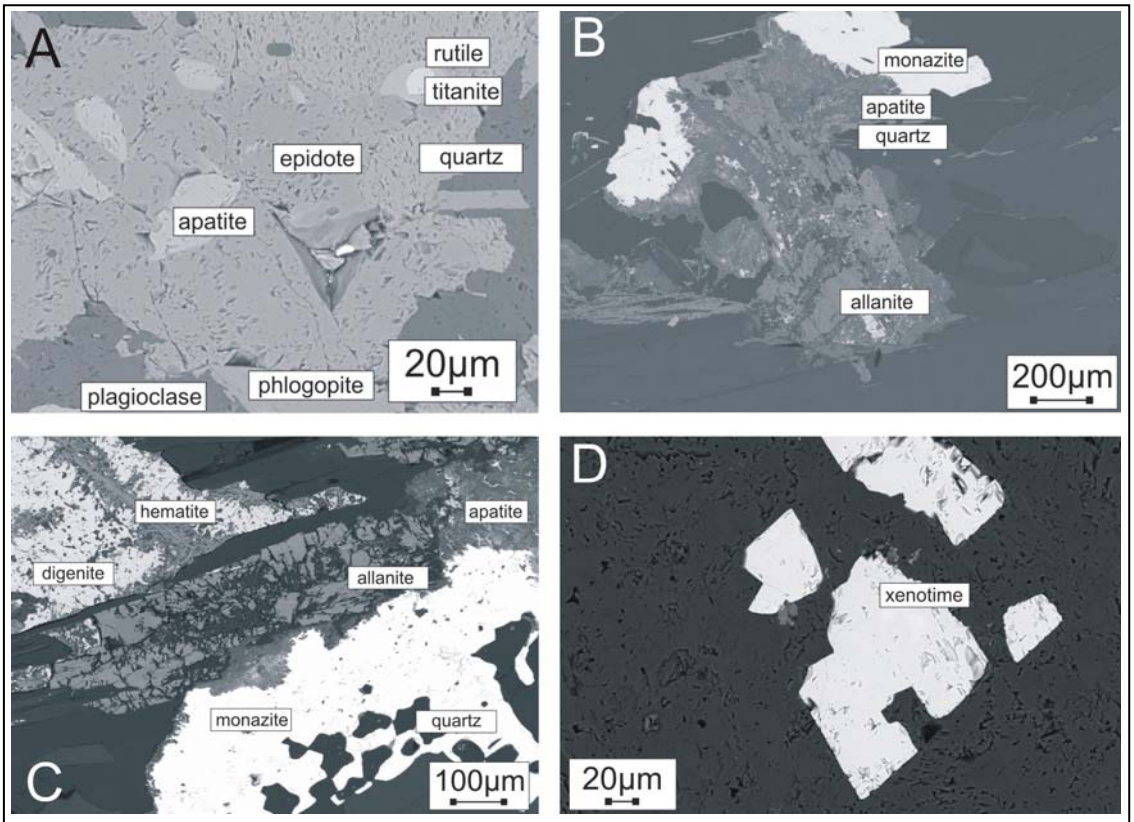

Figure 4.3 Backscattered electron images (SEM) (EHT= 20kV, WD=19mm, nominal probe current 750pA) A) epidote – apatite alteration in the Malundwe footwall**.** Apatite forms inclusions within epidote and locally rutile is observed replacing titanite. B) Monazite, apatite and allanite alteration in the Chimiwungo hanging wall. C) Monazite, apatite and allanite alteration in the Chimiwungo upper ore schist. D) Xenotime in the Malundwe footwall.

Texturally late rare earth element minerals monazite, apatite, allanite and xenotime are observed locally within the hanging wall, ore schist and footwall lithologies. In addition, rutile and hematite are represented in both the ore

schist, hanging wall and footwall lithologies and post date the sulphide and gangue phases (figure 4.3).

A sulphide mineral paragenesis has been recognised for the Malundwe and Chimiwungo deposits (figure 4.4). An early pyrite (FeS_2) stage predates the main phase of copper-cobalt mineralization with pyrite replaced by chalcopyrite. Minor pyrite is also observed locally in the hanging wall gneiss at Chimiwungo and Malundwe and is a potential source for sulphur for the Cu±Co sulphide mineralization.

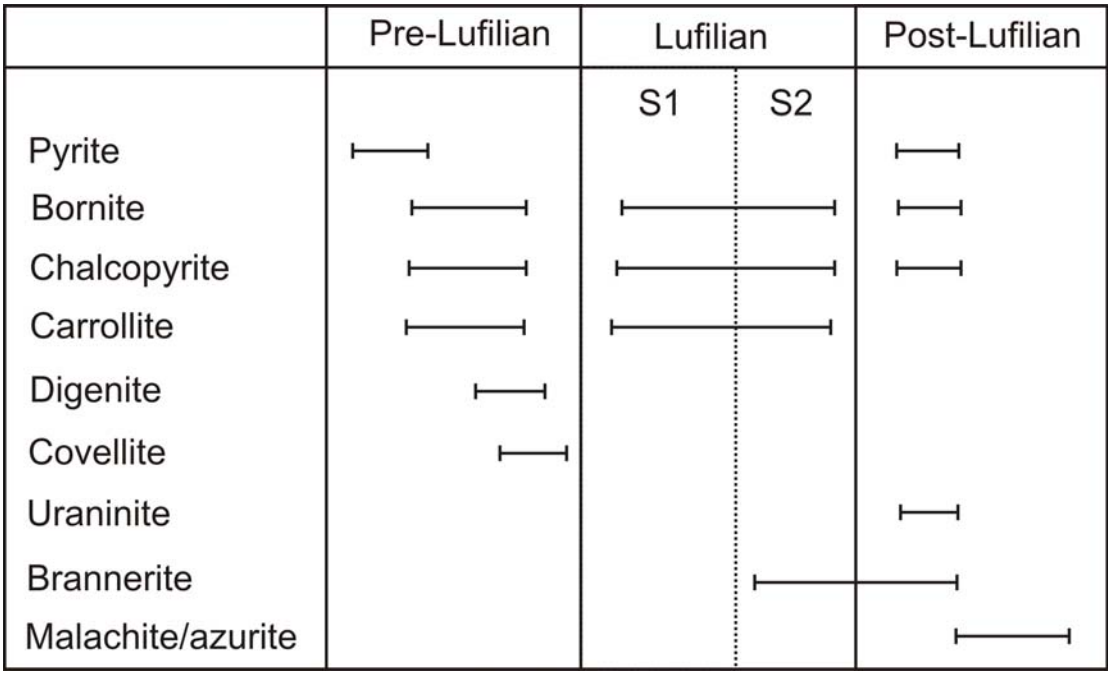

Figure 4.4 Ore paragenesis of the Malundwe and Chimiwungo copper ± cobalt (± uranium) deposits showing timing of pre-Lufilian basement mineralization, Lufilian metamorphic sulphide remobilization, post-Lufilian vein hosted mineralization and supergene enrichment (malachite/azurite)

The main stage of Copper-Cobalt mineralization consists of bornite and chalcopyrite (+ carrollite, Chimiwungo only). The sulphide mineralization commonly forms in pairs of copper sulphides that form a weak down hole zoning of pyrite-chalcopyrite ($CuFeS_2$), chalcopyrite-carrollite ($CuCo_2S_4$) (Chimiwungo only) and chalcopyrite-bornite (Cu_5FeS_4). Bornite and chalcopyrite are locally observed replaced by digenite (CuS_2) that was subsequently altered to covellite (CuS). Digenite is also observed as individual grains that are often crosscut by a lattice of secondary hematite. Carrollite was observed as exsolution lamellae and as inclusions within chalcopyrite,

indicating that copper and cobalt mineralization are synchronous. Other sulphide phases are observed locally at Chimiwungo, including cubanite ($CuFe_2S_3$) and pyrrhotite ($Fe_{1-X}S$) (figure 4.10). Pentlandite has also been identified at Lumwana (Nisbet, *pers comms.* 2004) although was not observed in this study.

The uranium mineralization at Chimiwungo and Malundwe consists of vein hosted uraninite (UO_2) and disseminated brannerite $(U,Ca,Ce)(Ti,Fe)_2O_6$ that are located in discrete zones in the ore schist, hanging wall and footwall units. Copper is remobilized in late undeformed veins that cross-cut the stratigraphy. Quartz veins within the ore and internal gneiss units locally host massive grains of the primary sulphide assemblage. Carbonate veins can be locally mineralized with traces of copper oxides. Vein hosted sulphide mineralization is the result of late metamorphic fluids remobilising the sulphide phases.

Copper oxides malachite and azurite are observed at Chimiwungo and Malundwe replacing the primary sulphide mineralization. The copper oxides are located where the primary sulphide ore bodies are above the water table and represent less than 5% of the copper mineralization. Trace amounts of copper oxides are observed associated with vein hosted uraninite, as well as traces of molybdenite.

4.2.3 Internal gneiss units

The internal gneiss units at Malundwe and Chimiwungo are unmineralized to weakly mineralized but massive sulphide may occur locally along tectonic contacts. Carrollite (~10%) lamellas form within the chalcopyrite (~50%) and are crosscut by the pyrite (~40%) (figure 4.5.1).

Plagioclase (~2%) was altered to a very fine grained high birerefringence clay seen in patches and in late fractures. Rutile grains (<1%) form a 1mm by 8mm band in muscovite which has overprinted plagioclase and chlorite (figure 4.5.2). Locally chlorite represents up to 50% of the rock forming large aggregates of grains with inclusions of quartz and crosscut by late biotite. Late fine grained laths of muscovite and chlorite crosscut minor (<1%) titanite and

calcite. Calcite is observed locally within the Chimiwungo internal gneiss as large rhomb shaped grains (figure 4.5.3).

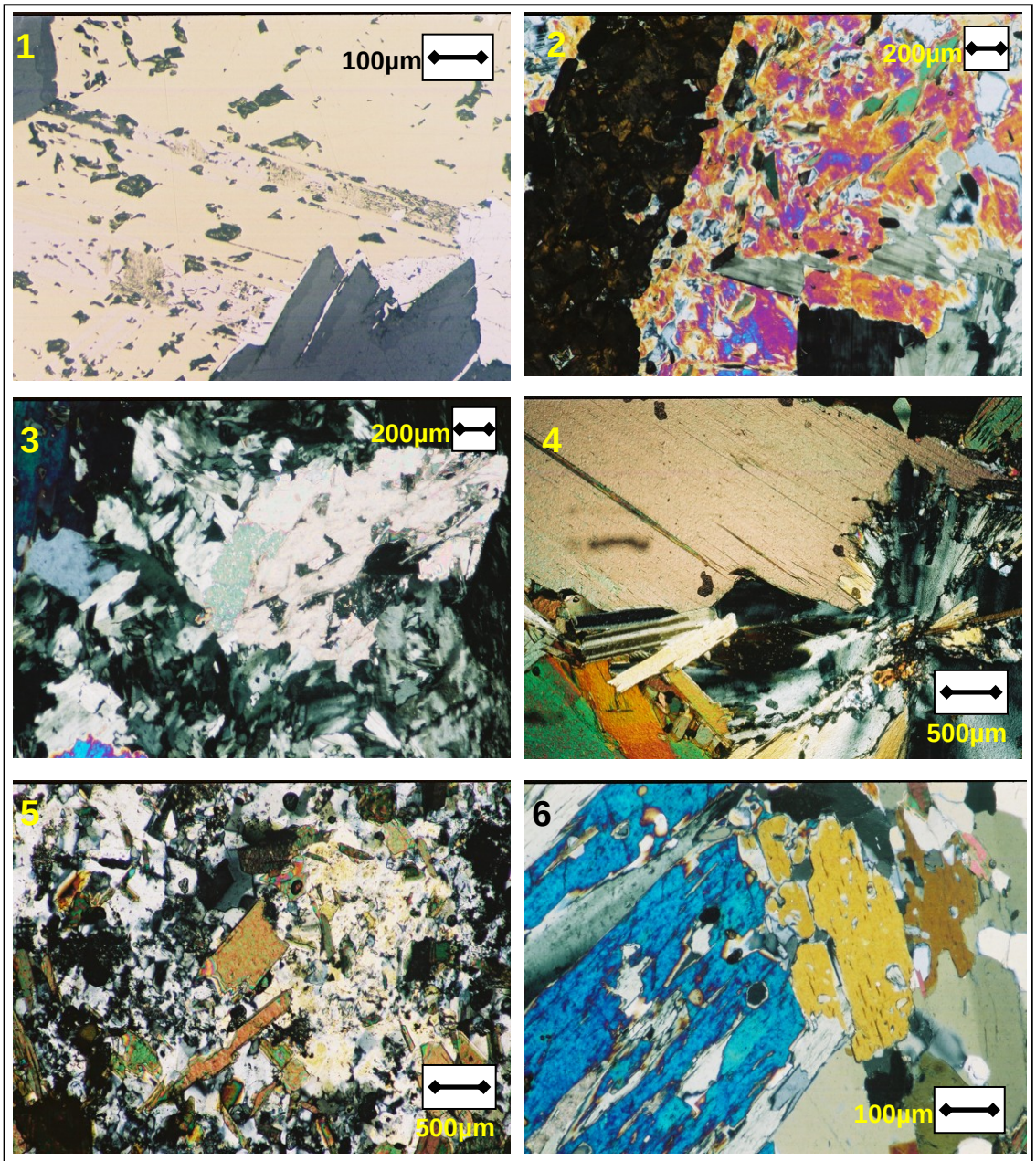

Figure 4.5 Internal gneiss transmitted and reflected light photomicrographs: 1) (Eq-Chi-062-20a) Carrollite lamellae formed within the chalcopyrite and are crosscut by the pyrite. Gangue is chlorite (ref) **2) (Eq-Chi-062-20b)** 8mm rutile band in muscovite that's replaced feldspar, and large chlorites (trans, cpl) **3) (Eq-Chi-062-20b)** Calcite rhomb crosscut by late muscovite and chlorite (trans, cpl.) **4) (Eq-Chi-062-21)** Large interlocking biotites crosscut by chlorite (trans, cpl) **5) (Eq-Chi-062-21)** Scapolite alteration crosscut by late biotite grains (trans, cpl) **6) (Eq-Chi-062-22)** Ferroactinolite crosscutting k-fels, but crosscut by chlorite, both of which are crosscut by tremolite (trans, cpl) (transmitted light=trans, reflected=ref, cross-polars=cpl, plane polars=ppl)

An internal gneiss unit sampled to investigate the slip along the contact between amphibolite and quartz-biotite-muscovite-kyanite gneiss consisted of

large interlocking biotite (~35%) grains up to 15mm long and large chlorite grains (~35%). Matrix minerals located around the edge of the shear are made up of biotite and feldspar (~7%) (< 2mm long) and rutile (~3%) (< 4mm long) (figure 4.5.4).

Areas of fine grained scapolite are crosscut by late biotite grains. Due to the similar optical properties of quartz and scapolite a visual estimation of these minerals is difficult but together they would account for ~20% of the thin-section (figure 4.5.5).

Amphibole bearing internal gneiss units are common at Chimiwungo, consisting of quartz (~55%), which form anastomosing bands of interlocking anhedral grains up to 2-3mm in diameter that are separated by a quartz – feldspar (~5%) matrix with grains ranging from 50 to 400μm in diameter. The rock contains large porphyroblasts of ferroactinolite (~20%) and kyanite (~5%) and tremolite (~10%). Ferroactinolite is often crosscut by laths of chlorite. The matrix contains up to 40 percent feldspar in places with associated clay alteration minerals. This rock also contain muscovite (~2%), biotite (~3%), chlorite (~7%) and rutile (~3%) (figure 4.5.6). Garnet porphyroblast grains, often associated with amphibole are common in the internal gneiss units and are observed with inclusions of feldspar and quartz.

4.2.4 Footwall units

Chimiwungo and Malundwe footwall units consist of augen to banded gneiss, amphibolite and mottled kyanite schist that have been interpreted as units of the Meso to Palaeoproterozoic basement. The footwall of the Malundwe deposit is also host to epidote schist units and overlies overturned Lower Roan quartzite to whiteschist.

The mottled kyanite schist units contain patches of intense chloritic alteration that overprint kyanite. Kyanite (~30%) grains exhibit two texturally distinct morphologies. Early kyanite grains are commonly poikilitic augens (~3mm diameter) in a fabric dominated by quartz (~30%) and biotite (~10%) (figures 4.6.1 & 4.6.2).

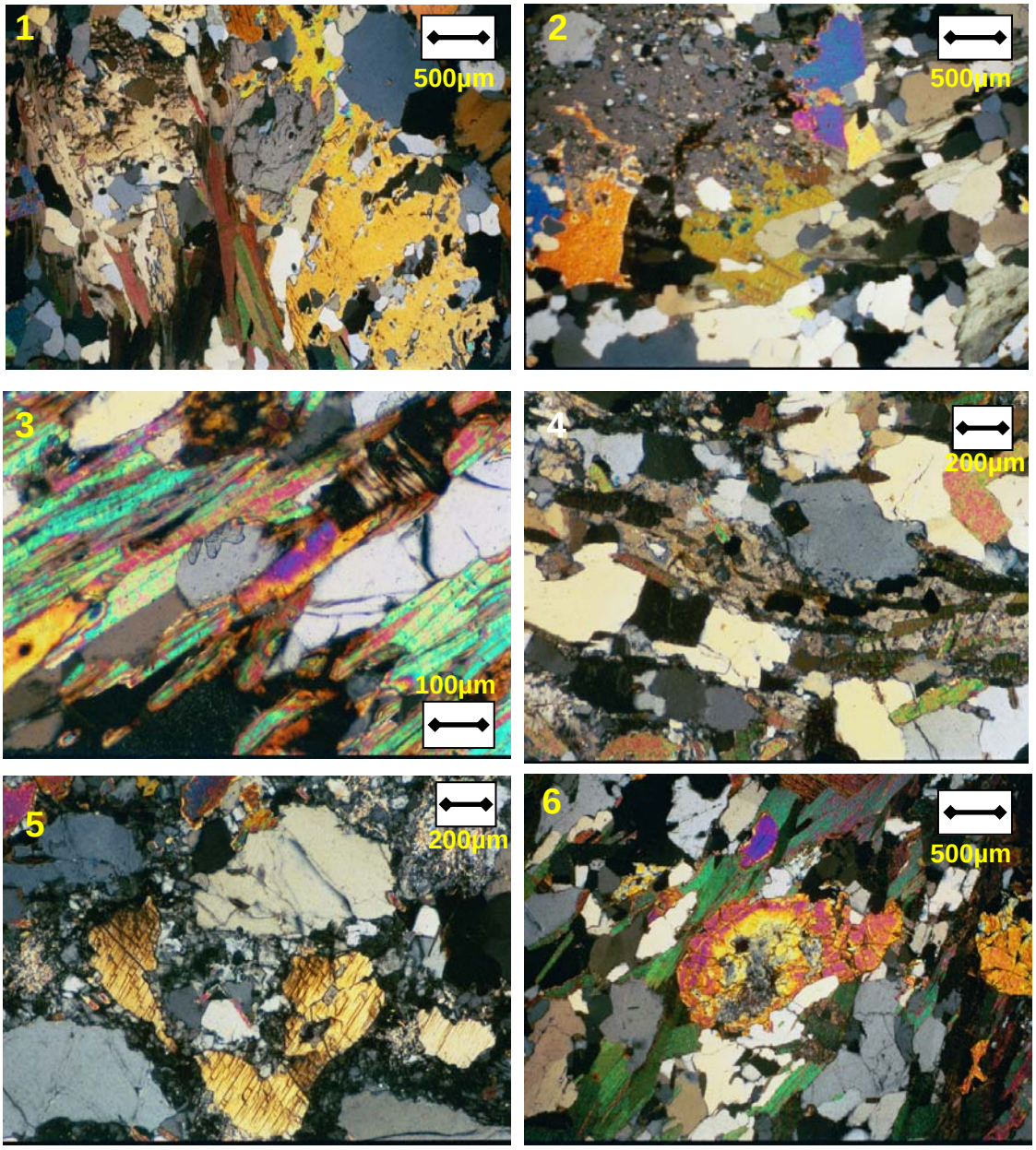

Figure 4.6 Footwall transmitted light photomicrographs (cross-polars) 1) (Eq-Mal-094-13) Kyanite with inclusions of quartz and biotite, crosscut by late biotite, muscovite and chlorite **2) (Eq-Mal-094-13)** Poikilitic kyanite crosscut by biotite, quartz, chlorite, and early kyanite **3) (Eq-Mal-094-16)** Epidote grains and prismatic zoisite in quartz-biotite-muscovite fabric **4) (Eq-Mal-094-15)** Quartz and feldspar (altered to sericite) bands defining fabric with phlogopite weakly aligned and that overprinted the fabric **5) (Eq-Mal-094-15)** Quartz replaced kyanite and sericite altered from feldspar. Late epidote grain, top left **6) (Eq-Mal-094-15)** Epidote with complex zoning crosscutting biotite and quartz

The early euhedral kyanites form clusters separated by aligned biotite, chlorite (~24%) and anhedral quartz grains. Late kyanite porphyroblasts are poikilitic with quartz and biotite inclusions that form augens within the fabric. Large kyanite porphyroblasts locally exhibit simple twinning and are crosscut by late biotite, muscovite and chlorite (figures 4.6.1 & 4.6.2).

The fabric of the mottled kyanite schist is dominated by biotite and chlorite with minor muscovite. Coarse light brown biotite/phlogopite define the S_1 fabric and are cross-cut by darker fine grained S_2 biotite/phlogopite. Muscovite has a high birerefringence and typically forms large (<3mm) anhedral plates that crosscut kyanite, quartz and chlorite. Chlorite is commonly aligned with the S_2 biotite/phlogopite fabric. Scapolite is a common phase observed in the mottled schist units at Malundwe where it can be observed as large grains that are difficult to distinguish from kyanite in hand specimen.

An epidote schist observed in the footwall of the Malundwe deposit is typically fine grained with a strong fabric defined by biotite (~30%) and muscovite (~20%). Epidote (~10%) forms grains parallel with the schistosity up to 0.5mm in length. Eq-Mal-094-16 (figure 4.6.3) shows segregations of quartz (~30%) rich and mica rich bands. The quartz bands are discontinuous and comprise interlocking polygonal grains. Magnetite (~5%) forms elongated grains parallel to the schistosity. Zoisite (~5%) is part of the epidote group and forms prismatic grains that are colourless in plane polarised light. Unlike epidote, zoisite grains are orientated perpendicular to the S_1 fabric. In the epidote schist, epidote and zoisite are commonly observed together (figure 4.6.3).

The footwall core samples also contain a mottled schist with epidote with a fabric defined by polycrystalline quartz (~30%) bands separated by a matrix of plagioclase feldspar (~19%) altered to sericite (~5%) (figure 4.6.4). Biotite (~30%) grains are weakly aligned within the fabric, although are also observed as large unfoliated interlocking grains. Kyanite was replaced by fine grained quartz, and plagioclase feldspar was partially altered to sericite (figure 4.6.5).

Kyanite also forms long (2-3mm) grains aligned with the fabric that are crosscut by biotite and large epidote grains (~5%) form euhedral porphyroblasts (200-600μm) that crosscut the fabric and exhibit complex zoning of cross polarised light (figure 4.6.6). The opaques are dominated by magnetite (~1%) grains which are texturally late and replaced the matrix feldspar. Titanite and calcite are also observed locally.

CHAPTER 4: HOST ROCK AND ORE MINERALOGY

4.3 Metamorphic history

At Lumwana, the host rock to the mineralization exhibits a gneissic fabric, with separation into crude discontinuous phlogopite rich and quartz-plagioclase rich bands. The S_1 fabric is also defined by aligned phlogopite grains, resulting from recrystallization during the Lufilian Orogeny. A top to the north deformation direction is widely observable from a variety of kinematic indicators preserved throughout the succession including, porphyroblast rotation and s-c fabrics. The relative timings for key mineral forming events are indicated in figure 4.7

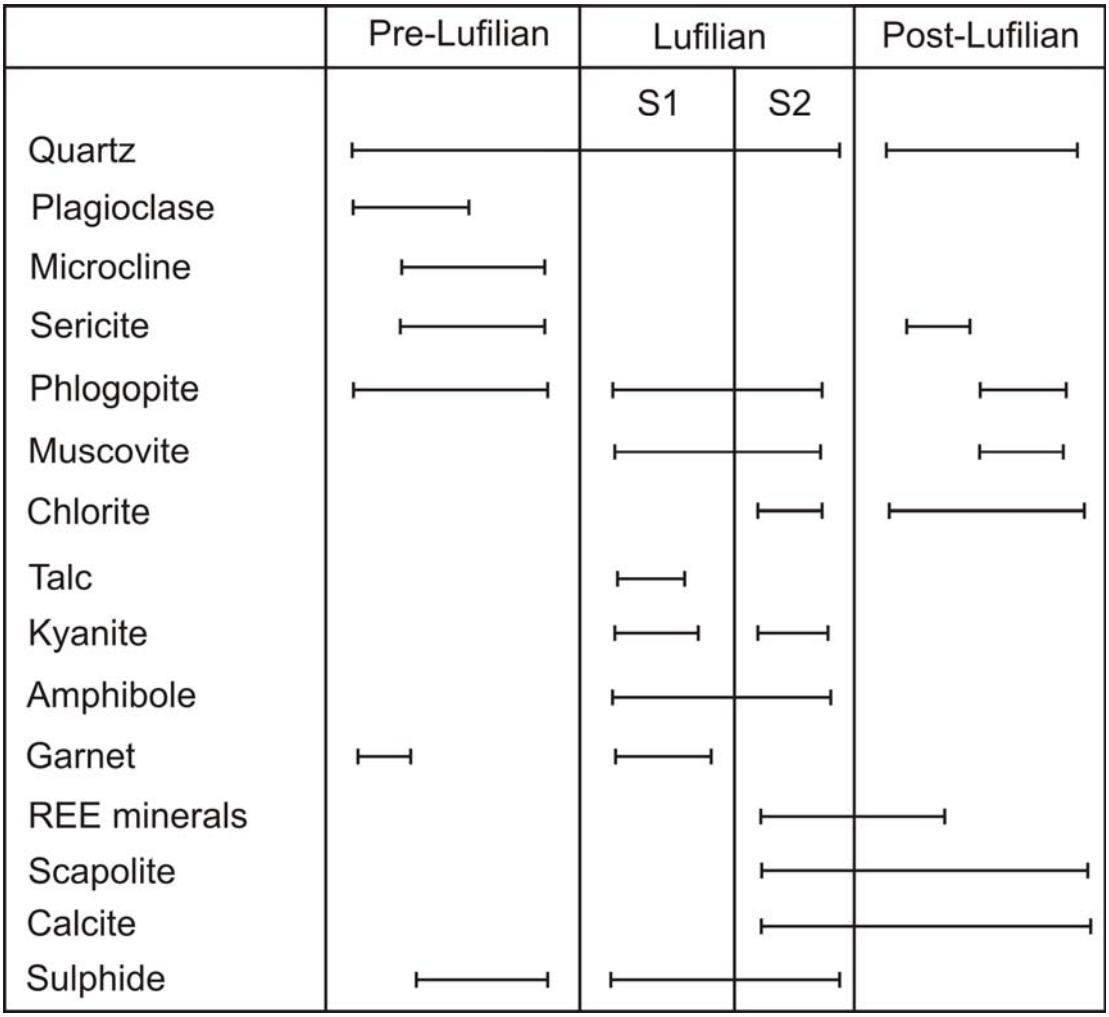

Figure 4.7 Relative mineral timings at Lumwana indicated by micro-textural relationships in reflected and transmitted light, SEM and microprobe analysis

The pre-Lufilian gneissic fabric is overprinted by Lufilian fabric S_1 that correlates with the sulphide mineralization. An S_2 retrograde metamorphic event is observable that is associated with a quartz-muscovite dominant assemblage that forms anastomosing bands sub-parallel to the S_1 fabric.

However, low strain muscovite development is observed in the Chimiwungo and Malundwe deposits with development restricted to hanging wall gneiss units commonly with associated quartz veins.

S_3 fabrics are not observed in the host rocks to the Lumwana mineralization as D_3 deformation was only prevalent in the Katangan cover rocks above the décollement. A discontinuous crenulation fabric S_4 can be observed in the Malundwe hanging wall schist units and ore schist, but is only observed in the ore schist at Chimiwungo.

Kyanite is observed in the hanging wall (Chimiwungo only), ore schist, footwall and Lower Roan units that are only present at Malundwe. Kyanite in the hanging wall is more common within the schistose banded gneiss units proximal to the ore schist. The hanging wall kyanite typically forms aggregates of grains up to 1mm in diameter that overprint the fabric. The ore schist includes large kyanite augens up to 15mm in diameter, which are deformed within the S_1 fabric. The S_2 retrograde muscovite dominant event observed in the ore schist was destructive to kyanite and is also observed in the footwall mottled schist where kyanite porphyroblasts are altered to fine grained quartz and sericite (figure 4.7).

Two phases of kyanite are observed within the footwall mottled schist units, an early phase deformed within the fabric, texturally similar to the ore schist kyanite, and a later phase of larger intensely poikiloblastic porphyroblasts, which overprint the fabric. The mineral deposits, Chimiwungo and Malundwe, represent Lufilian shear zones within the pre-Lufilian gneisses of the Mwombezhi Dome.

Talc-kyanite (whiteschist) assemblages in the Mwombezhi Dome basement indicate peak metamorphism of 750ºC ± 25ºC and 13 ± 1 kb corresponding to burial depths of approximately 50 km (Cosi *et al.* 1992; John *et al.* 2004) (figure 4.8).

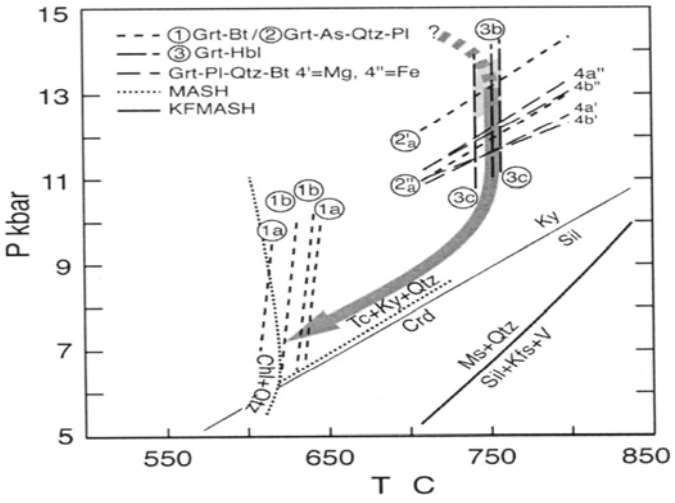

Figure 4.8 *PT* diagram for Lufilian Arc whiteschists. 1, garnet-biotite thermometry (Kleemann and Reinhardt 1994) 2, garnet-alumosilicate-quartz-plagioclase equilibrium (Koziol 1989) with 2' indicating peak and 2" retrograde conditions; 3, garnet-hornblende thermometry (Graham and Powell 1984); 4, garnet-plagioclase-quartz-biotite equilibrium (Hoisch 1990). Thick arrows show possible *PT* paths. Shaded areas indicate uncertainties of *PT* estimates (after John *et al.* 2004)

Metamorphic monazites from the whiteschist assemblages have been dated at 524 to 532 Ma (John *et al.* 2004) (figure 4.8).

4.4 Relative timing and textural controls on the Cu-Co mineralization

The textures of the sulphide minerals are controlled by the fabric development. Sulphides typically formed coarse grains elongated within the fabric, and are commonly hosted within low strain quartz bands, where the sulphides pseudomorphed the euhedral polygonal quartz grains.

Kyanite is deformed within the fabric and locally has inclusions of copper sulphides, constraining the timing of ore formation as either pre or syn metamorphism. It is unlikely that copper was introduced during the muscovite event as areas of intense quartz-muscovite alteration are commonly unmineralized and cross-cutting relationships indicate that it post dates the mineralization. However, where the S_2 quartz-muscovite alteration overprints the S_1 fabric, copper sulphides have been remobilized into pressure shadows around porphyroblasts, and into low strain micro-structural dilatant sites.

Timing the introduction of all the sulphur into the system is also important to the formation of sulphides. The presence of minor euhedral pyrite within the hanging wall gneiss to schist units indicates that sulphur was present in the succession prior to the introduction of copper. Pyrite is also observed within the Upper Roan mafics and calc-silicates of the Malundwe footwall. Sulphides also replace gangue (biotite, muscovite, quartz and feldspar) and are crosscut

by large muscovite and chlorite laths indicating that any metamorphic remobilisation of sulphides had finished before the late muscovite retrogressive event. Late carbonate fracture veining crosscuts all previous phases and locally hosts minor sulphides (typically pyrite), when in close proximity to the ore horizons.

At the Malundwe and Chimiwungo deposits scapolite is observed within the internal gneiss units and in late biotite rich shears crosscutting the hanging wall units. Scapolite has been recognised within the Lower Roan meta-sedimentary rocks of the Zambian Copperbelt and is thought indicate the former presence of evaporite minerals within the sequence (Hitzman 2000). No ore-scapolite crosscutting relationships have been observed at Lumwana. Rare examples of the evaporite mineral gypsum have been identified in hand specimen within veins cross-cutting the footwall units. The uranium mineralization is hosted by late veins indicating that it post dates copper and cobalt. The occurrence of brannerite suggests that the uraninite is synchronous with the rare earth element mineralization observed locally in the ore and host rock assemblages.

4.5 Alteration history

The host rocks to the Lumwana deposits have undergone intense wall-rock alteration with various styles of mineralization resulting from the changing chemistry of the fluids and rocks before during and after the Lufilian Orogeny.

Alteration style	Relative timing	Associations
sericite	All	replaces feldspar
garnet	pre-Lufilian	amphibole and plagioclase
phlogopite-muscovite	S_1	S_1 shear zones
muscovite-quartz	S_2	S_2 shear zones
chlorite-muscovite	S_2	S_2 shear zones
epidote	post-S_2	locally throughout
REE minerals	post-S_2	locally throughout
scapolite	post-S_2	phlogopite
hematite	post-Lufilian	locally throughout
carbonate veinlets	post-Lufilian	locally throughout

Table 4.1 Alteration styles of the Lumwana deposits observed in thin-section and backscattered electron microscopy and timings determined by textural relationships

CHAPTER 5: GEOCHEMICAL CHARACTERISTICS OF THE LUMWANA DEPOSITS

5.1 Introduction

A representative sample suite of ore and host rocks were analyzed using methods of whole rock geochemistry, electron microprobe and stable isotope analysis ($\delta^{34}S$), in order to assess the geochemical characteristics of the Lumwana deposits. In addition, the existing whole rock assay data was examined with reference to the current interpretation of the geology.

5.2 Whole-rock geochemistry

A total of 110 core samples from the Chimiwungo and Malundwe deposit were collected and analyzed for major and trace element concentrations using X-Ray Fluorescence (XRF; see appendix B1) analysis. In addition, historical core assay data was collected and plotted against current logs. Whole rock assay analysis had been conducted on half core at approximately metre intervals across the mineralization.

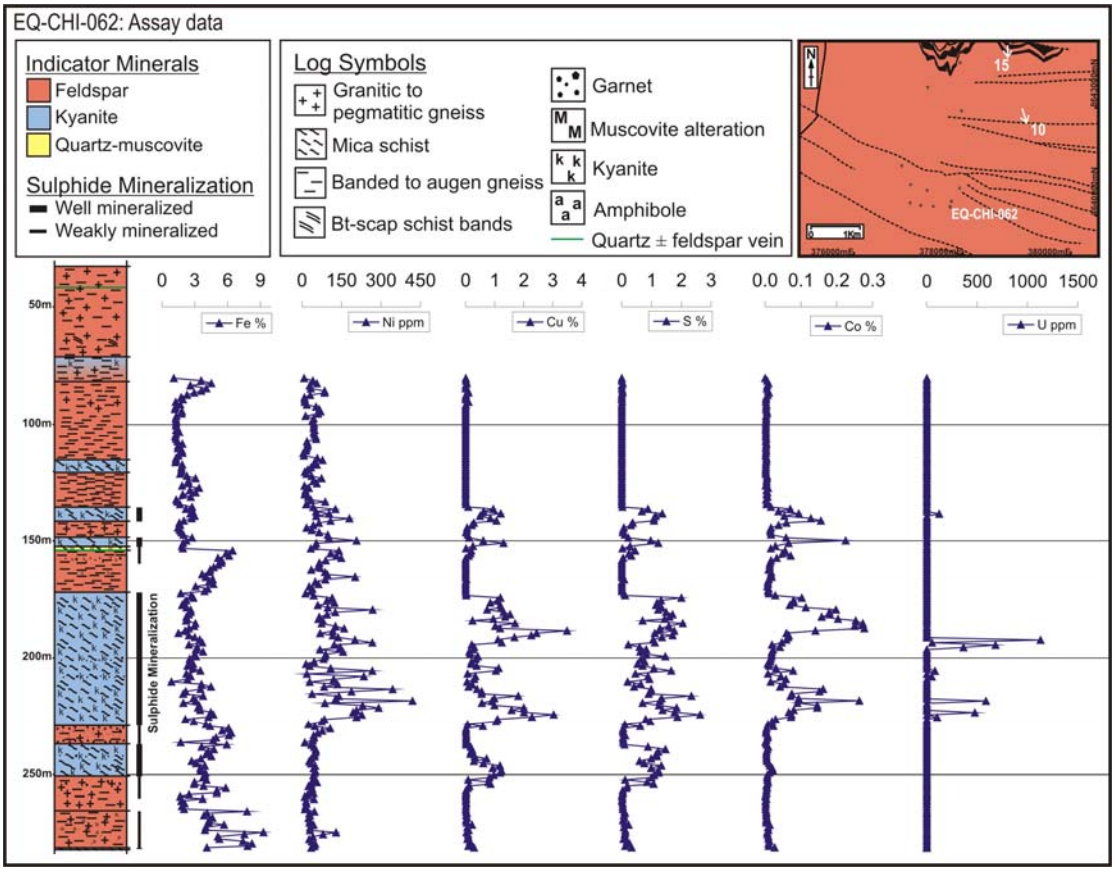

Figure 5.1 Assay data for Eq-Chi-062 plotted against summary log

The copper and sulphur assay values correlate well down hole and have highest concentrations in the phlogopite-muscovite-quartz-kyanite ore schist.

Cobalt and nickel are also enriched in the ore zone although copper and cobalt peaks are often slightly offset indicating either multiple mineralizing events or separate controlling factors for cobalt precipitation.

Ore samples with garnet present exhibit lower copper and cobalt grades that correlate with a reduction in sulphur content. The nickel trend of the assay data shows similarities to the copper cobalt and sulphur, supporting the petrographic observation of the cobalt sulphide phases siegenite ($(Ni,Co)_3S_4$), bravoite ($(Fe,Ni,Co)S_2$) and carrollite ($Cu(Co,Ni)_2S_4$) that have been identified in the Chimiwungo deposit (figure 5.1).

Although iron is one of the principal components of the sulphide mineralization including pyrite, chalcopyrite, bornite, and bravoite, iron is also a component of gangue mineral phases, such as hematite, magnetite, chlorite, biotite, garnet and amphibole. As a result of the frequent occurrence of iron bearing mineral phases iron is not a vector to the sulphide mineralization (figure 5.1 & 5.2).

The uranium assay values also correlate with the ore schist units in discrete zones that are offset from the copper peaks. However, the uranium mineralization is also observed locally outside of the copper deposits and post dates the sulphide mineralization. The absence of copper or sulphur in the hanging wall kyanite schist to gneiss units supports the theory that they represent a separate alteration event to the copper cobalt mineralization.

5.2.1 XRF results

43 samples from Eq-Chi-062 within the Chimiwungo South ore body were examined and 3 were removed due to excessive radioactivity. The remaining 40 samples were analyzed for selected major and trace element suite, of which 5 fusion bead results were removed due to anomalous results. The concentration of elements reflects the mineralogy and allows the determination of geochemical signatures for sampled units as well as various styles of alteration. Down hole geochemical data are plotted for Eq-Chi-062 (figures 5.2, 5.3, 5.4 & 5.5).

CHAPTER 5: GEOCHEMICAL CHARACTERISTICS OF THE LUMWANA DEPOSITS

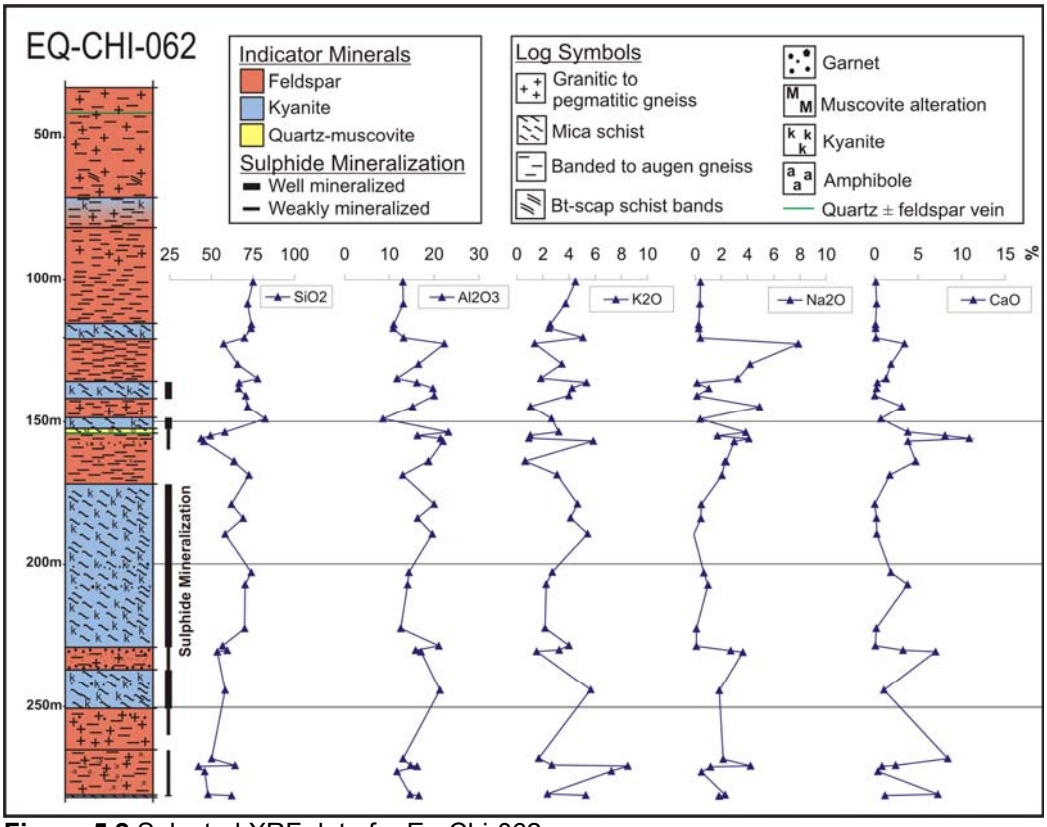

Figure 5.2 Selected XRF data for Eq-Chi-062

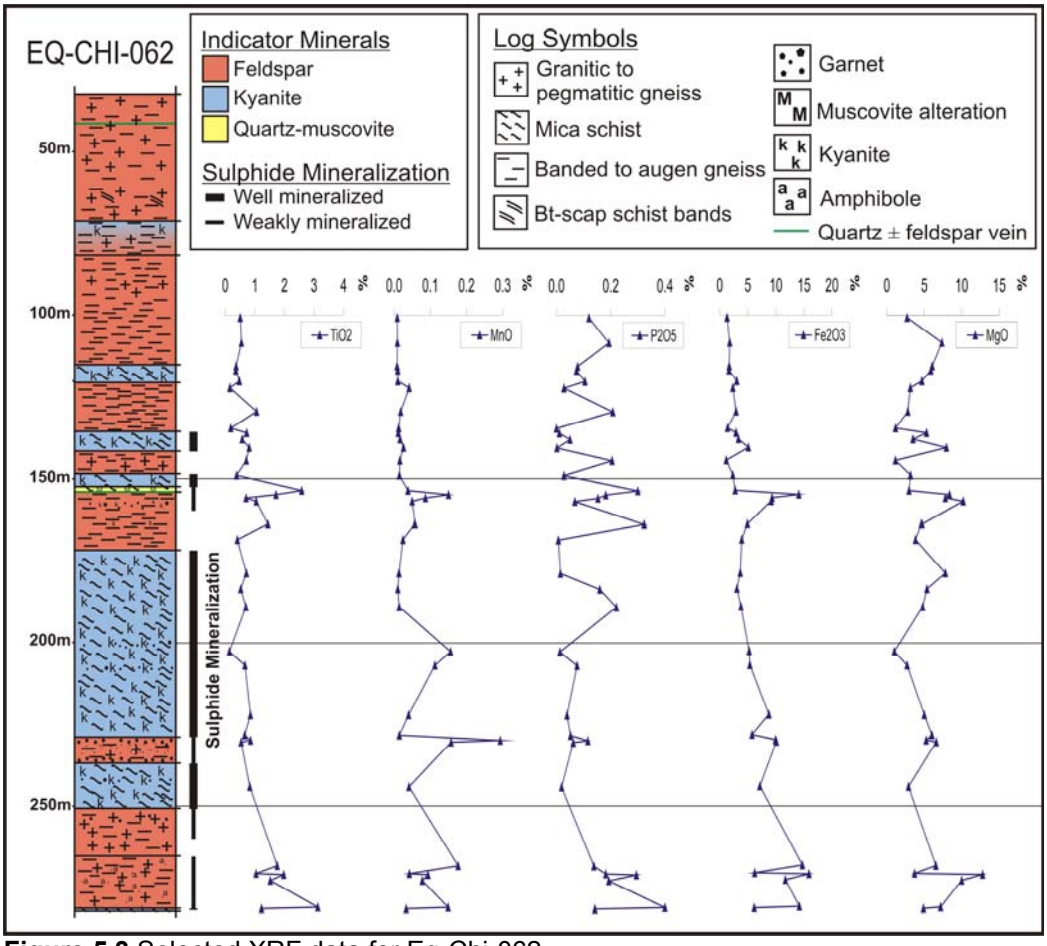

Figure 5.3 Selected XRF data for Eq-Chi-062

CHAPTER 5: GEOCHEMICAL CHARACTERISTICS OF THE LUMWANA DEPOSITS

The mineralogy may be subdivided into ore and gangue minerals. Ore minerals are principally sulphides and are reflected in the geochemistry by an increase mode of copper, cobalt, nickel and sulphur (figure 5.4).

The geochemical signature of the silicate gangue phases within the ore schist units is an increase in the mode of aluminum and depletion in calcium and sodium. Aluminum is enriched in the kyanite schist to gneiss units in the ore and host rock assemblages although the highest aluminum values (23 to 24 percent) are in the pegmatitic quartz-feldspar units with late metamorphic muscovite-chlorite alteration. Aluminum and potassium exhibit similar downhole trends reflecting the mode of phlogopite and microcline (figure 5.2).

Iron and magnesium are major components of the ore and host rock assemblages and exhibit similar downhole trends primarily representing the composition of phlogopite to biotite and to a lesser extent amphibole. This relationship is examined in more detail in the microprobe data.

There is a correlation between garnet bearing units and the calcium peaks (up to 7 percent CaO) and manganese. However, the highest CaO value is 11 percent which reflects late carbonate veinlets that crosscut the middle gneiss (figure 5.2&5.3).

Titanium varies from 1 to 1.5 percent in the ore schist compared to 0.5 to 1 percent in the hanging wall. Internal gneiss units typically have higher values that range up to 3.5 percent in amphibole bearing units (figure 5.3).

Phosphorous shows a lot of variation in concentration in the hanging wall with less variation in the sulphide mineralized zone. Phosphate minerals monazite ($(La,Ce,Nd,Th)PO_4$), allanite ($(Y,Ce,Ca)_2(Al,Fe^{3+})_3(SiO4)_3(OH)$), xenotime ($YPO_4$) and apatite ($Ca_5(PO4)_3(OH,F,Cl)$), have been identified on scanning electron microscope and are texturally late, post dating the sulphide mineralization (figure 4.3).

CHAPTER 5: GEOCHEMICAL CHARACTERISTICS OF THE LUMWANA DEPOSITS

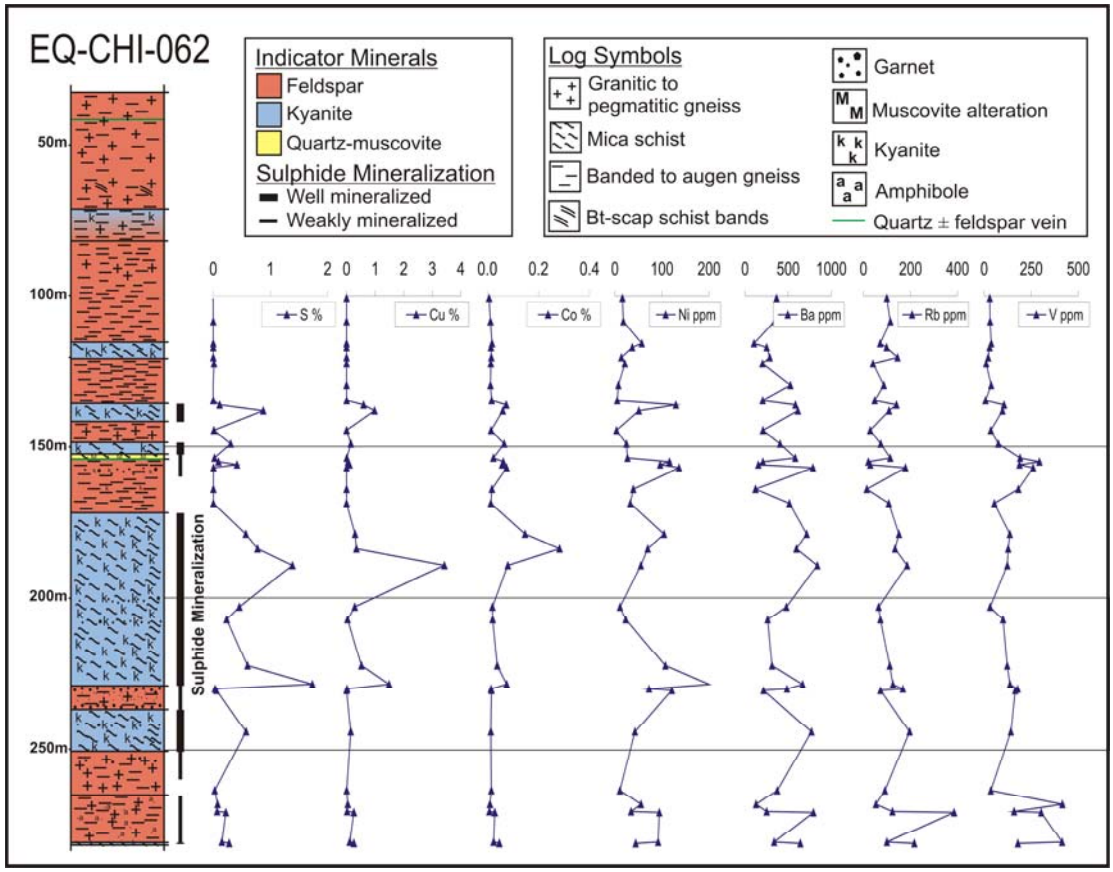

Figure 5.4 Selected XRF data for Eq-Chi-062

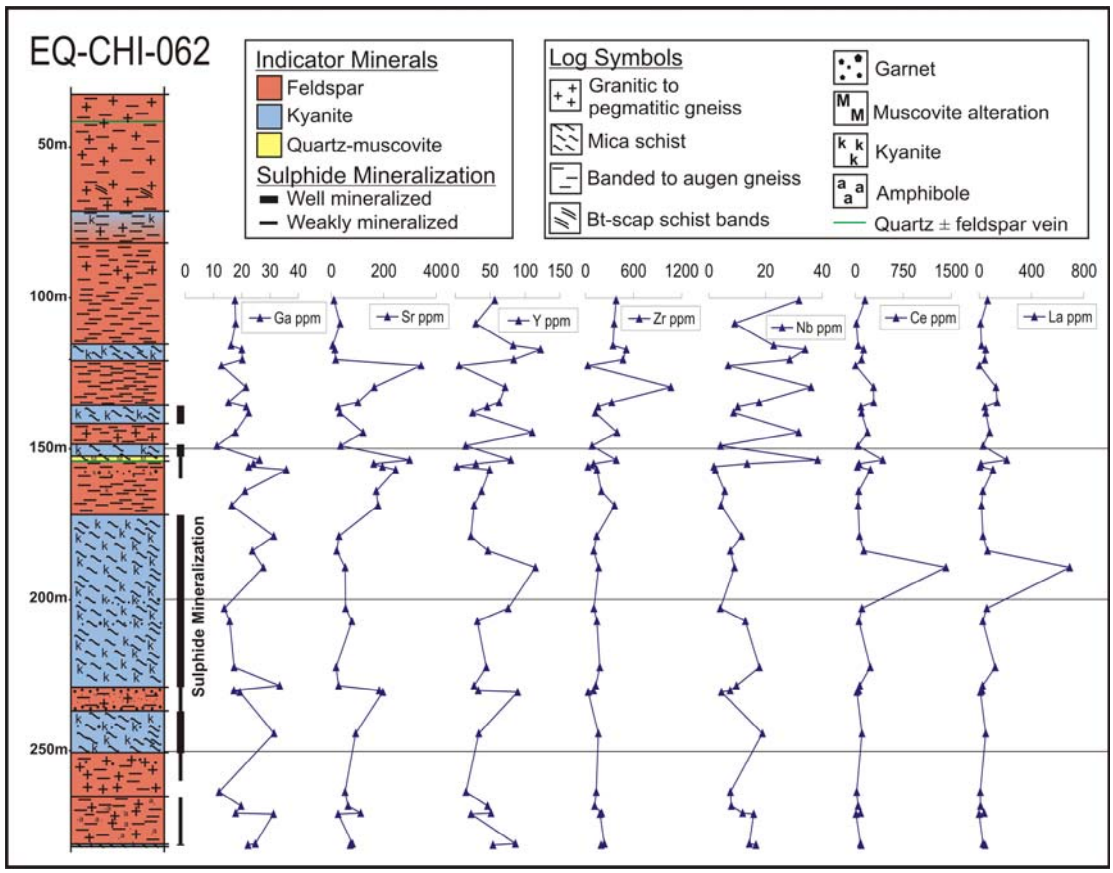

Figure 5.5 Selected XRF data for Eq-Chi-062

CHAPTER 5: GEOCHEMICAL CHARACTERISTICS OF THE LUMWANA DEPOSITS

Trace elements can often substitute for major elements of similar ionic size and charge resulting in similar downhole trends (table 5.1).

Major Element	Substituting Trace Element(s)
Ti	V
Al	Ga
Fe	Cr, Co, Ni
Mg	Cr, Co, Ni
Ca	Sr, REEs
K	Rb, Ba, Sr

Table 5.1 Trace elements substituting for major elements of similar ionic size and charge (after Best & Christiansen 2001)

An example of ionic substitution is vanadium which substitutes for titanium in the mineral lattice resulting in vanadium and titanium exhibiting similar downhole trends. Rubidium and barium are of similar ionic size and charge to potassium and hence exhibit similar trends. Strontium substitutes for both calcium and potassium and as such reflects a combination of both the potassium and the calcium trends. In addition, the trace element gallium is of similar ionic charge to aluminium resulting in a similar downhole trend due to ionic substitution (figures 5.2, 5.3, 5.4 & 5.5).

5.2.2 Isocon diagrams

For many years isocon diagrams have been applied to the study of hydrothermal alteration and used in the analysis of changes in volumes and element concentrations during metasomatism by the method of Gresens (1967). The net gains and losses in components during alteration are calculated by this method and as such account for the volume and compositional changes that accompany the process. Gresens' equation was modified to produce a linear relationship between the concentration of a component in the altered rock and the concentration of a component in the original (Grant 1986) (figure 5.6).

The construction of an isocon diagram factors out compositional and volumetric changes and all immobile elements will have a value of ΔC_i of zero and therefore sit on a line that trends through the origin, with a slope of Mo/Ma.

CHAPTER 5: GEOCHEMICAL CHARACTERISTICS OF THE LUMWANA DEPOSITS

$$C_i^A = \frac{M^O}{M^A}(C_i^O + \Delta C_i)$$

Figure 5.6 Equation to factor out volume and composition change to allow identification of immobile elements. A and O are the superscripts for the altered and unaltered samples respectively. C^A_i and C^O_i are the concentrations of component "i" in the altered and unaltered samples respectively. M^O and M^A are the reference masses of unaltered and altered samples respectively. ΔC_i is the difference in concentration between the original and altered samples (Grant 1986)

The isocon is the line that connects the immobile elements of equal concentration, separating relative enrichment from relative depletion. The isocon is determined by a straight line best fit through a series of points and the immobile elements should plot on the line (Grant 1986).

Ambiguity over the protolith to the ore and host rocks at Lumwana due to the metasomatism and metamorphic recrystallization of samples makes identifying with certainty altered and unaltered samples of the same rock problematic. As such, various styles of ore and host rock have been compared on isocon plots, to highlight the geochemical variations between units.

Isocon plots are used for the determination of mobile and immobile elements using scaled data so that concentrations of different magnitudes plot on the same graph (Grant 1986). TiO_2, Zr, Sc, Nb, Ce and Y are commonly considered immobile elements and should plot on the isocon. However, the rare earth element mineralization and titanium mineral phases result in traditionally immobile elements not plotting on the isocon at Lumwana. A lack of correlation between immobile elements can also reflect a variation in the protolith of the samples.

Chimiwungo

Following petrographic examination five samples that represent different units and alteration styles (Eq-Chi-062) were selected and plotted on isocon

diagrams in order to characterize the geochemical characteristics of the Chimiwungo deposit and variations between units (figure 5.7).

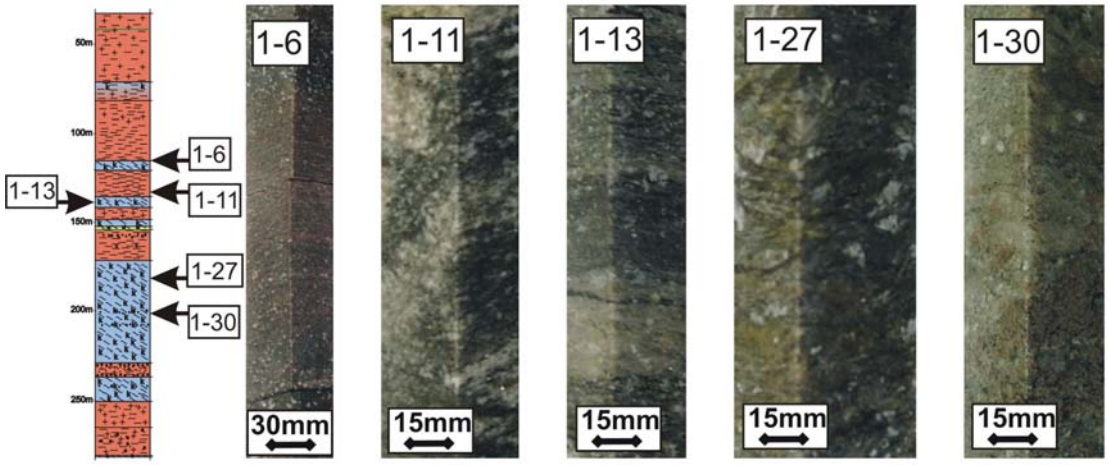

Figure 5.7 Selected Chimiwungo samples with stratigraphic position. **1-6:** Hanging wall kyanite gneiss to schist with iron oxide alteration. **1-11:** Banded hanging wall gneiss with alteration cross-cutting the fabric. **1-13:** Upper ore schist with S_2 muscovite-quartz alteration forming banded texture. **1-27:** Copper-cobalt ore schist with S_2 extensional shear fabric and remobilised sulphides. **1-30:** Weakly sulphide mineralised ore schist with garnet alteration. Sample numbers refer to XRF data (Appendix B1)

Figure 5.8A illustrates the relative concentrations of major, trace and immobile elements of hanging wall banded gneiss (1-11) in comparison to hanging wall kyanite gneiss (1-6). These units were chosen to examine the transition of a banded gneiss to an unmineralized kyanite schist to gneiss in order to highlight the geochemical characteristics of the metasomatism.

The isocon is selected by the straight line best fit through titanium, zirconium, yttrium and niobium. Notable features are the increased mode of sodium and calcium in the banded gneiss representing the plagioclase feldspar component that is not present in the kyanite gneiss. As expected, strontium is also enriched in the hanging wall gneiss as it substitutes for calcium due to having a similar ionic charge and size (table 5.1 & table 5.2A).

The hanging wall kyanite gneiss is relatively enriched in magnesium and phosphorous, reflecting phlogopite and phosphate minerals respectively (figure 5.8A).

CHAPTER 5: GEOCHEMICAL CHARACTERISTICS OF THE LUMWANA DEPOSITS

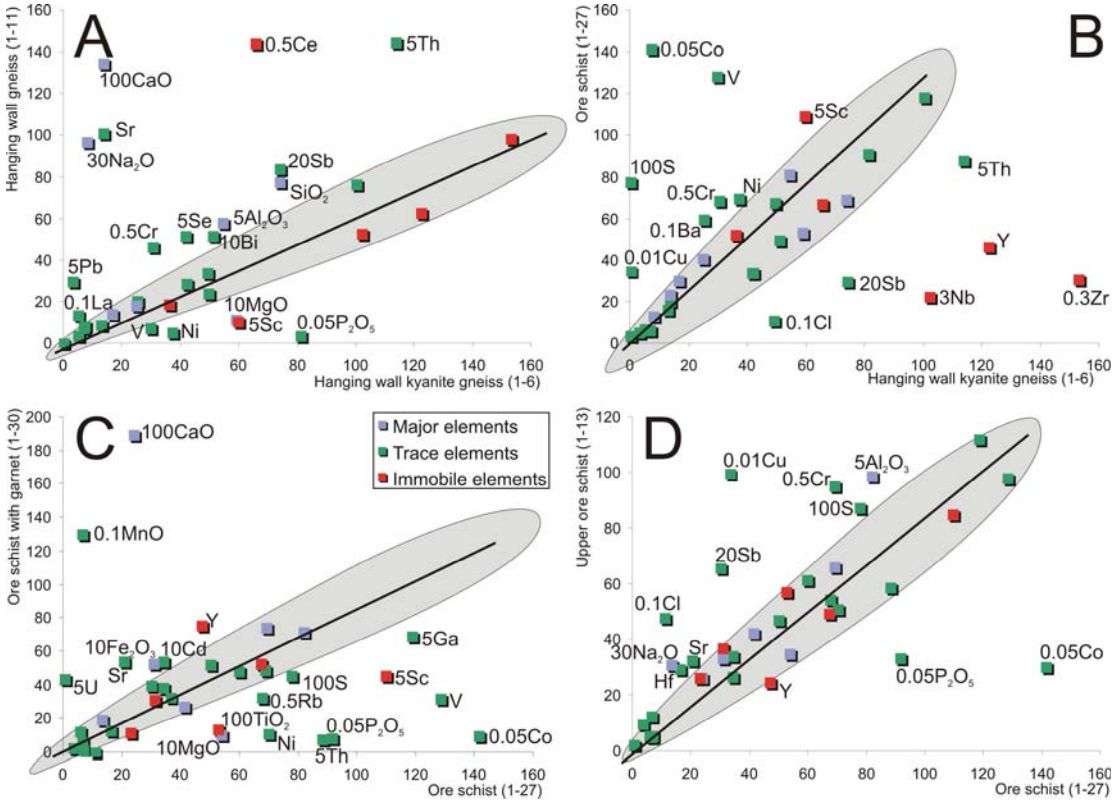

Figure 5.8 Selected isocon plots for the Chimiwungo deposit. **Eq-Chi-62** (after Grant 1986). Blue squares are major elements (%). Green squares are trace elements (ppm). A summary of graphs is shown in figure 5.2

A well mineralized (Cu-Co) kyanite bearing ore schist sample (1-27) with an S_2 shear fabric was selected to compare the ore schist mineralization to the unmineralized kyanite gneiss to schist (1-6) of the Chimiwungo hanging wall, and test the hypothesis that they share a common protolith.

	X	Increased mode	Y	Increased mode	Correlation
A	**(1-6)**	MgO, V, Ni, P_2O_5, Sc	**(1-11)**	CaO, Na_2O, SiO_2, Al_2O_3, Sr, Sb, Th, Se, Cr, Pb, La, Ce	K_2O, Fe_2O_3, S, Cl, MnO, Cu, Ga, Co, Ba, Rb, Hf, U, TiO_2, Zr, Y, Nb
B	**(1-6)**	Cl, Sb, Th, Y, Nb, Zr	**(1-27)**	Co, Cu, V, S, Cr Ni, Ba, Sc	SiO_2, Al_2O_3, Fe_2O_3, MgO, CaO, K_2O, Na_2O, MnO, P_2O_5, Pb, Rb, Sr, Hf, U, La, Se, Ga, TiO_2, Ce
C	**(1-27)**	MgO, S, Ga, Rb, Ni, Th, V, Co, P_2O_5, Sc, TiO_2	**(1-30)**	CaO, Fe_2O_3, MnO, Sr, U, Y	K_2O, SiO_2, Al_2O_3, Na_2O, Cl, Cu, Cr, Pb, Ba, Hf, La, Sb, Se, Zr, Nb, Ce
D	**(1-27)**	P_2O_5, Co, Y	**(1-13)**	Na_2O, Al_2O_3, Cl, Hf, Sr, Sb, S, Cr, Cu	SiO_2, Fe_2O_3, MgO, CaO, K_2O, MnO, V, Ni, Pb, Ba, Rb, Th, U, La, Se, Ga, TiO_2, Zr, Sc, Nb, Ce

Table 5.2 Relative element concentrations between XRF analyzed Chimiwungo samples. Blue denotes major elements, green trace elements and red immobile elements

CHAPTER 5: GEOCHEMICAL CHARACTERISTICS OF THE LUMWANA DEPOSITS

Ore schist sample (1-27) when compared to the hanging wall kyanite gneiss (1-6) have similar concentrations of all major elements, and apart from the main ore elements copper, cobalt and sulphur, it is also enriched in nickel, chrome, vanadium and barium. The hanging wall kyanite gneiss is relatively enriched in chlorine, thorium and antimony as well as rare earth elements zirconium, yttrium and niobium. The selected isocon correlates with cerium and titanium, which are commonly considered immobile, but here reflect the sample mineralogy with rutile and REE phosphate minerals observed in both samples. The relative enrichment of immobile elements (Y, Nb &, Zr) in the unmineralized kyanite gneiss in comparison to the ore schist indicates that the ore schist has been subject to increased levels of metasomatism. However, another possibility is that the poor correlation of the selected isocon with the immobile elements suggests that the hanging wall kyanite gneiss and the ore schist do not share a common protolith (figure 5.8B, table 5.2B).

The antithetic garnet-sulphide relationship is examined by comparing XRF data for ore schist sample (1-27) and ore schist with garnet sample (1-30) (figure 5.7, figure 5.8C & table 5.2C). Petrographic observations indicate that the garnet alteration pre-dates the Lufilian deformation and metasomatism and that they are relics of the protolith. The presence of garnet in the sample (1-30) is reflected in the geochemistry by relatively higher concentrations of calcium, iron, manganese, strontium and cadmium, which supports the trends of the downhole data (figures 5.2 to 5.5). Uranium and yttrium are also relatively enriched in the garnet bearing sample.

The ore schist (1-27) is relatively enriched in cobalt, sulphur, magnesium, thorium, nickel, vanadium, phosphorous and scandium when compared to the ore schist with garnet, representing the cobalt sulphides and phlogopite-muscovite alteration associated with the copper sulphides (figure 5.8C).

The geochemical variations between copper dominant ore schist and cobalt dominant ore schist are studied by examining a sample of the upper ore schist with S_2 quartz-muscovite alteration (1-13; Cu:0.98%, Co:602ppm) and a

sample of cobalt ore schist with S_2 extensional shear fabric (1-27; Cu:0.35%, Co:2828ppm) (figure 5.7, figure 5.8D & table 5.2D).

An isocon line is selected that plots in close proximity to all immobile elements suggesting that the upper ore schist sample (1-13) and the ore schist sample (1-27) are altered versions of the same protolith. The ore schist (1-27) is enriched in phosphorous, cobalt and yttrium and the upper ore schist (1-13) is comparably enriched in copper, sulphur, aluminum and sodium. The relative increase of copper and sulphur in the upper ore schist reflects the higher proportion of copper sulphides, as observed in thin-section. Similarly, the increased cobalt abundance is to be expected in the cobalt rich ore schist sample. The relative increase in the sodium content of the upper ore schist suggests a progressive increase in the degree of alteration from the upper ore schist to the ore schist, reflecting the sericitization of plagioclase and metasomatic removal of sodium. This observation also supports the hypothesis that the S_2 muscovite-quartz alteration bands are indicative of pre-existing quartz-feldspar bands in a banded gneiss protolith.

Malundwe

Six representative samples from Eq-Mal-094 have been selected and plotted on isocon diagrams in order to study the geochemical characteristics of the alteration styles of the Malundwe deposit (figure 5.9, figure 5.10 & table 5.3).

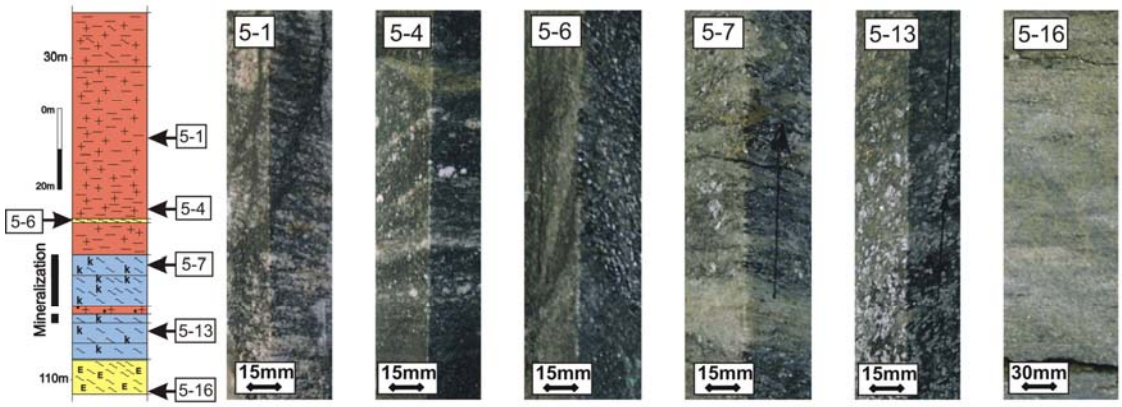

Figure 5.9 Selected Malundwe samples from Eq-Mal-94 with stratigraphic position. **5-1:** Hanging wall gneiss **5-4:** Hanging wall augen gneiss with epidote alteration cross-cutting the fabric. **5-6:** hanging wall phlogopite schist with S_4 crenulation cleavage. **5-7:** Copper-cobalt ore schist with anastomosing fabric and remobilised sulphides. **5-13:** Weakly sulphide mineralised ore schist with garnet alteration. **5-16:** Epidote schist. Sample numbers refer to XRF data (Appendix B2)

CHAPTER 5: GEOCHEMICAL CHARACTERISTICS OF THE LUMWANA DEPOSITS

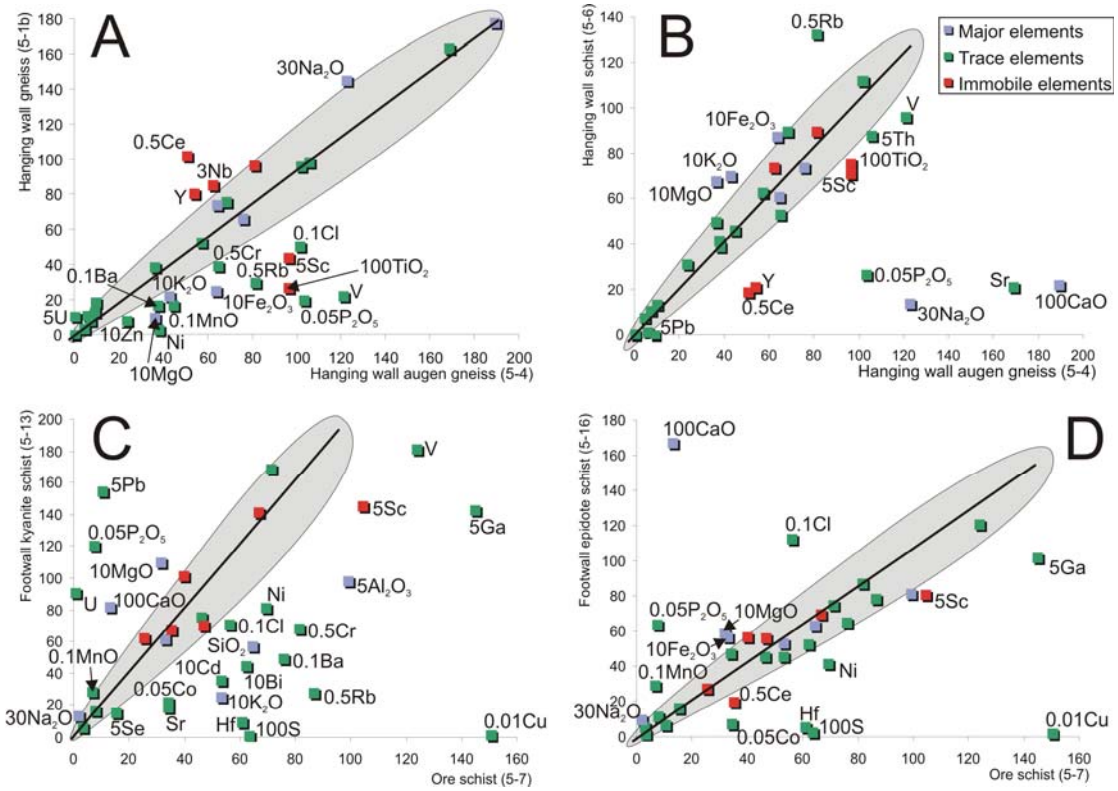

Figure 5.10 Selected isocon plots for the Malundwe deposit. **Eq-Mal-094** (after Grant 1986). Blue squares are major elements (%). Green squares are trace elements (ppm). A summary of graphs is shown in table 5.3.

	X	Increased mode	Y	Increased mode	Correlation
A	**(5-4)**	MgO, K_2O, Fe_2O_3, Ni, Ba, MnO, Cr, Rb, Cl, P_2O_5, V, TiO_2, Sc	**(5-1b)**	Y, Nb, Ce Na_2O, U	SiO_2, Al_2O_3, CaO, S, Cu, Co, Pb, Sr, Hf, Th, La, Sb, Se, Ga, Zr,
B	**(5-4)**	Na_2O, CaO, V, Th, Pb, P_2O_5, Sr, TiO_2, Sc, Y, Ce	**(5-6)**	MgO, K_2O, Fe_2O_3, Rb	SiO_2, Al_2O_3, S, Cl, MnO, Cu, Co, Cr, Ni, Ba, Hf, U, La, Sb, Se, Ga, Zr, Nb
C	**(5-7)**	Al_2O_3, SiO2, K_2O, V, Ga, Ni, Cl, Cr, Ba, Rb, Co, Se, Sr, Hf, S, Cu, Sc	**(5-13)**	MgO, CaO, Na_2O, Pb, P_2O_5, U, MnO	Fe_2O_3, Th, La, Sb, Cd, TiO_2, Zr, Y, Nb, Ce
D	**(5-7)**	Cu, Co, Hf, S, Ni, Ga, Ce, Sc	**(5-16)**	CaO, MgO, Fe_2O_3, Cl, MnO, P_2O_5	SiO_2, Al_2O_3, K_2O, Na_2O, Cr, V, Pb, Ba, Rb, Sr, Th, U, La, Sb, Se, TiO_2, Zr, Y, Nb

Table 5.3 Relative element concentrations between XRF analyzed Malundwe samples. Blue denotes major elements, green trace elements and red immobile elements.

In order to examine the possibility that the banded gneiss is a deformed and altered variant of the granite gneiss, figure 5.10A compares a sample of hanging wall granite gneiss (5-1b) with a sample of augen gneiss (5-4) (figure 5.9). The selected isocon line correlates poorly with the immobile elements suggesting that they do not share a common protolith. The augen gneiss has relatively higher concentrations of magnesium, potassium, and iron than the

granite gneiss and is depleted in sodium. The geochemical characteristics correlate with the observed microscopy of the samples with an increased proportion of phlogopite, muscovite and microcline in the augen gneiss and a higher proportion of plagioclase in the granite gneiss (table 5.3A).

The augen gneiss (5-4) is also comparatively enriched in phosphorous, chlorine and titanium when compared to the granite gneiss (5-1b) (figure 5.10A, table 5.3A). These geochemical characteristics respectively reflect the epidote-apatite alteration, observed discordant to the S_1 fabric and the presence of titanite in the augen gneiss (figure 5.10A and figure 4.1).

The augen gneiss sample (5-4) was selected for comparison with an unmineralized phlogopite-quartz schist sample (5-6) to test the hypothesis that the variations in mineralogy are the result of phlogopite alteration of an augen gneiss protolith (figure 5.9, figure 5.10B & table 5.3B).

An isocon line was selected that closely correlates with the immobile elements zirconium and niobium. The isocon line also correlates with many of the major and trace elements, providing support for the stated hypothesis. A relative increase of the concentrations of magnesium, potassium and iron in the phlogopite-quartz schist sample, reflect the petrographic observations with an increased mode of phlogopite. A relative decrease in the mode of sodium and calcium in the schist sample (5-6), are the result of relatively higher proportions of plagioclase and epidote in the augen gneiss (5-4) (5.10B).

The ore schist is mineralogically and texturally similar to the unmineralized footwall kyanite schist and may share a common protolith. To establish whether or not this is the case, XRF data for ore schist with S_2 muscovite-quartz bands (sample 5-7) and unmineralized footwall kyanite schist with intense chlorite alteration (sample 5-13) have been compared (figure 5.9, figure 5.10C and table 5.3C). The isocon line was selected by the correlation of immobile elements titanium, zirconium, yttrium, niobium and cerium that all plot close to a straight line through the origin. This indicates that the footwall

kyanite schist has been altered from a geochemically similar protolith to the ore schist (figure 5.10C).

As expected, the ore schist is enriched in ore components copper, cobalt and sulphur. Trace elements associated with ore enrichment include nickel, chrome and vanadium. The ore schist is also relatively enriched in aluminium, silica and potassium as a result of the higher mode of phlogopite and kyanite. Trace element enrichment associated with the silicate phases includes barium, rubidium and gallium, a result of ionic substitution of potassium and aluminium respectively (figure 5.10C, table 5.3C). An unexpected enrichment in the ore schist is strontium as it typically exhibits the same trend as calcium. However, strontium can also substitute for potassium (table 5.1).

The hanging wall kyanite schist (5-13) is comparatively enriched in magnesium, calcium, phosphorous uranium and lead, and to a lesser extent sodium and manganese. The enrichment of calcium and phosphorous indicate the presence of apatite in the footwall kyanite schist, that was not observed in thin-section. The uranium and lead enrichment may reflect the radioactive breakdown of uranium to lead, whereas the magnesium enrichment reflects the pervasive chlorite alteration in the footwall kyanite schist. The generalised formula for common members of the chlorite group is $(Fe,Mg,Al)_6(Si,Al)_4O_{10}(OH)_8$. The geochemical characteristics and distribution of chlorite are examined in more detail through microprobe analysis in section 5.3.

Isocon plot 5-7D examines the geochemical differences between Malundwe ore schist (5-7) and footwall epidote schist (5-16) (figure 4.6). The selected isocon line correlates well with the immobile elements titanium, zirconium, yttrium and niobium, as well as major elements silica, aluminium, and potassium. The ore schist is comparatively enriched in copper, cobalt, sulphur and nickel reflecting the sulphide mineralization. The epidote schist is relatively enriched in calcium and phosphorous supporting the petrographic observation of epidote and apatite.

CHAPTER 5: GEOCHEMICAL CHARACTERISTICS OF THE LUMWANA DEPOSITS

5.3 Geochemical characteristics of silicate phases

Phlogopite, muscovite, chlorite, amphibole and garnet phases were analyzed on the Cameca SX50 WDS electron microprobe (Natural History Museum, London), using polished-thin sections of selected samples (appendix B2). Operating conditions were 15kV (accelerating voltage), 20nA (beam current) and count time of 20 s. The geochemical characteristics, relationship between sulphide and increased mode of phlogopite and muscovite, as well as the metamorphic history were investigated.

In total 497 points were probed from selected ore and host rock samples from Chimiwungo and Malundwe (table 5.4). In order to interpret the data, petrographic relationships were examined including mineral zonation, mineral associations and where possible, the relative timing of phases and their relationship to structure and metamorphism, which are described in chapter 4.

	Chimiwungo	**Malundwe**	**Total**
Phlogopite	95	113	**208**
Muscovite	59	65	**124**
Chlorite	44	28	**72**
Amphibole	43	12	**55**
Garnet	24	14	**38**
Total	**265**	**232**	**497**

Table 5.4 Summary of microprobe analysis (raw data in appendix B3)

Phlogopite, muscovite and chlorite all have associations with sulphide mineralization at both Chimiwungo and Malundwe. Garnet and amphibole, although not mutually exclusive from sulphide, do exhibit an apparent antithetic relationship with sulphide mineralization. The molecular proportions for phlogopite were calculated using the method of Tindle and Webb (1990) (table 5.5).

Phlogopite is a magnesium variety of biotite with a ratio of magnesium to iron atoms, of greater than two to one (Deer *et al.* 1966). Any phase with an X_{Fe} ratio (iron/iron+magnesium) of less than 0.5 is phlogopite, and any value greater is defined as biotite.

CHAPTER 5: GEOCHEMICAL CHARACTERISTICS OF THE LUMWANA DEPOSITS

	1	2	3	4	5
SiO_2	36.17	39.34	36.89	38.58	35.61
TiO_2	2.04	0.73	1.35	1.28	1.62
Al_2O_3	15.95	19.09	18.63	17.18	16.57
FeO	17.29	4.50	13.35	5.38	18.16
MnO	0.11	<0.05	0.12	0.13	0.07
MgO	12.29	21.07	14.75	20.59	12.75
K_2O	9.83	9.44	9.70	9.83	9.23
Na_2O	<0.05	0.37	0.23	0.10	0.11
Cl	0.18	<0.05	0.18	0.11	0.30
F	0.04	0.20	0.27	0.00	0.21
Totals	**93.87**	**94.78**	**95.46**	**93.18**	**94.63**
Number of ions in structural formula based on 24 oxygens					
Si	5.5	5.5	5.4	5.5	5.4
Ti	0.2	0.1	0.1	0.1	0.2
Al	2.9	3.1	3.2	2.9	3.0
Fe	2.2	0.5	1.6	0.6	2.3
Mn	0.0	0.0	0.0	0.0	0.0
Mg	2.8	4.4	3.2	4.4	2.9
K	1.9	1.7	1.8	1.8	1.8
Na	0.0	0.1	0.1	0.0	0.0
Cl	0.0	0.0	0.0	0.0	0.1
F	0.0	0.1	0.1	0.0	0.1
OH	3.9	3.9	3.8	4.0	3.8

Table 5.5 Typical concentrations (weight %) of phlogopites from various Lumwana rocks (< = below detection limit): 1) hanging wall granite gneiss (Malundwe, 5-4 #5) 2) ore schist with cobalt (Chimiwungo, 1-27 #5) 3) lower ore schist (Chimiwungo, 1-43 #14) 4) epidote schist (Malundwe, 5-16 #3) 5) Footwall amphibolite with garnet (Chimiwungo, 2-4). Number of ions in formula is calculated on the basis of 24 oxygens (Tindle and Webb 1990) (zap # refers to raw data in appendix B3 and figure 5.11)

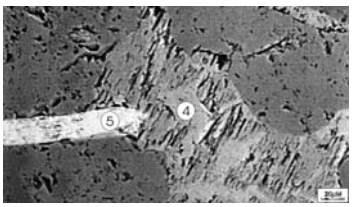

1) 5-4, zap #5

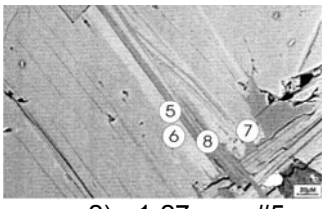

2) 1-27, zap #5

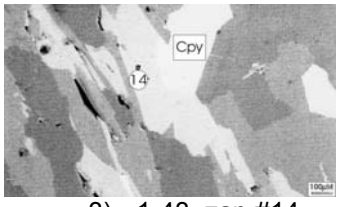

3) 1-43, zap #14

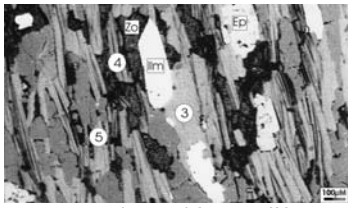

4) 5-16 zap #3

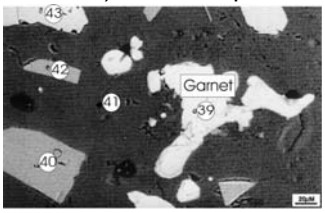

5) 2-4 zap #40

Early and late silicate phases were identified by cross-cutting relationships in samples. Where possible, the relationship to the structural fabric was also noted.

Figure 5.11 Backscattered electron images (electron microprobe) of phlogopite samples from Chimiwungo and Malundwe. 1) Light grey phlogopite crosscutting dark grey quartz and grey muscovite. 2) Dark grey S_2 chlorite overprinting grey S_1 muscovite. Locally chlorite replaced white phlogopite along cleavage planes. 3) S_1 light grey phlogopite partially overprinted by white chalcopyrite aligned with the S_2 fabric. 4) Grey phlogopite and slightly darker grey quartz define the S_1 fabric. Phlogopite is altering to fine muscovite along cleavages. 5) Grey tabular laths of phlogopite host by dark grey feldspar with white garnet (grossular) inclusions

Almost all of the analyzed phlogopites have a ratio of magnesium to iron atoms, of greater than two to one, with the exception of 2 analyses from the Chimiwungo deposit that were replacing garnet (figure 5.12).

5.3.1 Chimiwungo silicate geochemistry

At Chimiwungo, samples of the upper ore schist, ore schist and lower ore schist were selected to examine the variations within mineral phases between ore horizons. In addition samples of hanging wall kyanite schist to gneiss were selected to examine the variations between sulphide mineralized kyanite schist and barren hanging wall kyanite schist. The Internal gneiss units that separate the ore horizons were also selected including samples of garnet-amphibolite. Samples were chosen from Eq-Chi-062 with exception of 2-2 and 2-4 that are from Eq-Chi-201 (figure 5.6).

Hole Number	Sample ID	Depth	Sample type
EQ-CHI-062	1-2	104.90	Hanging wall schist
EQ-CHI-062	1-6	117.16	Hanging wall kyanite schist to gneiss
EQ-CHI-062	1-13	138.05	Upper ore schist
EQ-CHI-062	1-19	155.00	Amphibolite band with garnet
EQ-CHI-062	1-20	156.00	Amphibolite band
EQ-CHI-062	1-27	183.80	Ore schist with cobalt
EQ-CHI-062	1-30	202.86	Ore schist with garnet
EQ-CHI-062	1-32	222.52	Ore schist
EQ-CHI-062	1-41	273.00	Internal gneiss with sulphide
EQ-CHI-062	1-43	281.37	Lower ore schist
EQ-CHI-201	2-2	253.53	Internal gneiss with garnet alteration
EQ-CHI-201	2-4	257.20	Footwall amphibolite with garnet

Table 5.6 Samples analyzed with the electron microprobe from the Chimiwungo deposit

The ratio of magnesium to iron in phlogopites is consistent within samples between early and late phases, but varies between samples. Ore schist and hanging wall kyanite schist samples exhibit low X_{Fe} ratios, whereas internal gneiss units and samples mineralized with garnet exhibit higher values. Interestingly, the phlogopite X_{Fe} ratios appear to relate to the whole rock X_{Fe} ratio analyzed using XRF analysis. The downhole X_{Fe} ratio of probed muscovites from Chimiwungo also exhibit a similar trend to the whole rock XRF data (figure 5.12).

CHAPTER 5: GEOCHEMICAL CHARACTERISTICS OF THE LUMWANA DEPOSITS

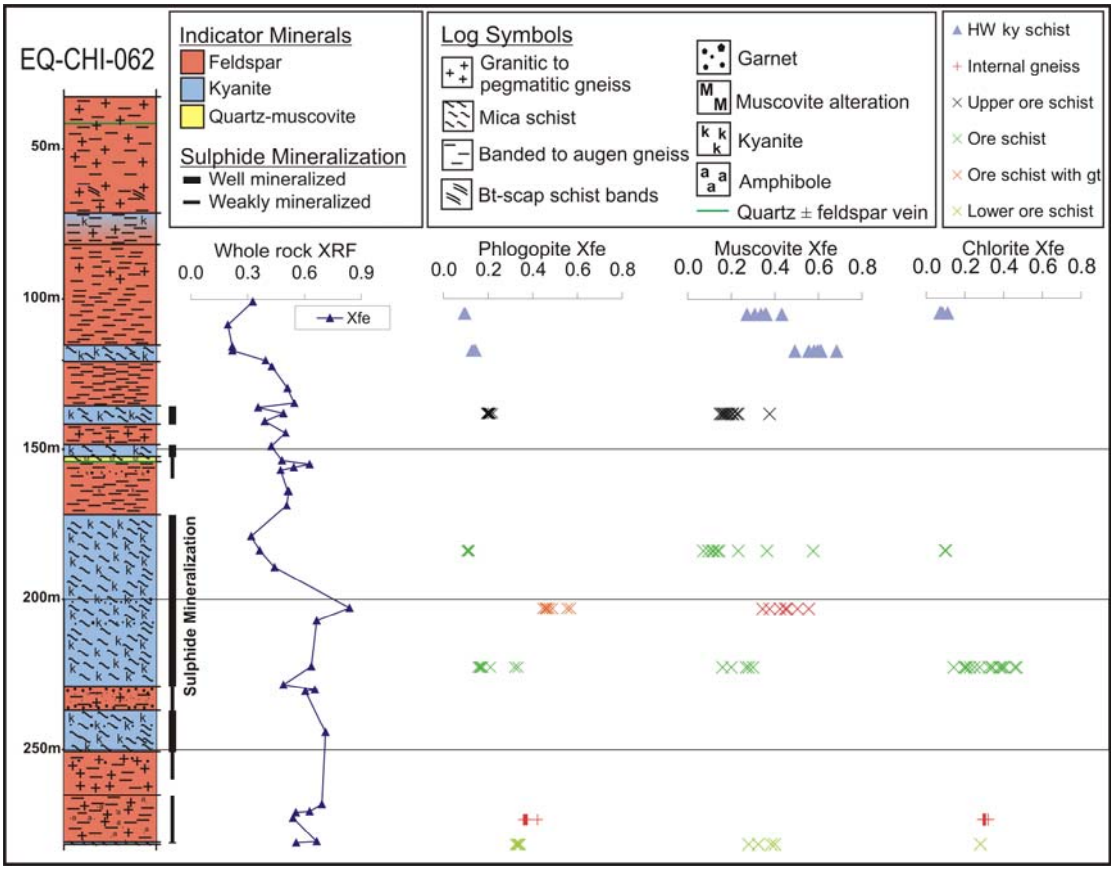

Figure 5.12 Downhole plot for whole rock X_{Fe} ratios as well as probed phlogopite, muscovite and chlorite for Chimiwungo deposit (Eq-Chi-062)

At Chimiwungo chlorite commonly replaces phlogopite and exhibits a similar downhole trend of X_{Fe} ratios. An inverse correlation between iron and magnesium is observed and the X_{Fe} ratios reflect the mineralogy of the sample with chlorite phases that cross-cut sulphide mineralization exhibiting high iron values, and hence relatively higher X_{Fe} numbers (figure 5.11 & 5.12).

Phlogopite

Although observed in all units at Chimiwungo and Malundwe, phlogopite is enriched in ore schist units and associated with sulphide. Early and late phases were identified by cross-cutting relationships and preferred orientation direction but show no significant variation in chemistry within a sample. Phlogopite of any phase in direct contact with sulphide exhibit moderately higher X_{Fe} values, indicating that iron is sequestered from the sulphide, into the silicate, during metamorphism.

CHAPTER 5: GEOCHEMICAL CHARACTERISTICS OF THE LUMWANA DEPOSITS

A	1		2	3		4
Sample	**1-2**	**1-6**	**1-13**	**1-27**	**1-32**	**1-43**
SiO_2	39.35	40.07	37.34	39.46	38.57	36.87
TiO_2	0.81	0.80	0.93	0.80	0.98	1.39
Al_2O_3	18.67	18.39	19.05	19.08	18.89	18.24
FeO	4.05	5.83	7.94	4.69	7.27	13.23
MnO	0.01	0.03	0.07	0.03	0.03	0.08
MgO	21.65	20.51	17.37	20.88	18.31	14.77
CaO	0.01	0.00	0.11	0.00	0.00	0.00
Na_2O	0.38	0.00	0.24	0.40	0.23	0.22
K_2O	9.99	8.83	9.71	9.53	9.61	9.73
BaO	0.05	0.05	0.08	0.08	0.12	0.10
F	0.69	0.45	0.17	0.15	0.00	0.25
Cl	0.07	0.11	0.19	0.03	0.14	0.18
Total	95.80	95.18	93.24	95.37	94.42	95.31
N	6	13	12	11	12	8

B	5	6		7	8
Sample	**1-30**	**1-19**	**1-41**	**2-2**	**2-4**
SiO_2	36.28	37.53	36.98	36.48	35.89
TiO_2	1.62	1.58	1.47	1.71	1.63
Al_2O_3	18.98	16.91	16.52	16.15	16.44
FeO	18.26	15.82	15.04	20.14	18.22
MnO	0.05	0.11	0.11	0.16	0.09
MgO	10.87	13.40	14.31	11.20	12.40
CaO	0.00	0.00	0.00	0.00	0.02
Na_2O	0.00	0.00	0.17	0.15	0.12
K_2O	9.05	9.55	9.89	9.68	9.52
BaO	0.10	0.10	0.10	0.10	0.10
F	0.18	0.11	0.28	0.26	0.23
Cl	0.15	0.50	0.17	0.26	0.26
Total	95.71	95.87	95.20	96.42	95.10
N	9	5	13	2	3

Table 5.7 Mean average phlogopite microprobe data for selected samples from Chimiwungo. 1) Hanging wall kyanite schist to gneiss. 2) Upper ore schist. 3) Ore schist 4) Lower ore schist. 5) Ore schist with garnet. 6) Internal gneiss. 7) Internal gneiss garnet-amphibolite. 8) Lower ore schist garnet-amphibolite. (Samples are from Eq-Chi-062 with exception of 2-2 and 2-4 that are from Eq-Chi-201)

Iron and Magnesium values of probed phlogopites from the Chimiwungo deposit show a broadly inversely proportional relationship. Ore schist phlogopites exhibit a range of mean average iron values of 4.69 to 7.94 with the exception of the lower ore schist and the ore schist with garnet that have mean values of 13.23 and 18.26 wt % respectively. The internal gneiss units and footwall gneiss units show high mean average iron values that are similar to the lower ore schist and ore schist with garnet and range from 15.04 in the

internal banded gneiss to 20.14 in the internal gneiss garnet-amphibolite (table 5.7 and figure 5.13).

The mean average magnesium values for Chimiwungo probed phlogopites are highest in the hanging wall kyanite schist to gneiss units and ore schist units with values of 20.51 to 21.65 and 17.37 to 20.88 wt % magnesium respectively. The lower ore schist and internal gneiss units exhibit lower magnesium values of 10.87 to 14.77 wt %, a function of the inverse proportional relationship between iron and magnesium (table 5.7 and figure 5.13).

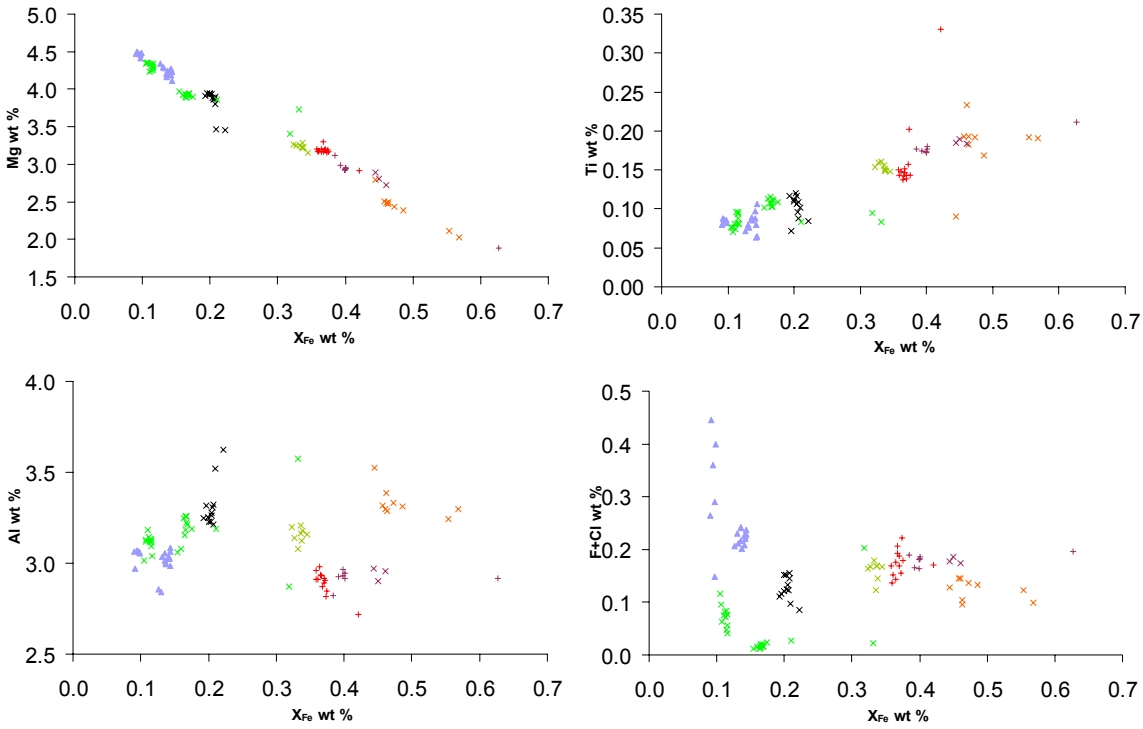

Figure 5.13 Phlogopite plots for Chimiwungo using calculated weight percent values. Key shown on figure 5.12

Titanium values of phlogopites are low in the hanging wall with a mean average of 0.80 to 0.81 compared to 0.80 to 0.98 wt % in the ore schist. Lower ore schist and ore schist with garnet samples have values of 1.39 and 1.62 wt % TiO_2 respectively and are similar to the internal gneiss units that exhibit values ranging from 1.47 to 1.71 wt % TiO_2 (table 5.7 and figure 5.13).

Mean average aluminium values for probed phlogopite from the Chimiwungo deposit show little variation between hanging wall kyanite schist to gneiss

units and ore schist including the lower ore schist and ore schist with garnet, with values ranging from 18.24 to 19.08 wt % Al_2O_3. The internal gneiss garnet-amphibolite units exhibit a lower mean average values of 16.15 to 16.91 wt % Al_2O_3 (table 5.7 and figure 5.13).

The halogen content of phlogopite can be used to discriminate between styles of alteration and high fluorine phlogopites have been observed associated with sulphide mineralization at Nchanga. However, at Chimiwungo little variation is observed in fluorine with values ranging from 0 to 0.28 wt % although higher values of 0.45 to 0.69 wt % were observed in the hanging wall kyanite schist to gneiss units. Mean average chlorine values are also low at Chimiwungo with values ranging from 0.03 to 0.26 although higher values are observed in one internal gneiss unit of 0.50 wt % (table 5.7).

Figure 5.13 shows calculated total halogen values plotted against X_{Fe} ratio for probed phlogopites from the Chimiwungo deposit. Little variation is observed in total halogen content although the hanging wall kyanite gneiss does show higher values as a result of the increase in the mode of fluorine.

Muscovite

Early and late phases of muscovite were probed from Chimiwungo. Figure 5.14 shows plots of calculated element weight percent against X_{Fe} ratio for probed muscovite from the Chimiwungo deposit. The concentration of potassium correlates with the X_{Fe} ratio with high iron contents responding to low potassium. Magnesium values show variation within individual samples whereas iron exhibits little variation in probed muscovite, except where muscovite cross-cuts sulphide or garnet, resulting in higher iron values. Muscovite laths with a relatively higher mode of magnesium are observed replacing phlogopite. Muscovite also exhibits fluorine-sodium avoidance. Fluorine bearing muscovites are mainly observed in ore schist with garnet, although one example was analysed from a hanging wall kyanite schist (sample 1-6) (figure 5.14).

CHAPTER 5: GEOCHEMICAL CHARACTERISTICS OF THE LUMWANA DEPOSITS

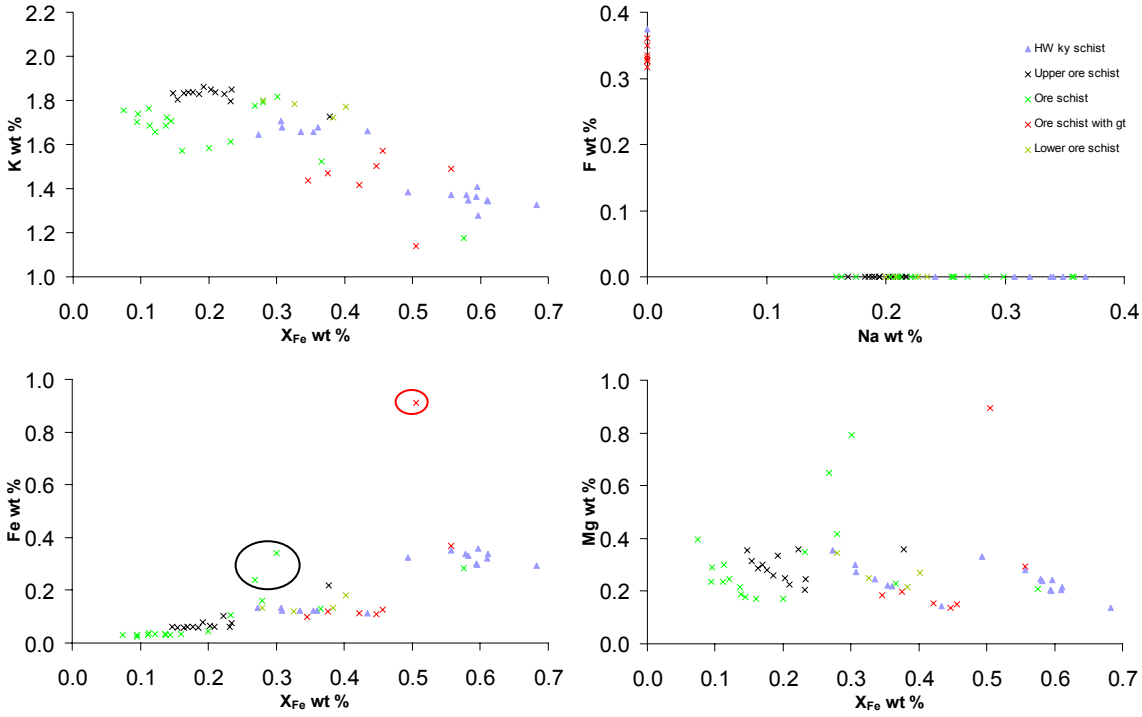

Figure 5.14 Muscovite plots for Chimiwungo using calculated weight percent values. Black circle represents muscovite cross-cutting sulphide; Red circle represents muscovite cross-cutting garnet

Chlorite

The hanging wall kyanite schist to gneiss samples exhibit the highest magnesium values of approximately 8 to 8.5 wt % whereas ore schist samples have a range of magnesium values from approximately 5 to 8 wt %. Chlorites probed from internal gneiss samples exhibit magnesium values ranging from approximately 5.8 to 6.8 wt % (figure 5.15).

Figure 5.16 shows two species of chlorite present at Chimiwungo, sheridanite within the hanging wall and ore schist samples and ripidolite within the internal gneiss and ore schist samples.

CHAPTER 5: GEOCHEMICAL CHARACTERISTICS OF THE LUMWANA DEPOSITS

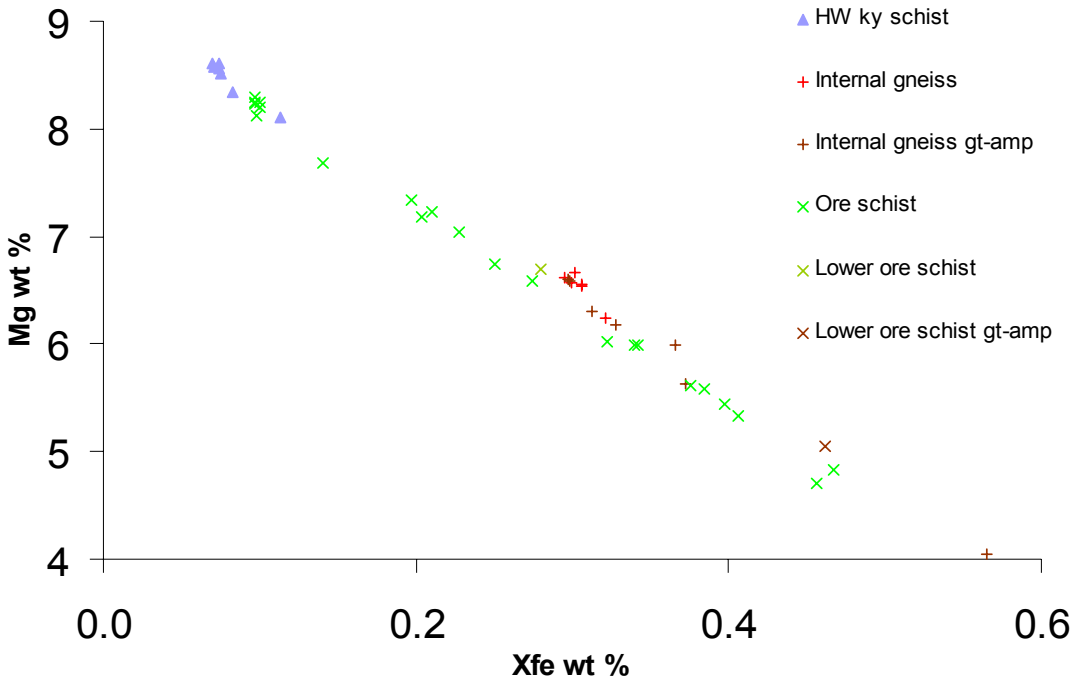

Figure 5.15 Probed chlorite data for Chimiwungo using calculated weight percent values

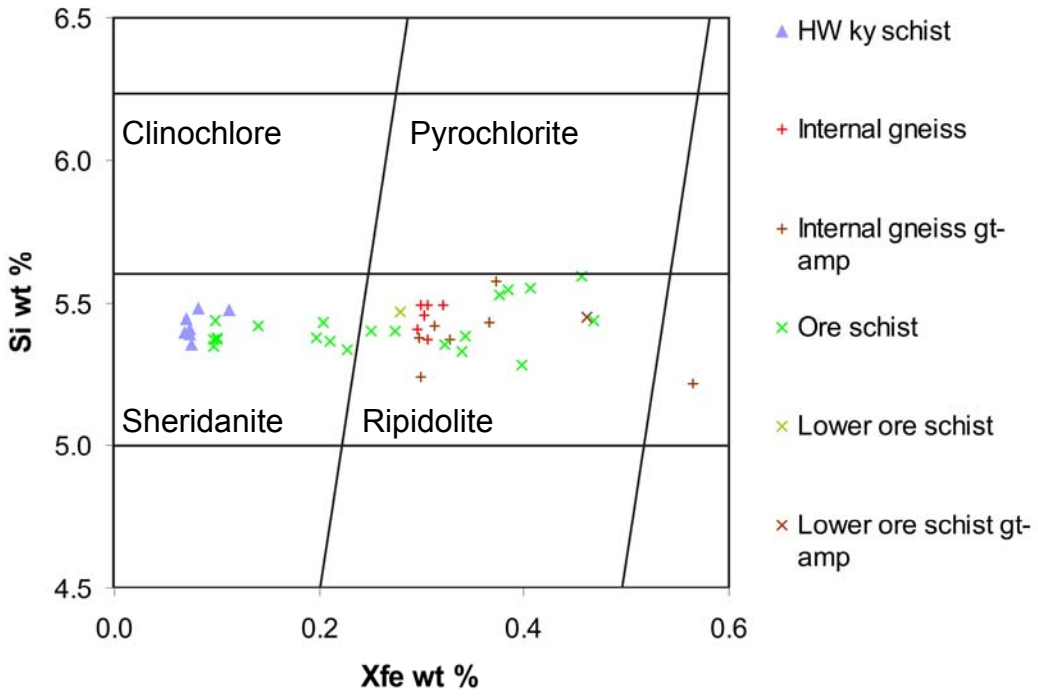

Figure 5.16 Hey diagram for the Chimiwungo deposit using calculated weight percent values

CHAPTER 5: GEOCHEMICAL CHARACTERISTICS OF THE LUMWANA DEPOSITS

5.3.2 Malundwe silicate geochemistry

At Malundwe samples probed from the hanging wall consist of gneiss with phlogopite alteration, augen gneiss with epidote alteration and phlogopite schist. Ore schist samples probed included ore schist, ore schist with garnet, and ore schist with quartz phlogopite alteration. Footwall samples analyzed with the electron microprobe included kyanite schist, kyanite schist with epidote and epidote schist (table 5.8, 5.9 and figure 5.17).

Hole Number	Sample ID	Depth	Sample type
EQ-MAL-094	5-2	57.28	Hanging wall granite gneiss + phlogopite alteration
EQ-MAL-094	5-3	65.86	Hanging wall granite gneiss + phlogopite alteration
EQ-MAL-094	5-4	67.88	Hanging wall granite gneiss + phlogopite-epidote alteration
EQ-MAL-094	5-5	70.37	Hanging wall phlogopite-quartz schist
EQ-MAL-094	5-7	82.63	Ore schist (bornite-chalcopyrite)
EQ-MAL-094	5-10	90.44	Ore schist with coarse muscovite-quartz band
EQ-MAL-094	5-11	91.80	Ore schist with garnet
EQ-MAL-094	5-12	95.84	Ore schist with quartz-phlogopite alteration
EQ-MAL-094	5-13	97.96	Footwall kyanite schist with chloritic alteration
EQ-MAL-094	5-15	100.55	Footwall kyanite schist
EQ-MAL-094	5-16	112.97	Epidote schist

Table 5.8 Samples analyzed with the electron microprobe from the Malundwe deposit

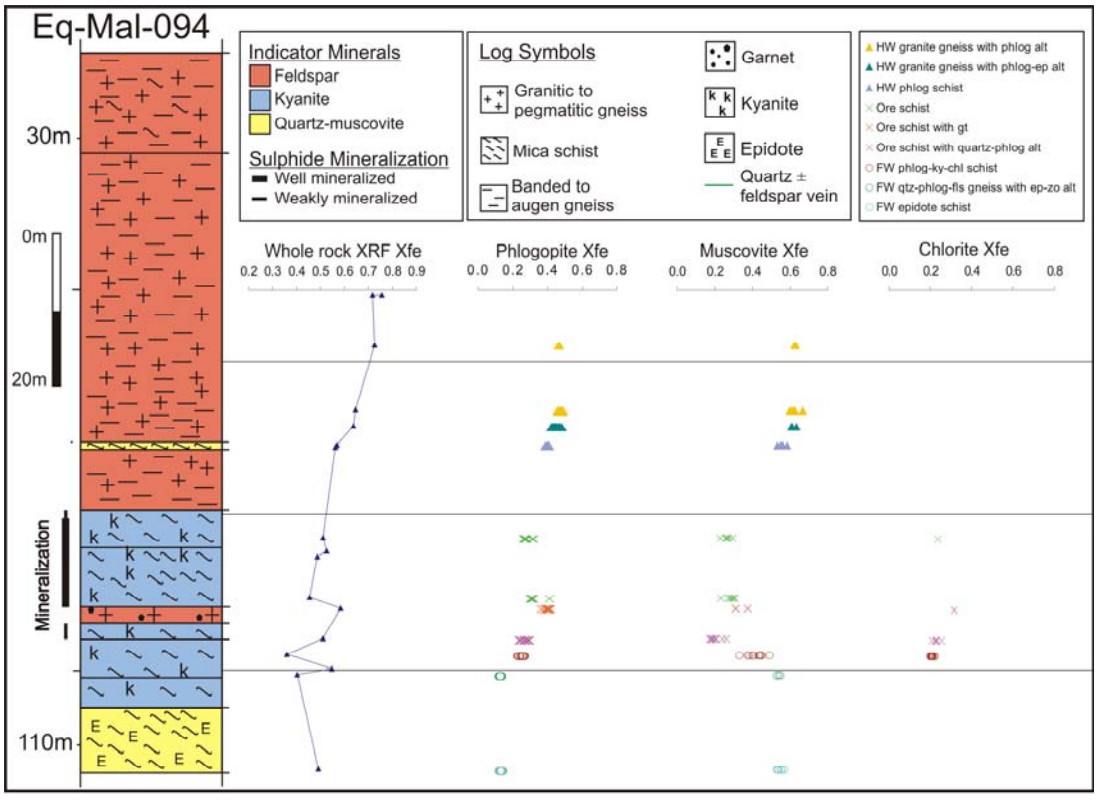

Figure 5.17 Downhole plot for whole rock X_{Fe} ratios as well as probed phlogopite, muscovite and chlorite for ore and host rock units of the Malundwe deposit (Eq-Mal-094)

Phlogopite

As observed at Chimiwungo the downhole trend of the X_{Fe} ratios for phlogopite are similar to the X_{Fe} ratios of the whole rock XRF analyses (figure 5.17).

A	1		2	3
Sample	**5-2**	**5-3**	**5-4**	**5-5**
SiO_2	36.47	36.17	36.53	36.67
TiO_2	2.29	2.60	2.25	2.11
Al_2O_3	16.43	15.77	15.76	16.10
FeO	17.69	18.04	17.54	15.64
MnO	0.11	0.12	0.13	0.09
MgO	11.65	11.22	12.03	12.97
CaO	0.00	0.00	0.00	0.01
Na_2O	0.04	0.09	0.00	0.14
K_2O	10.22	10.17	9.84	10.22
BaO	0.04	0.07	0.11	0.11
F	0.48	0.39	0.07	0.22
Cl	0.20	0.21	0.17	0.16
Total	95.78	94.98	94.59	94.60
N	1	22	10	11

B	4		5	6	7	8	9
Sample	**5-7**	**5-10**	**5-11**	**5-12**	**5-13**	**5-15**	**5-16**
SiO_2	37.22	37.29	37.34	37.37	36.90	41.27	38.83
TiO_2	1.14	1.10	1.50	1.11	1.17	1.17	1.37
$Al2O_3$	18.65	19.12	17.68	18.99	18.67	20.27	17.13
FeO	10.95	12.28	12.72	10.66	9.72	5.26	5.49
MnO	0.03	0.08	0.08	0.06	0.02	0.05	0.08
MgO	15.62	15.42	15.08	16.22	16.56	16.04	20.18
CaO	0.00	0.00	0.01	0.00	0.00	0.05	0.06
Na_2O	0.29	0.00	0.15	0.21	0.32	0.15	0.12
K_2O	9.47	9.42	9.66	9.82	9.32	10.14	9.75
BaO	0.08	0.06	0.09	0.08	0.14	0.10	0.13
F	0.31	0.21	0.25	0.18	0.45	0.00	0.00
Cl	0.18	0.20	0.18	0.24	0.23	0.10	0.12
Total	94.30	95.36	94.91	95.10	93.67	94.73	93.40
N	8	8	13	17	8	8	8

Table 5.9 mean average microprobe data for selected samples from Malundwe. 1) Hanging wall gneiss with phlogopite alteration. 2) Hanging wall augen gneiss with epidote alteration 3) Hanging wall phlogopite schist. 4) Ore schist. 5) Ore schist with garnet. 6) Ore schist with quartz phlogopite alteration. 7) Footwall kyanite schist. 8) Footwall kyanite schist with epidote. 9) Footwall epidote schist.

At Malundwe the hanging wall phlogopites exhibit higher X_{Fe} ratios than the ore schist, a result of a higher mode of iron than magnesium in the hanging wall whereas the ore schist and footwall phlogopites exhibit a higher mode of

magnesium than iron. The probed phlogopites from the footwall samples at Malundwe exhibit the same relationship to a greater degree with higher modes of magnesium and lower modes of iron than both the ore schist and hanging wall phlogopites, (table 5.9 and figure 5.17).

Malundwe phlogopites exhibit a higher mode of titanium than at Chimiwungo, with mean average values of up to 2.6 wt % TiO_2. As observed at Chimiwungo high titanium values correspond to high iron values. The hanging wall phlogopites probed at Malundwe exhibit a narrow range of calculated aluminum weight percent values (figure 5.18).

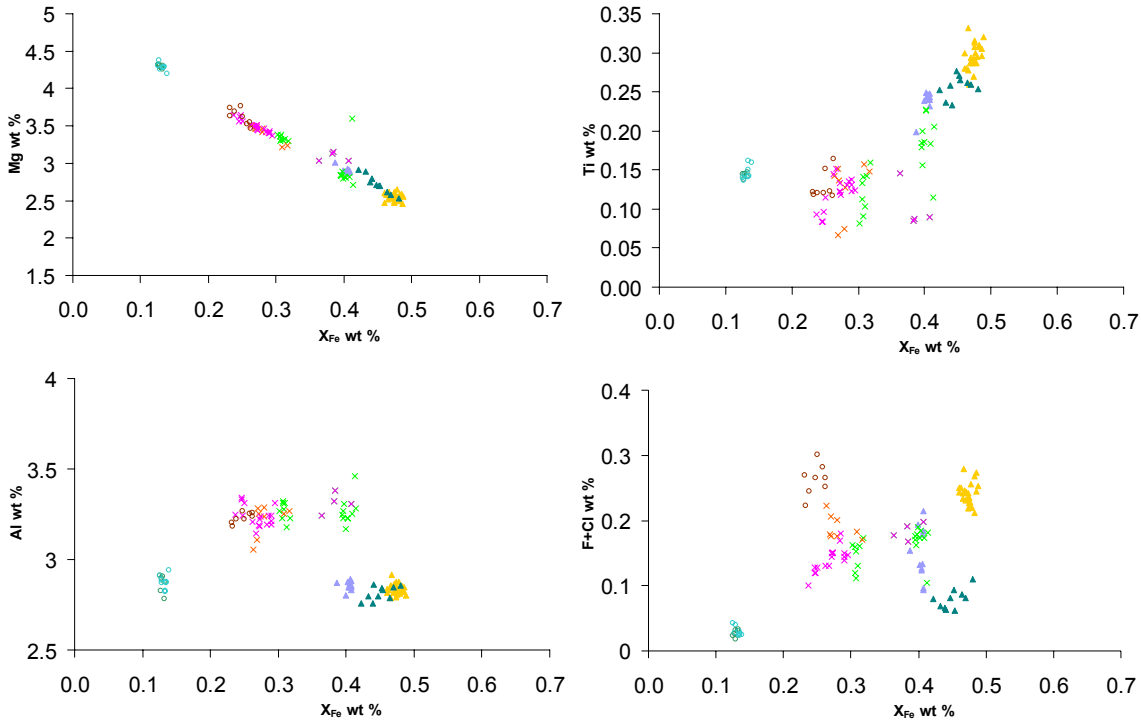

Figure 5.18 Probed phlogopite plots for Malundwe using calculated weight percent values (key shown in figure 5.17)

The aluminum values, when plotted against the X_{Fe} ratio, form distinct groups with hanging wall phlogopites exhibiting low aluminium values when compared to the ore schist and footwall with the exception of phlogopites probed from the footwall epidote schist and the foot wall kyanite schist with epidote that also exhibit low aluminum values. The total halogen content of phlogopites probed at Malundwe are plotted against the X_{Fe} ratio and although variations are observed within samples this does not correspond to different

phases of mineralization and no high fluorine phlogopites are observed (table 5.9 and figure 5.18).

Muscovite

Muscovite probed from Malundwe exhibit many similar geochemical traits to the muscovite probed at Chimiwungo including a similar downhole X_{Fe} ratio to phlogopite and whole rock XRF data (figure 5.17) and fluorine-sodium avoidance (figure 5.19).

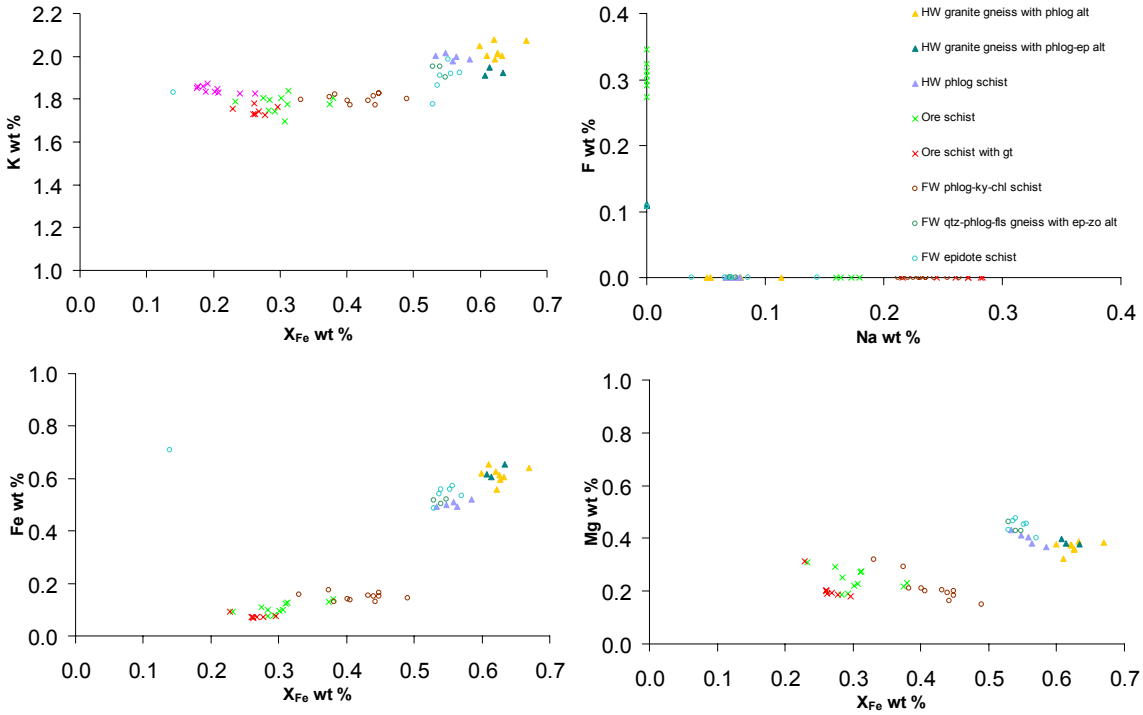

Figure 5.19 Probed muscovite plots for Malundwe using calculated weight percent values

The calculated potassium weight percent of probed muscovite from the Malundwe deposit exhibit a narrow band of values when compared to Chimiwungo with values ranging from approximately 1.7 to 2.1 wt % (figure 5.19).

Two phases of muscovite mineralization are geochemically discernable at Malundwe although can not be attributed to a metamorphic event as no variations in crystal morphology or structural orientation where observed. Ore schist muscovites are characteristically low in magnesium and iron which is also a characteristic of muscovite probed from the Malundwe footwall kyanite

schist. Muscovite probed from samples of the hanging wall schist and gneiss units as well as the epidote schist and kyanite schist with epidote alteration exhibit higher magnesium and iron values. The probed muscovite potassium values from Malundwe are higher in the hanging wall gneiss and schist units than the hanging wall schist to gneiss units at Chimiwungo.

Chlorite

Chlorite phases probed at Malundwe are also commonly observed replacing phlogopite and have an inverse correlation between iron and magnesium. Chlorite at Malundwe show a more restricted range with less variation in X_{Fe} values than at Chimiwungo, which may be a result of the sample selection, with no chlorite observed in the Malundwe hanging wall samples. Footwall kyanite schist samples exhibit lower X_{Fe} ratios (figure 5.17).

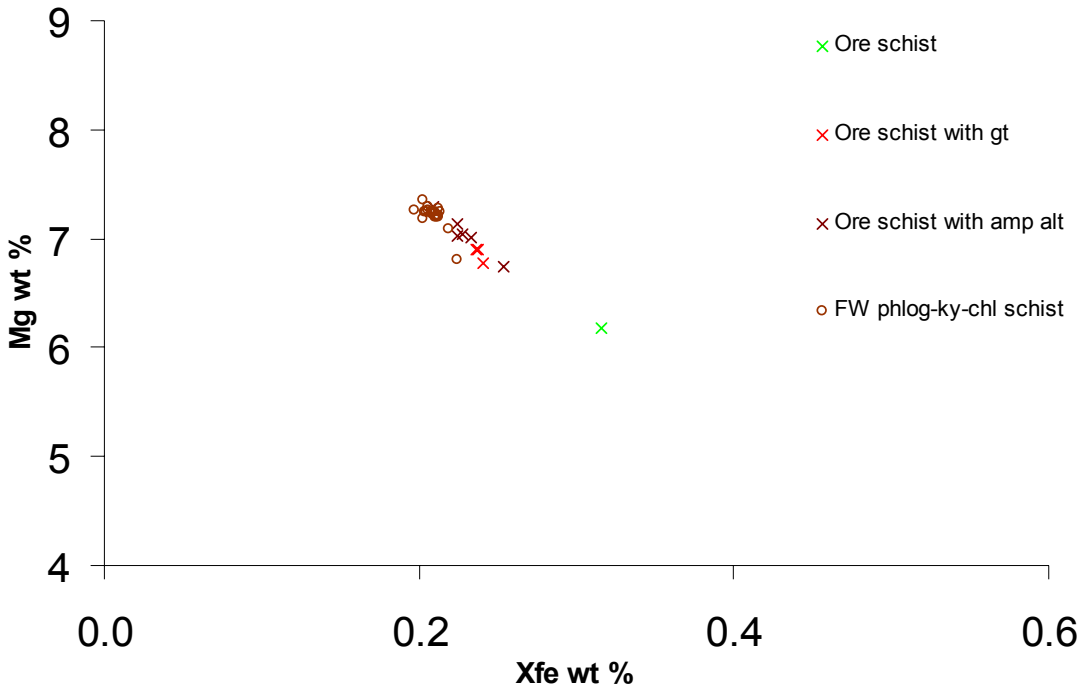

Figure 5.20 Probed chlorite plots for Malundwe using calculated weight percent values

Calculated magnesium values for chlorite from the Malundwe deposit exhibit less range than at Chimiwungo with approximate values ranging from 6 to 7.5 weight percent (figure 5.20).

CHAPTER 5: GEOCHEMICAL CHARACTERISTICS OF THE LUMWANA DEPOSITS

As observed at Chimiwungo, two species of chlorite are observed sheridanite, within the footwall kyanite schist and ore schist and ripidolite within the ore schist and ore schist with garnet (figure 5.21)

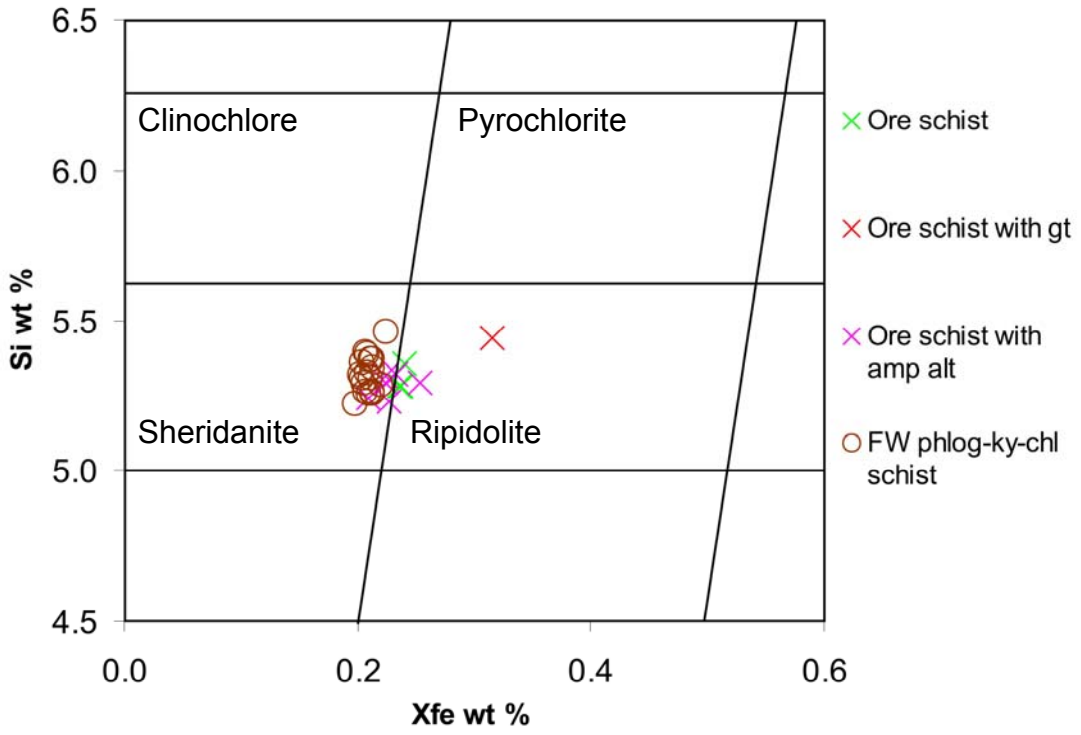

Figure 5.21 Hey diagram for Malundwe deposit using calculated weight percent values

5.3.3 Garnet and amphibole

Through electron microprobe analysis, the majority of the garnet probed at Malundwe and Chimiwungo has been identified as almandine ($Fe_3Al_2(SiO_4)_3$), although one grain of pyrope ($Mg_3Al_2(SiO_4)_3$) (sample 2-2) and one grain of grossular ($Ca_3Al_2(SiO_4)_3$) (sample 2-4, figure 5.11) were identified within the Chimiwungo internal gneiss amphibolites and footwall amphibolites respectively (figure 5.22).

Amphibole analyzed from the ore and host rock assemblages of the Chimiwungo deposit have been identified as gedrite, pargasite, tschermakite and hornblende that indicate pressures ranging from 8.3 to 11.8Kbars. Amphiboles exhibit fluorine-sodium avoidance and amphibole within the ore schist exhibit the highest total halogens.

CHAPTER 5: GEOCHEMICAL CHARACTERISTICS OF THE LUMWANA DEPOSITS

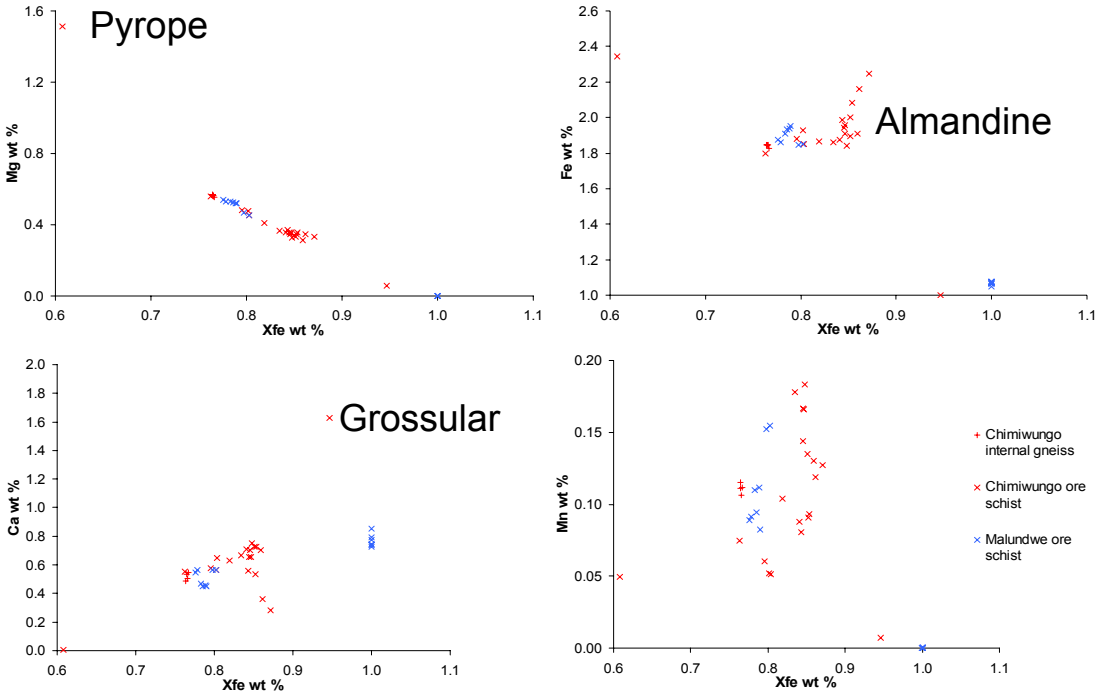

Figure 5.22 Calculated element weight percent plots for garnets analyzed from Chimiwungo and Malundwe

5.4 Stable Isotope Analysis

Sulphur isotope studies were carried out on sulphide minerals from the Chimiwungo and Malundwe deposits using the isotope facilities at the Scottish Universities Environmental Research Centre (SUERC). The aim of the investigation was to determine the source of the sulphur component and investigate the mechanisms of ore formation in both deposits. This would facilitate a comparison between the new $\delta^{34}S$ data and the existing data from the Copperbelt deposits, as well as with the typical sulphur isotope compositions in nature.

5.4.1 Sample selection and method

$\delta^{34}S$ analysis on the cores of 15 sulphide samples from Chimiwungo and 11 from Malundwe were selected to represent the various styles of sulphide mineralization observed in the deposits. In addition, 2 examples of background pyrite from the Malundwe footwall amphibolites were selected.

CHAPTER 5: GEOCHEMICAL CHARACTERISTICS OF THE LUMWANA DEPOSITS

In total, selected samples included sulphides from the main ore horizons, background pyrite from unmineralized samples, and quartz vein hosted sulphides that cross-cut both the mineralization and the barren gneiss units.

The four sulphides sampled in this analysis were pyrite, pyrrhotite, chalcopyrite and bornite and where possible specific minerals were selected for analysis. However, this was problematic as primary sulphides commonly exhibit exsolution textures and can be replaced by minor secondary digenite and covellite.

Conventional sulphur isotope analyses of hand-picked sulphide separates were performed following the standard technique of Robinson and Kusakabe (1975), as well as extraction of more massive sulphides using a dentist's drill. In addition, use of the in situ laser combustion system allowed greater resolution of sampling, to sub-millimetric levels on polished samples. Typically samples were rastered under the laser beam to combust individual zones extending around 500 µm by 100 µm following the technique described in detail by Kelley and Fallick (1990) and Wagner *et al.* (2002).

Determination of the sulphur isotope composition of the purified SO_2 gas from both techniques were carried out on a VG SIRA II gas mass spectrometer. The reference gas in the mass spectrometer was calibrated by running a suite of international and lab standards regularly through the system. The standards employed were the international standards NBS-123 and IAEA-S-3, and SUERC standard CP-1. These gave $\delta^{34}S$ values of +6.3‰, -36.5‰ and -12.8‰ respectively, with 1σ reproducibility around ±0.2‰ at the time of these analyses.

Data are reported in $\delta^{34}S$ notation as per mil (‰) variations from the Vienna Canyon Diablo Troilite (V-CDT) standard. A mineral specific sulphur isotope fractionation between the host mineral and the SO_2 gas produced via combustion (Kelley and Fallick 1990). Fractionation corrections for pyrite (raw gas $\delta^{34}S$ +0‰), chalcopyrite (raw gas $\delta^{34}S$ +0‰) and bornite (raw gas $\delta^{34}S$

+0.3‰) were determined experimentally through comparison with conventionally drilled material from the same block.

5.4.2 Results

A total of fifty six $\delta^{34}S$ values have been obtained by both conventional and in situ laser analysis (appendix B4). All results plotted together give a broad range of values from +2.3 to +18.5‰ with background pyrite ranging in values from +3.9 to +6.2‰, sulphide samples from the Malundwe deposit ranging from +5.6 to +15.2‰, whereas Chimiwungo has a broader range of values of +2.3 to +18.5‰ (figure 5.23).

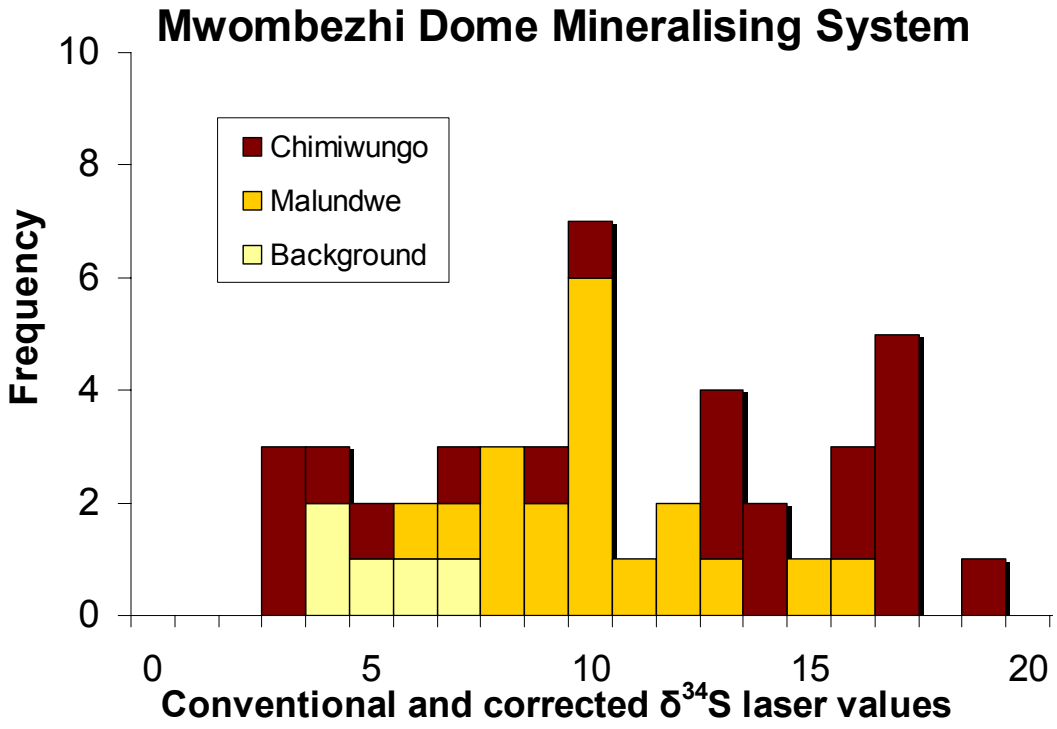

Figure 5.23 Conventional s-line and corrected $\delta^{34}S$ laser values for Chimiwungo Malundwe and background sulphide analysis

At Chimiwungo, the full range of $\delta^{34}S$ values are observed in the main ore schist unit, whereas the upper ore schist has a range of $\delta^{34}S$ values from +3.0 to +15.7 and the lower ore schist has a range of +6.9 to 8.3‰. Sulphides hosted by cross-cutting quartz veins exhibit a range of values from +3 to +16.5‰. Variations in $\delta^{34}S$ are observed within hand specimen sample indicating that the process of metamorphic homogenization has had little effect on the sulphides analyzed from Lumwana.

5.4.3 Discussion

The aim of this study was to test the hypothesis that the Chimiwungo and Malundwe deposits are the result of epigenetic alteration, shearing and mineralization of pre-Katangan basement due to thermochemical sulphate reduction (TSR) rather than syngenetic mineralization due to bacteriogenic sulphate reduction (BSR) (figure 5.24).

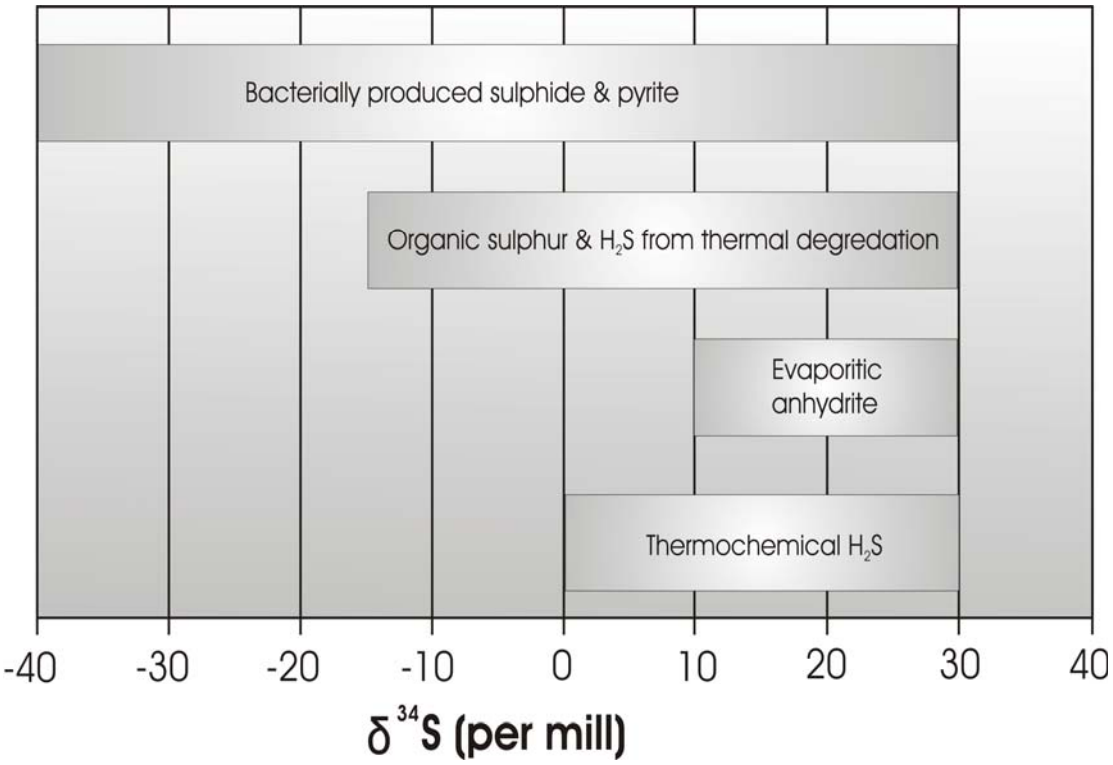

Figure 5.24 The $\delta^{34}S$ signature of various sulphur sources and sulphides (Emery & Robinson, 1993)

Malundwe has one dominant ore horizon whereas Chimiwungo has three, and given previous studies in the Copperbelt, a variation in $\delta^{34}S$ values between the ore horizons at Chimiwungo was anticipated due to the fractionation of the ore during the migration of the mineralizing fluid (figure 5.25). However, at Chimiwungo, no fractionation could be observed between the ore horizons.

The range of $\delta^{34}S$ values measured from Lumwana fall within the range of values measured from the Copperbelt of -17 to +23‰ (McGowan *et al.* 2006). Sediment-hosted copper deposits exhibit a wide range of $\delta^{34}S$ values from -22‰ to +12‰ at White Pine and -44‰ to -2‰ at the Kupferschiefer and indicate that bacteriogenic reduction of sulphate is an important mechanism for ore formation (Gustafson & Williams, 1981) (figure 5.26).

CHAPTER 5: GEOCHEMICAL CHARACTERISTICS OF THE LUMWANA DEPOSITS

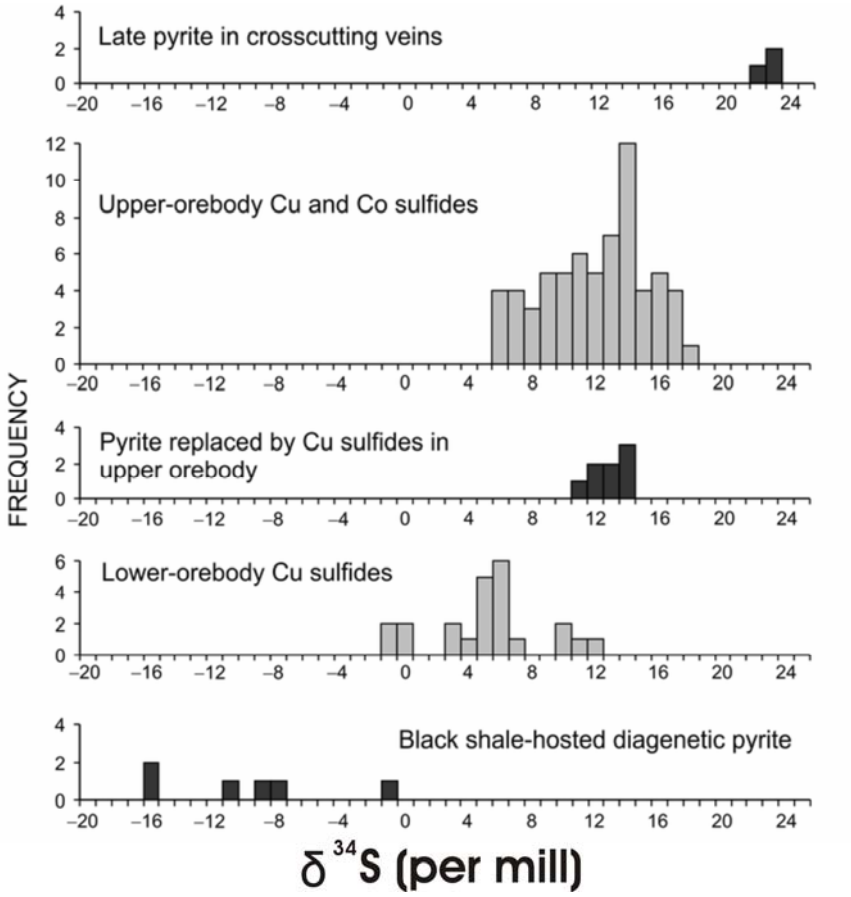

Figure 5.25 Frequency histograms to show results of conventional and laser sulphur isotope analyses of paragenetically different sulphides from Nchanga. CDT— Cañon Diablo troilite (After McGowan *et al*. 2003)

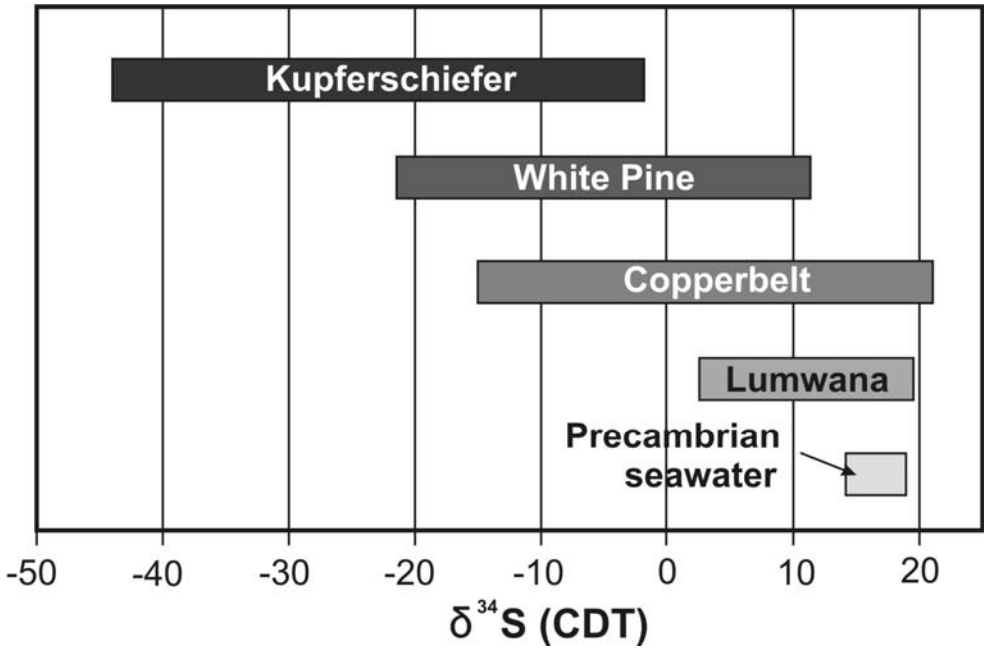

Figure 5.26 $\delta^{34}S$ data for various Copperbelt deposits as well as for the Kupferschiefer and White Pine sediment-hosted copper deposits and calculated $\delta^{34}S$ value of Precambrian seawater (After McGowan, 2003).

CHAPTER 5: GEOCHEMICAL CHARACTERISTICS OF THE LUMWANA DEPOSITS

The mechanism of ore formation at Lumwana is interpreted as thermochemical sulphate reduction (TSR), indicated by the relatively heavy $\delta^{34}S$ values and the absence of the light bacteriogenic $\delta^{34}S$ values observed in the Copperbelt. This supports the hypothesis that the Chimiwungo and Malundwe deposits are the result of epigenetic alteration, shearing and mineralization of pre-Katangan basement The Lumwana sulphides exhibit variations in $\delta^{34}S$ values within individual hand specimens suggesting that these heavy results are not the result of metamorphic homogenisation. Existing sulphur isotope data, in light of the data obtained during this study, are discussed in more detail in Chapter 6.

CHAPTER 6: DISCUSSION

6.1 Discussion of the geochemical results and observations

With respect to the new data presented here, the discussion examines the geochemical characteristics of the Malundwe deposit with those of the Chimiwungo deposit. In order to test the hypothesis made by previous authors (Benham *et al.* 1976; McGregor 1965) that the Lumwana deposits represent "Copperbelt Style" mineralization, a comparison has been made between the whole rock geochemistry of the Lumwana deposits and the Zambian Copperbelt (Nchanga). In addition, the relationship of the silicate phases to the sulphide mineralization and the sulphur isotope analysis are discussed.

6.1.1 Geochemical characteristics of the Lumwana deposits

The hanging wall gneiss from Malundwe (5-1b) and Chimiwungo (1-11) are geochemically similar supporting the interpretation that they are both units of the Mwombezhi Dome basement. The Malundwe hanging wall gneiss shows minor enrichment in sodium, calcium and strontium (figure 6.1 A).

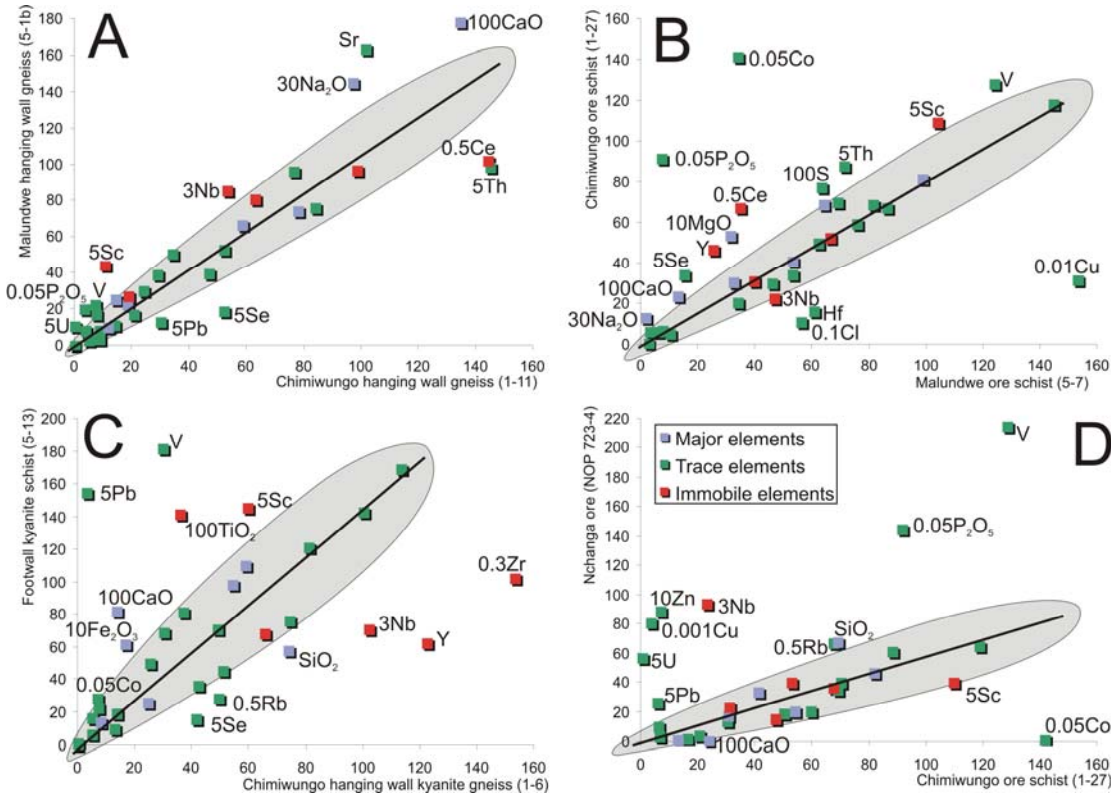

Figure 6.1 Selected isocon plots for Chimiwungo, Malundwe and the Zambian Copperbelt (Nchanga) (after Grant 1986). Blue squares are major elements (%). Green squares are trace elements (ppm). A summary of graphs is shown in table 6.1 (Nchanga data after McGowan 2003)

CHAPTER 6: DISCUSSION

The ore schist at Malundwe (5-7) and Chimiwungo (1-27) also correlate well supporting the theory that there is little variation in their protolith. The Chimiwungo is enriched in cobalt reflecting the observation that cobalt phases are not present at Malundwe. The Malundwe ore schist sample is relatively enriched in copper reflecting the higher grade of copper mineralization (6.1 B).

	X	Increased mode	Y	Increased mode	Correlation
A	**(1-11)**	Th, Se, Pb, Ce	**(5-1b)**	CaO, Na_2O, Sr, P_2O_5, V, U, Sc, Nb	SiO_2, Al_2O_3, Fe_2O_3, MgO, K_2O, S, Cl, MnO, Cu, Co, Cr, Ni, Ba, Rb, Hf, La, Sb, Ga, TiO_2, Zr, Y
B	**(5-7)**	Cu, Cl, Hf, Nb	**(1-27)**	MgO, CaO, Na_2O, Co, Th, P_2O_5, V, S, Se, Ce, Y, Sc	SiO_2, Al_2O_3, Fe_2O_3, K_2O, MnO, Cr, Ni, Pb, Ba, Rb, Sr, U, La, Sb, Ga, TiO_2, Zr
C	**(1-6)**	SiO_2, Rb, Se, Nb, Zr, Y	**(5-13)**	CaO, Fe_2O_3, Pb, V, Co, TiO_2, Sc	Al_2O_3, MgO, K_2O, Na_2O, S, Cl, MnO, P_2O_5, Cu, Cr, Ni, Ba, Sr, Hf, Th, U, La, Sb, Ga, Ce
D	**(1-27)**	CaO, Co, Sc	**(NOP 723-4)**	SiO_2, Rb, P_2O_5, V, Zn, Cu, U, Pb, Nb	Al_2O_3, Fe_2O_3, MgO, K_2O, Na_2O, S, Cl, MnO, Cr, Ni, Ba, Sr, Hf, Th, La, Sb, Se, Ga, TiO_2, Zr, Y, Ce

Table 6.1 Relative element concentrations between XRF analysed Malundwe and Chimiwungo samples as well as Nchanga ore sample from the Zambian Copperbelt. Blue denotes major elements, green trace elements and red immobile elements (Nchanga data from McGowan 2003).

Isocon plot 6.1 C compares the hanging wall kyanite schist (1-6) sampled from Chimiwungo with the footwall kyanite gneiss of the Malundwe footwall. The hanging wall kyanite schist exhibits an apparent enrichment in silica reflecting the higher mode of quartz. The footwall kyanite schist is relatively enriched in calcium and iron. In isocon plot 6.1 D a Chimiwungo ore schist sample (1-27) is compared to Copperbelt mineralization from Nchanga (NOP 723-4).

The sulphide mineralization from both deposits is geochemically similar with aluminium, magnesium, potassium, sodium and iron plotting on the isocon. The Chimiwungo ore is relatively enriched in calcium, cobalt and scandium. Copper, zinc, vanadium, uranium and lead are enriched in the Nchanga Ore, an association that has also been described in the Copperbelt (McGowan 2003). No whole rock data was available to compare the Lumwana mineralization to the basement hosted copper deposits of the Kafue Anticline.

CHAPTER 6: DISCUSSION

6.1.2 Relationship of silicate phases to sulphide mineralization

Textural relationships between silicate and sulphide phases of the Lumwana deposits suggest that sulphide mineralization is associated with widespread pre-Lufilian metasomatism resulting in the break down of feldspar and the formation of phlogopite.

Several studies of metamorphosed ore deposits have documented distinct variations in oxide, sulphide and silicate mineralogies in and around metamorphosed ore deposits (Nesbitt 1986). Sulphur and oxygen from massive sulphide deposits react with the iron component of ferromagnesian silicates or oxides to produce more magnesium or zinc rich varieties in proximity to ore (Spry 2000). At Lumwana, silicates observed overprinting sulphide typically exhibit higher iron values although locally phlogopite alters to high magnesium chlorite. The phlogopites with highest mode of magnesium at Lumwana are observed in the footwall of the Malundwe deposit, which may represent an oxidation halo around the footwall quartzite, due to its high hematite-magnetite content. At Lumwana no sulphidation haloes are observed around the mineralization indicating that the silicate geochemistry is not a vector to the sulphide mineralization.

The transitional contacts between host rock and ore schist reflect a basement gneiss protolith that is altered to the ore schist. The alteration is observed in thin-section and reflected in the XRF geochemistry by the loss of plagioclase ($(Na,Ca)(Si,Al)_4O_8$) and scapolite $(Na,Ca)_4[Al_3Si_9O_{24}]Cl$ with increased alteration. Microcline ($KAlSi_3O_8$) is also removed but potassium is buffered by the increased mode of muscovite ($KAl_2(Si_3Al)O_{10}(OH,F)_2$) and phlogopite ($KMg_3(Si_3Al)O_{10}(F,OH)_2$) to biotite ($K(Mg,Fe^{2+})_3[AlSi_3O_{10}](OH,F)_2$) in the ore zone.

6.1.3 Sulphur isotope analysis

Published sulphide $\delta^{34}S$ data for various Copperbelt deposits (figure 6.2) show ranges of –11‰ to +11‰ for Chambishi (Annels 1989); –10.5‰ to +10.9‰ for Mufulira: +2.9‰ to +11.7‰ for Nkana North Limb and +6.5‰ to

+15.9‰ for Chibuluma (Dechow & Jensen 1965), and –7‰ to +9‰ for Konkola (Sweeney *et al.* 1986).

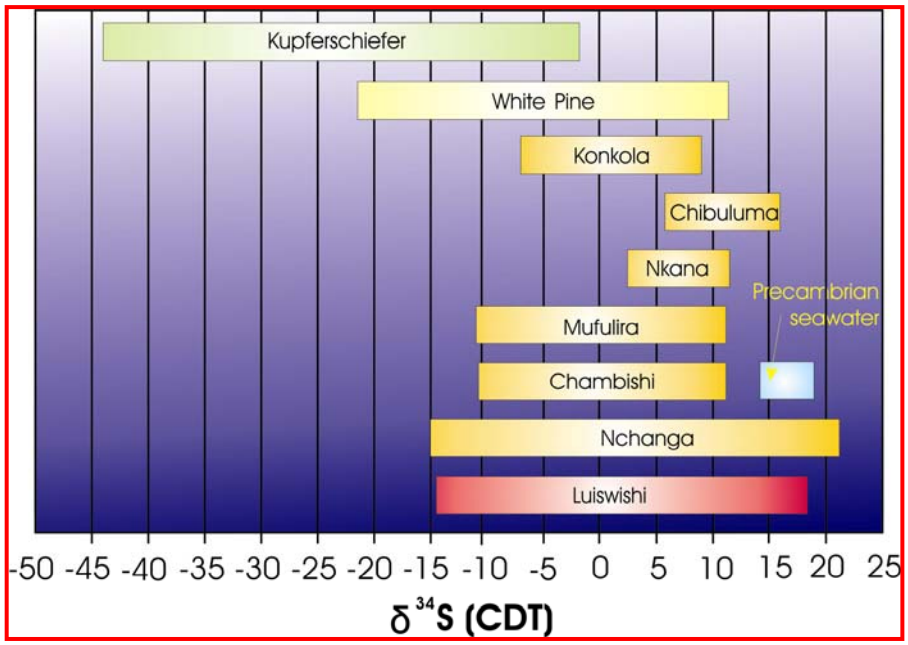

Figure 6.2 $\delta^{34}S$ values of selected sediment hosted copper deposits (after Dechow & Jensen 1965; Claypool *et al.* 1980; Gustafson & Williams 1981; Annels 1989; Sweeney *et al.* 1986; McGowan 2003; Lerouge 2005)

Dechow & Jensen (1965) explained the heavy and sometimes narrow range of $\delta^{34}S$ of the Copperbelt sulphides by suggesting metamorphic homogenization of original sedimentary $\delta^{34}S$ signatures (Gustafson and Williams 1981). The metamorphic re-equilibration of sulphides results in the homogenization of $\delta^{34}S$ values on a millimetre scale (Crowe *et al*. 1990; Velasco *et al*. 1998). However, within a specimen at Chimiwungo, variations of several parts per mil are observed, thus indicating that this process has not occurred.

Dechow & Jensen (1965) also carried out $\delta^{34}S$ analyses of sulphide samples from the pre-Katangan basement mineralization of the Kafue Anticline and Domes Region. These included 8 samples from the Lumwana sulphide mineralization that range from +6.0‰ to +13.3‰. Through use of highly precise conventional S-line and laser isotope analysis, this study has extended that range to +2.3 to +18.5‰. The $\delta^{34}S$ of copper sulphides at Lumwana are indicative of sulphide derived from the thermochemical reduction of a sulphate-enriched fluid (Machel *et al*. 1995). In such systems,

the likely sulphate source would have been remobilized evaporite minerals (e.g. Sverjensky 1987; Naylor *et al*. 1989).

Figure 6.3 examines available $\delta^{34}S$ data for the Central African copper mineralization, which includes the Zambian and Congolese Copperbelt, the basement mineralization of the Kafue Anticline and the Domes Region mineralization. Typically basement hosted mineralization is analogous to the Zambian Copperbelt mineralization, suggesting a possible genetic link. However, the basement mineralization typically lacks the light diagenetic pyrite values that are interpreted to result from bacteriogenic sulphate reduction (McGowan 2003).

Examples of light values are yielded from the basement at Fimpimpa and in the Mtuga Aplite which require further investigation to gain an understanding of the mechanism of ore formation.

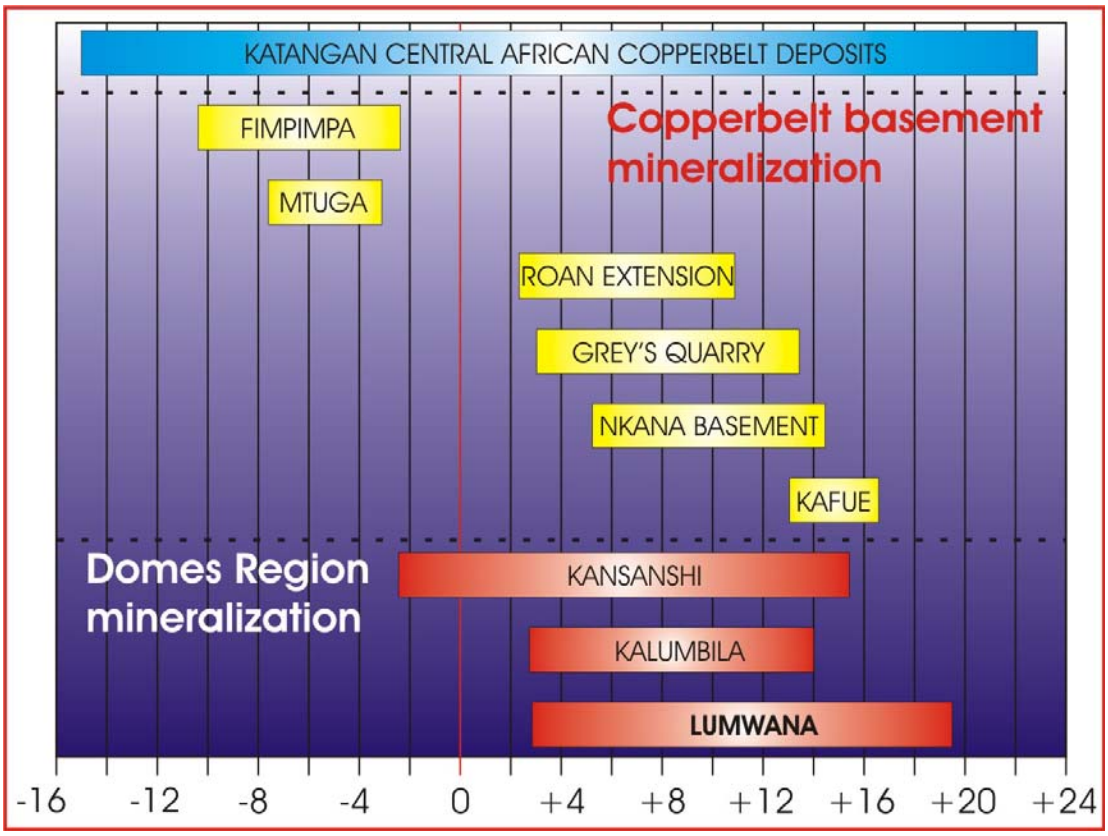

Figure 6.3 $\delta^{34}S$ values of the Central African Copperbelt, basement hosted mineralization and Domes Region mineralization (after Dechow & Jensen 1965; Gustafson & Williams 1981; Annels 1989; Sweeney *et al.* 1986; McGowan 2003)

CHAPTER 6: DISCUSSION

6.2 The nature and origin of the Lumwana ore schist

The Lumwana deposits consist of unmineralized quartz-feldspar ± phlogopite basement gneiss to Cu±Co mineralized quartz-phlogopite-muscovite-kyanite-sulphide schist. Transitional contacts are observed that result from the increased removal of feldspar associated with increased fabric development and deformation. Although the host rocks to the Lumwana copper sulphide mineralization have been correlated with the Lower Roan by previous authors (Benham *et al.* 1976; McGregor 1965), the observation of progressive alteration from hanging wall to ore schist suggests that this is untenable.

6.2.1 Comparison of the Lumwana deposits with pre-Katangan basement mineralization of the Zambian Copperbelt

Minor mineralized basement is widespread in the Kafue Anticline but has been subject to little scientific analysis. Whilst commonly of low grade when compared to the mineralization of the Zambian Copperbelt, higher grade mineralization has been identified associated with basement shear zones (Mendelsohn 1961; Pienaar 1961; Wakefield 1978).

Mineralogical and textural similarities are apparent between the Lumwana deposits and the basement mineralization of the Kafue Anticline. The Fimpimpa mineralization is vein hosted but occurs within a basement shear zone and feldspathized quartz diorite. Garnetiferous quartz-mica schist and biotite gneiss host the 8 metre wide shear zone that can be traced for more than a kilometre. The shear zone is sporadically mineralized with malachite, chalcopyrite and bornite with the entire width containing less than 0.4% copper (Pienaar 1961). The Lumwana deposits are also hosted by shear zones indicated by c-s fabrics, mylonites and porphyroblast rotation.

The Samba deposit of the Lufubu Metamorphic Complex (Rainaud *et al.* 2005) is the largest concentration of copper mineralization in the pre-Katangan basement of the Kafue Anticline. The sulphide mineralization of the Samba deposit is similar to Lumwana, consisting of disseminations, stringers and veinlets of pyrite, chalcopyrite and bornite in deformed quartz-sericite schist (Wakefield 1978).

CHAPTER 6: DISCUSSION

Textural and mineralogical similarities are apparent between the Lumwana and Samba deposits, including the observations that sulphides are aligned with the foliation and that bornite and pyrite have an antithetic relationship (Wakefield 1978) (observed at Chimiwungo). The deformed rocks at Samba are typically L-S tectonites that are also prevalent in the quartzites at Lumwana.

Wakefield (1978) also describes a pervasive sericitization of plagioclase at the Samba prospect that increases towards the mineralized zone. The degree of sericitization correlates with the intensity of the D_1 deformation. However, local zones of undeformed and totally sericitized rock indicate that alteration predates the D_1 deformation. Although the Samba deposit has been subject to greenschist PT conditions, the early sericitization is highly analogous to the alteration observed at Lumwana. This is responsible for the transition from basement gneiss to ore schist.

The origin of the protolith to the mineralization is ambiguous at Lumwana with transitional contacts from unmineralized quartz-feldspar ± phlogopite basement gneiss to Cu±Co mineralized quartz-phlogopite-muscovite-kyanite-sulphide schist. The transitional contacts and structural controls on mineralization have led to the hypothesis that these deposits represent metasomatically altered, mineralized and sheared basement. This challenges the interpretation that the ore schist horizons correlate with units of the Lower Roan, representing mineralized neo-Proterozoic sediments with amphibolite grade metamorphism (Benham *et al.* 1976, McGregor 1965).

6.2.2 Migration of hydrothermal fluids

At Lumwana the ore schist has undergone 3 dominant phases of alteration, an early potassic stage that results in the formation of phlogopite and the destruction of feldspar. The alteration envelops the ore and increases in intensity into the ore zone with increased fabric development and shearing. The transitional contacts observed at Lumwana are the result of an alteration event associated with mineralization that removed feldspar from ore horizons resulting in depleted Na and Ca and relatively higher Al components.

However, the host rocks to the Lumwana deposits have undergone intense wall-rock alteration with various styles of mineralization resulting from the changing chemistry of the fluids and rocks before, during and after the Lufilian Orogeny. Unfortunately, K-Ar and Rb-Sr dating of mica provide a cooling age of 500 Ma, corresponding to when the temperature dropped below 350-400°C rather than the timing of the alteration (Cosi *et al.* 1992).

In the Zambian Copperbelt the host rocks to the mineralization exhibit various styles of alteration although the timing and origin of the alteration is controversial. Three main styles of alteration are observed including calcium-magnesium, potassic and sodic alteration (Mendelsohn 1961; Fleischer *et al.* 1976; Sweeney *et al.* 1991; Binda 1995).

6.2.3 Deposition of copper and cobalt

The syngenetic “Copperbelt Style” origin of the mineralization proposed by previous authors (McGregor 1965; Benham *et al.* 1976) is not possible as the mineralization is hosted by units of the Mwombezhi Dome basement.

Sulphides are deformed by the S_1 fabric and overprinted by kyanite which formed at peak metamorphism. This indicates that copper was introduced to the basement either syn or pre-peak metamorphism. S_2 metamorphism with associated quartz-muscovite alteration has remobilized sulphides into low strain micro-structural dilatant sites including pressure shadows around porphyroblasts.

Several different styles of mineralization can commonly be observed in the Copperbelt that either overlap or form spatially distinct zones and include disseminated, pre-folding vein-hosted, post-folding vein-hosted, shear zone hosted and oxidation-supergene mineralization (Selley *et al.* 2005). The primary Copperbelt mineralization is overprinted with secondary chalcocite, copper carbonate, sulphate, cuprite and native copper (after Selley *et al.* 2005) (table 2.2). A progressive change from primary sulphide to secondary sulphide assemblages commonly occurs within 30 to 70 metres of the surface (Mendelsohn 1961) however, chalcocite and malachite extend to greater

depths of more than 1km at Konkola and greater than 600 metres at Nchanga (McKinnon and Smit 1961). Post folding vein-hosted mineralization includes chalcopyrite, accessory bornite, pitchblende, brannerite and molybdenite. The uranium mineralization is typically sub economic in the Zambian Copperbelt with the exception of the Mindola uranium orebody and typically occurs in the late veins and as local disseminations (Selley *et al.* 2005).

6.2.4 Deposition of uranium

Cosi *et al.* (1992) propose a uranium deposit model where the oxidising conditions of the Lower Roan Group hematite rich quartzite results in uraninite mineralization, whereas the reducing sulphide ore schist horizons are mineralized with disseminated brannerite. Textural relationships indicate that reduced brannerite pre-dates the remobilized sulphide and that the uranium bearing fluids left large amounts of Cl and CO_2 (Cosi *et al.* 1992). Only vein hosted uranium within the ore schist horizons were observed as part of this study.

6.2.5 Metamorphic remobilization of sulphide

Textures of remobilized sulphide minerals are controlled by the fabric development, typically forming coarse grains elongate within the S_2 quartz-muscovite fabric. It is unlikely that copper was introduced during the muscovite event as areas of intense quartz-muscovite alteration are commonly unmineralized. However, where quartz-muscovite alteration overprints the S_1 fabric, copper sulphides have been remobilised into pressure shadows around porphyroblasts, and into low strain dilatant sites.

Sulphides also locally replace silicate phases (phlogopite, muscovite, quartz and feldspar) and are crosscut by large muscovite and chlorite laths indicating that any metamorphic remobilisation of sulphides had finished before the late muscovite retrogressive event.

6.3 Genetic model for the Lumwana copper-cobalt deposits

A genetic model for the formation of the Lumwana deposits is proposed where alteration and sulphide mineralization of pre-Katangan basement occurred

during the development of a passive continental margin during the dispersal of Rodinia between 880 to 600 Ma (John *et al.* 2003). Copper and Cobalt bearing magnesium rich basinal brines are transported along extensional basement structures. This results in the sericitization of feldspar and the copper sulphide mineralization with associated phlogopite. The convergence of the Kalahari and Congo cratons resulted in continent-continent collision with the Kalahari craton overriding the passive continental margin at 530 Ma (John *et al.* 2004). This stage is responsible for the remobilization of sulphides into pressure shadows and for the formation of whiteschist assemblages. The final collision was followed by rapid erosion, tectonic uplift and cooling (John *et al.* 2004).

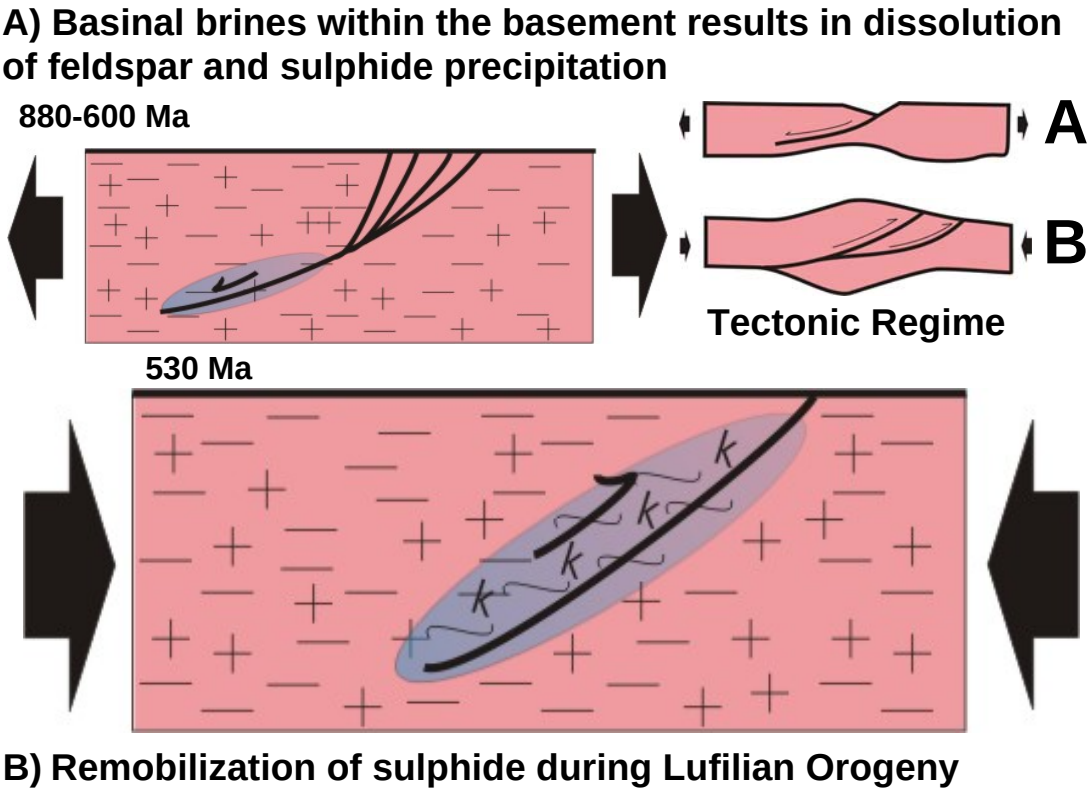

Figure 6.4 Genetic model for the formation of the Lumwana deposits

CHAPTER 7: CONCLUSIONS

7.1 Conclusions

The main conclusions to be drawn from this Lumwana-based study are summarized below:

- The Lumwana Cu±Co deposits Malundwe and Chimiwungo are examples of pre-Katangan mineralized basement that are located in the Domes Region of the Lufilian Arc.

- The host rocks to the mineralization are highly sheared amphibolite grade schist to gneiss units with kinematic indicators such as s-c fabrics and pressure shadows on porphyroblasts suggesting a top to the North shear sense. Peak metamorphism of 750ºC ± 25ºC and 13 ± 1 Kb indicated by whiteschist assemblages occurred during the Lufilian Orogeny at ~530Ma, with burial depths of ~50km.

- The transitional contacts and structural controls on mineralization indicates that these deposits represent metasomatically altered, mineralized and sheared basement, rather than mineralized neo-Proterozoic sediments with amphibolite grade metamorphism.

- The transitional contacts observed at Lumwana are due to an alteration event associated with mineralization that removed feldspar from ore horizons resulting in depleted Na and Ca and relatively higher Al components.

- Sulphides are deformed by the S1 fabric and overprinted by kyanite which formed at peak metamorphism. This indicates that copper was introduced to the basement either syn or pre-peak metamorphism. Post S1 metamorphism with associated quartz-muscovite alteration has remobilized sulphides into low strain zones and pressure shadows around porphyroblasts.

CHAPTER 7: CONCLUSIONS

- $\delta^{34}S_{SULPHIDES}$ give values of +2.3 to +18.5‰ that fall within the range of values observed in the Copperbelt of -17 to +23‰. The mechanism of ore formation at Lumwana was dominated by thermochemical sulphate reduction (TSR), indicated by the relatively heavy $\delta^{34}S$ values and the absence of the light bacteriogenic $\delta^{34}S$ values observed in the Copperbelt.

- Electron microprobe data of muscovite, phlogopite and chlorite show little variation between early and late mineral phases indicating that metamorphic homogenization of silicate assemblages occurred.

- The lithologies and structural controls on mineralization at Lumwana show similarities to various styles of basement mineralization observed in the Kafue Anticline suggesting that pre-Katangan basement had a key role in the formation of the Central African Copperbelt.

7.2 Implications for future exploration

The implications of this study for future copper-cobalt exploration in Zambia are as follows:

- The observation of potassic alteration associated with basement sulphide mineralization is a key vector to the sulphide mineralization of the Mwombezhi dome.

- The role of basement structures in the formation of deposits including the role of shear zones in the remobilization of sulphide as observed at Lumwana and at Samba in the Zambian Copperbelt.

- This study has highlighted the importance of pre-Katangan basement as a host of large economic copper-cobalt ore bodies as well as a viable source for the Cu-Co budget of the Central African Copperbelt.

CHAPTER 7: CONCLUSIONS

7.3 Recommendations for further work

Other techniques to be applied the samples collected during this project include:

- Further examination of sulphides and their relationship to structure.
- Halogen studies.
- Pb isotopes.

The following broad suggestions for future work are proposed:

- Investigation of lower PT analogues in the basement of the Zambian Copperbelt (Kafue Anticline) to further assess the timing and geochemistry of basement hosted mineralization.
- Expansion of the study to a regional level to examine the sulphide mineralization including basement hosted, Katangan and vein hosted mineralization, in order to develop a model for the Central African Copperbelt.

REFERENCES

ANNELS, A.E. 1974. Some aspects of the stratiform ore deposits of the Zambian Copperbelt and their genetic significance. *In*: BARTHOLOME, P. (ed) *Gisements stratiformes et provinces cupriferes*. Centenaire Societe Geologique Belgique, Leige, 235-254.

ANNELS, A.E. 1979. The genetic relevance of recent studies at Mufulira Mine, Zambia. *Annales Société Géologique de Belgique,* **102**, 431-449.

ANNELS, A.E. 1989. Ore genesis in the Zambian Copperbelt, with particular reference to the northern sector of the Chambishi Basin. In: BOYLE, R.W., BROWN, A.C., JEFFERSON, C.W., JOWETT, E.C., and KIRKHAM, R.V., (eds.) *Sediment-hosted Stratiform Copper Deposits*. Geological Association of Cananda, Special Paper 36, 427-452.

ANNELS, A.E., VAUGHAN, D.J., & CRAIG, J.R., 1983. Conditions of ore mineral formation Zambian Copperbelt deposits with special reference to the role of cobalt. *Mineralium Deposita*, **18**, 71-88.

ARMSTRONG, R.A., MASTER, S., & ROBB, L.J., 2005. Geochronology of the Nchanga Granite, and constraints on the maximum age of the Katanga Supergroup, Zambian Copperbelt. *Journal of African Earth Sciences*, **42**, 32-40.

ARMSTRONG, R.A., ROBB, L.J., MASTER, S., KRUGER, F.J., & MUMBA, P.A.C.C., 1999. New U-Pb age constraints on the Katangan sequence, Central African Copperbelt. *Journal of African Earth Sciences*, **28 (4a)**, 6-7.

BENHAM D.G., GREIG, D.D., & VINK, B.W., 1976. Copper occurrences of the Mwombezhi Dome area, northwestern Zambia. *Economic Geology*, **71**, 433-442.

BEST, M., & CHRISTIANSEN, E., 2001. *Igneous Petrology*. Blackwell Science, Abingdon.

BINDA, P.L., 1975. Detrital bornite grains in the Late Precambrian B greywackes of Mufulira, Zambia. *Mineralium Deposita*, **10**, 101-107.

BINDA, P.L., 1994. Stratigraphy of Zambian Copperbelt orebodies. *Journal of African Earth Sciences*, **19 (4),** 251-264.

BINDA, P.L., & MULGREW, J.R., 1974. Stratigraphy of copper occurrences in the Zambian Copperbelt. *In*: BARTHOLOME, P., (ed.) *Gisements stratiformes et provinces cuprifères*. Société Geologique Belgique, Liege, 215-233.

BINDA, P.L., & PORADA, H. 1995. Observations on the Katangan breccias of Zambia. *In*: WENDORFF, M., and TACK, L., (eds.) *Late Proterozoic Belts in Central and Southwestern Africa. Proceedings IGCP302*. *Annales Musee Royale Afrique, Central Turveren Belgique*, **101**, 49-62.

REFERENCES

BODISELITSCH, B., KOEBERL, C., MASTER, S., & REIMOLD, W.U., 2005. Estimating Duration and Intensity of Neoproterozoic Snowball Glaciations from Ir Anomalies. *Science*, **308**, 239-242.

CAHEN, L., SNELLING, N.J., DELHAL, J., & VAIL, J.R., 1984. *The geochronology and evolution of Africa*. Clarendon, Oxford.

CAILTEUX, J., BINDA, P.L., KATEKESHA, W.M., KAMPUNZU, A.B., INTIOMALE, M.M., KAPENDA, D., KAUNDA, C., NGONGO, K., TSHIAUKA, T., & WENDORFF, M., 1994. Lithostratigraphical correlation of the Neoproterozoic Roan Supergroup from Shaba (Zaire) and Zambia, in the central African copper-cobalt metallogenic province. *Journal of African Earth Sciences*, **19**, 265-278.

CAILATEUX, J., KAMPUNZU, A.B., LEROUGE, C., KAPUTO, A.K., & MILESI, J.P., 2005. Genesis of sediment-hosted stratiform copper-cobalt deposits, Central African Copperbelt. *Journal of African Earth Sciences*, **42**, 134-158.

CLAYPOOL, G.E., HOLSER, W.T., KAPLAN, I.R. SAKAI, H., & ZAK, I., 1980. The age curves of sulphur and oxygen isotopes in marine sulphate and their mutual interpretation. *Chemical Geology*, **28**, 199-260.

CONDIE, K.C., 2002. The supercontinent cycle; are there two patterns of cyclicity?. *Journal of African Earth Sciences*, **35**, 179-183.

COSI, M., De BONIS, A., GOSSO, G., HUNZIKER, J., MARTINOTTI, G., MORATTO, S., ROBERT, J.P., & RUHLMAN, F., 1992. Late Proterozoic thrust tectonics, high-pressure metamorphism and uranium mineralization in the Domes area, Lufilian Arc, northwestern Zambia. *Precambrian Research*, **58**, 215-240.

CRAIG, J.R., & VAUGHAN, D.J., 1981. *Ore microscopy and ore petrography*. John Wiley & Sons, Canada, p.406.

CROWE, D.E., VALLEY, J.W., & BAKER, K.L., 1990. Micro-analysis of sulphur-isotope ratios and zonation by laser microprobe. *Geochimica et Cosmochimica Acta*, **54**, 2075-2092.

DALY, M.C., CHAKROBORTY, S.K., KASOLO, P., MUSIWA, M., MUMBA, P., NAIDU, B., NAMATEBA, C., NGAMBI, O., & COWARD M.P., 1984. The Lufilian Arc and Irumide Belt of Zambia: results of a geotraverse across their intersection. *Journal of African Earth Sciences*, **2**, 311-318.

DARNLEY, A.G., 1960. Petrology of some Rhodesian copperbelt orebodies and associated rocks. *Inst. Min. & Met., B*., **638**, 137-173.

DAVIDSON, C.M., 1931. The geology and ore deposits of Chambishi, Northern Rhodesia. *Economic Geology*., **26**, 131-154.

REFERENCES

DAVIS, G.H., & REYNOLDS, S.J., 1984. *Structural Geology of Rocks and Regions,* 2nd *Edition*. John Wiley and Sons Inc: New York.

DECHOW, E., & JENSEN, M.L., 1965. Sulphur isotopes of some central African sulphide deposits. *Economic Geology*, **60**, 894-941.

DEER, W.A., HOWIE, R.A. & ZUSSMAN, J., 1966. *An introduction to the rock-forming minerals.* Longman: London.

DIEDERIX, D., 1977. *The geology of the Nchanga Mining Licence Area*. Unpublished Company Report – Nchanga Consolidated Copper Mines Limited Chingola Division, p.59.

DODSON, M.H., 1979. Theory of cooling ages. *In*: JAGER, E., and HUNZIKER, J.C., (ed.) *Lectures in isotope geology*. Springer, Berlin, p. 194-202.

DRYSDALL, A.R., JOHNSON, R.L., MOORE, T.A., & THIEME, J.G., 1972. Outline of the geology of Zambia. *Geologie en Mijnbouw*, **53**, 265-276.

DUANE, M.J., & SAGGERSON, E.P., 1995. Brine expulsion, fluid transport and metallization spanning 2 Gyr in basins of southern and central Africa. *Basin Research*, **7**, 97-108.

FLEISCHER, V.D., GARLICK, W.G., & HALDANE, R., 1976. Geology of the Zambian Copperbelt. *In*: WOLF, K.H. (ed.) *Handbook of Stratabound and Stratiform Ore Deposits*, Volume 9, Elsevier Scientific Publishing Company, Amsterdam, p. 223-353.

FRANCIOS, A.P., 1973. *L'extremité occidentale de l'arc cuprifrère shabien. Memoir*, Gécamines Geology Department, Likasi, Zaire.

FRANCIOS, A.P., & CAILTEUX, J., 1981. La couverture Kantangienne entre les socles de Zilo et de la Kabompo, Republique du Zaire, region de Kolwezi. *Annales Sciences Geologiques*, **87**. Musee royal de l'Afrique Centrale, Tervuren, Belgique, 50pp.

GARLICK, W.G., 1972. Sedimentary environment of Zambian copper deposition. *Geologie en Mijnbouw*, **51**, 277-298.

GARLICK, W.G., 1961. The Syngenetic Theory. *In*: MENDELSOHN, F. (ed.) *The Geology of the Northern Rhodesian Copperbelt*. Macdonald: London, p.146-165.

GARLICK, W.G., & BRUMMER, J.J., 1951. The age of the granites of the Northern Rhodesian copperbelt. *Economic Geology and the Bulletin of the Society of Economic Geologists*, **46**, 478-497.

REFERENCES

GRANT, J.A., 1986. The isocon diagram; a simple solution to Gresens' equation for metasomatic alteration. *Economic Geology and the Bulletin of the Society of Economic Geologists*, **81**, 1976-1982.

GRAY, A., 1929. *The outline of the geology and ore deposits of the Nkana concession*. 15th Int. Geol. Cong.

GREYLING, L.N., ROBB, L.J., MASTER, S., BOIRON, M.C., & YAO, Y., 2005. The nature of early basinal fluids in the Zambian Copperbelt: A case study from the Chambishi deposit. *Journal of African Earth Sciences*, **42**, 159-172.

GUSTAFSON, L.B., & WILLIAMS, N., 1981. Sediment-hosted stratiform deposits of copper, lead, and zinc. *Economic Geology* 75th anniversary volume, 138-178.

HANSON, G.N., & GAST, P.W., 1967. Kinetic studies in contact metamorphic zones. *Geochimica et Cosmochimica Acta*, **31**, 1119-1153.

HANSON, R.E., 2003. Proterozoic geochronology and tectonic evolution of southern Africa. *In*: YOSHIDA, M., WINDLEY, B.F., and DASGUPTA, S., (eds.) *Proterozoic East Gondwana: Supercontinent Assembly and Breakup*. *Geological Society*, London, Special publication, **206**, 427-463.

HANSON, R.E., WARDLAW, M.S., WILSON, T.J., & MWALE, G., 1993. U-Pb zircon ages from the Hook granite massif and Mwembeshi dislocation: constraints on Pan-African deformation, plutonism and transcurrent shearing in central Zambia. *Precambrian Research*, **63**, 189-209.

HITZMAN, M.W., 2000. Source basins for sediment-hosted stratiform Cu deposits; implications for the structure of the Zambian Copperbelt. *Journal of African Earth Sciences*, **30**, 855-863.

JACKSON, G.C.A., 1932, The Geology of the Nchanga district. Q.J. *Geol. Soc. London*, **88**, 443-514.

JACKSON, M.P.A., WARIN, O.N., WOAD, G.M., & HUDEC, M.R., 2003. Neoproterozoic allochthonous salt tectonics during the Lufilian orogeny in the Katangan Copperbelt, Central Africa: *GSA Bulletin*, **115**, 314- 330.

JOHN, T., SCHENK, V., HAASE, K., SCHERER, E., & TEMBO, F., 2003. Evidence for a Neoproterozoic ocean in south-central Africa from mid-oceanic-ridge-type geochemical signatures and pressure-temperature estimates of Zambian eclogites: *Geology*, **31**, 243-246.

JOHN, T., SCHENK, V., MEZGER, K., & TEMBO, F., 2004. Timing and PT evolution of whiteschist metamorphism in the Lufilian Arc-Zambezi Belt Orogen (Zambia); implications for the assembly of Gondwana. *Journal of Geology*, **112**, 71-90.

REFERENCES

JOHNSON, S.P., & OLIVER, G.J.H., 2002. High fO (sub 2) metasomatism during whiteschist metamorphism, Zambezi Belt, northern Zimbabwe. *Journal of Petrology*, **43**, 271-290.

KAMPUNZU, A.B., & CAILTEUX, J., 1997. Tectonic evolution of the Lufilian Arc (Central Africa copper belt) during Neoproterozoic Pan African Orogenesis*. Abstracts, Intraplate Magmatism and Tectonics of Southern Africa Conference, Harare*, 25-26.

KAMPUNZU, A.B., & CAILTEUX, J., 1999. Tectonic evolution of the Lufilian Arc (Central Africa copper belt) during Neoproterozoic Pan African Orogenesis. *Gondwana Research*, **2**, 401-421.

KEY, R.M., LIYUNGU, A.K., NJAMU, F.M., SOMWE, V., BANDA, J., MOSLEY, P.N., & ARMSTRONG, R.A., 2001. The western arm of the Lufilian Arc in NW Zambia and its potential for copper mineralization. *Journal of African Earth Sciences*, **33**, 503-528.

KIRKHAM, R.V., 1976. Environments of formation of copper sulphide-native copper deposits in volcanic sequences. *International Geological Congress, Abstracts*, **1 (25)**, section 4, 169-170.

KIRKHAM, R.V., 1989. Distribution, settings, and genesis of sediment-hosted stratiform copper deposits. *Special Paper - Geological Association of Canada*, **36**, 3-38.

LEROUGE, C., CAILTEUX, J., KAMPUNZU, A. B., MILESI, J. P., FLEHOC, C., 2005. Sulphur isotope constraints on formation conditions of the Luiswishi deposit, ore; Democratic Republic of Congo (DRC). *Journal of African Earth Sciences*, **42 (1-5)** [SPECIAL ISSUE], 173-182.

MACHEL, H.G., KROUSE, H.R., & SASSEN, R., 1995. Products and distinguishing crieria of bacterial and thermochemical sulphate reduction. *Applied Geochemistry*, **10**, 373-389.

MASTER, S., RAINAUD, C., ARMSTRONG, R.A., PHILLIPS, D., & ROBB, L.J., 2002. Contributions To the geology and mineralization of the Central African Copperbelt II: Neoproterozoic deposition of the Katanga Supergroup with implications for regional and global correlations. *In*. *Geocongress-IAGOD Joint Meeting, Windhoek, Namibia, Extended Abstracts* on CD-ROM.

MASTER, S., RAINAUD, C., ARMSTRONG, R.A., PHILLIPS, D., & ROBB, L.J., 2005. Provenance ages of the Neoproterozoic Katanga Supergroup (Central African Copperbelt), with implications for basin evolution. *Journal of African Earth Sciences*, **42**, 41-60.

McGOWAN, R., 2003. *The Origin of the Nchanga Copper-Cobalt Deposits of the Zambian Copperbelt*. Unpub. PhD thesis, University of Southampton, 247 p.

REFERENCES

McGOWAN, R.R., ROBERTS, S., FOSTER, R., BOYCE, A., & COLLER, A., 2003. Origin of the copper-cobalt deposits of the Zambian Copperbelt: An epigenetic view from Nchanga. *Geology*, **31**, 497–500.

McGOWAN, R.R., ROBERTS, S., BOYCE, A.J, 2006. Origin of the Nchanga Copper-Cobalt Deposits of the Zambian Copperbelt. Mineralium Deposita, **40**, 617-638.

McGREGOR, J.A., 1965. *The Lumwana Copper Project in Zambia*. Unpub. PhD thesis, University of Southampton.

McKINNON, D.M., and SMIT, N.J., 1961. Nchanga. *In*: MENDELSOHN, F., (ed.) *The Geology of the Northern Rhodesian Copperbelt*. Macdonald: London, 234-275.

MENDELSOHN, F., 1961. *The Geology of the Northern Rhodesian Copperbelt*. Macdonald: London, 423p.

MINISTRY of MINES and MINERAL DEVELOPMENT, 1998. *Zambia: Investment opportunities in the mining industry*. Ministry of Mines and Mining Development, Zambia, 33 p.

MOINE, B., GUILLOUX, L., & AUDEOUD, D., 1986. Major element geochemistry of the host rocks in some sediment-hosted copper deposits. *Special Publication of the Society for Geology Applied to Mineral Deposits*, **4**, 443-460.

MOLAK, B., 1995. Some structural and petrological aspects of the Cu (Co) mineralization in the Copperbelt and northwestern provinces of Zambia. *Royal Museum of Central Africa (Begium) Annales de la Societe Geologique*, **101**, 95-102.

MULELA, D., & SEIFERT, A.V., 1998. Geology of the Mwombezhi Dome and Jiwundu Swamp areas: Explaination of degree sheet 1225 NE quarter and 1125, part of SE quarter. *Report of the Geological Survey of Zambia*, **83**, 28 p.

NAYLOR, H., TURNER, P., VAUGHAN, D.J., BOYCE, A.J., & FALLICK, A.E., 1989. Genetic studies of red bed mineralization in the Triassic of the Cheshire Basin, northwest England. *Journal of the Geological Society of London*, **146**, 685-699.

NESBITT, B.E., 1986(a). Oxide-sulphide-silicate equilibria associated with metamorphosed ore deposits. Part I: Theoretical considerations. *Economic Geology*, **81**, 831-840.

REFERENCES

NESBITT, B.E., 1986(b). Oxide-sulphide-silicate equilibria associated with metamorphosed ore deposits. Part II: Pelitic and felsic volcanic terrains. *Economic Geology*, **81**, 841-856.

NYAMBE, I.A., & KAWAMYA, V.M., 2005. Approaches to sustainable minerals development in Zambia. *In*. MARKER, B. R., PETTERSON, M. G., McEVOY, F., STEPHENSON, M. H., (eds.) *Sustainable Minerals Operations in the Developing World.* Geological Society Special Publication 250: London, p.73-86.

PIENAAR, P.J., 1961. Mineralization in the basement. *In*. MENDELSOHN, F., (ed.) *The Geology of the Northern Rhodesian Copperbelt*. Macdonald: London, p. 30-40.

PORADA, H., 1989. Pan-African rifting and orogenesis in southern to equatorial Africa and eastern Brazil. *Precambrian Research*, **44**, 103-136.

PORADA, H., & BERHORST, V., 2000. Towards a new understanding of the Neoproterozoic-early Palaeozoic Lufilian and northern Zambezi belts in Zambia and the Democratic Republic of Congo. *Journal of African Earth Sciences*, **30**, 727-771.

RAINAUD, C., ARMSTRONG, R.A., MASTER, S., & ROBB, L.J., 1999. A fertile Palaeoproterozoic magmatic arc beneath the central African Copperbelt. *Proceedings of the ... Biennial SGA Meeting*, **5**, 1427-1430.

RAINAUD, C., MASTER, S., ARMSTRONG, R.A., & ROBB, L.J., 2005. Geochronology and nature of the Palaeoproerzoic basement in the Central African Copperbelt (Zambia and the Democratic Republic of Congo), with regional implications. *Journal of African Earth Sciences*, **42**, 1-31.

RAINAUD, C., MASTER, S., ARMSTRONG, R.A., PHILLIPS, D., & ROBB, L.J., 2005. Monazite U-Pb dating and ^{40}Ar-^{39}Ar thermochronology of metamorphic events in the Central African Copperbelt during the Pan-African Lufilian Orogeny. *Journal of African Earth Sciences*, **42**, 183-199.

RAMSAY, C.R., & RIDGEWAY, J., 1977. Metamorphic patterns in Zambia and their bearing on problems of Zambian tectonic history. *Precambrian Research*, **4**, 321-337.

RICHARDS, J.P., KROGH, T.E., & SPOONER, E.T.C., 1988. Fluid Inclusion Characteristics and U-Pb Rutile Age of Late Hydrothermal Alteration and Veining at the Musoshi Stratiform Copper Deposit, Central African Copper Belt, Zaire. *Economic Geology*, **83**, 118-139.

ROBB, L.J., 2005. *Introduction to Ore-forming Processes*. Blackwell Science, Abingdon.

SCHREYER, W., 1973. Whiteschist: a high-pressure rock and its geologic significance. *Journal of Geology*, **81**, 735-739.

REFERENCES

SELLEY, D., BROUGHTON, D., SCOTT, R., HITZMAN, M., BULL, S., LARGE, R., McGOLDRICK, P., CROAKER, M., POLLINGTON, N., & BARRA, F., 2005. A new look at the geology of the Zambian Copperbelt. *Economic Geology*, (100 Anniversary volume), 965-1000.

SPRY, P.G., 2000. Sulfidation and oxidation haloes as guides in the exporation for metamorphosed massive sulfide ores. *In*. Metamorphosed and Metamorphogenic Ore Deposits. *Reviews in Economic Geology*, **11**, 149-161.

STEVEN, N., & ARMSTRONG, R., 2003. A metamorphosed proterozoic carbonaceous shale-hosted Co-Ni-Cu depsoit at Kalumbila, Kabompo Dome: The Copperbelt Ore Shale in Northwestern Zambia. *Economic Geology*, **98 (5)**, 893-909.

SUTTON, S.J., & MAYNARD, J.B., 2005. A fluid mixing model for copper mineralization at Konkola north, Zambian Copperbelt. *Journal of African Earth Sciences*, **42**, 95-118.

SVERJENSKY, D.A., 1987. The role of the migrating oil-field brines in the formation of sediment-hosted copper-rich deposits. *Economic Geology*, **82**, 1130-1141.

SWEENEY, M.A., & BINDA, P.L., 1989. The role of diagenesis in the formation of the Konkola Cu-Co orebody of the Zambian Copperbelt. *In*. BOYLE, R.W., BROWN, A.C., JEFFERSON, C.W., JOWETT, E.C., & KIRKHAM, R.V., (eds.) *Sediment-hosted stratiform Copper deposits*: *Geological Association of Canada Special Paper*, **36**, 499-518.

SWEENEY, M.A., & BINDA, P.L., 1994. Some constraints on the formation of the Zambian Copperbelt deposits. *Journal of African Earth Sciences*, **19**, 303-313.

SWEENEY, M.A., BINDA, P.L., & VAUGHAN, D.J., 1991. Genesis of the ores of the Zambian copperbelt. *Ore Geology Reviews*, **6**, 51-76.

SWEENEY, M.A., VAUGHAN, D.J., & BINDA, P.L., 1991. The geochemistry of the basement complex of the Zambian Copperbelt, Implications for mineralzation. *In*: PAGEL and LEROY, (eds.) *Transport and Deposition of Metals.* Balkema, Rotterdam, p.359-362.

SWEENEY, M.A., TURNER, P., & VAUGHAN, D.J., 1986. Stable isotope and geochemical studies of the role of early diagenesis in ore formation, Konkola Basin, Zambian Copperbelt. *Economic Geology*, **81**, 1836 - 1852.

REFERENCES

TINDLE, A.G., & WEBB, P.C., 1990. Estimation of lithium contents in trioctahedral micas using microprobe data; application to micas from granitic rocks. *European Journal of Mineralogy,* **2**, 595-610.

WAKEFIELD, J., 1978. Samba: a deformed porphyry-type copper deposit in the basement of the Zambian Copperbelt. *Transactions of the Institution of Mining and Metallurgy*, **87**, 43-52.

WENDORFF, M., 2002. Stratigraphy of the Fungurume Group – evolving foreland basin succession in the Lufilian fold-thrust belt, Neoproterozoic-Lower Palaeozoic, Democratic Republic of Congo. *South African Journal of Geology*, **106**, 17-34.

WENDORFF, M., 2005. Evolution of Neoproterozoic-Lower Palaeozoic Lufilian arc, Central Africa: a new model based on syntectonic conglomerates. *Journal of the Geological Society, London*, **162**, 5-8.

WENDORFF, M., 2005. Sedimentary genesis and lithostratigraphy of Neoproterozoic megabreccia from Mufulira, Copperbelt of Zambia. *Journal of African Earth Sciences*, **42**, 61-81.

WHYTE, R.J., & GREEN, M.E., 1971. Geology and pelaeogeography of Chibuluma West Orebody, Zambian Copperbelt. *Economic Geology*, **66**, 400-424.

VAN EDEN, J.G., 1974. Depositional and diagenetic environment related to sulphide mineralization, Mufulira, Zambia. *Economic Geology*, **69**, 59-79.

VELASCO, F., SANCHEZ-ESPANA, J., BOYCE, A.J., FALLICK, A.E., SAEZ, R. & ALMODOVAR, G.R. 1998. A new sulphur isotopic study of some IPB deposits: Evidence of a textural control on sulphur isotope composition. *Mineralium Deposita*, **34**, 4-18.

APPENDIX A

APPENDIX A1: List of boreholes investigated

Malundwe							
Borehole	**Company**	**Eastings**	**Northings**	**R.L.**	**Dip**	**Azimuth**	**Depth (m)**
EQMAL083	EQCV	370985	8646598	1271.4	-90	4	110
EQMAL084	EQCV	370941	8646601	1270.6	-90	4	116
EQMAL094	EQCV	371084	8646701	1281.8	-80	94	114
EQMAL251	EQCV	370710	8648997	1313.2	-80	94	107
MAD010	AGIP	370020	8647784	1298.9	-90	0	303
MAD015	AGIP	369867	8648892	1293.6	-90		285
MAD018	AGIP	370963	8645660	1320.3	-90	0	262
MAD056	AGIP	370953	8648048	1335.1	-90	0	281
MAD067	AGIP	370908	8646185	1300.1	-90	0	345
MAD112	AGIP	372712	8644659	1337.2	-90	0	162
MAD122	AGIP	373127	8642742	1340.7	-90	0	274
MMB226	RST	372535	8644590	1343.4	-90	0	520
				Malundwe Total			**2879**
Chimiwungo							
Borehole	**Company**	**Eastings**	**Northings**	**R.L.**	**Dip**	**Azimuth**	**Depth (m)**
CHI017W1	PD	377950	8640493	1362.1	-90	0	252
CHI017W2	PD	377950	8640493	1362.1	-90	0	245
EQCHI062	EQCV	377775	8640150	1372.0	-80	0	281
EQCHI065	EQCV	377475	8640150	1369.2	-80	4	244
EQCHI067	EQCV	377271	8640152	1366.5	-80	4	222
EQCHI128	EQCV	377055	8640550	1371.6	-80	4	132
EQCHI188	EQCV	376950	8640850	1376.6	-80	0	93
EQCHI201	EQCV	377800	8640250	1369.3	-80	4	294
MM158	RST	377672	8642679	1349.6	-90	0	671
MM614	RST	377359	8640451	1357.8	-80		350
MM735	RST	377040	8640213	1364.6	-90	0	197
MMC456	RST	377970	8642834	1358.0	-90	0	184
MMC477	RST	377367	8642371	1332.3	-90	0	180
MMC723	RST	377989	8641936	1334.6	-90	0	233
				Chimiwungo Total			**3578**
Mwombezhi Dome - Basement gneiss							
Borehole	**Company**	**Eastings**	**Northings**	**R.L.**	**Dip**	**Azimuth**	**Depth (m)**
MM635	RST	378010	8653486	1369.8	-90	0	151
Copperbelt Deposit							
Borehole	**Company**	**Eastings**	**Northings**	**R.L.**	**Dip**	**Azimuth**	**Depth (m)**
KS17							1903
				Total logged core			**8511**

APPENDIX A

APPENDIX A2: CHIMIWUNGO SUMMARY LOGS

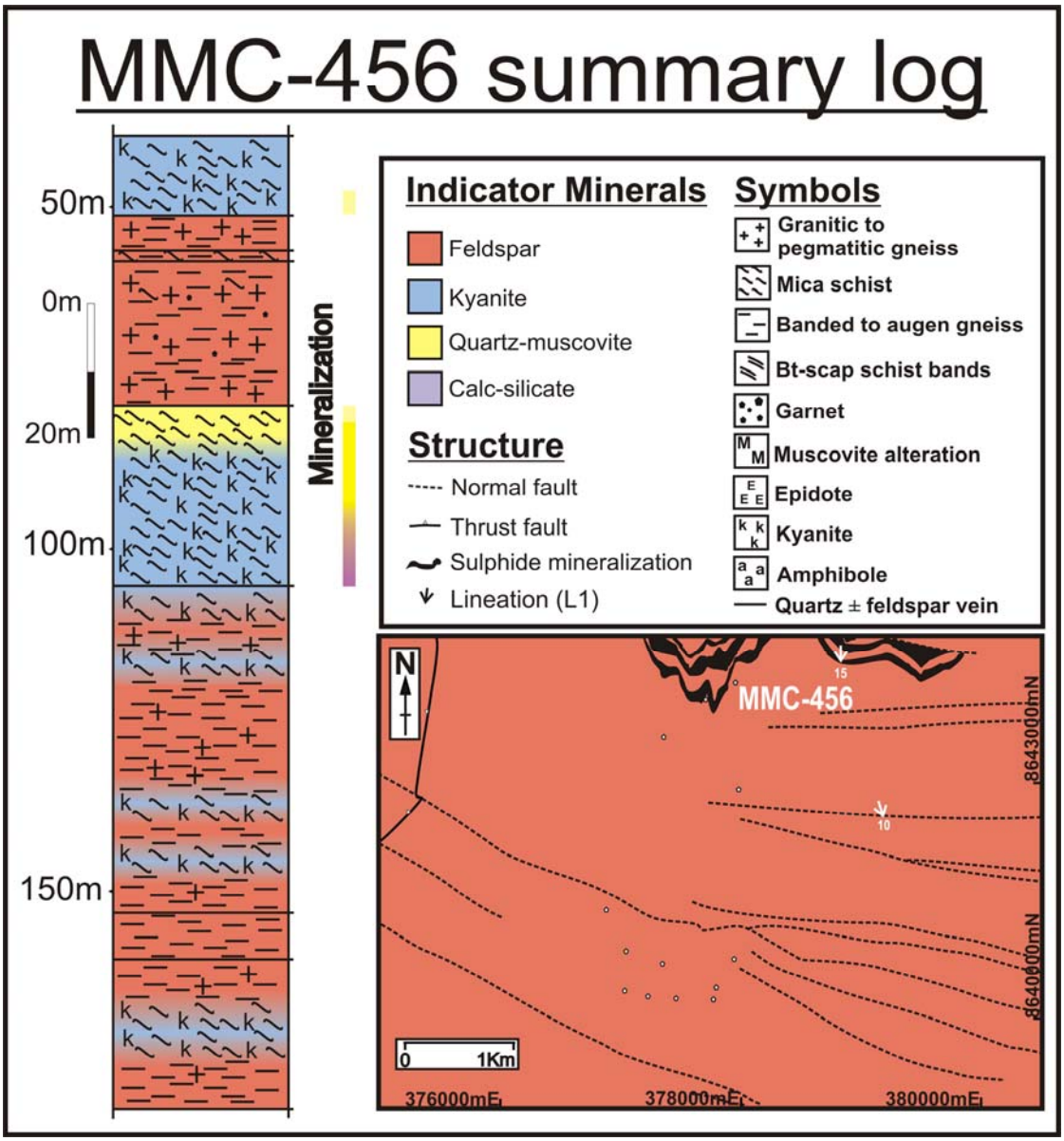

APPENDIX A

APPENDIX A2: CHIMIWUNGO SUMMARY LOGS

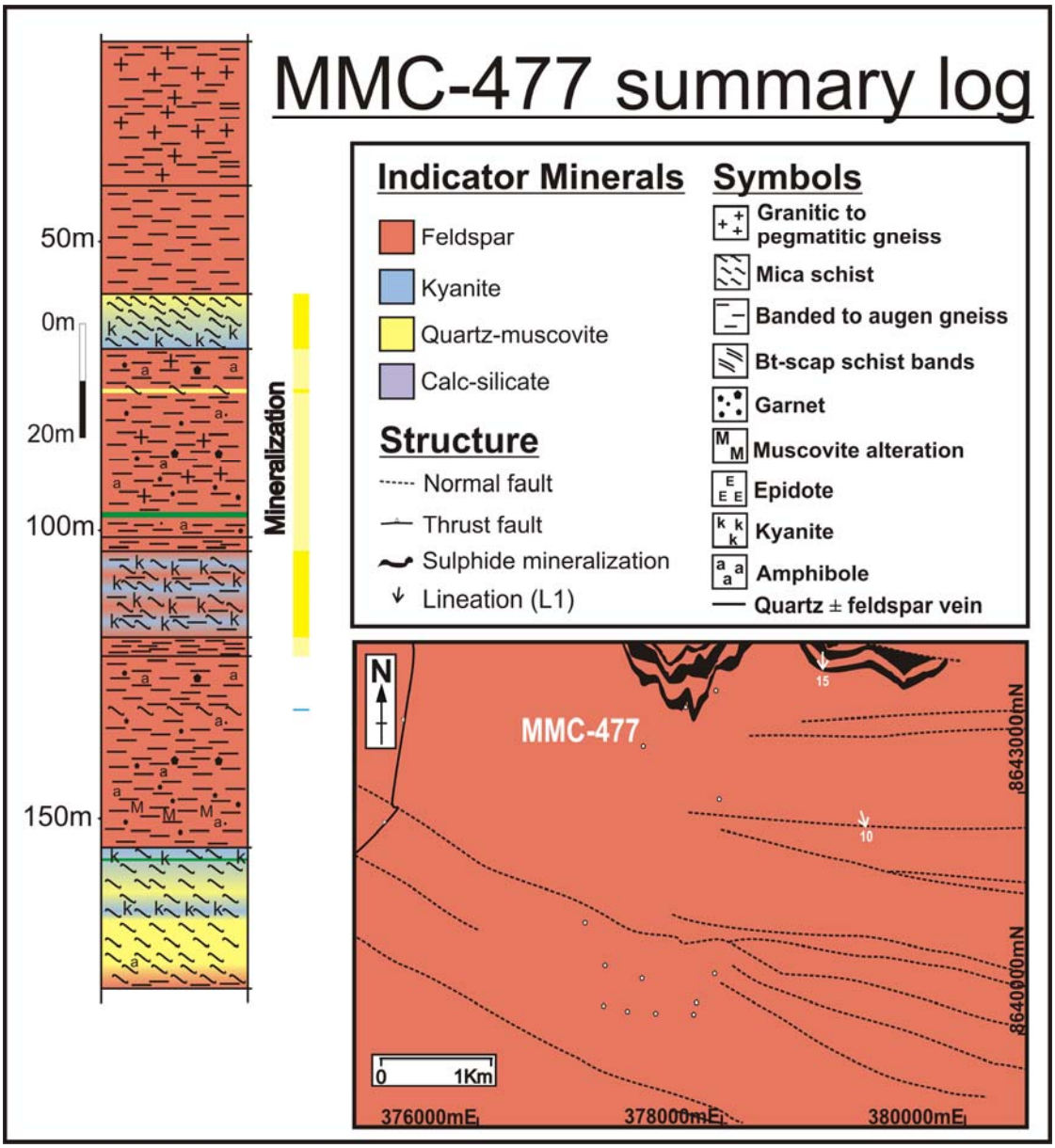

APPENDIX A

APPENDIX A2: CHIMIWUNGO SUMMARY LOGS

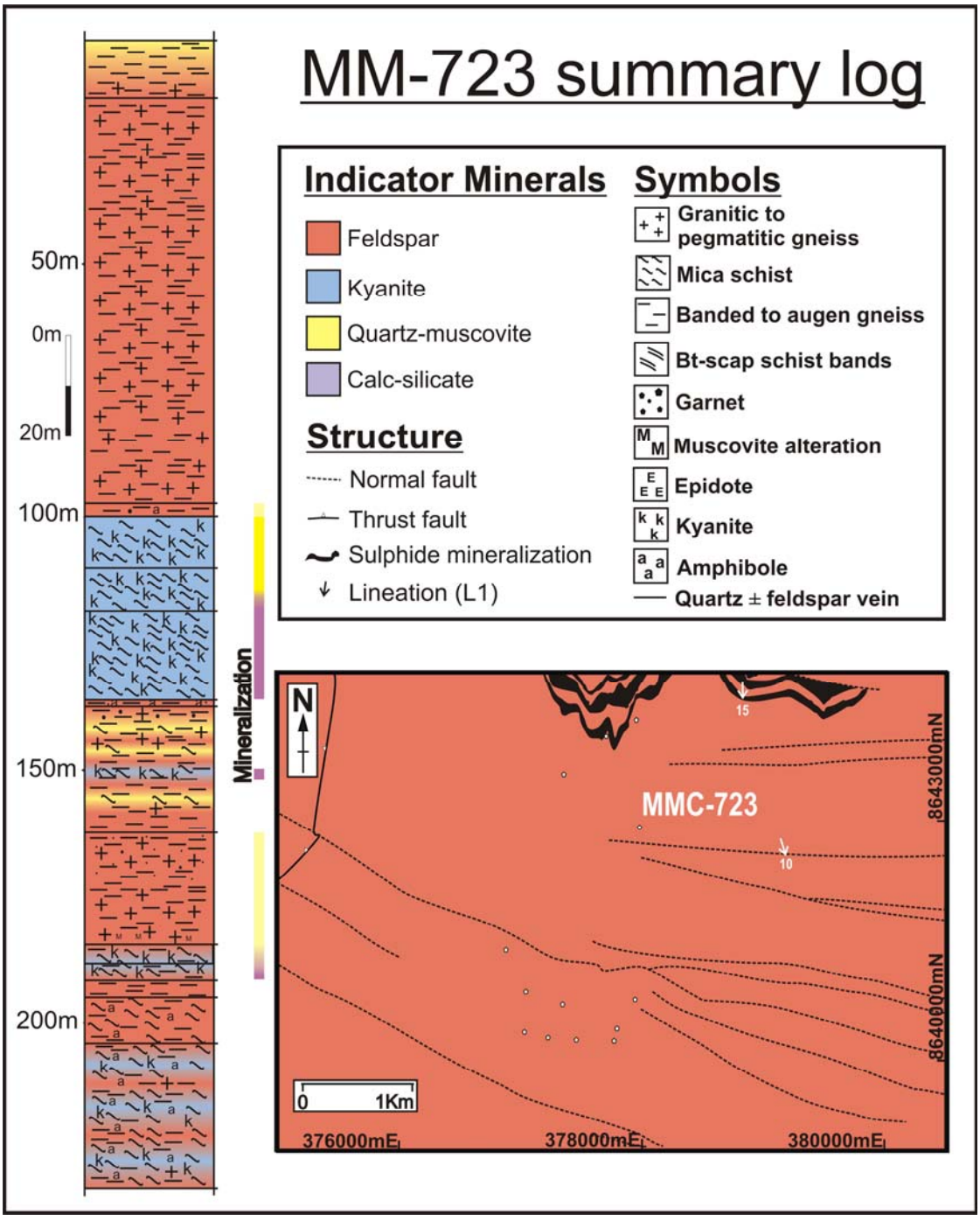

APPENDIX A

APPENDIX A2: CHIMIWUNGO SUMMARY LOGS

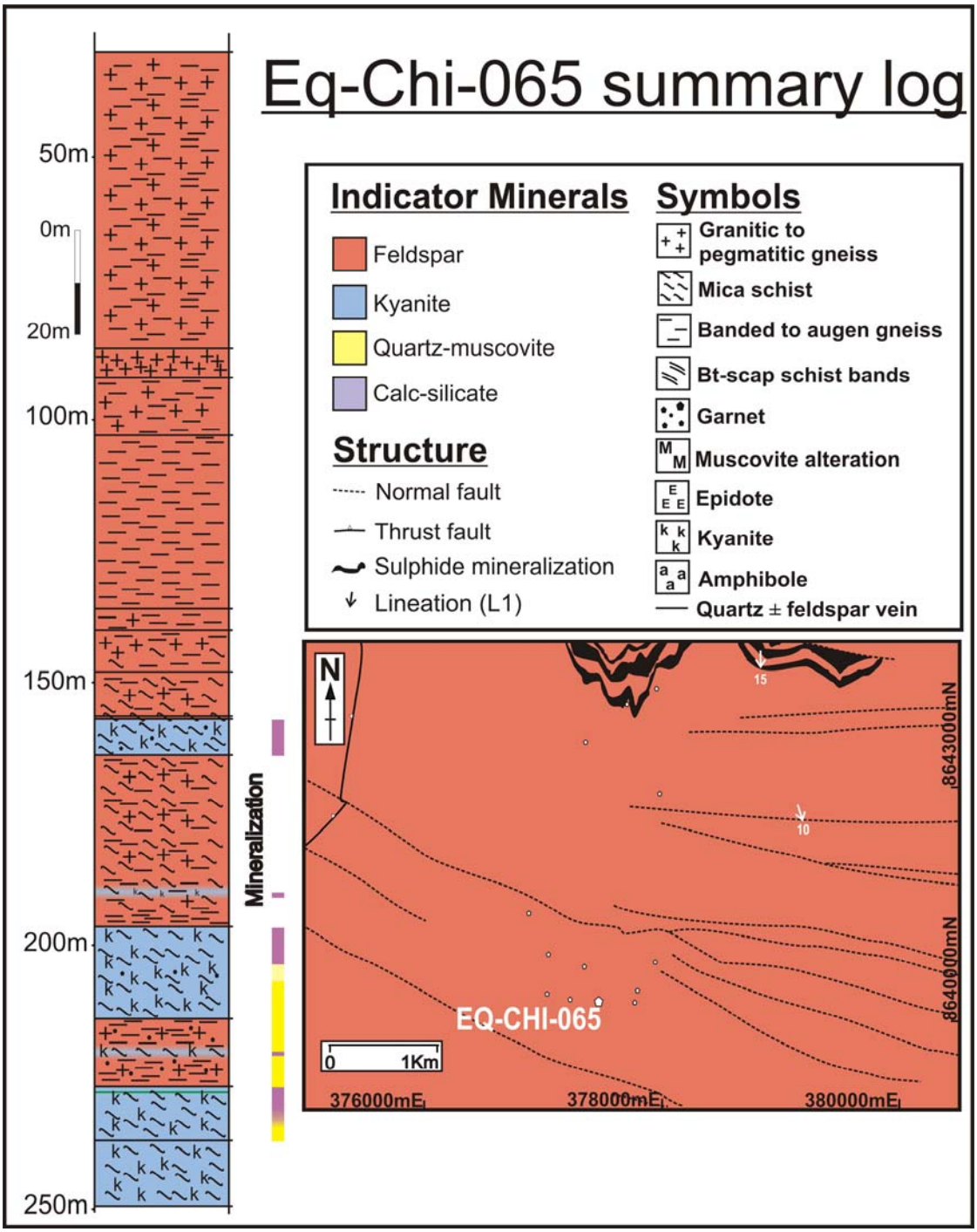

APPENDIX A

APPENDIX A2: CHIMIWUNGO SUMMARY LOGS

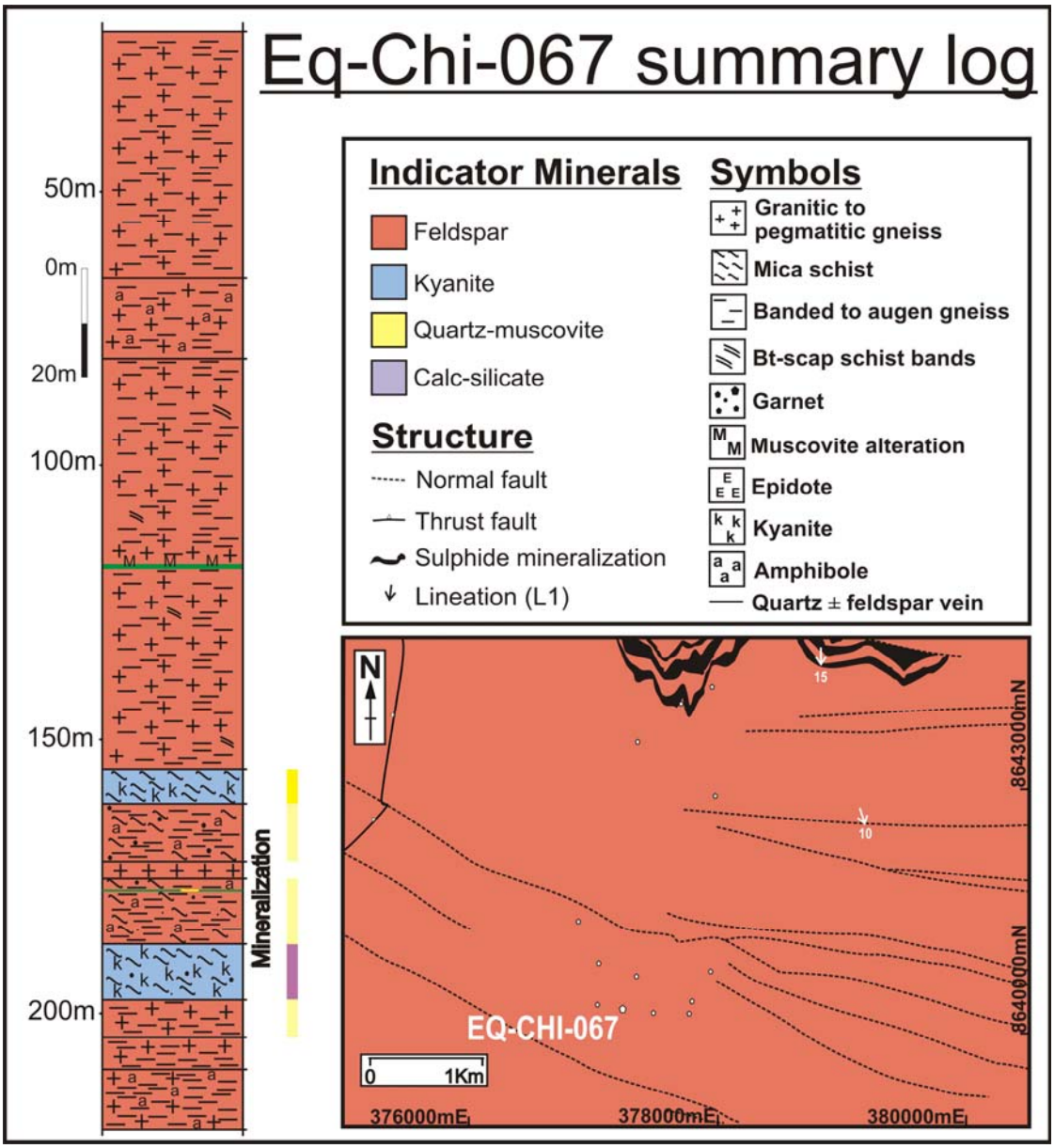

APPENDIX A

APPENDIX A2: CHIMIWUNGO SUMMARY LOGS

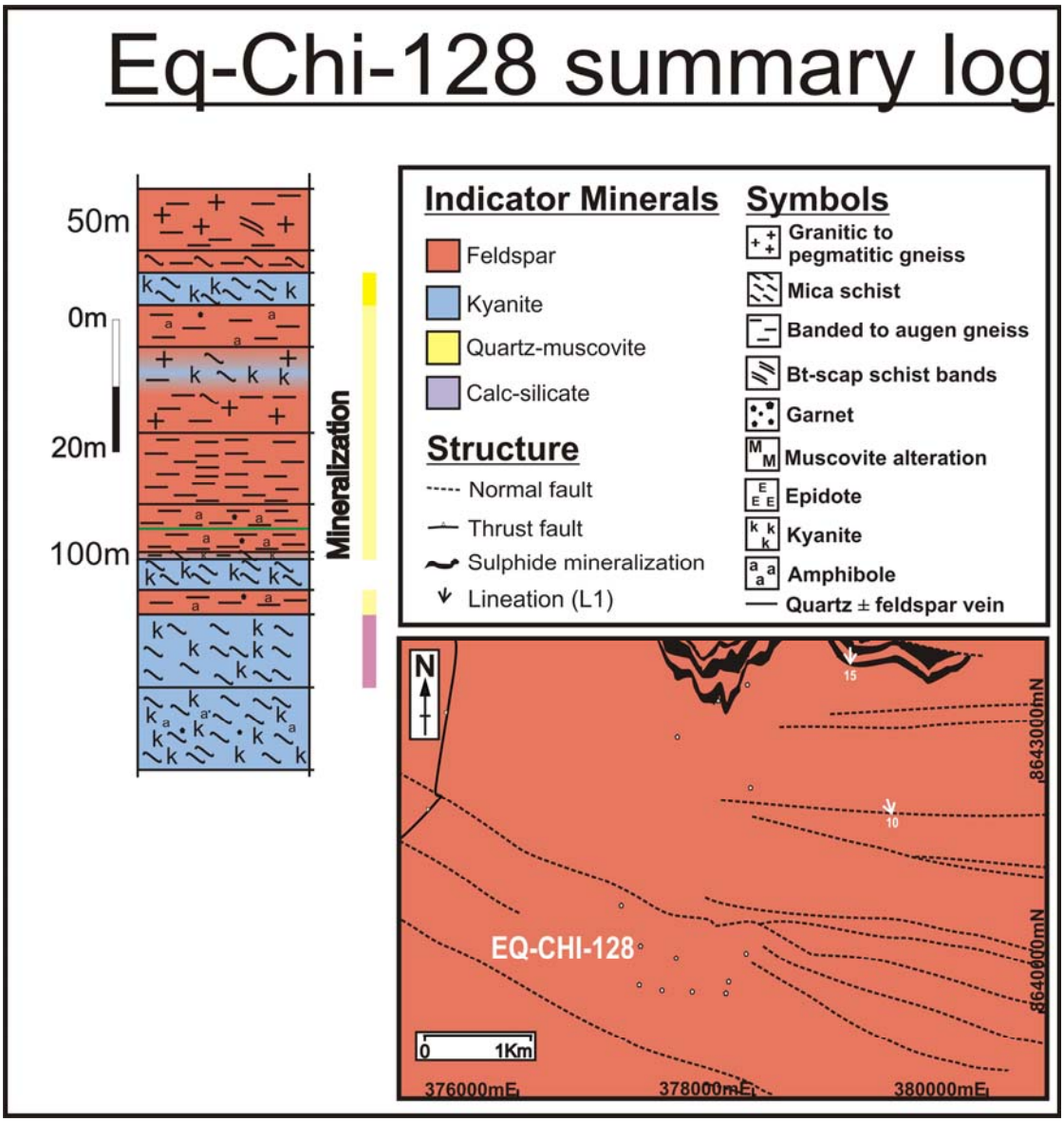

APPENDIX A

APPENDIX A2: CHIMIWUNGO SUMMARY LOGS

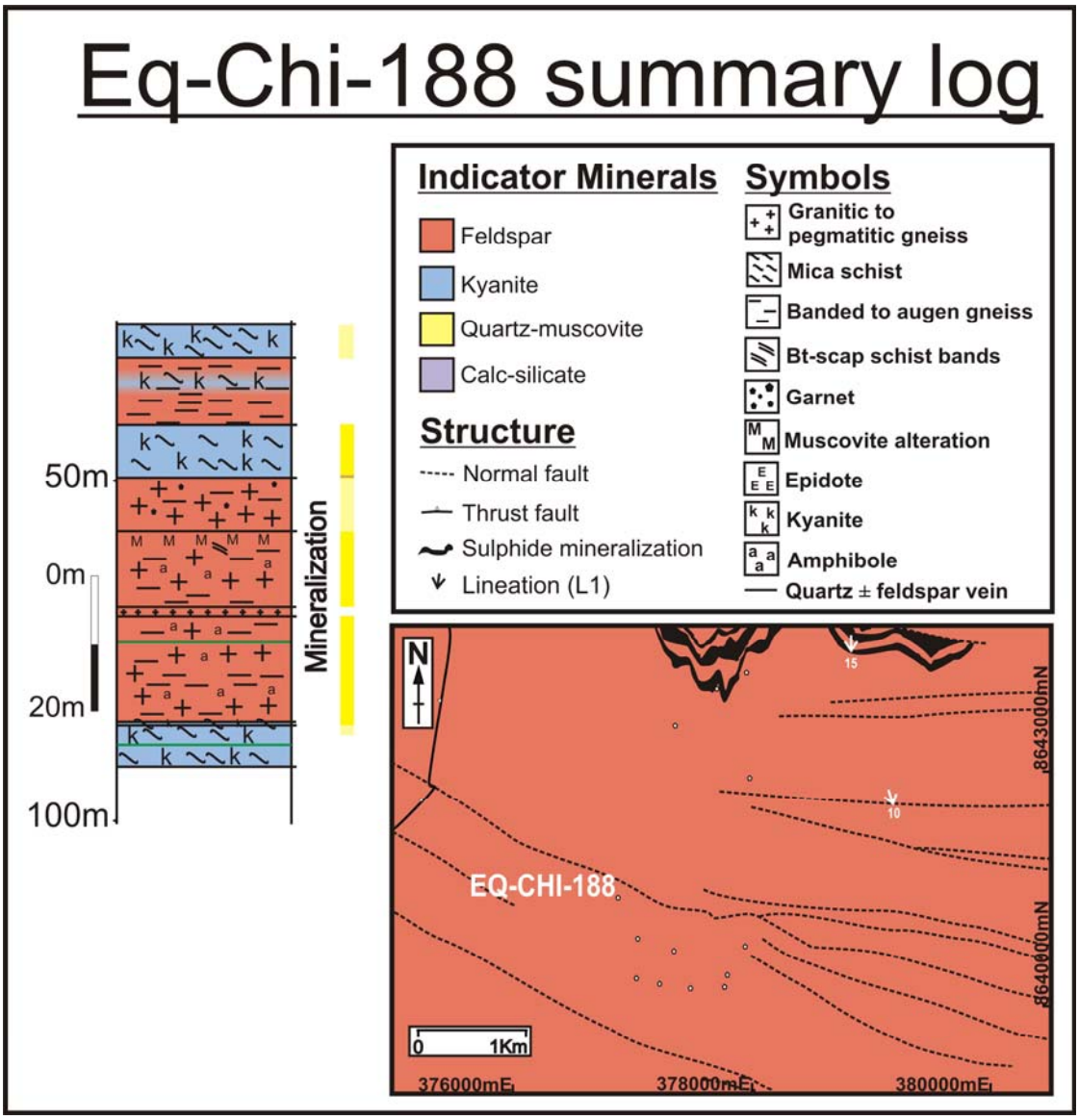

APPENDIX A

APPENDIX A2: CHIMIWUNGO SUMMARY LOGS

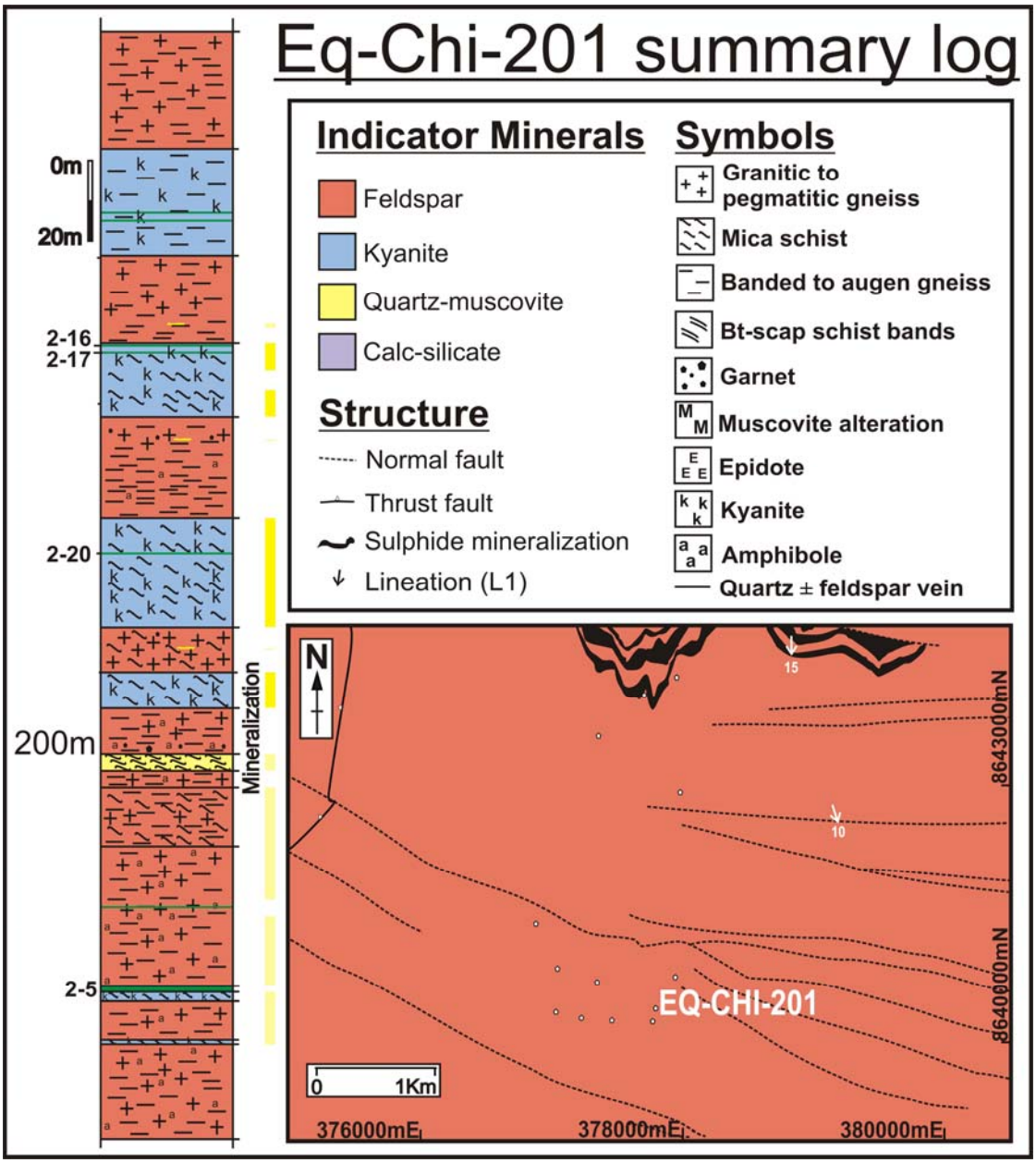

APPENDIX A

APPENDIX A2: CHIMIWUNGO SUMMARY LOGS

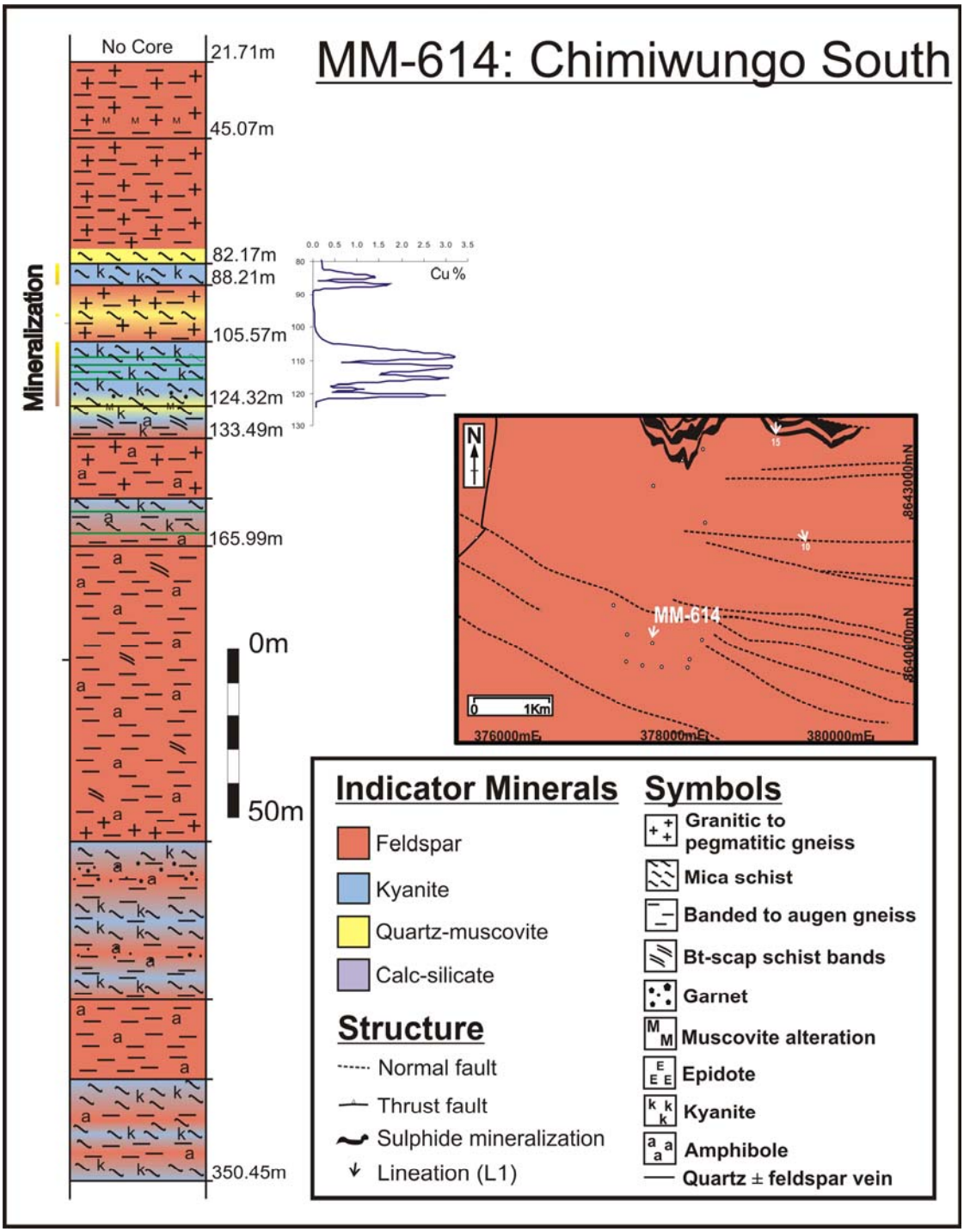

APPENDIX A

APPENDIX A2: CHIMIWUNGO SUMMARY LOGS

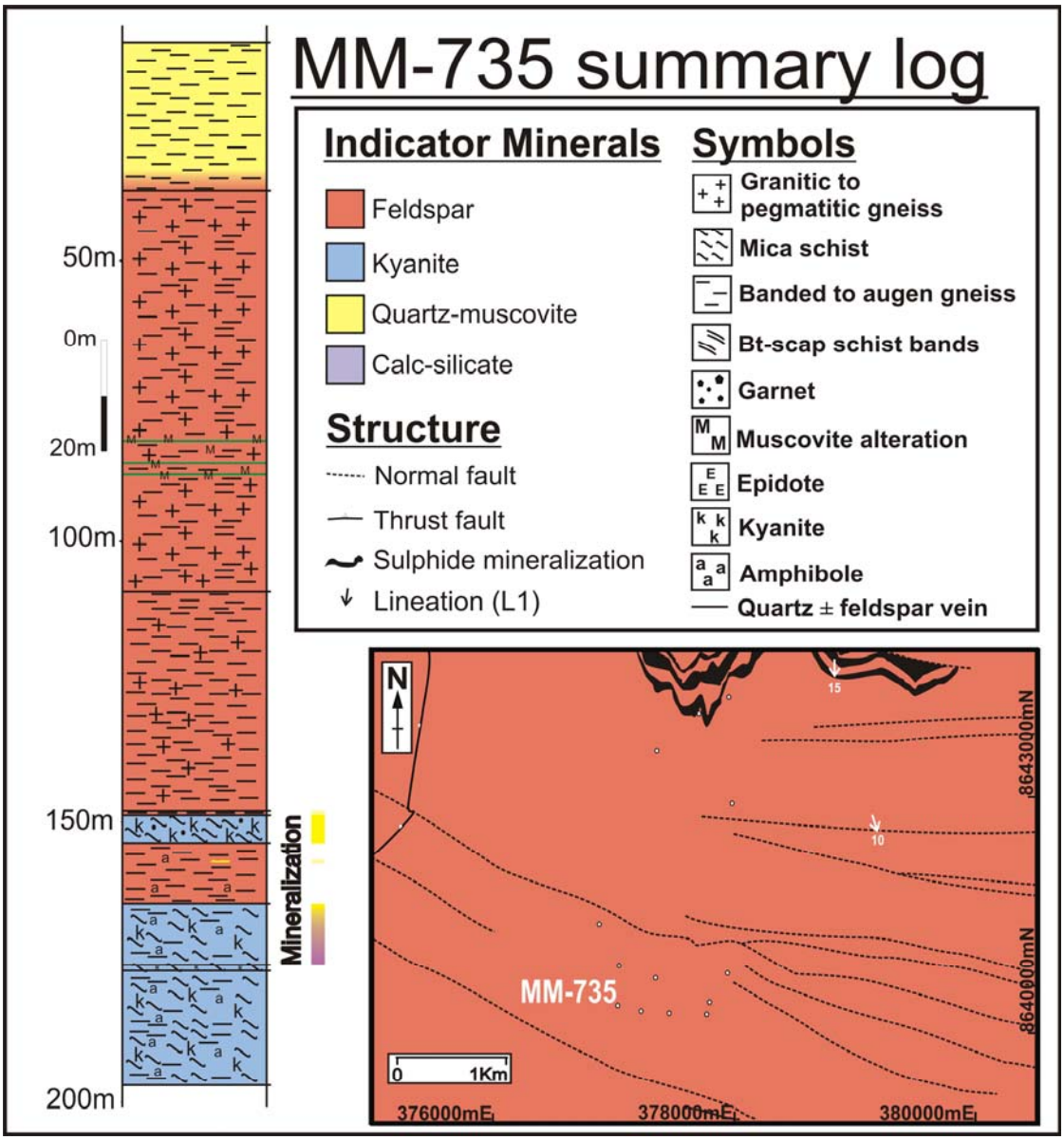

APPENDIX A

APPENDIX A3: MALUNDWE SUMMARY LOGS

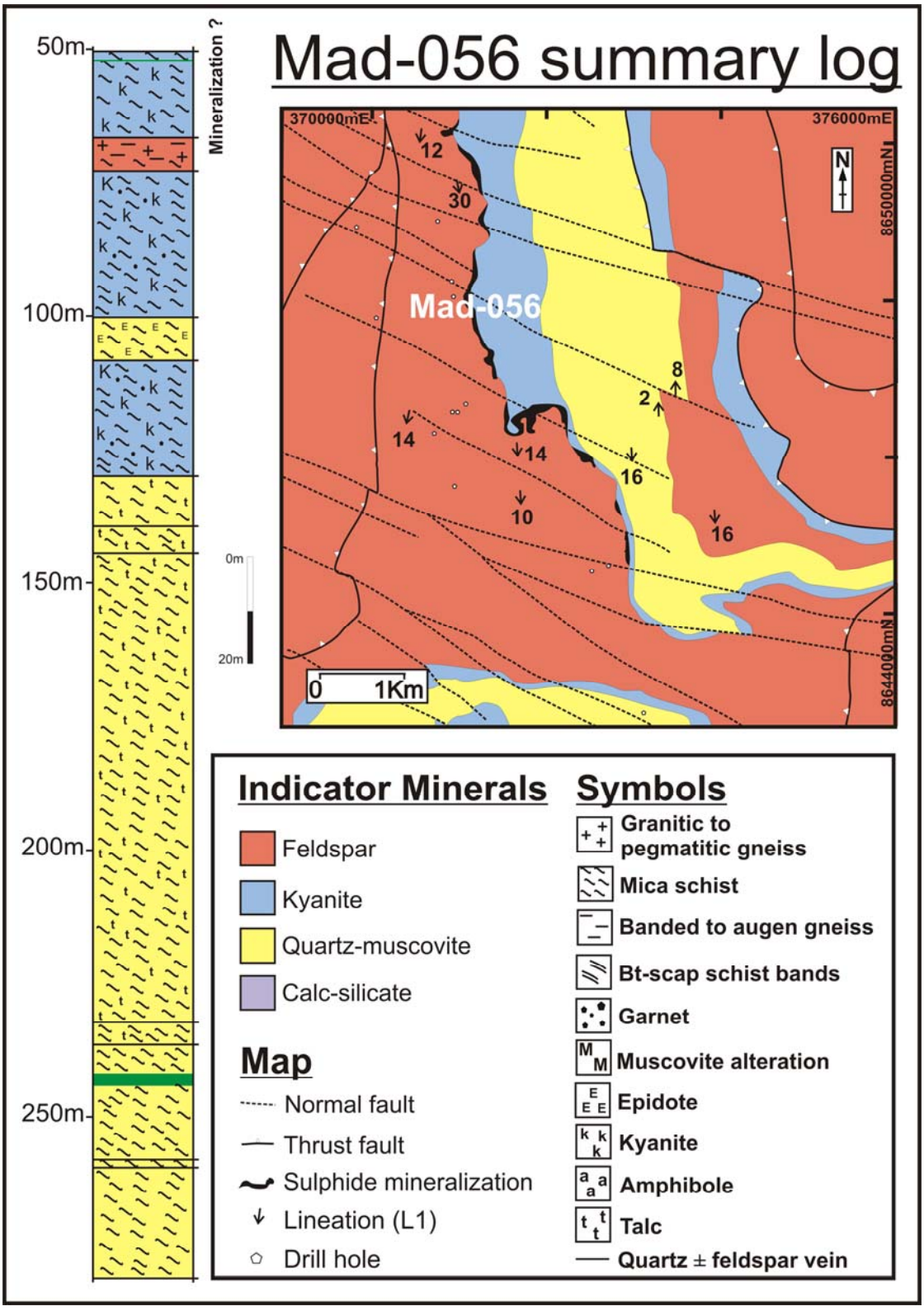

APPENDIX A

APPENDIX A3: MALUNDWE SUMMARY LOGS

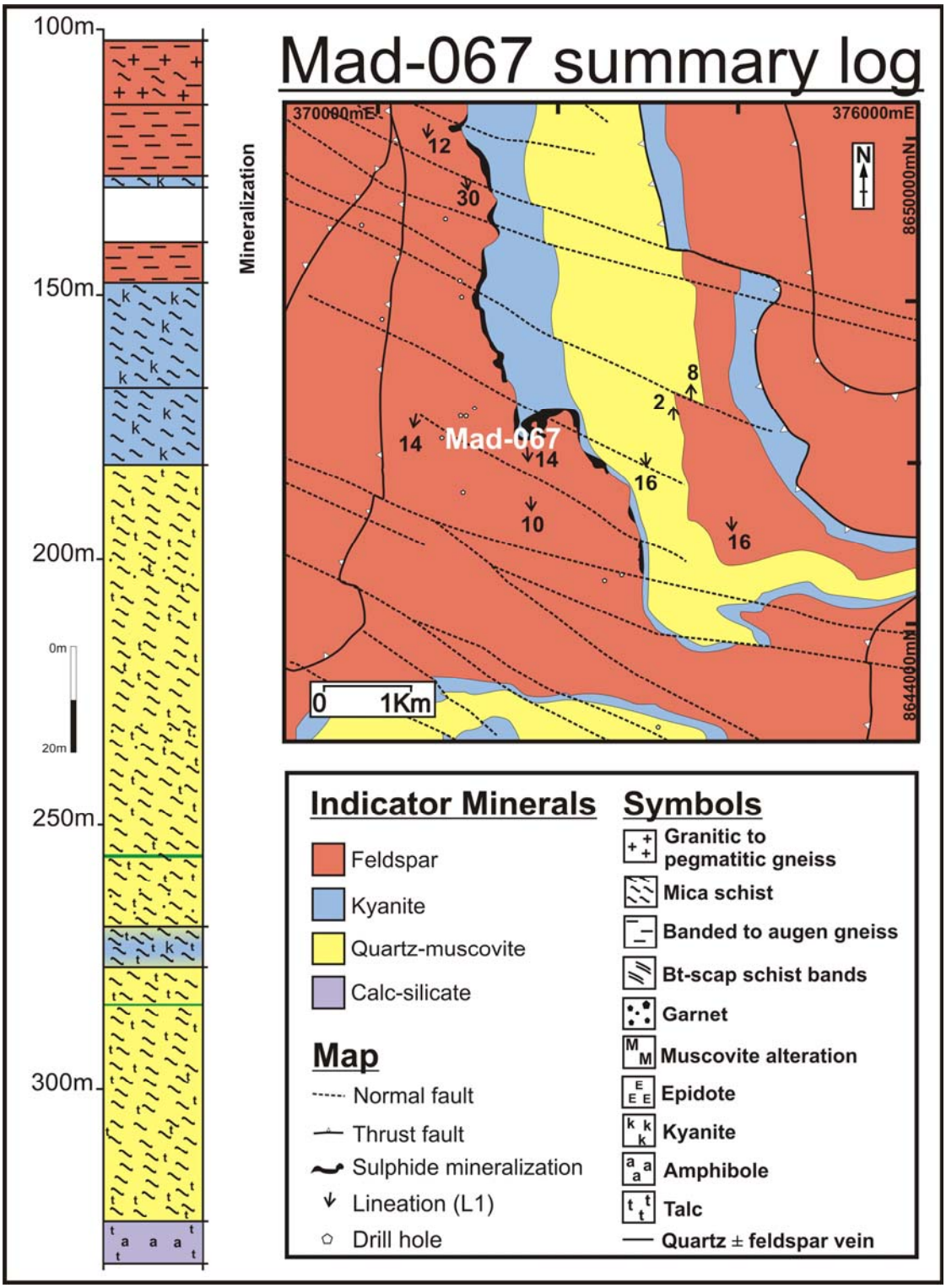

APPENDIX A

APPENDIX A3: MALUNDWE SUMMARY LOGS

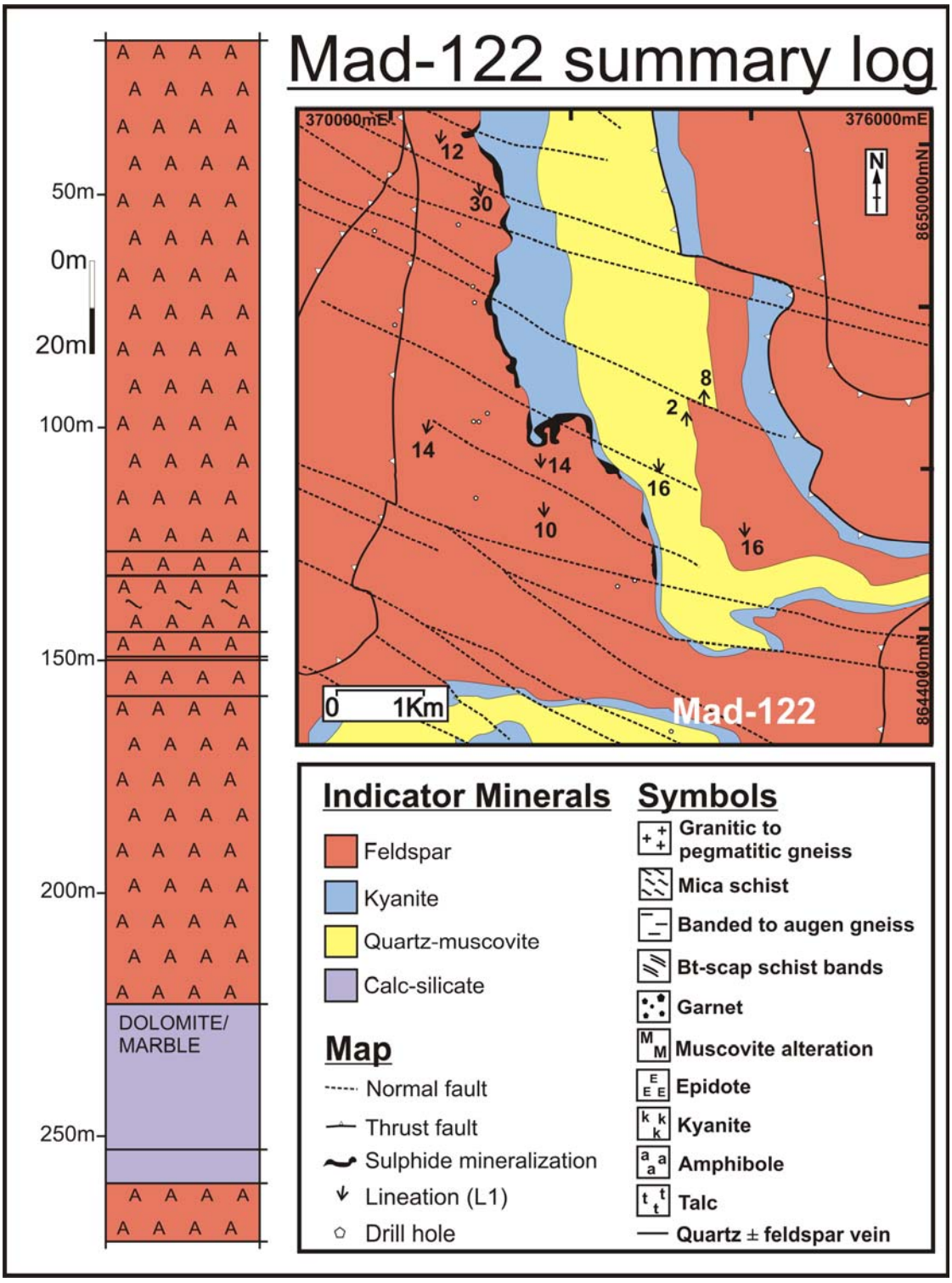

APPENDIX A

APPENDIX A3: MALUNDWE SUMMARY LOGS

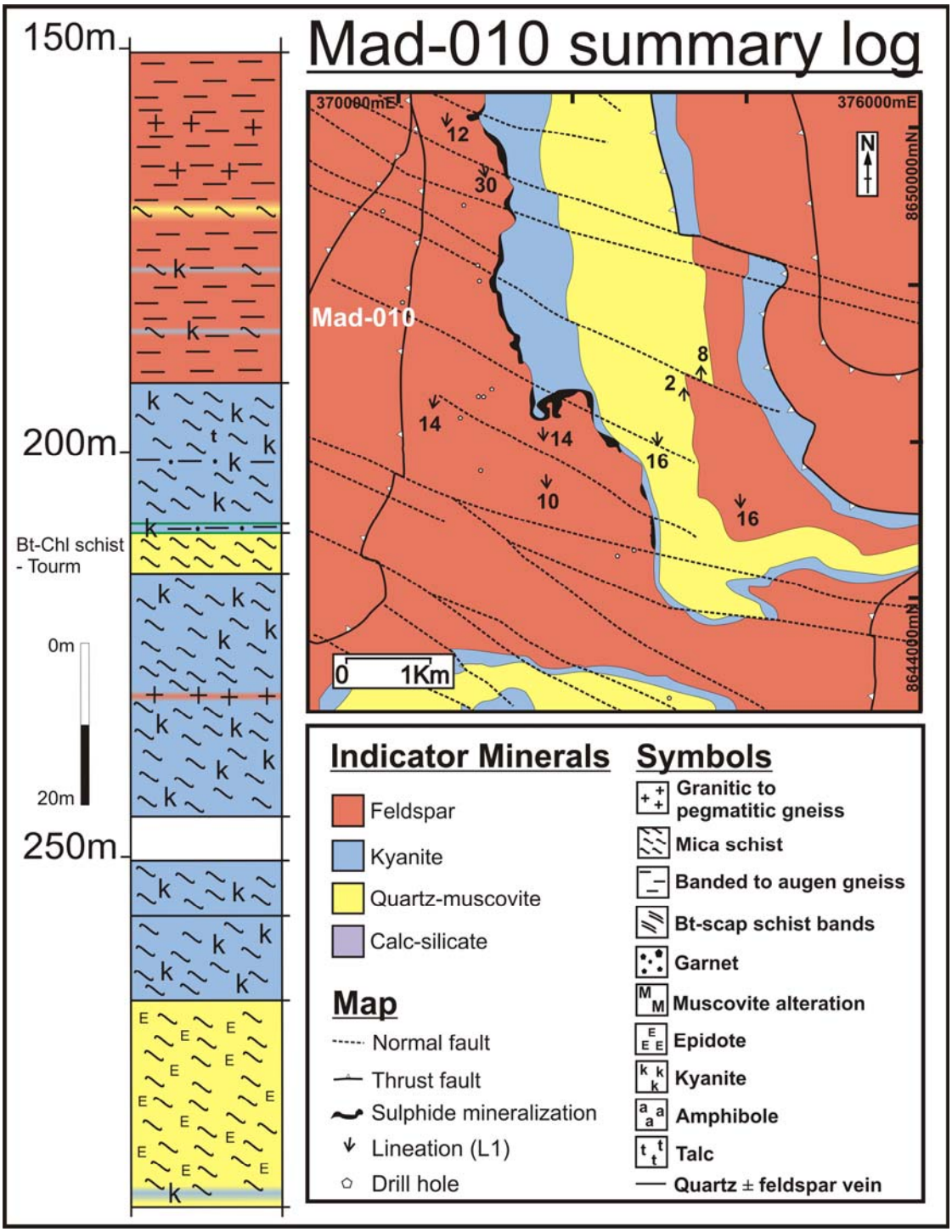

APPENDIX A

APPENDIX A3: MALUNDWE SUMMARY LOGS

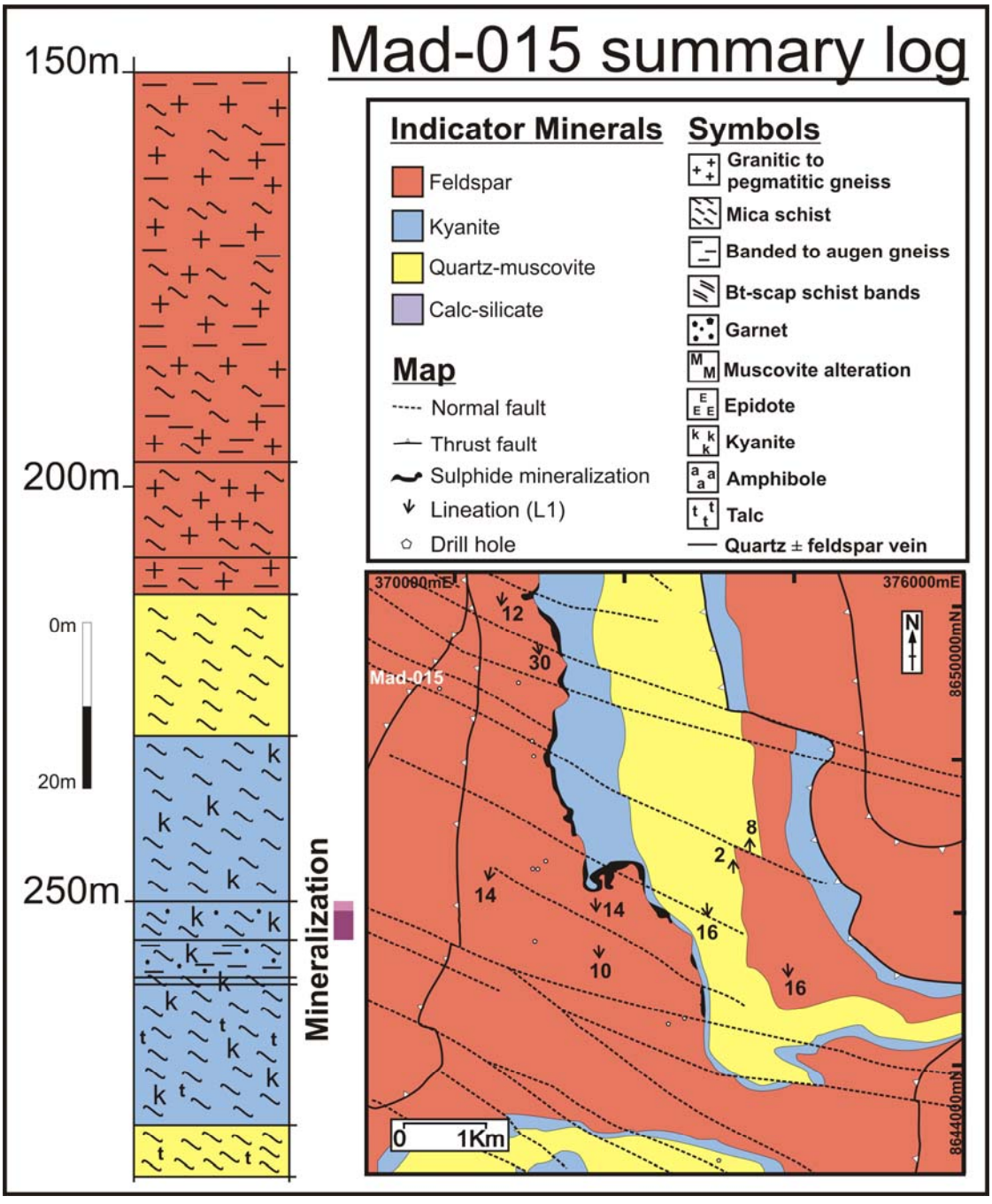

APPENDIX A

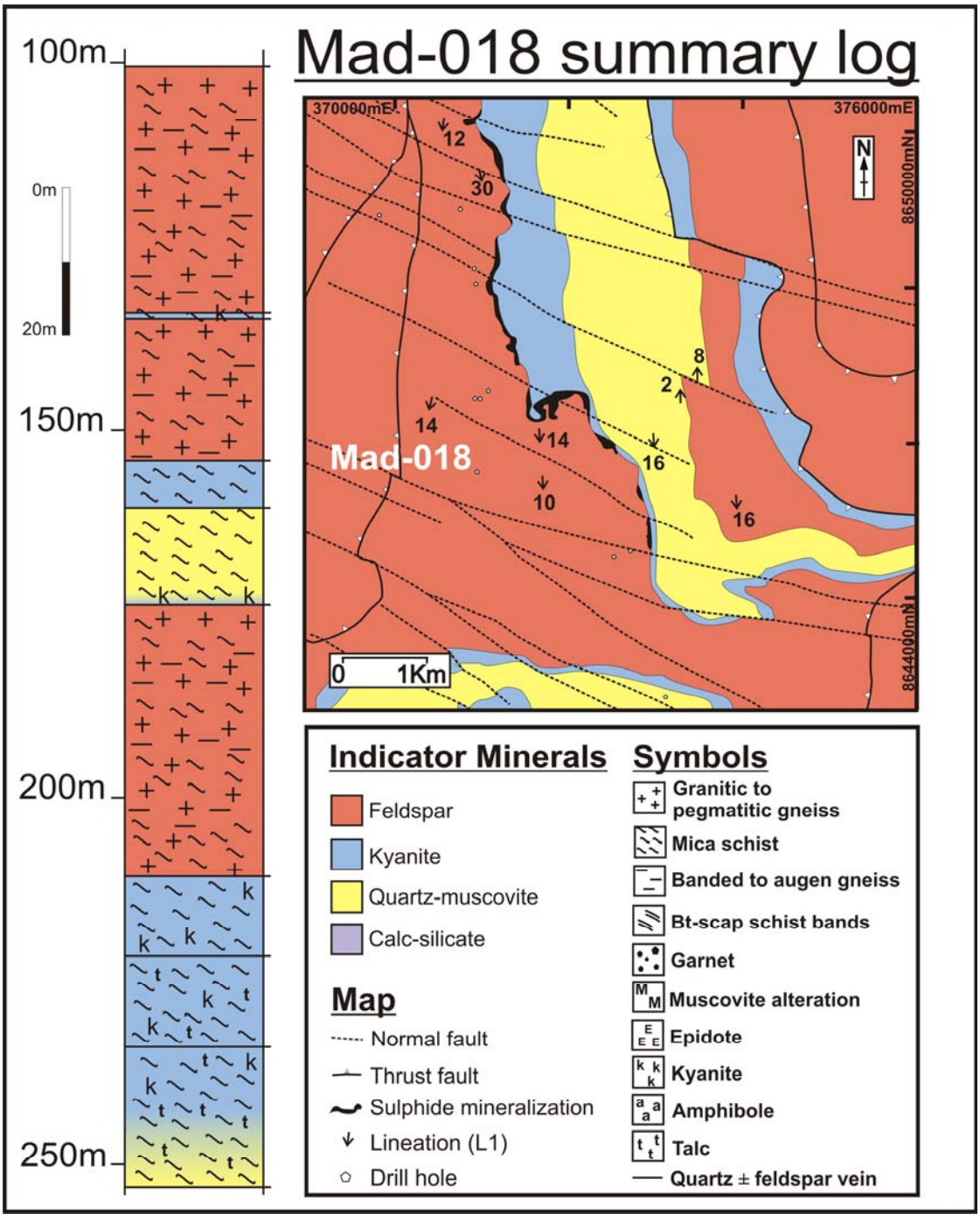

APPENDIX A3: MALUNDWE SUMMARY LOGS

APPENDIX A

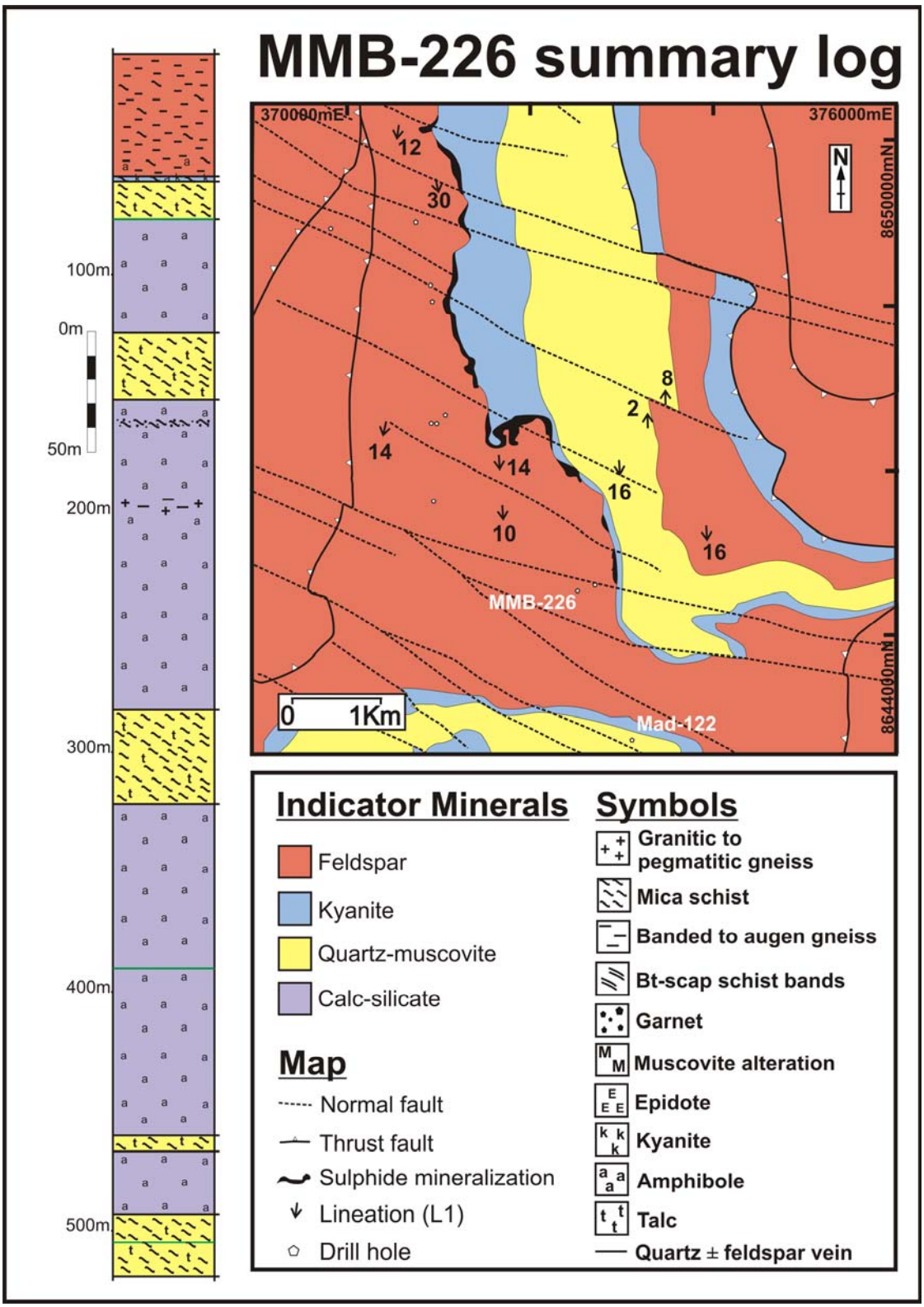

APPENDIX A3: MALUNDWE SUMMARY LOGS

APPENDIX A

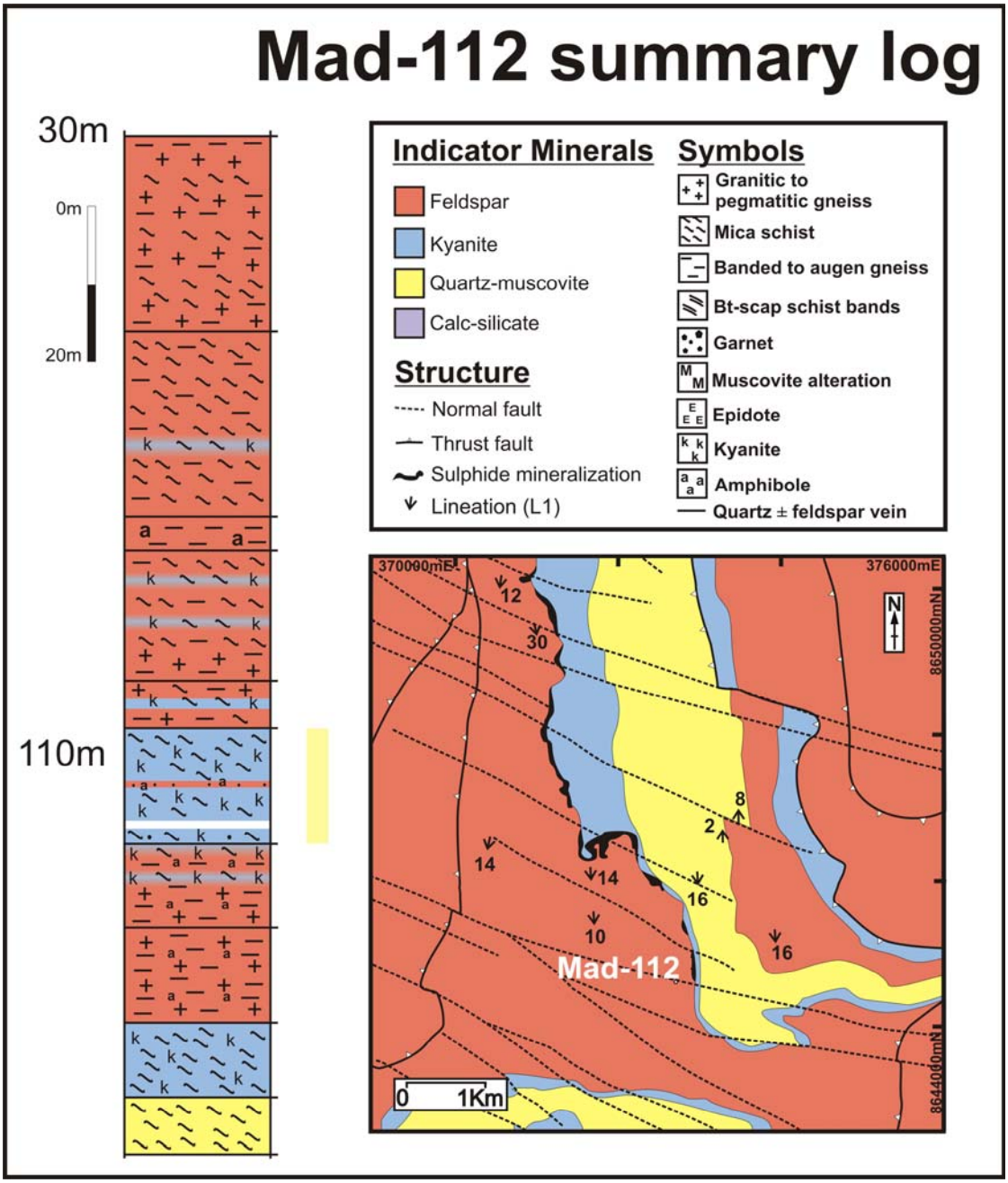
Mad-112 summary log
30m
0m
20m
110m
Indicator Minerals
Feldspar
Kyanite
Quartz-muscovite
Calc-silicate
Structure
Normal fault
Thrust fault
Sulphide mineralization
Lineation (L1)
Symbols
Granitic to pegmatitic gneiss
Mica schist
Banded to augen gneiss
Bt-scap schist bands
Garnet
Muscovite alteration
Epidote
Kyanite
Amphibole
Quartz ± feldspar vein
370000mE
376000mE
8650000mN
8644000mN
N
12
30
8
2
14
14
16
10
16
Mad-112
0
1Km

APPENDIX B

APPENDIX B1: XRF data – precision, accuracy and detection limits

Bead		Pellet					
SiO2	0.005%	Co	2ppm	Pb	2ppm	Ce	7ppm
TiO2	0.005%	Cr	5ppm	Ba	2ppm	Mo	2ppm
Al2O3	0.005%	V	5ppm	Rb	6ppm	Sn	2ppm
Fe2O3	0.005%	Ni	2ppm	Sr	2ppm	Sb	3ppm
MnO	0.005%	Sc	7ppm	Y	2ppm	W	3ppm
MgO	0.005%	Cu	2ppm	Zr	2ppm	Ag	3ppm
CaO	0.005%	Zn	2ppm	Nb	2ppm	Se	1ppm
K2O	0.005%	As	2ppm	Th	2ppm	Cd	2ppm
Na2O	0.005%	Bi	2ppm	U	3ppm	Ge	2ppm
P2O5	0.005%	Tl	2ppm	La	5ppm	Ga	2ppm

XRF elemental detection limits

The precision of XRF data is dependent on the concentration relative to the elemental detection limit. The accuracy of the data collected is monitored by reference to internationally certified standards.

In addition to the registered standards BCR-1 and Mag-1, a copper and a cobalt standard were used (made by adding 10% copper and 3% cobalt respectively to a certified standard). The reported concentrations of selected elements for BCR-1 and Mag-1 and the results measured during XRF analysis at the University of Southampton are provided below.

	percent							ppm						
BCR-1	SiO2	Al2O3	Fe2O3	MgO	CaO	K2O	Na2O	Co	Cu	Zn	Ba	Pb	Zr	V
Reported*	54.11	13.64	12.47	3.48	6.95	1.69	3.27	37	19	130	681	14	190	407
Measured 1	56.49	13.63	12.89	2.53	6.71	1.68	3.17	40	25	124	686	15	189	398
Measured 2	56.49	13.62	12.88	2.53	6.72	1.68	3.16	35	25	124	676	15	188	397
Mag-1														
Reported*	50.36	16.37	6.55	3.00	1.37	3.55	3.83	20	30	130	479	24	126	140
Measured 1	59.98	16.25	7.36	3.90	1.43	3.77	2.77	22	30	135	530	29	134	167
Measured 2	59.93	16.25	7.37	3.89	1.43	3.77	2.77	23	30	136	521	28	134	166

Reported values for internationally certified standards from:

GOVINDARAJU, K. 1994. Geostandards Newsletter, **18**, 15.

Accuracy has been determined to be 5% RSD or better based on regular assessments of accuracy for the Southampton XRF involving submission to international reference exercises to compare blind results with internationally certified standards. This was confirmed by most of the results summarized in the table. Analytical results compared favourably with recommended values and are within the 5% RSD limits for both major and minor elements. Reproducibility between samples is good. This was confirmed by the repeats of the Cu + Co standards.

APPENDIX B

APPENDIX B1: Chimiwungo XRF data

Chimiwungo bead data (%)

	SiO_2	TiO_2	Al_2O_3	Fe_2O_3	MnO	MgO	CaO	K_2O	Na_2O	P_2O_5	LOI
1-1	75.04	0.51	13.02	1.32	0.01	2.72	0.17	4.48	0.41	0.12	2.02
1-3	71.85	0.55	13.11	1.79	0.01	7.38	0.27	3.73	0.35	0.19	2.77
1-5	74.05	0.37	10.98	1.70	0.01	6.08	0.14	2.55	0.26	0.08	1.16
1-6	73.78	0.36	10.88	1.66	0.01	5.89	0.13	2.46	0.26	0.07	1.74
1-7	69.82	0.47	13.19	3.05	0.01	4.69	0.19	5.06	0.39	0.11	2.29
1-8	57.34	0.16	22.27	2.34	0.04	3.15	3.47	1.37	7.87	0.03	2.55
1-10	65.72	1.06	16.51	2.93	0.02	2.81	1.91	3.44	4.19	0.21	1.14
1-11	77.76	0.19	11.70	1.41	0.01	1.17	1.35	1.84	3.24	0.00	0.97
1-12	66.64	0.73	16.13	2.92	0.01	5.32	0.35	5.32	0.14	0.01	2.73
1-13	66.35	0.57	19.74	3.34	0.02	3.50	0.26	4.23	1.04	0.05	2.32
1-16	71.77	0.71	15.19	1.17	0.02	1.17	3.16	1.04	4.91	0.21	0.68
1-17	82.41	0.38	8.55	2.34	0.01	3.18	0.74	2.66	0.38	0.03	1.79
1-18	58.09	2.58	23.18	2.76	0.04	2.98	3.83	3.21	3.86	0.30	3.13
1-19	49.41	1.72	16.28	14.09	0.15	8.39	8.11	1.03	1.70	0.18	2.95
1-20	43.76	0.70	21.40	9.33	0.09	7.83	10.89	0.92	4.09	0.15	8.52
1-21	45.42	1.05	21.99	9.18	0.05	10.21	3.86	5.85	2.97	0.07	2.02
1-22	63.86	1.44	18.78	4.93	0.06	4.71	4.75	0.64	2.36	0.32	0.95
1-22	63.42	1.44	18.66	4.92	0.06	4.61	4.74	0.64	2.26	0.32	0.95
1-23a	72.62	0.41	12.98	3.94	0.02	3.84	1.77	3.08	2.05	0.01	1.07
1-26	62.06	0.71	19.99	3.65	0.01	7.83	0.06	4.64	0.46	0.02	2.62
1-27	69.06	0.53	16.31	3.06	0.01	5.37	0.24	4.11	0.43	0.16	2.81
1-28	58.22	0.70	19.60	3.79	0.01	4.80	0.27	5.41	-0.10	0.22	4.57
1-30	73.99	0.14	14.37	5.25	0.16	1.02	1.90	2.71	0.65	0.01	1.27
1-31	70.25	0.67	14.08	5.37	0.11	2.71	3.81	2.24	0.98	0.08	0.97
1-32	70.04	0.85	12.56	8.77	0.04	5.02	0.23	2.16	0.09	0.04	3.64
1-33	56.74	0.66	21.04	5.76	0.01	6.04	0.12	3.98	0.09	0.05	3.67
1-34	59.49	0.86	15.88	9.94	0.29	5.26	3.28	3.24	2.71	0.12	1.24
1-35	53.54	0.54	17.07	10.10	0.16	6.62	7.02	1.51	3.64	0.06	1.82
1-36	58.24	0.83	21.32	7.15	0.04	2.91	1.11	5.65	1.84	0.02	2.77
1-38	50.09	1.76	13.05	14.74	0.18	6.57	8.41	1.68	2.14	0.14	0.69
1-39	64.25	1.04	14.75	6.24	0.04	3.72	2.45	2.68	4.23	0.18	0.76
1-40	42.29	1.97	16.20	15.91	0.09	12.81	0.87	8.48	1.17	0.30	1.35
1-42	47.92	3.13	14.64	14.20	0.15	7.19	7.29	2.34	2.29	0.40	0.71
1-43	62.12	1.23	16.58	6.14	0.03	4.91	1.22	5.27	1.81	0.14	1.94
2-1	63.65	1.04	14.10	7.77	0.08	3.90	3.15	3.00	3.29	0.15	0.75
2-2	73.95	0.37	8.84	10.82	0.67	1.69	3.32	0.15	0.85	0.04	-0.35
2-3	49.72	1.79	13.89	16.03	0.16	6.30	7.80	1.30	2.22	0.20	1.62
2-4	48.54	3.35	13.47	16.20	0.24	5.79	8.08	1.07	2.63	0.42	1.21
2-5	100.72	0.01	0.09	0.06	0.00	0.05	0.04	0.01	-0.05	-0.01	0.05
2-7	59.48	0.91	17.29	5.23	0.03	9.82	0.45	5.48	1.34	0.16	27.00
2-8	54.22	2.47	13.90	11.82	0.12	6.55	7.32	1.13	2.64	0.32	0.85

Note: Bead samples were fused with a flux (lithium tetraborate) into glass disks (following ignition of the samples >900ºC and noting of LOI) using platinum equipment at 1200ºC.

APPENDIX B

APPENDIX B1: Chimiwungo XRF data

Chimiwungo pellet data (ppm)

	Co	Cr	V	Ni	Sc	Cu (%)	Zn	Bi	Pb	Ba	Rb	Sr	Y	Zr	Nb	Hf	Th	U	La	Ce	Sb	Se	Ga	S (%)	Cl (%)
1-1	69	40	30	16	12	0.00	1	5	0	366	99	10	57	384	32	10	16	2	64	153	3	6	18	0.00	0.01
1-2a	150	32	52	65	14	0.00	6	5	0	140	109	9	102	424	20	10	22	1	51	172	3	7	16	0.00	0.03
1-2b	182	68	47	68	12	0.00	5	5	1	138	109	9	105	459	21	11	25	2	60	187	2	9	16	0.00	0.05
1-3	123	67	32	18	13	0.00	5	5	1	342	114	34	29	358	9	10	4	-2	11	18	3	4	18	0.00	0.06
1-4	149	70	23	12	10	0.00	3	5	0	292	128	14	79	454	33	12	17	-3	32	103	3	10	17	0.00	0.03
1-5	183	98	38	57	12	0.00	3	5	0	104	71	5	83	344	23	8	17	-2	18	45	4	9	16	0.00	0.05
1-6	141	60	30	37	12	0.00	5	5	1	252	99	14	122	510	34	13	23	-2	50	131	4	8	20	0.00	0.05
1-7	156	53	22	14	8	0.00	8	6	1	288	145	17	84	469	29	12	27	-2	43	99	4	10	20	0.00	0.06
1-8	138	23	11	21	3	0.00	27	5	7	203	41	343	5	30	7	4	0	-1	2	3	3	4	13	0.00	0.26
1-10	122	44	38	8	15	0.00	8	6	2	526	87	164	72	1067	36	23	20	0	128	286	2	5	22	0.00	0.04
1-11	170	94	7	5	2	0.00	4	5	6	205	48	101	63	328	18	9	29	-1	138	288	4	10	15	0.00	0.03
1-12	740	124	106	130	17	0.60	8	5	1	585	141	26	46	157	10	29	18	4	43	88	4	7	22	0.11	0.08
1-13	602	191	98	51	17	0.98	5	5	1	614	109	33	25	123	9	30	12	1	52	99	3	5	22	0.87	0.05
1-15	2199	207	238	260	23	0.54	12	5	3	321	143	8	48	126	19	25	12	25	148	296	3	3	24	0.82	0.09
1-16	146	80	36	4	7	0.00	5	5	4	208	29	121	110	395	32	10	16	2	80	191	2	6	18	0.01	0.03
1-17	655	159	76	25	12	0.15	12	5	0	407	74	35	15	82	4	10	4	0	30	44	2	4	11	0.30	0.07
1-18	235	137	192	27	31	0.01	20	6	9	582	114	299	80	384	38	11	42	15	211	430	4	1	26	0.20	0.06
1-19	622	249	294	116	47	0.05	43	6	29	209	21	162	30	102	14	5	1	0	14	60	7	2	24	0.90	0.72
1-20	582	233	189	96	11	0.11	47	5	97	155	30	195	2	32	2	8	-4	0	6	34	3	1	22	0.41	0.96
1-21	754	217	261	137	37	0.00	28	6	6	788	179	245	49	143	2	6	12	4	106	237	2	1	36	0.00	0.28
1-22	177	133	182	39	29	0.00	12	5	3	121	15	172	38	198	6	6	1	3	29	53	2	4	21	0.00	0.15
1-23a	133	75	55	33	8	0.00	17	6	3	516	108	179	27	364	4	10	12	-1	18	45	5	3	16	0.00	0.11
1-23b	86	69	32	13	7	0.00	8	5	4	595	67	177	51	359	7	10	14	0	43	77	3	4	15	0.00	0.07
1-24	759	182	117	50	18	0.51	8	5	1	552	109	26	24	126	10	22	10	0	20	32	2	3	19	0.91	0.02
1-25	261	54	15	4	5	0.14	1	5	1	584	75	35	6	50	1	8	4	1	35	75	3	8	19	0.18	-0.01
1-26	1480	180	137	104	26	0.30	7	5	3	716	152	29	22	140	12	16	8	19	29	66	3	3	31	0.57	0.02
1-27	2828	138	128	70	22	0.35	7	5	1	596	135	20	47	103	8	16	18	0	64	134	2	7	24	0.78	0.01
1-28	801	165	124	55	19	3.43	1	16	18	839	186	53	115	164	9	117	39	26	691	1416	0	4	28	1.39	0.02
1-30	200	98	32	11	9	0.28	2	5	3	480	65	54	76	105	4	13	2	9	60	106	2	8	14	0.46	-0.01
1-31	210	161	101	23	18	0.04	10	5	3	263	73	78	32	143	13	6	8	1	28	58	3	7	16	0.23	0.04
1-32	388	147	123	108	17	0.52	25	6	1	314	112	18	44	179	18	26	26	3	123	234	3	3	17	0.60	0.16
1-33	759	183	138	201	25	1.49	25	6	3	668	125	28	27	129	10	52	10	4	26	70	1	3	33	1.74	0.07
1-34	146	205	178	73	25	0.02	54	6	6	486	168	183	33	101	8	4	4	0	22	53	3	2	17	0.03	0.19
1-35	157	184	166	121	41	0.00	62	5	4	215	73	197	89	35	4	2	0	-1	11	27	4	5	19	0.05	0.42
1-36	134	205	143	43	25	0.15	10	5	4	772	197	93	34	161	19	10	19	0	50	105	4	2	31	0.57	0.10
1-37	154	80	36	11	7	0.00	11	5	7	374	92	53	15	134	8	5	10	-1	9	23	2	7	12	0.03	0.08
1-38	103	239	416	56	55	0.04	60	6	1	129	53	64	46	114	8	6	2	-1	12	44	7	2	20	0.08	0.42
1-39	84	122	159	34	26	0.02	27	5	2	253	124	112	51	203	12	7	15	1	39	84	4	3	18	0.07	0.16
1-40	290	117	304	94	28	0.26	78	6	1	794	386	26	23	183	16	15	-2	3	-5	13	6	2	31	0.22	0.27
1-41	263	102	255	81	31	0.05	51	6	1	685	320	11	31	243	16	9	3	5	11	33	8	4	22	0.05	0.22
1-42	245	207	415	92	41	0.11	46	6	2	338	100	81	86	235	14	10	4	2	30	82	7	1	25	0.15	0.35
1-43	471	149	180	44	25	0.25	15	6	1	641	217	72	54	196	17	14	15	-1	45	92	1	3	22	0.28	0.18
2-1	96	153	157	45	24	0.01	43	6	3	388	147	102	59	199	16	6	21	1	70	139	3	7	19	0.03	0.19
2-2	311	140	45	11	12	0.00	4	5	3	19	4	23	97	141	6	5	5	0	5	28	4	13	5	0.01	0.04
2-3	225	386	397	102	70	0.14	72	6	18	96	48	77	68	154	10	10	2	1	15	47	7	4	23	0.38	1.07
2-4	185	157	399	81	47	0.13	51	6	-1	92	34	85	67	259	17	11	4	1	26	76	6	4	23	0.12	0.57
2-5	308	105	1	-4	0	0.00	-6	4	0	33	2	4	-2	11	1	1	1	-2	1	2	3	21	1	0.00	-0.02
2-7	153	148	179	80	24	0.00	17	5	1	251	162	71	22	145	12	5	10	0	2	13	3	3	21	0.00	0.04
2-8	169	134	335	56	50	0.03	22	6	1	106	34	49	84	229	20	9	7	6	25	65	-10	4	22	0.03	0.12

Note: Pellet samples were prepared by mixing approximately 10g of sample powder (crushed in an iron tema mill) with a small amount of binding agent (8% PVA in water), which was then pressed into powder pellets with a force of 10-12t/in^2 and allowed to dry overnight at approximately 80ºC.

APPENDIX B

APPENDIX B2: Malundwe XRF data

Malundwe bead data (%)

	SiO_2	TiO_2	Al_2O_3	Fe_2O_3	MnO	MgO	CaO	K_2O	Na_2O	P_2O_5	LOI
3-1	73.75	0.14	14.50	1.57	0.01	0.77	2.13	3.80	2.93	0.01	1.08
3-2	72.91	0.42	12.10	2.61	0.05	1.05	5.28	3.55	0.47	0.04	1.58
4-2	76.04	0.32	12.39	2.61	0.02	4.41	0.16	3.32	0.17	0.05	1.45
4-3	58.94	0.75	21.14	4.77	0.03	4.73	1.98	6.35	0.34	0.02	3.24
4-4	62.59	1.28	17.25	4.61	0.03	3.91	6.18	2.43	0.41	0.11	1.95
4-5	56.70	0.69	26.84	2.83	0.03	2.95	1.78	5.51	0.55	0.05	3.94
4-7	54.51	0.92	25.19	3.95	0.02	9.38	0.13	3.45	-0.06	0.03	3.34
4-8	54.73	1.05	22.79	3.93	0.02	4.91	0.15	7.61	0.18	0.02	2.63
5-1a	46.67	2.60	13.54	18.26	0.10	5.87	5.25	4.81	1.04	0.42	1.59
5-1b	74.07	0.27	13.38	2.51	0.02	0.99	1.78	2.24	4.84	0.03	0.50
5-2	76.43	0.17	12.44	1.55	0.02	0.58	2.96	1.76	3.80	0.03	0.91
5-3	62.26	0.67	16.20	6.16	0.04	3.38	1.17	4.95	4.68	0.03	0.93
5-4	64.10	0.96	15.08	6.34	0.04	3.60	1.89	4.24	4.08	0.20	1.02
5-5	47.16	1.64	14.61	15.36	0.08	11.72	0.25	8.76	0.33	0.14	1.57
5-6	61.10	0.76	14.78	8.75	0.04	6.81	0.22	7.03	0.47	0.05	2.11
5-7	64.18	0.66	19.76	3.25	0.01	3.13	0.13	5.30	0.05	0.01	2.91
5-8	68.95	0.65	15.71	4.17	0.01	3.77	0.08	3.65	-0.21	0.03	2.19
5-9	65.62	0.66	17.48	4.29	0.03	4.52	0.17	6.23	0.33	0.03	2.48
5-10	74.57	0.05	15.40	1.99	0.02	2.40	1.44	3.95	0.42	0.02	2.17
5-11	64.18	0.78	15.88	5.73	0.04	4.08	1.17	4.84	0.65	0.09	2.62
5-13	57.43	1.42	19.74	6.18	0.03	11.01	0.82	2.58	0.46	0.21	5.40
5-14	71.98	0.51	12.85	5.18	0.04	4.29	1.05	3.39	0.31	0.14	2.18
5-15	68.90	0.41	12.17	4.35	0.03	6.47	3.46	3.16	0.62	0.08	2.24
5-16	63.71	0.70	16.35	5.71	0.03	5.94	1.68	5.36	0.34	0.17	3.27
6-1	69.10	0.31	8.94	6.13	0.03	9.54	0.15	4.96	0.41	0.01	1.88
6-2	76.19	0.26	9.42	3.87	0.02	5.32	0.17	3.96	0.62	0.00	1.85
6-3	76.22	0.06	11.51	2.43	0.01	3.58	0.50	3.42	2.26	0.02	1.61
6-4	56.32	0.72	24.13	3.32	0.01	2.64	0.60	8.00	0.45	0.02	3.58
6-5	43.68	0.58	23.33	14.93	0.08	7.72	3.50	4.19	0.57	0.06	8.24
6-6	71.29	0.86	14.56	2.74	0.01	2.85	0.71	3.95	0.68	0.11	1.97
6-7	61.07	0.74	20.53	3.84	0.01	2.59	0.13	6.79	-0.11	0.05	2.79
6-8	56.86	0.86	17.70	8.67	0.03	3.16	2.74	4.17	2.65	0.06	0.96
6-9	59.29	0.75	22.13	2.74	0.01	2.83	0.11	6.08	-0.20	0.04	2.98
6-11	67.64	0.47	13.86	3.77	0.03	3.20	1.82	3.90	0.86	0.05	1.58
6-12	60.94	0.86	15.62	4.77	0.02	12.01	0.18	4.48	0.44	0.08	2.55
6-12r	65.56	0.89	14.07	4.38	0.02	10.39	0.20	4.37	0.48	0.09	2.03

APPENDIX B

APPENDIX B2: Malundwe XRF data

Malundwe pellet data (ppm)

	Co	Cr	V	Ni	Sc	Cu (%)	Zn	Bi	Pb	Ba	Rb	Sr	Y	Zr	Nb	Hf	Th	U	La	Ce	Sb	Se	Ga	S	Cl
3-1	58	81	19	1	6	0.01	5	5	3	496	89	153	23	57	8	5	9	-1	13	27	3	3	14	0.00	0.02
3-2	88	114	35	7	9	0.10	5	5	4	664	98	115	107	287	24	12	36	4	52	107	3	4	16	0.06	0.11
3-3	133	198	168	55	21	0.04	16	5	3	1267	202	53	12	136	23	6	11	4	10	9	2	3	30	0.04	0.17
3-5	323	192	106	47	17	0.92	12	6	4	434	150	8	51	204	21	38	20	3	39	91	1	7	23	0.34	0.18
3-6	245	66	29	12	6	0.00	5	4	6	178	105	46	64	226	16	6	92	16	33	69	4	12	15	0.00	0.06
4-2	134	91	52	18	12	0.04	5	5	0	335	141	8	29	229	6	9	32	4	12	30	3	5	15	0.05	0.10
4-3	149	201	135	63	24	0.52	9	5	10	958	225	167	37	120	14	25	19	0	47	89	4	2	33	0.36	0.12
4-4	141	175	168	56	34	0.95	10	6	7	270	129	85	49	336	25	42	22	3	33	84	3	3	25	0.74	0.13
4-5	92	140	78	20	13	1.14	42	8	13	560	141	89	47	138	31	47	23	33	24	51	1	2	26	0.39	0.07
4-6	144	172	125	47	25	0.23	6	6	2	757	99	24	57	306	33	18	19	2	31	75	4	2	28	0.17	0.03
4-7	108	171	151	31	25	1.05	14	7	23	999	245	24	37	197	26	44	19	1	29	57	3	2	34	0.41	0.13
4-8	152	312	155	83	25	1.92	23	10	3	372	115	9	57	230	18	77	14	5	31	68	3	3	30	0.59	0.08
5-1a	118	155	297	98	27	0.00	52	6	1	337	262	250	105	234	53	6	3	1	68	112	4	2	32	0.00	0.25
5-1b	74	80	22	3	9	0.00	8	5	3	173	60	164	81	322	29	8	20	2	114	205	4	4	19	0.00	0.05
5-2	70	90	17	0	6	0.00	5	5	2	238	45	77	52	329	17	8	20	1	69	144	4	5	15	0.01	0.08
5-3	91	165	81	37	11	0.00	27	5	1	354	175	97	18	146	33	5	11	-3	13	31	3	2	22	0.00	0.12
5-4	83	129	121	38	19	0.00	23	6	2	372	162	168	54	269	21	7	21	-2	54	101	3	2	20	0.00	0.10
5-5	190	265	283	105	31	0.01	59	6	0	425	405	7	17	135	14	4	-1	-5	3	11	8	1	25	0.00	0.16
5-6	158	107	96	39	14	0.06	31	6	-1	419	266	22	21	299	25	11	18	-2	14	38	5	3	22	0.00	0.11
5-7	680	162	124	69	21	1.53	7	6	2	756	173	34	25	132	16	61	14	1	32	70	2	3	29	0.63	0.06
5-8	266	157	102	30	16	2.23	6	11	2	435	158	14	18	147	12	84	12	-1	23	57	2	3	21	0.94	0.08
5-9	297	126	117	31	21	0.62	11	7	1	726	232	20	25	124	10	30	7	-2	23	50	1	3	24	0.26	0.09
5-10	224	66	12	4	6	0.04	3	4	1	541	137	37	19	12	2	3	3	-1	25	36	3	8	18	0.06	0.03
5-11	636	119	141	58	19	0.64	17	5	3	697	210	43	27	113	10	30	10	16	18	47	2	6	20	0.13	0.15
5-12	278	158	74	41	13	3.34	5	12	4	212	89	30	32	110	11	112	12	8	38	80	1	8	19	1.20	0.08
5-13	442	137	182	82	29	0.01	17	5	31	499	57	19	63	340	24	10	34	93	67	136	4	3	29	0.01	0.07
5-14	170	88	78	17	9	0.00	21	5	2	408	108	50	62	383	16	10	25	0	37	94	4	7	17	0.00	0.09
5-15	149	79	55	19	8	0.00	9	6	3	312	101	98	73	329	18	8	26	0	57	132	3	6	19	0.00	0.10
5-16	156	176	121	42	16	0.00	12	5	1	650	158	48	28	191	19	6	15	1	15	40	2	3	21	0.03	0.11
6-1	138	122	87	210	16	0.00	26	5	-1	145	201	7	10	212	13	6	18	-3	12	64	4	5	15	0.00	0.12
6-2	276	54	68	52	9	0.02	12	5	5	147	158	23	25	477	27	13	15	-2	11	33	3	12	12	0.00	0.07
6-3	191	76	47	30	4	0.00	11	5	1	149	118	63	11	320	8	8	11	-1	29	81	3	8	12	0.00	0.05
6-4	85	182	137	15	24	1.38	4	6	2	987	243	44	45	149	14	52	16	2	63	109	3	4	33	0.43	0.03
6-5	229	110	77	141	18	0.00	15	5	2	479	114	19	251	175	16	5	35	7	62	141	2	1	29	0.00	0.08
6-6	93	112	106	21	19	0.37	5	5	0	543	152	41	57	327	23	26	35	1	68	131	2	3	19	0.15	0.03
6-7	91	201	128	28	22	2.20	-1	6	2	765	243	27	25	133	10	79	15	-4	39	79	3	2	27	0.83	0.04
6-8	146	172	151	33	23	0.53	12	6	3	553	179	74	55	197	16	26	20	2	67	136	5	4	26	0.17	0.22
6-9	77	197	118	18	20	2.29	-1	6	2	883	175	29	29	132	15	82	29	1	90	164	5	2	30	0.86	0.02
6-10	110	242	127	25	21	2.02	-1	5	1	734	162	23	42	153	15	74	17	-1	42	73	2	4	27	0.78	0.02
6-11	218	78	60	15	10	0.01	5	5	3	407	132	83	45	171	13	6	25	1	30	60	1	10	19	0.01	0.11
6-12	217	134	170	83	21	0.00	11	5	1	314	152	6	42	150	13	5	13	7	11	25	2	6	21	0.00	0.10

APPENDIX B

APPENDIX B3: Electron microprobe data

	Zap	Na2O	F	MgO	SiO2	Al2O3	SO3	K2O	P2O5	CaO	Cl	TiO2	Cr2O3	MnO	FeO	CoO	NiO	SrO	BaO	Total
1-6	#1	1.13	0.00	1.26	47.84	34.65	0.01	8.22	0.03	0.00	0.01	0.62	0.02	0.00	3.09	0.00	0.02	0.00	0.13	97.0
1-6	#2	1.23	0.00	1.03	46.89	34.37	0.03	8.01	0.03	0.00	0.00	0.61	0.05	0.00	2.70	0.02	0.03	0.00	0.12	95.1
1-6	#3	1.18	0.00	1.23	48.41	34.65	0.04	8.12	0.04	0.00	0.01	0.59	0.00	0.01	3.06	0.00	0.00	0.00	0.20	97.5
1-6	#4	0.48	0.00	20.29	40.09	18.46	0.00	8.85	0.00	0.00	0.14	0.86	0.00	0.01	5.70	0.04	0.00	0.00	0.01	94.9
1-6	#5	0.42	0.00	20.30	39.16	18.23	0.06	8.92	0.03	0.01	0.09	0.92	0.01	0.00	5.96	0.02	0.02	0.00	0.07	94.2
1-6	#6	0.44	0.00	20.03	39.01	18.12	0.04	8.55	0.00	0.01	0.13	0.82	0.01	0.08	5.86	0.00	0.09	0.00	0.02	93.2
1-6	#7	0.47	0.00	21.10	41.09	17.66	0.00	9.03	0.02	0.00	0.12	0.78	0.00	0.01	5.65	0.00	0.00	0.00	0.07	96.0
1-6	#8	0.91	0.00	1.25	48.49	34.26	0.05	7.68	0.00	0.00	0.01	0.74	0.04	0.00	3.28	0.02	0.00	0.00	0.12	96.8
1-6	#9	0.43	0.00	20.83	40.04	18.67	0.03	8.83	0.01	0.01	0.10	0.73	0.00	0.04	5.62	0.03	0.04	0.00	0.04	95.5
1-6	#10	1.00	0.00	1.10	47.99	34.44	0.00	8.03	0.01	0.00	0.00	0.58	0.01	0.03	3.07	0.01	0.00	0.00	0.17	96.4
1-6	#11	0.44	0.00	20.17	39.14	18.45	0.00	8.99	0.02	0.00	0.13	0.61	0.00	0.04	6.03	0.03	0.02	0.00	0.00	94.1
1-6	#12	1.07	0.00	1.43	48.56	33.64	0.00	8.21	0.01	0.00	0.01	0.34	0.00	0.04	3.20	0.00	0.01	0.00	0.18	96.7
1-6	#13	1.03	0.00	1.72	50.03	33.17	0.02	8.37	0.00	0.00	0.00	0.22	0.00	0.00	2.98	0.01	0.00	0.00	0.11	97.7
1-6	#14	0.49	0.00	20.27	40.78	18.57	0.08	9.06	0.00	0.00	0.12	1.04	0.03	0.01	6.06	0.02	0.00	0.00	0.06	96.6
1-6	#15	0.46	0.00	20.38	40.25	18.66	0.01	8.94	0.00	0.00	0.09	0.62	0.00	0.02	6.05	0.07	0.05	0.00	0.08	95.7
1-6	#16	1.20	0.00	0.70	47.66	35.67	0.00	7.96	0.00	0.00	0.00	0.40	0.04	0.03	2.69	0.00	0.04	0.00	0.12	96.5
1-6	#17	1.01	0.00	1.07	48.50	34.85	0.00	8.13	0.00	0.00	0.01	0.61	0.00	0.02	2.97	0.00	0.05	0.00	0.13	97.3
1-6	#18	0.40	0.00	20.68	40.09	18.44	0.01	9.15	0.02	0.00	0.12	0.83	0.00	0.06	5.87	0.03	0.02	0.00	0.05	95.8
1-6	#19	1.13	0.00	1.05	48.25	34.85	0.00	8.47	0.00	0.00	0.01	0.58	0.03	0.00	2.74	0.02	0.05	0.00	0.14	97.3
1-6	#20	0.47	0.00	20.72	39.65	18.95	0.06	8.71	0.00	0.01	0.09	0.76	0.01	0.02	6.15	0.02	0.05	0.00	0.04	95.7
1-6	#21	0.39	0.00	20.89	40.58	17.40	0.00	8.05	0.00	0.00	0.14	0.69	0.00	0.03	5.38	0.04	0.02	0.00	0.04	93.7
1-6	#22	0.52	0.00	20.47	40.53	18.98	0.00	9.06	0.00	0.00	0.08	0.85	0.00	0.02	5.73	0.08	0.04	0.00	0.05	96.4
1-6	#23	0.44	0.00	20.56	40.53	18.55	0.00	8.62	0.02	0.02	0.12	0.85	0.00	0.02	5.78	0.02	0.04	0.00	0.06	95.6
1-19	#24	1.58	0.00	4.77	37.44	15.30	0.00	1.84	0.00	11.46	3.30	0.40	0.19	0.18	22.22	0.09	0.01	0.00	0.08	98.9
1-19	#25	0.00	0.00	18.75	27.67	21.28	0.00	0.30	0.00	0.00	0.09	0.13	0.02	0.41	19.87	0.13	0.02	0.00	0.02	88.7
1-19	#26	1.54	0.00	4.90	37.38	16.92	0.02	1.67	0.00	11.48	2.67	0.54	0.01	0.20	21.02	0.14	0.02	0.00	0.04	98.6
1-19	#27	1.49	0.00	5.64	38.45	15.96	0.03	1.32	0.00	11.57	2.25	0.42	0.06	0.16	19.95	0.13	0.03	0.00	0.02	97.5
1-19	#28	1.70	0.00	9.89	42.37	16.47	0.04	0.54	0.04	10.90	0.19	0.60	0.05	0.17	14.91	0.05	0.04	0.00	0.01	97.9
1-19	#29	1.43	0.00	8.47	42.19	16.20	0.03	0.34	0.02	11.25	0.38	0.12	0.02	0.17	16.44	0.02	0.05	0.00	0.00	97.2
1-19	#30	1.61	0.00	8.66	41.30	16.96	0.00	0.49	0.04	10.85	0.34	0.39	0.08	0.20	16.64	0.01	0.02	0.00	0.03	97.6
1-19	#31	0.01	0.00	4.88	38.25	21.40	0.00	0.01	0.06	5.76	0.01	0.03	0.02	1.74	28.19	0.08	0.03	0.00	0.02	100.5
1-19	#32	0.03	0.00	4.84	38.37	21.21	0.00	0.00	0.06	6.00	0.00	0.04	0.04	1.61	28.18	0.07	0.00	0.00	0.01	100.5
1-19	#33	1.53	0.00	9.92	42.65	15.48	0.00	0.40	0.00	10.99	0.23	0.33	0.08	0.17	15.64	0.07	0.05	0.00	0.03	97.5
1-19	#34	0.02	0.00	20.38	26.43	22.08	0.00	0.03	0.06	0.00	0.09	0.04	0.02	0.12	17.74	0.10	0.00	0.00	0.02	87.1
1-19	#35	0.00	0.00	21.05	26.97	22.19	0.01	0.01	0.04	0.00	0.06	0.05	0.02	0.08	17.06	0.13	0.03	0.00	0.01	87.7
1-19	#36	1.48	0.00	5.07	37.59	16.25	0.03	1.72	0.03	11.40	2.71	0.51	0.04	0.15	21.16	0.10	0.00	0.00	0.07	98.3
1-19	#37	1.62	0.00	5.89	38.89	14.78	0.02	1.41	0.06	11.40	2.55	0.36	0.00	0.19	21.09	0.09	0.04	0.00	0.03	98.4
1-19	#38	1.61	0.00	9.70	41.87	16.12	0.00	0.48	0.05	11.30	0.29	0.58	0.03	0.18	14.87	0.07	0.00	0.00	0.02	97.2
1-19	#39	0.14	0.00	13.31	37.71	16.88	0.06	9.22	0.03	0.01	0.39	1.57	0.05	0.11	15.75	0.12	0.03	0.00	0.09	95.5
1-19	#40	1.65	0.00	9.67	41.81	16.52	0.02	0.52	0.04	11.03	0.20	0.57	0.04	0.13	14.79	0.08	0.03	0.00	0.04	97.1
1-19	#41	1.58	0.00	4.96	37.82	16.64	0.00	1.61	0.00	11.33	2.73	0.38	0.02	0.18	21.10	0.08	0.00	0.00	0.05	98.5
1-19	#42	1.63	0.00	9.42	41.81	16.33	0.05	0.48	0.01	11.18	0.26	0.56	0.03	0.19	15.18	0.01	0.01	0.00	0.00	97.1
1-19	#43	0.00	0.00	4.77	38.12	21.23	0.00	0.00	0.05	6.52	0.00	0.08	0.08	1.68	27.92	0.10	0.08	0.00	0.00	100.6
1-19	#44	0.03	0.00	4.85	37.92	21.17	0.02	0.00	0.02	6.34	0.01	0.08	0.00	1.67	28.08	0.08	0.01	0.00	0.00	100.3
1-19	#45	1.52	0.00	6.66	40.32	16.84	0.00	0.49	0.00	11.31	0.72	0.34	0.09	0.22	19.67	0.09	0.01	0.00	0.04	98.3
1-19	#46	1.76	0.00	5.60	37.78	16.68	0.41	0.82	0.00	10.92	0.90	0.28	0.00	0.18	20.20	0.09	0.00	0.00	0.03	95.6
1-30	#47	0.15	0.00	11.25	36.54	19.45	0.00	9.11	0.00	0.00	0.11	1.65	0.10	0.01	17.28	0.00	0.03	0.00	0.09	95.8
1-30	#48	0.20	0.00	10.81	36.62	18.95	0.00	9.15	0.02	0.00	0.16	1.51	0.08	0.10	18.24	0.03	0.01	0.00	0.11	96.0
1-30	#49	0.02	0.00	3.50	38.17	21.12	0.05	0.02	0.00	7.43	0.00	0.15	0.03	1.55	28.25	0.00	0.01	0.00	0.04	100.3
1-30	#50	0.01	0.00	2.94	37.93	21.30	0.00	0.01	0.01	6.31	0.03	0.05	0.03	1.35	29.91	0.02	0.00	0.00	0.00	99.9
1-30	#51	0.76	0.00	1.44	44.79	33.72	0.04	8.55	0.02	0.00	0.02	0.69	0.07	0.00	3.22	0.03	0.00	0.00	0.32	93.7
1-30	#52	0.02	0.00	3.88	38.27	21.34	0.08	0.01	0.00	7.73	0.01	0.11	0.06	0.78	28.22	0.08	0.02	0.00	0.00	100.6
1-30	#53	0.04	0.00	4.76	38.40	21.25	0.00	0.00	0.00	6.51	0.02	0.02	0.06	1.12	27.20	0.03	0.01	0.00	0.02	99.4
1-30	#54	0.05	0.00	3.13	37.84	21.08	0.01	0.00	0.00	6.58	0.02	0.14	0.00	1.20	29.91	0.01	0.02	0.00	0.00	100.0
1-30	#55	0.26	0.00	11.42	36.79	19.07	0.03	9.04	0.00	0.00	0.10	1.74	0.03	0.00	17.14	0.09	0.00	0.00	0.16	95.9
1-30	#56	0.81	0.00	0.96	49.18	35.98	0.02	8.76	0.00	0.00	0.01	0.72	0.03	0.01	0.91	0.06	0.00	0.00	0.20	97.6
1-30	#57	0.04	0.00	4.05	37.96	21.24	0.01	0.01	0.00	6.68	0.01	0.08	0.02	0.78	29.20	0.03	0.04	0.00	0.04	100.2
1-30	#58	0.80	0.00	1.02	48.48	35.69	0.02	8.91	0.00	0.00	0.02	0.83	0.08	0.00	1.09	0.00	0.00	0.00	0.30	97.2
1-30	#59	0.17	0.00	11.37	36.75	18.93	0.00	9.32	0.00	0.03	0.10	1.74	0.05	0.04	17.51	0.09	0.01	0.00	0.15	96.3
1-30	#60	0.85	0.00	0.80	48.17	36.31	0.01	8.56	0.00	0.00	0.01	0.68	0.05	0.03	1.05	0.00	0.00	0.00	0.27	96.8
1-30	#61	0.88	0.00	0.70	47.78	36.20	0.01	9.03	0.01	0.00	0.00	0.67	0.04	0.00	1.01	0.02	0.01	0.00	0.21	96.6
1-30	#62	0.73	0.00	4.35	43.48	30.79	0.05	6.50	0.00	0.03	0.01	0.47	0.01	0.07	7.92	0.04	0.00	0.00	0.22	94.7
1-30	#63	0.25	0.00	11.16	36.37	18.77	0.09	8.99	0.00	0.00	0.11	2.08	0.07	0.03	16.99	0.09	0.01	0.00	0.12	95.1
1-30	#64	0.11	0.00	9.34	35.91	18.20	0.06	9.48	0.00	0.00	0.28	1.69	0.03	0.08	20.68	0.02	0.05	0.00	0.10	96.0
1-30	#65	0.07	0.00	8.99	35.86	18.52	0.00	9.61	0.00	0.00	0.25	1.68	0.00	0.08	21.06	0.09	0.02	0.00	0.11	96.3
1-30	#66	0.81	0.00	0.77	47.25	35.77	0.00	9.38	0.03	0.00	0.01	0.72	0.10	0.00	1.15	0.02	0.00	0.00	0.23	96.2
1-30	#67	0.22	0.00	12.55	35.30	20.00	0.02	7.71	0.03	0.00	0.09	0.80	0.04	0.00	17.93	0.06	0.05	0.00	0.07	94.9
1-30	#68	0.01	0.00	2.92	37.78	20.98	0.02	0.01	0.03	4.23	0.00	0.04	0.03	1.76	32.37	0.02	0.01	0.00	0.02	100.2
1-30	#69	0.04	0.00	2.79	37.76	21.06	0.03	0.02	0.03	3.30	0.00	0.03	0.05	1.88	33.67	0.02	0.03	0.00	0.02	100.7
1-30	#70	0.00	0.00	4.12	38.35	21.34	0.04	0.01	0.00	6.84	0.00	0.07	0.01	0.90	28.58	0.01	0.03	0.00	0.03	100.3
1-30	#71	0.02	0.00	3.01	37.91	20.87	0.07	0.00	0.01	8.33	0.02	0.17	0.00	1.31	28.32	0.00	0.03	0.00	0.00	100.0
1-30	#72	0.22	0.00	10.98	36.38	18.95	0.02	9.06	0.00	0.00	0.12	1.71	0.06	0.07	17.54	0.03	0.00	0.00	0.05	95.2
1-19	#73	0.07	0.00	13.25	37.34	17.00	0.04	9.82	0.00	0.00	0.58	1.55	0.00	0.15	15.68	0.13	0.03	0.00	0.07	95.7
1-19	#74	0.11	0.00	13.41	37.38	16.97	0.04	9.65	0.02	0.00	0.54	1.62	0.05	0.07	16.00	0.13	0.00	0.00	0.15	96.1
1-19	#75	0.13	0.00	13.60	37.60	16.86	0.04	9.44	0.00	0.00	0.43	1.57	0.04	0.14	15.65	0.15	0.06	0.00	0.07	95.8
1-19	#76	0.10	0.00	13.45	37.62	16.83	0.02	9.61	0.00	0.00	0.55	1.60	0.05	0.09	16.05	0.18	0.04	0.00	0.13	96.3
1-19	#77	1.52	0.00	9.22	42.02	16.04	0.00	0.49	0.00	11.16	0.29	0.63	0.08	0.20	15.44	0.03	0.01	0.00	0.05	97.2
1-19	#78	1.69	0.00	9.34	41.65	15.77	0.05	0.44	0.05	11.01	0.25	0.63	0.02	0.21	15.53	0.04	0.05	0.00	0.03	96.7
1-19	#79	1.60	0.00	9.23	41.93	15.87	0.05	0.43	0.00	11.41	0.32	0.60	0.03	0.19	15.19	0.13	0.04	0.00	0.04	97.0
1-19	#80	1.49	0.00	10.28	43.00	15.73	0.03	0.48	0.00	10.12	0.13	0.60	0.06	0.22	15.23	0.05	0.01	0.00	0.05	97.5
1-19	#81	1.61	0.00	9.37	42.38	15.76	0.05	0.38	0.00	11.35	0.30	0.57	0.04	0.17	15.12	0.07	0.00	0.00	0.01	97.2
1-19	#82	1.61	0.00	9.53	41.95	16.45	0.01	0.47	0.02	11.34	0.25	0.53	0.00	0.11	14.94	0.03	0.03	0.00	0.05	97.3
1-19	#83	1.76	0.00	9.60	42.42	16.80	0.00	0.54	0.08	11.08	0.27	0.66	0.03	0.18	15.43	0.03	0.01	0.00	0.00	98.9
1-19	#84	1.66	0.00	9.61	42.01	16.08	0.04	0.53	0.01	11.23	0.22	0.61	0.01	0.19	14.86	0.13	0.01	0.00	0.01	97.2

APPENDIX B

APPENDIX B3: Electron microprobe data

	Zap	Na2O	F	MgO	SiO2	Al2O3	SO3	K2O	P2O5	CaO	Cl	TiO2	Cr2O3	MnO	FeO	CoO	NiO	SrO	BaO	Total
5-4	#1	0.10	0.00	11.58	36.82	15.64	0.01	10.00	0.00	0.00	0.16	2.30	0.00	0.10	17.87	0.00	0.02	0.00	0.12	94.7
5-4	#2	0.07	0.00	11.35	36.38	15.85	0.07	9.83	0.01	0.00	0.18	2.26	0.02	0.13	17.89	0.04	0.06	0.00	0.11	94.3
5-4	#3	0.10	0.00	10.97	35.90	15.65	0.00	9.67	0.01	0.00	0.23	2.17	0.01	0.11	18.11	0.02	0.04	0.00	0.08	93.1
5-4	#4	0.17	0.00	0.00	62.39	18.14	0.03	16.22	0.00	0.09	0.02	0.01	0.00	0.03	0.00	0.00	0.04	0.00	0.79	97.9
5-4	#5	0.04	0.00	12.29	36.17	15.95	0.00	9.83	0.00	0.03	0.18	2.04	0.04	0.11	17.29	0.06	0.03	0.00	0.05	94.1
5-4	#6	0.25	0.00	1.83	45.80	27.92	0.01	10.91	0.00	0.00	0.00	1.40	0.03	0.02	5.18	0.00	0.01	0.00	0.11	93.5
5-4	#7	0.07	0.00	12.99	36.78	15.58	0.00	9.85	0.00	0.00	0.18	2.24	0.00	0.15	16.93	0.06	0.06	0.00	0.11	95.0
5-4	#8	0.25	0.00	1.80	44.86	28.90	0.05	10.72	0.00	0.00	0.02	0.94	0.03	0.00	5.55	0.00	0.03	0.00	0.12	93.3
5-4	#9	0.25	0.00	1.91	45.61	28.13	0.04	10.69	0.01	0.00	0.00	1.18	0.08	0.01	5.26	0.02	0.00	0.00	0.15	93.3
5-4	#10	0.07	0.00	12.83	36.44	15.73	0.04	9.78	0.07	0.00	0.15	2.08	0.05	0.10	17.42	0.04	0.06	0.00	0.14	95.0
5-4	#11	0.11	0.00	11.93	36.32	15.90	0.01	9.94	0.04	0.00	0.17	2.38	0.04	0.20	17.57	0.00	0.00	0.00	0.16	94.8
5-4	#12	0.06	0.00	12.32	37.24	15.64	0.03	9.98	0.06	0.00	0.15	2.29	0.02	0.07	17.19	0.00	0.03	0.00	0.09	95.2
5-4	#13	0.03	0.00	12.05	36.59	16.00	0.04	9.86	0.00	0.00	0.18	2.35	0.12	0.18	17.82	0.05	0.00	0.00	0.12	95.4
5-4	#14	0.09	0.00	12.00	36.63	15.70	0.00	9.68	0.04	0.00	0.15	2.43	0.09	0.14	17.34	0.01	0.00	0.00	0.13	94.4
5-10	#15	0.27	0.00	15.24	37.14	18.87	0.00	9.40	0.00	0.00	0.20	1.46	0.01	0.15	12.67	0.12	0.03	0.00	0.07	95.6
5-10	#16	0.73	0.00	1.15	46.49	34.94	0.00	10.00	0.01	0.00	0.00	0.95	0.02	0.00	0.90	0.04	0.01	0.00	0.25	95.5
5-10	#17	0.68	0.00	1.54	46.83	33.12	0.05	10.42	0.03	0.00	0.03	0.72	0.00	0.00	0.83	0.00	0.02	0.00	0.14	94.4
5-10	#18	0.26	0.00	15.41	37.62	19.57	0.02	9.45	0.02	0.01	0.18	1.04	0.02	0.07	12.14	0.08	0.07	0.00	0.04	96.0
5-10	#19	0.18	0.00	15.29	37.26	19.36	0.06	9.33	0.00	0.00	0.20	0.94	0.00	0.05	12.26	0.10	0.02	0.00	0.10	95.1
5-10	#20	0.70	0.00	1.10	45.90	34.68	0.03	10.52	0.02	0.00	0.01	0.49	0.01	0.00	0.84	0.01	0.00	0.00	0.20	94.5
5-10	#21	0.15	0.00	15.63	37.04	19.43	0.03	9.51	0.05	0.00	0.18	0.84	0.00	0.10	12.36	0.06	0.01	0.00	0.08	95.5
5-10	#22	0.25	0.00	15.56	37.31	19.06	0.00	9.45	0.00	0.00	0.19	0.75	0.01	0.08	12.02	0.08	0.02	0.00	0.07	94.9
5-10	#23	0.81	0.00	0.93	45.40	36.12	0.00	10.20	0.01	0.01	0.01	0.04	0.02	0.01	0.66	0.00	0.01	0.00	0.19	94.4
5-10	#24	0.76	0.00	0.95	45.61	35.53	0.00	10.14	0.00	0.00	0.00	0.13	0.02	0.05	0.70	0.00	0.01	0.00	0.24	94.1
5-10	#25	0.16	0.00	15.51	37.34	18.89	0.00	9.48	0.00	0.00	0.19	1.22	0.03	0.06	12.20	0.11	0.02	0.00	0.02	95.2
5-10	#26	0.64	0.00	1.45	46.69	33.05	0.05	10.48	0.00	0.00	0.00	0.67	0.05	0.00	0.97	0.00	0.02	0.00	0.17	94.2
5-10	#27	0.21	0.00	15.33	37.05	19.10	0.06	9.41	0.02	0.00	0.22	1.28	0.05	0.07	12.16	0.09	0.00	0.00	0.07	95.1
5-10	#28	0.73	0.00	1.25	46.05	33.89	0.02	10.41	0.00	0.00	0.00	0.68	0.01	0.00	0.88	0.01	0.01	0.00	0.22	94.2
5-10	#29	0.09	0.00	14.46	29.71	17.57	0.84	4.40	0.05	0.11	0.20	0.91	0.08	0.09	18.09	0.12	0.03	0.00	0.08	86.8
5-10	#30	0.23	0.00	15.40	37.59	18.64	0.01	9.32	0.00	0.00	0.22	1.31	0.02	0.07	12.46	0.09	0.05	0.00	0.06	95.5
5-10	#31	0.73	0.00	1.22	45.88	34.93	0.02	10.29	0.00	0.00	0.02	0.68	0.03	0.00	0.87	0.00	0.00	0.00	0.19	94.9
5-16	#32	0.25	0.00	2.17	45.37	28.86	0.00	11.16	0.07	0.00	0.02	0.89	0.03	0.02	4.78	0.03	0.00	0.00	0.30	93.9
5-16	#1	0.00	0.62	0.41	25.01	13.28	0.21	0.23	0.02	1.99	0.23	0.00	0.00	0.01	0.85	0.02	0.00	0.00	0.01	42.9
5-16	#2	0.00	0.25	1.63	35.62	23.20	0.02	7.83	0.00	0.09	0.05	0.61	0.00	0.01	3.28	0.04	0.00	0.00	0.15	72.8
5-16	#3	0.00	0.10	20.59	38.58	17.18	0.01	9.83	0.04	0.00	0.11	1.28	0.07	0.13	5.38	0.08	0.03	0.00	0.09	93.5
5-16	#4	0.00	0.12	20.16	38.69	17.07	0.02	9.96	0.06	0.02	0.11	1.32	0.01	0.06	5.62	0.03	0.05	0.00	0.13	93.4
5-16	#5	0.00	0.19	19.73	38.02	16.87	0.00	8.47	0.01	0.31	0.17	1.27	0.06	0.02	5.05	0.10	0.02	0.00	0.12	90.4
5-16	#6	0.00	0.26	2.24	45.01	29.31	0.00	10.44	0.09	0.00	0.01	0.73	0.06	0.00	4.61	0.02	0.03	0.00	0.14	92.9
5-16	#7	0.00	0.24	1.93	45.02	29.55	0.00	10.79	0.03	0.00	0.02	0.74	0.00	0.00	4.56	0.00	0.02	0.00	0.25	93.2
5-16	#8	0.00	0.27	2.32	46.06	29.07	0.00	10.85	0.00	0.00	0.03	0.74	0.00	0.00	4.85	0.04	0.01	0.00	0.31	94.5
5-16	#9	0.00	0.14	20.36	39.32	17.24	0.01	9.98	0.00	0.04	0.12	1.32	0.00	0.09	5.90	0.02	0.01	0.00	0.06	94.6
5-16	#10	0.00	0.54	2.21	45.70	29.37	0.00	10.89	0.00	0.01	0.11	0.69	0.00	0.00	4.95	0.00	0.00	0.00	0.24	94.7
5-16	#11	0.00	0.10	20.25	38.84	17.22	0.02	10.09	0.00	0.00	0.13	1.52	0.03	0.11	5.61	0.06	0.01	0.00	0.16	94.2
5-16	#12	0.00	0.09	19.90	38.81	17.64	0.00	10.12	0.01	0.00	0.11	1.50	0.04	0.13	5.72	0.00	0.03	0.00	0.16	94.3
5-16	#13	0.00	0.16	20.46	39.63	17.06	0.02	9.58	0.01	0.09	0.10	1.34	0.00	0.06	5.66	0.00	0.00	0.00	0.12	94.3
5-16	#14	0.00	0.10	19.96	38.79	17.02	0.00	10.02	0.03	0.00	0.17	1.34	0.06	0.05	5.26	0.05	0.02	0.00	0.10	93.0
5-16	#15	0.00	0.12	20.35	39.27	16.98	0.04	9.93	0.00	0.06	0.10	1.42	0.03	0.09	5.60	0.06	0.00	0.00	0.13	94.2
1-32	#16	0.00	0.14	19.33	25.58	21.70	0.16	0.08	0.03	0.67	0.22	0.05	0.00	0.01	16.42	0.03	0.10	0.00	0.00	84.5
1-32	#17	0.00	0.06	15.66	38.23	16.69	0.00	9.70	0.00	0.00	0.82	0.86	0.02	0.00	13.04	0.10	0.02	0.00	0.06	95.3
1-32	#18	0.00	0.01	26.52	27.93	23.52	0.00	0.01	0.00	0.01	0.02	0.08	0.04	0.06	7.75	0.18	0.08	0.00	0.03	86.2
1-32	#19	0.00	0.03	22.02	26.89	22.50	0.00	0.02	0.00	0.01	0.08	0.04	0.03	0.00	14.88	0.06	0.09	0.00	0.00	86.6
1-32	#20	0.00	0.04	24.23	27.29	22.54	0.06	0.01	0.00	0.03	0.08	0.11	0.06	0.02	11.02	0.20	0.10	0.00	0.01	85.8
1-32	#21	0.00	0.11	16.22	33.10	19.69	0.02	6.58	0.07	0.00	0.09	0.72	0.04	0.11	14.35	0.15	0.07	0.00	0.14	91.4
1-32	#22	0.00	1.33	0.99	45.94	34.93	0.05	9.44	0.04	0.00	0.00	0.61	0.03	0.00	0.31	0.02	0.00	0.00	0.41	94.1
1-32	#23	0.00	1.39	0.87	46.04	36.22	0.04	9.29	0.04	0.00	0.02	0.48	0.02	0.00	0.30	0.00	0.02	0.00	0.42	95.1
1-32	#24	0.00	0.00	17.67	25.57	22.65	0.07	0.01	0.05	0.03	0.11	0.04	0.04	0.09	20.76	0.14	0.03	0.00	0.02	87.3
1-32	#25	0.00	0.01	19.94	26.40	22.84	0.03	0.00	0.03	0.02	0.08	0.04	0.01	0.09	18.26	0.08	0.10	0.00	0.00	87.9
1-32	#26	0.00	0.00	23.86	26.96	23.19	0.02	0.01	0.03	0.00	0.04	0.08	0.04	0.03	12.50	0.21	0.03	0.00	0.01	87.0
1-32	#27	0.00	0.05	24.18	26.79	22.55	0.04	0.00	0.03	0.01	0.09	0.10	0.02	0.03	11.46	0.22	0.00	0.00	0.03	85.6
1-32	#28	0.00	0.01	25.28	27.63	23.27	0.03	0.00	0.00	0.00	0.04	0.06	0.03	0.01	11.05	0.14	0.05	0.00	0.00	87.6
1-32	#29	0.00	0.15	18.16	38.07	18.97	0.03	9.68	0.00	0.00	0.11	0.78	0.03	0.02	8.64	0.20	0.04	0.00	0.13	95.0
1-32	#30	0.00	0.10	22.32	26.66	22.46	0.07	0.05	0.00	0.00	0.07	0.04	0.03	0.05	13.33	0.08	0.01	0.00	0.02	85.3
1-32	#31	0.00	0.67	3.20	45.43	32.29	0.02	10.26	0.05	0.00	0.05	0.27	0.06	0.00	2.09	0.00	0.00	0.00	0.05	94.4
1-32	#32	0.00	0.59	3.85	44.42	30.95	0.00	10.34	0.00	0.00	0.21	0.35	0.03	0.00	2.95	0.04	0.01	0.00	0.11	93.8
1-32	#33	0.00	0.62	2.06	46.47	32.81	0.01	10.41	0.00	0.00	0.07	0.24	0.06	0.02	1.42	0.04	0.00	0.00	0.07	94.3
1-32	#34	0.00	0.04	15.36	27.19	21.23	0.04	0.62	0.00	0.04	0.28	0.04	0.01	0.10	22.96	0.22	0.09	0.00	0.00	88.2
1-32	#35	0.00	0.02	17.40	27.05	21.02	0.01	0.54	0.00	0.02	0.15	0.05	0.03	0.08	21.22	0.15	0.01	0.00	0.01	87.8
1-32	#36	0.00	0.00	18.48	27.36	21.25	0.00	0.28	0.00	0.02	0.08	0.07	0.05	0.11	20.61	0.15	0.06	0.00	0.00	88.5
1-32	#37	0.00	0.04	18.48	27.14	21.30	0.07	0.44	0.00	0.01	0.14	0.09	0.08	0.08	19.86	0.15	0.06	0.00	0.02	87.9
1-32	#38	0.00	0.00	15.45	25.90	21.08	0.02	0.01	0.07	0.04	0.29	0.05	0.01	0.09	24.16	0.19	0.04	0.00	0.04	87.4
1-32	#39	0.00	0.03	19.75	26.50	22.24	0.07	0.02	0.01	0.02	0.11	0.05	0.00	0.11	18.33	0.11	0.03	0.00	0.02	87.4
1-32	#40	0.00	1.37	0.86	45.75	35.67	0.01	9.28	0.00	0.00	0.02	0.50	0.02	0.02	0.38	0.00	0.01	0.00	0.34	94.2
1-32	#41	0.00	0.28	18.61	39.20	18.46	0.03	9.35	0.01	0.00	0.06	1.06	0.00	0.00	6.31	0.15	0.03	0.00	0.13	93.7
1-32	#42	0.00	0.28	18.64	38.41	19.20	0.03	9.41	0.00	0.00	0.06	1.04	0.02	0.00	6.73	0.17	0.00	0.00	0.14	94.1
1-32	#43	0.00	0.26	18.75	38.81	18.99	0.04	9.69	0.01	0.01	0.05	1.09	0.06	0.08	6.57	0.11	0.01	0.00	0.17	94.7
1-32	#44	0.00	0.22	18.55	38.17	19.43	0.05	9.60	0.00	0.00	0.08	0.96	0.05	0.05	6.64	0.18	0.04	0.00	0.08	94.1
1-32	#45	0.00	0.24	18.26	37.85	18.99	0.02	9.81	0.00	0.02	0.07	1.03	0.06	0.02	6.53	0.18	0.02	0.00	0.11	93.2
1-32	#46	0.00	0.31	18.52	38.65	19.15	0.00	9.42	0.03	0.00	0.10	1.02	0.04	0.04	7.00	0.19	0.07	0.00	0.13	94.7
1-32	#47	0.00	0.24	18.49	38.56	19.50	0.00	9.80	0.04	0.00	0.07	1.01	0.05	0.01	6.44	0.18	0.01	0.00	0.12	94.5
1-32	#48	0.00	0.16	18.39	38.45	19.51	0.05	9.80	0.01	0.00	0.06	0.96	0.04	0.04	6.50	0.18	0.04	0.00	0.16	94.3
1-32	#49	0.00	0.18	18.94	39.51	18.48	0.04	9.68	0.02	0.00	0.05	0.96	0.00	0.03	6.17	0.18	0.00	0.00	0.13	94.4
1-32	#50	0.00	0.35	18.77	38.99	19.27	0.00	9.43	0.05	0.00	0.08	1.01	0.03	0.03	6.64	0.20	0.06	0.00	0.14	95.0

Detection limit=0.01%

APPENDIX B

APPENDIX B3: Electron microprobe data

	Zap	Na2O	F	MgO	SiO2	Al2O3	SO3	K2O	P2O5	CaO	Cl	TiO2	Cr2O3	MnO	FeO	CoO	NiO	SrO	BaO	Total
5-15	#51	0.00	0.14	20.82	39.62	17.74	0.01	10.13	0.01	0.04	0.08	1.38	0.00	0.09	5.47	0.10	0.03	0.00	0.08	95.7
5-15	#52	0.00	0.24	2.30	46.64	29.09	0.00	10.95	0.03	0.00	0.03	0.58	0.02	0.00	4.57	0.07	0.05	0.00	0.18	94.7
5-15	#53	0.00	0.31	2.40	46.46	28.74	0.04	11.04	0.02	0.00	0.07	0.59	0.03	0.02	4.77	0.00	0.03	0.00	0.16	94.7
5-15	#54	0.00	0.20	1.82	43.74	28.94	0.00	10.25	0.00	0.00	0.08	0.80	0.03	0.03	3.87	0.00	0.00	0.00	0.23	90.0
5-15	#55	0.00	0.10	20.86	39.56	17.80	0.01	10.00	0.00	0.07	0.10	1.39	0.03	0.04	5.35	0.05	0.01	0.00	0.08	95.5
5-15	#56	0.00	3.87	0.00	38.75	19.72	2.68	0.19	0.01	11.41	0.40	0.00	0.02	0.00	0.15	0.00	0.06	0.00	0.04	77.3
5-15	#57	0.00	0.12	19.99	38.46	17.14	0.00	9.86	0.05	0.00	0.13	1.34	0.02	0.03	5.30	0.09	0.03	0.00	0.05	92.6
5-15	#58	0.00	0.08	20.57	39.29	17.39	0.02	10.06	0.00	0.01	0.14	1.34	0.03	0.04	5.61	0.05	0.02	0.00	0.14	94.8
5-15	#59	0.00	0.12	20.87	40.18	17.39	0.01	9.03	0.00	0.17	0.11	1.32	0.00	0.10	5.43	0.09	0.01	0.00	0.05	94.8
5-15	#60	0.00	0.10	20.49	39.95	17.39	0.01	10.02	0.09	0.08	0.13	1.40	0.04	0.09	5.60	0.04	0.03	0.00	0.06	95.1
5-15	#61	0.00	0.26	2.22	45.87	17.39	0.02	10.98	0.00	0.00	0.02	0.71	0.03	0.01	4.44	0.02	0.00	0.00	0.11	93.3
5-15	#62	0.00	0.28	2.08	45.35	17.39	0.01	11.03	0.02	0.00	0.02	0.87	0.07	0.03	4.34	0.00	0.00	0.00	0.25	94.0
5-15	#63	0.00	0.25	2.03	44.96	17.39	0.02	10.55	0.00	0.01	0.06	0.97	0.00	0.00	4.39	0.00	0.00	0.00	0.23	92.0
1-43	#1	0.00	1.70	0.79	46.00	17.39	0.02	10.33	0.07	0.00	0.02	0.74	0.00	0.03	1.17	0.01	0.00	0.02	0.21	93.3
1-43	#2	0.00	1.23	0.89	45.57	17.39	0.06	10.27	0.01	0.00	0.01	0.69	0.03	0.00	1.06	0.00	0.00	0.04	0.23	93.6
1-43	#3	0.00	1.07	0.76	45.51	17.39	0.00	9.96	0.00	0.00	0.00	0.72	0.07	0.00	1.18	0.17	0.00	0.00	0.20	93.7
1-43	#4	0.22	14.76	0.21	36.84	17.39	0.04	9.77	0.00	0.00	0.17	1.35	0.05	0.09	13.44	0.01	0.12	0.04	0.07	95.6
1-43	#5	0.27	14.83	0.22	36.30	17.39	0.00	9.70	0.01	0.00	0.16	1.35	0.07	0.06	13.45	0.03	0.12	0.03	0.08	94.5
1-43	#6	0.28	14.98	0.27	37.49	17.39	0.01	9.46	0.01	0.00	0.21	1.47	0.06	0.07	13.28	0.05	0.12	0.04	0.10	95.8
1-43	#7	0.25	14.88	0.28	36.96	17.39	0.00	9.85	0.00	0.00	0.20	1.45	0.07	0.09	12.89	0.00	0.14	0.05	0.09	95.4
1-43	#8	0.00	0.00	7.94	58.58	17.39	0.02	0.05	0.00	7.20	0.00	0.03	0.00	0.00	0.02	0.03	0.03	0.05	0.01	98.6
1-43	#9	0.24	14.94	0.18	36.90	17.39	0.02	9.88	0.06	0.00	0.20	1.39	0.02	0.09	12.69	0.00	0.08	0.06	0.15	95.4
1-43	#10	0.17	14.59	0.21	36.45	17.39	0.01	9.67	0.03	0.00	0.17	1.40	0.05	0.09	13.16	0.03	0.16	0.02	0.10	94.4
1-43	#11	0.00	22.48	0.00	27.34	17.39	0.03	0.00	0.00	0.02	0.02	0.13	0.04	0.12	15.55	0.00	0.15	0.05	0.02	87.6
1-43	#12	0.00	1.35	0.87	45.68	17.39	0.00	10.29	0.00	0.00	0.00	0.86	0.05	0.05	1.62	0.01	0.01	0.00	0.24	94.7
1-43	#13	0.27	14.44	0.17	37.14	17.39	0.02	9.80	0.00	0.00	0.17	1.34	0.00	0.05	13.56	0.04	0.14	0.02	0.08	95.6
1-43	#14	0.27	14.75	0.23	36.89	17.39	0.02	9.70	0.00	0.00	0.18	1.35	0.00	0.12	13.35	0.00	0.17	0.05	0.09	95.8
1-41	#1	0.28	14.44	0.21	36.91	17.39	0.00	9.88	0.03	0.00	0.18	1.28	0.00	0.13	14.79	0.01	0.05	0.04	0.08	95.1
1-41	#2	0.00	21.96	0.02	27.34	17.39	0.05	0.01	0.05	0.05	0.03	0.10	0.00	0.17	16.77	0.06	0.08	0.03	0.04	87.9
1-41	#3	0.28	12.99	0.14	36.39	17.39	0.05	9.98	0.03	0.00	0.15	2.91	0.03	0.12	16.81	0.01	0.02	0.05	0.09	95.4
1-41	#4	0.00	21.69	0.07	26.56	17.39	0.03	0.02	0.02	0.04	0.04	0.11	0.00	0.22	16.87	0.00	0.04	0.00	0.00	87.2
1-41	#5	0.28	14.75	0.17	37.80	17.39	0.00	9.88	0.00	0.00	0.16	1.38	0.03	0.11	14.66	0.00	0.05	0.01	0.15	96.4
1-41	#6	0.25	14.39	0.20	37.35	17.39	0.00	9.92	0.03	0.00	0.15	1.42	0.00	0.05	15.23	0.03	0.04	0.00	0.07	95.9
1-41	#7	0.00	20.35	0.00	26.68	17.39	0.00	0.34	0.00	0.00	0.01	0.13	0.05	0.20	17.18	0.00	0.10	0.02	0.00	86.0
1-41	#8	0.32	14.89	0.16	36.53	17.39	0.08	9.32	0.00	0.00	0.17	1.31	0.05	0.10	15.39	0.00	0.07	0.03	0.13	95.2
1-41	#9	0.28	14.10	0.12	36.79	17.39	0.00	9.80	0.00	0.00	0.17	1.26	0.07	0.09	15.06	0.01	0.00	0.01	0.08	93.9
1-41	#10	0.33	14.09	0.14	36.65	17.39	0.04	10.03	0.06	0.00	0.19	1.33	0.06	0.16	14.60	0.01	0.05	0.01	0.11	94.0
1-41	#11	0.28	14.26	0.17	36.74	17.39	0.03	10.04	0.00	0.00	0.21	1.23	0.05	0.11	14.94	0.02	0.06	0.01	0.10	94.6
1-41	#12	0.27	14.15	0.13	36.24	17.39	0.00	9.87	0.02	0.00	0.16	1.26	0.05	0.11	14.81	0.04	0.07	0.00	0.04	93.5
1-41	#13	0.00	0.00	8.06	59.38	17.39	0.05	0.11	0.00	6.67	0.01	0.00	0.00	0.02	0.13	0.00	0.00	0.00	0.01	99.1
1-41	#14	0.00	22.12	0.03	26.98	17.39	0.04	0.01	0.03	0.01	0.03	0.07	0.00	0.16	16.83	0.03	0.10	0.03	0.00	87.4
1-41	#15	0.00	22.30	0.04	27.17	17.39	0.02	0.01	0.07	0.02	0.02	0.08	0.07	0.21	16.59	0.02	0.04	0.04	0.02	88.6
1-41	#16	0.00	21.59	0.01	26.94	17.39	0.02	0.00	0.00	0.00	0.02	0.15	0.05	0.20	17.00	0.03	0.06	0.03	0.01	86.8
1-41	#17	0.38	14.36	0.11	36.78	17.39	0.04	10.13	0.00	0.00	0.17	1.81	0.06	0.10	15.25	0.02	0.06	0.07	0.12	95.5
1-41	#18	0.20	14.59	0.26	37.72	17.39	0.00	9.97	0.01	0.00	0.18	1.31	0.06	0.12	14.56	0.00	0.00	0.05	0.12	96.4
1-41	#19	0.24	14.56	0.25	37.55	17.39	0.02	9.89	0.04	0.00	0.17	1.34	0.05	0.09	14.66	0.00	0.09	0.01	0.09	95.9
1-41	#20	0.22	14.47	0.21	37.31	17.39	0.00	9.91	0.00	0.00	0.17	1.24	0.02	0.12	14.78	0.00	0.05	0.01	0.09	95.8
2-2b	#21	0.01	3.33	0.11	37.67	17.39	0.00	0.03	0.05	7.65	0.01	0.15	0.03	2.29	28.02	0.01	0.01	0.00	0.02	100.9
2-2b	#22	0.04	2.86	0.09	37.04	17.39	0.02	0.02	0.03	7.41	0.01	0.13	0.01	2.36	29.23	0.04	0.01	0.04	0.00	101.0
2-2b	#23	0.07	11.20	0.05	24.61	17.39	0.03	0.03	0.01	0.05	0.07	0.07	0.05	0.64	30.90	0.00	0.04	0.00	0.03	89.1
2-2b	#24	0.00	0.00	9.73	63.14	17.39	0.01	0.08	0.02	3.70	0.00	0.00	0.03	0.00	0.09	0.00	0.03	0.00	0.03	99.0
2-2b	#25	0.00	0.15	0.24	20.18	17.39	0.06	0.06	0.00	7.13	0.24	1.35	0.00	0.28	2.72	0.00	0.00	0.02	0.02	39.8
2-2b	#26	0.00	7.37	1.80	40.79	17.39	0.02	0.45	0.00	10.99	0.31	0.33	0.03	0.27	20.46	0.00	0.07	0.00	0.00	97.5
2-2b	#27	0.00	3.12	0.03	37.25	17.39	0.00	0.01	0.04	7.84	0.00	0.14	0.00	2.64	28.00	0.00	0.02	0.02	0.00	100.3
2-2b	#28	0.04	2.79	0.12	37.14	17.39	0.03	0.03	0.01	8.81	0.01	0.19	0.04	2.73	27.78	0.00	0.01	0.00	0.02	100.9
2-2b	#29	0.00	8.45	2.07	40.11	17.39	0.02	0.60	0.00	10.80	0.29	0.50	0.01	0.33	17.39	0.01	0.03	0.02	0.01	96.5
2-2b	#30	0.00	9.15	1.96	40.98	17.39	0.03	0.83	0.01	11.07	0.25	0.72	0.03	0.26	16.58	0.07	0.01	0.02	0.00	97.3
2-2b	#31	0.03	9.00	2.09	40.71	17.39	0.00	0.77	0.00	10.87	0.26	0.62	0.05	0.27	16.92	0.04	0.03	0.04	0.00	97.6
2-2b	#32	0.00	9.70	1.94	42.73	17.39	0.02	0.44	0.09	11.07	0.19	0.69	0.13	0.22	16.83	0.00	0.05	0.06	0.04	97.9
2-2b	#33	0.02	9.31	1.96	41.16	17.39	0.06	0.92	0.01	10.77	0.23	0.69	0.04	0.25	16.17	0.00	0.04	0.02	0.03	97.0
2-2b	#34	0.00	9.00	1.89	40.71	17.39	0.04	0.82	0.00	11.07	0.24	0.70	0.04	0.31	17.19	0.00	0.06	0.00	0.01	97.9
2-2b	#35	0.06	8.93	2.06	41.00	17.39	0.04	0.55	0.03	11.09	0.29	0.76	0.04	0.22	17.20	0.04	0.05	0.03	0.03	98.1
2-2b	#36	0.08	12.61	0.06	24.21	17.39	0.00	0.02	0.05	0.02	0.06	0.10	0.04	0.31	29.03	0.00	0.03	0.00	0.00	87.7
2-2b	#37	0.21	8.18	0.15	35.45	17.39	0.00	9.63	0.00	0.00	0.36	1.82	0.02	0.23	24.47	0.00	0.05	0.00	0.12	96.7
2-2b	#38	0.00	2.93	0.00	35.96	17.39	0.03	0.00	0.01	7.55	0.00	0.12	0.00	2.42	28.80	0.02	0.06	0.00	0.06	98.6
2-2b	#39	0.01	2.94	0.01	36.03	17.39	0.00	0.00	0.04	7.49	0.00	0.10	0.01	2.42	28.57	0.02	0.06	0.08	0.03	98.4
2-2b	#40	0.02	3.88	0.06	37.30	17.39	0.02	0.01	0.00	7.84	0.02	0.10	0.05	1.74	27.55	0.03	0.05	0.00	0.01	100.3
2-2b	#41	0.01	13.09	1.49	46.35	17.39	0.00	0.30	0.00	11.44	0.11	0.50	0.00	0.14	13.50	0.01	0.00	0.02	0.02	98.0
2-2b	#42	0.32	14.22	0.15	37.51	17.39	0.01	9.74	0.01	0.00	0.17	1.60	0.10	0.09	15.81	0.00	0.07	0.00	0.08	96.2
2-2b	#43	0.00	20.03	0.11	27.06	17.39	0.07	0.02	0.00	0.02	0.04	0.08	0.05	0.11	20.39	0.05	0.09	0.06	0.02	89.5
2-2b	#44	0.00	9.80	1.95	40.60	17.39	0.07	0.78	0.01	11.16	0.26	0.68	0.00	0.15	15.84	0.00	0.01	0.00	0.01	97.4

Detection limit=0.01%

APPENDIX B

APPENDIX B3: Electron microprobe data

	Zap	Na2O	F	MgO	SiO2	Al2O3	SO3	K2O	P2O5	CaO	Cl	TiO2	Cr2O3	MnO	FeO	CoO	NiO	SrO	BaO	Total
1-27	#1	0.00	1.12	0.80	45.57	17.39	0.04	8.78	0.06	0.00	0.00	0.64	0.02	0.01	1.15	0.02	0.03	0.00	0.30	92.7
1-27	#2	0.00	1.98	0.87	47.42	17.39	0.01	10.26	0.01	0.00	0.00	0.74	0.06	0.00	0.28	0.00	0.00	0.00	0.24	94.2
1-27	#3	0.00	1.72	0.84	46.40	17.39	0.00	9.34	0.00	0.00	0.01	0.45	0.04	0.00	0.93	0.02	0.02	0.03	0.29	93.2
1-27	#4	0.00	1.42	0.78	45.56	17.39	0.01	9.95	0.05	0.00	0.00	1.08	0.04	0.00	0.27	0.01	0.00	0.02	0.16	92.2
1-27	#5	0.20	21.07	0.37	39.34	17.39	0.00	9.44	0.00	0.00	0.03	0.73	0.02	0.02	4.50	0.01	0.25	0.01	0.00	95.1
1-27	#6	0.00	1.49	0.80	46.38	17.39	0.00	9.80	0.00	0.00	0.00	0.67	0.07	0.03	0.34	0.00	0.03	0.00	0.29	93.6
1-27	#7	0.16	20.60	0.42	39.52	17.39	0.04	9.54	0.00	0.00	0.03	0.78	0.00	0.06	4.57	0.00	0.17	0.00	0.08	95.6
1-27	#8	0.00	28.33	0.04	28.28	17.39	0.01	0.35	0.03	0.01	0.02	0.09	0.01	0.03	5.49	0.00	0.24	0.04	0.03	86.3
1-27	#9	0.18	20.81	0.41	39.15	17.39	0.00	9.56	0.01	0.00	0.03	0.78	0.00	0.00	4.79	0.09	0.12	0.01	0.08	95.1
1-27	#10	0.15	20.92	0.42	39.31	17.39	0.04	9.60	0.00	0.00	0.04	0.77	0.03	0.00	4.90	0.02	0.16	0.02	0.09	95.0
1-27	#11	0.00	1.14	1.06	44.22	17.39	0.03	9.95	0.00	0.00	0.01	0.68	0.00	0.04	0.26	0.00	0.00	0.03	0.32	91.3
1-27	#12	0.00	0.92	1.14	45.29	17.39	0.03	9.93	0.01	0.00	0.01	0.50	0.00	0.00	0.26	0.03	0.10	0.04	0.32	93.2
1-27	#13	0.00	0.88	1.03	45.11	17.39	0.07	9.92	0.02	0.00	0.01	0.50	0.00	0.00	0.27	0.00	0.54	0.01	0.27	94.4
1-27	#14	0.16	21.20	0.38	39.51	17.39	0.06	9.40	0.00	0.00	0.04	0.71	0.03	0.03	4.77	0.00	0.14	0.02	0.07	95.9
1-27	#15	0.00	1.22	0.98	45.69	17.39	0.05	9.60	0.00	0.00	0.00	0.74	0.03	0.03	0.30	0.00	0.03	0.02	0.30	93.4
1-27	#16	0.00	1.09	1.00	46.35	17.39	0.00	9.93	0.00	0.00	0.00	0.54	0.06	0.00	0.31	0.00	0.00	0.05	0.33	94.8
1-27	#17	0.00	1.01	0.75	44.17	17.39	0.03	6.59	0.04	0.07	0.00	0.47	0.06	0.00	2.43	0.01	0.02	0.05	0.21	89.6
1-27	#18	0.25	20.97	0.34	39.89	17.39	0.02	9.31	0.01	0.00	0.02	0.73	0.03	0.02	4.37	0.00	0.18	0.00	0.06	94.7
1-27	#19	0.13	21.72	0.41	40.40	17.39	0.01	9.50	0.00	0.02	0.04	0.70	0.05	0.03	4.67	0.02	0.19	0.00	0.08	97.7
1-27	#20	0.00	28.83	0.02	28.00	17.39	0.02	0.01	0.01	0.01	0.01	0.05	0.00	0.04	5.53	0.03	0.21	0.04	0.00	86.5
1-27	#21	0.00	28.90	0.01	28.23	17.39	0.02	0.02	0.00	0.00	0.01	0.06	0.07	0.08	5.70	0.00	0.18	0.01	0.00	87.2
1-27	#22	0.09	20.88	0.39	39.47	17.39	0.00	9.51	0.06	0.00	0.01	0.91	0.02	0.05	4.84	0.00	0.15	0.00	0.07	95.6
1-27	#23	0.00	28.86	0.01	28.05	17.39	0.06	0.00	0.01	0.00	0.00	0.05	0.04	0.06	5.72	0.02	0.21	0.03	0.01	86.7
1-27	#24	0.00	29.40	0.00	28.26	17.39	0.04	0.00	0.00	0.00	0.00	0.08	0.02	0.06	5.65	0.00	0.18	0.00	0.01	87.8
1-27	#25	0.00	29.12	0.02	28.22	17.39	0.06	0.00	0.05	0.01	0.01	0.09	0.05	0.05	5.55	0.00	0.15	0.05	0.01	87.6
1-27	#26	0.11	20.38	0.42	39.10	17.39	0.04	9.57	0.04	0.00	0.03	0.83	0.03	0.00	4.75	0.00	0.19	0.03	0.10	94.3
1-27	#27	0.00	1.17	0.98	46.40	17.39	0.00	9.94	0.02	0.00	0.01	0.61	0.04	0.06	0.22	0.03	0.00	0.00	0.34	94.2
1-27	#28	0.15	20.42	0.39	39.22	17.39	0.02	9.54	0.00	0.00	0.03	0.91	0.00	0.03	4.65	0.00	0.18	0.03	0.11	94.6
1-27	#29	0.09	20.70	0.43	39.15	17.39	0.04	9.83	0.01	0.00	0.03	0.92	0.00	0.05	4.80	0.01	0.17	0.00	0.09	95.4
2-4	#30	0.00	16.34	0.05	26.28	17.39	0.01	0.00	0.01	0.09	0.04	0.21	0.01	0.13	24.94	0.06	0.10	0.03	0.00	89.0
2-4	#31	0.04	4.06	1.34	36.46	17.39	0.00	2.19	0.00	11.51	2.55	0.57	0.06	0.09	23.51	0.00	0.04	0.02	0.02	97.4
2-4	#32	0.00	8.30	1.85	41.20	17.39	0.03	0.77	0.07	11.28	0.22	0.85	0.00	0.26	17.48	0.04	0.03	0.00	0.05	97.1
2-4	#33	0.00	8.20	1.73	40.98	17.39	0.07	0.69	0.02	11.21	0.25	0.82	0.03	0.26	17.78	0.01	0.06	0.01	0.06	96.5
2-4	#34	0.02	5.14	1.86	37.93	17.39	0.00	1.36	0.00	11.53	1.29	0.44	0.03	0.24	22.78	0.08	0.04	0.04	0.00	97.1
2-4	#35	0.00	2.67	1.27	58.20	17.39	0.00	1.56	0.06	8.00	2.22	0.52	0.02	0.05	17.75	0.05	0.01	0.00	0.01	102.4
2-4	#36	0.00	0.00	0.05	37.50	17.39	0.02	0.01	0.21	23.94	0.01	0.05	0.01	0.08	8.20	0.00	0.00	0.00	0.03	96.9
2-4	#37	0.24	12.44	0.14	36.12	17.39	0.01	9.83	0.01	0.00	0.27	1.67	0.04	0.06	18.15	0.00	0.05	0.08	0.07	95.4
2-4	#38	0.00	9.44	1.76	42.21	17.39	0.08	0.65	0.00	11.22	0.22	0.82	0.01	0.26	17.24	0.03	0.04	0.02	0.08	97.6
2-4	#39	0.00	0.44	0.09	34.54	17.39	0.03	0.03	0.00	17.59	0.01	0.17	0.00	0.10	8.90	0.05	0.03	0.04	0.03	83.8
2-4	#40	0.21	12.75	0.11	35.61	17.39	0.00	9.23	0.00	0.01	0.30	1.62	0.07	0.07	18.16	0.03	0.08	0.02	0.13	95.0
2-4	#41	0.00	0.00	8.18	59.33	17.39	0.00	0.05	0.02	6.75	0.00	0.00	0.00	0.00	0.06	0.00	0.03	0.00	0.03	99.1
2-4	#42	0.25	12.02	0.11	35.94	17.39	0.00	9.50	0.00	0.06	0.22	1.61	0.10	0.13	18.33	0.00	0.03	0.01	0.11	94.9
2-4	#43	0.01	2.79	0.01	36.90	17.39	0.00	0.00	0.04	8.53	0.00	0.14	0.00	2.00	28.52	0.00	0.04	0.03	0.07	100.4
2-4	#44	0.00	9.69	1.68	41.71	17.39	0.01	0.83	0.07	11.30	0.18	0.85	0.02	0.19	16.81	0.00	0.06	0.02	0.03	97.0
2-4	#45	0.00	8.93	1.71	41.04	17.39	0.06	0.87	0.01	11.31	0.22	0.88	0.01	0.28	17.27	0.04	0.01	0.05	0.06	96.8
2-4	#46	0.00	8.58	1.70	40.31	17.39	0.04	0.62	0.03	11.20	0.23	0.70	0.04	0.23	17.67	0.02	0.01	0.00	0.00	94.9
2-4	#47	0.13	2.77	0.08	32.93	17.39	0.00	0.01	0.02	7.87	0.01	0.06	0.00	1.27	28.85	0.00	0.06	0.00	0.00	93.6
2-4	#48	0.04	2.92	0.05	36.75	17.39	0.04	0.00	0.00	8.22	0.00	0.10	0.00	2.13	28.54	0.00	0.06	0.00	0.08	100.0
2-4	#49	0.00	2.65	0.05	37.27	17.39	0.00	0.00	0.00	8.25	0.00	0.12	0.00	1.93	28.75	0.00	0.04	0.00	0.00	100.3
1-2	#1	0.98	21.84	0.48	39.73	17.39	0.00	9.64	0.02	0.00	0.08	0.85	0.00	0.00	3.94	0.01	0.02	0.00	0.05	95.9
1-2	#2	0.78	21.44	0.47	38.85	17.39	0.03	9.98	0.02	0.00	0.07	0.83	0.00	0.02	3.98	0.00	0.02	0.00	0.05	95.2
1-2	#3	0.00	1.74	0.91	46.24	17.39	0.07	9.44	0.04	0.00	0.02	0.61	0.00	0.02	1.16	0.04	0.01	0.01	0.14	92.6
1-2	#4	0.00	1.49	1.32	45.84	17.39	0.05	9.83	0.00	0.00	0.00	0.73	0.00	0.02	1.17	0.01	0.00	0.00	0.11	93.4
1-2	#5	0.89	21.78	0.36	39.31	17.39	0.00	9.93	0.08	0.00	0.06	0.79	0.03	0.00	4.24	0.01	0.04	0.03	0.04	96.4
1-2	#6	0.00	28.52	0.04	28.69	17.39	0.05	0.13	0.03	0.06	0.01	0.04	0.06	0.06	6.46	0.05	0.02	0.04	0.02	87.3
1-2	#7	0.00	1.07	1.29	45.44	17.39	0.02	9.68	0.00	0.00	0.00	0.51	0.00	0.00	1.08	0.01	0.01	0.00	0.09	93.4
1-2	#8	0.62	21.66	0.35	39.34	17.39	0.01	10.09	0.00	0.00	0.07	0.83	0.00	0.02	4.18	0.00	0.02	0.00	0.06	96.0
1-2	#9	0.57	21.76	0.30	39.46	17.39	0.00	10.12	0.01	0.00	0.07	0.76	0.00	0.00	3.88	0.00	0.03	0.05	0.04	95.9
1-2	#10	0.00	1.11	1.42	46.04	17.39	0.01	9.74	0.00	0.01	0.00	0.70	0.02	0.03	1.09	0.01	0.00	0.02	0.06	95.0
1-2	#11	0.00	29.92	0.01	29.30	17.39	0.03	0.41	0.00	0.03	0.02	0.05	0.00	0.05	4.79	0.05	0.02	0.03	0.00	88.2
1-2	#12	0.00	30.86	0.04	28.85	17.39	0.01	0.01	0.00	0.01	0.02	0.06	0.00	0.03	4.10	0.00	0.01	0.05	0.00	87.9
1-2	#13	0.00	30.26	0.02	28.23	17.39	0.04	0.02	0.03	0.01	0.03	0.05	0.01	0.00	4.30	0.01	0.05	0.05	0.00	86.4
1-2	#14	0.00	30.27	0.04	28.38	17.39	0.08	0.02	0.00	0.01	0.02	0.00	0.03	0.01	4.40	0.02	0.05	0.00	0.00	87.4
1-2	#15	0.30	21.40	0.32	39.38	17.39	0.02	10.20	0.00	0.04	0.08	0.81	0.00	0.04	4.10	0.00	0.01	0.02	0.03	95.5
1-2	#16	0.00	0.72	1.30	45.41	17.39	0.03	9.69	0.00	0.00	0.00	0.44	0.00	0.03	0.99	0.00	0.00	0.00	0.09	94.2
1-2	#17	0.00	1.22	1.18	45.84	17.39	0.05	9.64	0.02	0.00	0.02	0.76	0.00	0.02	1.10	0.00	0.06	0.00	0.11	94.2
1-2	#18	0.00	30.36	0.05	28.71	17.39	0.00	0.08	0.04	0.03	0.03	0.04	0.00	0.02	4.14	0.00	0.04	0.04	0.00	86.8
1-2	#19	0.00	30.29	0.04	28.55	17.39	0.05	0.06	0.00	0.02	0.03	0.06	0.00	0.00	4.29	0.01	0.01	0.04	0.02	86.9
1-2	#20	0.00	1.35	1.22	45.70	17.39	0.06	9.67	0.03	0.05	0.07	0.72	0.00	0.04	1.07	0.03	0.01	0.00	0.17	93.5
1-2	#21	0.00	30.05	0.17	28.49	17.39	0.03	0.12	0.00	0.20	0.08	0.05	0.00	0.07	4.38	0.00	0.02	0.04	0.04	86.9
1-20b	#22	0.00	0.14	0.03	0.03	17.39	0.00	0.01	0.01	58.98	0.01	0.02	0.00	0.44	0.00	0.05	0.00	0.01	0.00	59.8
1-20b	#23	0.00	22.13	0.02	26.25	17.39	0.08	0.03	0.02	0.08	0.04	0.07	0.04	0.08	16.48	0.00	0.15	0.08	0.00	88.3
1-20b	#24	0.00	21.94	0.04	26.63	17.39	0.05	0.04	0.03	0.00	0.03	0.07	0.04	0.04	16.43	0.04	0.15	0.00	0.01	87.4

Detection limit=0.01%

APPENDIX B

APPENDIX B3: Electron microprobe data

	Zap	Na2O	F	MgO	SiO2	Al2O3	SO3	K2O	P2O5	CaO	Cl	TiO2	Cr2O3	MnO	FeO	CoO	NiO	SrO	BaO	Total
5-13	#1	0.02	0.00	22.77	27.28	17.39	0.00	0.72	0.00	0.01	0.07	0.25	0.06	0.02	11.77	0.05	0.05	0.00	0.01	85.4
5-13	#2	0.31	0.46	17.24	36.58	17.39	0.03	8.29	0.06	0.03	0.21	1.10	0.02	0.08	10.14	0.06	0.01	0.00	0.12	93.6
5-13	#3	0.02	0.00	24.12	26.82	17.39	0.05	0.03	0.00	0.01	0.05	0.06	0.01	0.06	11.58	0.11	0.08	0.00	0.03	85.7
5-13	#4	0.02	0.00	24.12	26.81	17.39	0.03	0.02	0.01	0.00	0.04	0.08	0.02	0.10	11.44	0.14	0.05	0.00	0.01	85.5
5-13	#5	0.02	0.00	24.45	26.42	17.39	0.00	0.03	0.01	0.03	0.03	0.07	0.01	0.10	11.33	0.08	0.06	0.00	0.00	86.0
5-13	#6	0.04	0.00	24.33	26.56	17.39	0.04	0.02	0.05	0.00	0.03	0.07	0.06	0.07	11.05	0.10	0.02	0.00	0.00	85.6
5-13	#7	0.05	0.00	24.19	26.88	17.39	0.04	0.07	0.00	0.00	0.08	0.06	0.03	0.06	10.97	0.11	0.02	0.00	0.00	85.6
5-13	#8	0.01	0.00	24.41	26.58	17.39	0.02	0.00	0.00	0.02	0.04	0.07	0.06	0.07	11.20	0.13	0.00	0.00	0.04	86.0
5-13	#9	0.80	0.00	1.04	44.93	17.39	0.00	10.33	0.00	0.00	0.01	0.63	0.03	0.03	1.24	0.03	0.03	0.00	0.46	93.8
5-13	#10	0.85	0.00	1.00	44.64	17.39	0.00	10.27	0.06	0.00	0.01	0.60	0.03	0.01	1.36	0.04	0.05	0.00	0.56	93.6
5-13	#11	0.88	0.00	1.05	45.22	17.39	0.00	10.50	0.01	0.00	0.04	0.71	0.03	0.06	1.15	0.00	0.00	0.00	0.39	93.9
5-13	#12	0.83	0.00	0.99	44.88	17.39	0.00	10.17	0.04	0.00	0.01	0.55	0.03	0.00	1.21	0.03	0.06	0.00	0.45	93.4
5-13	#13	0.99	0.00	0.80	44.44	17.39	0.02	10.15	0.00	0.00	0.00	0.46	0.03	0.04	1.14	0.00	0.00	0.00	0.51	93.2
5-13	#14	0.91	0.00	1.43	44.62	17.39	0.00	10.35	0.00	0.00	0.03	0.30	0.05	0.00	1.52	0.00	0.00	0.00	0.39	93.4
5-13	#15	0.89	0.00	0.90	44.62	17.39	0.00	10.44	0.03	0.00	0.00	0.42	0.04	0.00	1.30	0.00	0.01	0.00	0.31	93.1
5-13	#16	0.02	0.00	24.30	26.08	17.39	0.00	0.02	0.00	0.00	0.04	0.07	0.04	0.01	10.66	0.10	0.06	0.00	0.00	85.2
5-13	#17	0.02	0.00	24.34	26.71	17.39	0.04	0.01	0.03	0.00	0.04	0.10	0.05	0.07	11.36	0.07	0.02	0.00	0.00	85.8
5-13	#18	0.00	0.00	24.44	26.44	17.39	0.01	0.00	0.00	0.04	0.02	0.05	0.03	0.07	11.55	0.12	0.02	0.00	0.03	86.2
5-13	#19	0.02	0.00	24.29	26.34	17.39	0.02	0.00	0.00	0.01	0.04	0.05	0.05	0.08	11.71	0.15	0.04	0.00	0.00	86.0
5-13	#20	0.01	0.00	24.49	27.17	17.39	0.04	0.02	0.03	0.00	0.03	0.06	0.06	0.08	11.47	0.11	0.04	0.00	0.00	86.4
5-13	#21	0.35	0.38	16.81	37.64	17.39	0.05	9.73	0.00	0.00	0.20	1.08	0.05	0.01	9.08	0.10	0.03	0.00	0.16	94.3
5-13	#22	0.31	0.46	17.10	36.98	17.39	0.00	9.21	0.01	0.00	0.22	1.11	0.04	0.01	9.19	0.08	0.01	0.00	0.18	93.4
5-13	#23	0.36	0.41	16.71	36.55	17.39	0.02	9.55	0.01	0.00	0.21	1.08	0.02	0.01	9.32	0.10	0.08	0.00	0.09	93.0
5-13	#24	0.37	0.51	16.43	36.56	17.39	0.00	9.31	0.00	0.00	0.25	1.37	0.06	0.01	9.78	0.07	0.03	0.00	0.16	93.4
5-13	#25	0.29	0.44	15.83	37.12	17.39	0.00	8.74	0.00	0.00	0.24	1.48	0.03	0.00	10.04	0.08	0.00	0.00	0.15	93.1
5-13	#26	0.88	0.00	0.73	43.62	17.39	0.00	10.18	0.00	0.00	0.02	0.53	0.00	0.04	1.25	0.01	0.02	0.00	0.47	92.1
5-13	#27	0.80	0.00	0.97	44.11	17.39	0.00	10.31	0.03	0.00	0.00	0.56	0.04	0.00	1.40	0.00	0.00	0.00	0.45	92.2
5-13	#28	0.86	0.00	0.94	44.31	17.39	0.00	10.32	0.00	0.00	0.01	0.49	0.11	0.00	1.32	0.02	0.04	0.00	0.51	92.9
5-13	#29	0.05	0.00	24.40	26.88	17.39	0.00	0.01	0.00	0.01	0.04	0.08	0.05	0.05	11.26	0.17	0.01	0.00	0.00	85.3
5-13	#30	0.00	0.00	24.28	26.56	17.39	0.04	0.01	0.01	0.01	0.03	0.11	0.09	0.04	11.68	0.11	0.00	0.00	0.02	85.4
5-13	#31	0.02	0.00	24.81	26.74	17.39	0.00	0.00	0.00	0.01	0.03	0.06	0.00	0.08	11.24	0.08	0.01	0.00	0.02	86.0
5-13	#32	0.95	0.00	1.56	43.60	17.39	0.00	10.23	0.00	0.00	0.03	0.39	0.03	0.01	1.37	0.01	0.01	0.00	0.29	92.9
5-13	#33	0.26	0.42	16.30	36.89	17.39	0.01	9.91	0.00	0.00	0.23	1.07	0.06	0.01	10.30	0.14	0.00	0.00	0.18	94.7
5-13	#34	0.03	0.00	24.26	26.32	17.39	0.00	0.05	0.04	0.01	0.02	0.08	0.07	0.05	11.63	0.07	0.00	0.00	0.02	86.0
5-13	#35	0.29	0.47	16.05	36.87	17.39	0.01	9.79	0.01	0.00	0.25	1.11	0.06	0.02	9.93	0.08	0.03	0.00	0.12	93.8
5-13	#36	0.04	0.00	23.70	26.37	17.39	0.08	0.04	0.01	0.03	0.02	0.07	0.02	0.07	11.84	0.09	0.02	0.00	0.01	85.7
5-13	#37	0.04	0.00	24.15	26.58	17.39	0.01	0.00	0.02	0.02	0.03	0.15	0.02	0.08	11.55	0.10	0.07	0.00	0.00	85.8
5-12a	#38	0.20	0.15	16.59	37.52	17.39	0.00	9.84	0.01	0.00	0.20	0.78	0.04	0.07	9.63	0.05	0.00	0.00	0.09	94.8
5-12a	#39	0.16	0.17	16.36	36.95	17.39	0.02	9.82	0.01	0.00	0.21	1.04	0.01	0.05	9.74	0.08	0.01	0.00	0.10	94.0
5-12a	#40	0.26	0.17	16.58	36.72	17.39	0.00	9.82	0.00	0.00	0.21	0.76	0.00	0.03	9.65	0.05	0.02	0.00	0.07	93.7
5-12a	#41	0.04	0.00	24.81	26.59	17.39	0.03	0.00	0.00	0.01	0.03	0.07	0.00	0.10	11.68	0.10	0.05	0.00	0.01	87.1
5-12a	#42	1.89	0.00	9.30	36.29	17.39	0.00	0.03	0.00	1.47	0.01	0.23	0.05	0.00	2.63	0.00	0.00	0.00	0.03	85.6
5-12a	#43	1.93	0.00	6.98	35.65	17.39	0.01	0.02	0.01	0.95	0.00	0.82	0.01	0.02	5.28	0.00	0.00	0.00	0.03	85.6
5-12a	#44	1.92	0.00	6.99	35.73	17.39	0.03	0.04	0.00	0.92	0.00	0.89	0.00	0.04	5.47	0.00	0.02	0.00	0.03	85.9
5-12a	#45	2.12	0.00	8.84	37.16	17.39	0.01	0.02	0.03	0.75	0.01	0.19	0.01	0.04	3.52	0.05	0.01	0.00	0.05	85.9
5-12a	#46	0.76	0.00	1.48	46.05	17.39	0.03	10.73	0.02	0.00	0.00	0.29	0.05	0.00	0.68	0.02	0.00	0.00	0.19	94.1
5-12a	#47	0.78	0.00	1.20	45.20	17.39	0.00	10.47	0.00	0.00	0.03	0.23	0.04	0.01	0.67	0.00	0.01	0.00	0.35	93.0
5-12a	#48	0.34	0.13	17.06	37.75	17.39	0.01	9.67	0.01	0.00	0.17	0.86	0.04	0.05	9.45	0.11	0.04	0.00	0.03	94.9
5-12a	#49	0.63	0.00	2.23	46.25	17.39	0.03	10.67	0.00	0.00	0.02	0.32	0.03	0.00	0.84	0.00	0.00	0.00	0.14	93.5
5-12a	#50	0.66	0.00	1.76	46.45	17.39	0.00	10.63	0.02	0.00	0.01	0.31	0.03	0.00	0.73	0.04	0.01	0.00	0.21	93.8
5-12a	#51	0.68	0.00	1.70	46.00	17.39	0.01	10.71	0.00	0.00	0.00	0.29	0.03	0.04	0.69	0.03	0.00	0.00	0.21	93.3
5-12a	#52	1.89	0.00	6.95	36.28	17.39	0.00	0.03	0.00	0.96	0.00	0.76	0.06	0.05	5.53	0.00	0.06	0.00	0.03	86.6
5-12a	#53	1.89	0.00	6.70	36.06	17.39	0.00	0.05	0.00	0.80	0.00	0.48	0.03	0.07	5.67	0.01	0.03	0.00	0.00	86.3
5-12a	#54	0.20	0.14	16.91	37.29	17.39	0.00	9.80	0.03	0.00	0.22	0.89	0.05	0.08	9.92	0.08	0.05	0.00	0.08	94.8
5-12a	#55	0.79	0.00	1.30	44.04	17.39	0.00	10.25	0.00	0.00	0.03	0.32	0.01	0.00	0.61	0.02	0.00	0.00	0.35	90.8
5-12a	#56	0.80	0.00	1.32	44.85	17.39	0.02	10.52	0.04	0.00	0.00	0.31	0.00	0.00	0.59	0.03	0.00	0.00	0.34	93.1
5-12a	#57	1.83	0.00	7.37	35.89	17.39	0.04	0.07	0.01	1.05	0.02	0.68	0.05	0.07	4.99	0.00	0.03	0.00	0.00	85.8
5-12a	#58	1.81	0.00	6.92	36.16	17.39	0.00	0.05	0.06	0.94	0.01	0.69	0.04	0.06	5.48	0.01	0.03	0.00	0.02	86.3
5-12a	#59	1.82	0.00	6.75	36.67	17.39	0.03	0.03	0.03	0.75	0.00	0.56	0.00	0.02	5.69	0.00	0.02	0.00	0.01	86.8
5-12b	#60	0.20	0.21	15.87	37.41	17.39	0.04	9.73	0.00	0.00	0.17	1.21	0.03	0.03	11.53	0.07	0.07	0.00	0.10	95.8
5-12b	#61	0.23	0.19	15.56	36.87	17.39	0.00	9.91	0.00	0.00	0.25	1.13	0.04	0.05	11.61	0.11	0.02	0.00	0.03	95.3
5-12b	#62	0.22	0.18	15.72	37.45	17.39	0.02	9.74	0.00	0.00	0.25	1.12	0.01	0.08	11.45	0.05	0.03	0.00	0.09	95.1
5-12b	#63	0.02	0.00	22.66	26.48	17.39	0.00	0.00	0.04	0.01	0.04	0.06	0.00	0.07	13.74	0.09	0.05	0.00	0.01	86.7
5-12b	#64	0.00	0.00	24.35	26.93	17.39	0.00	0.02	0.00	0.01	0.04	0.03	0.00	0.08	12.58	0.08	0.06	0.00	0.01	87.6
5-12b	#65	0.00	0.00	23.80	26.82	17.39	0.00	0.02	0.03	0.02	0.05	0.09	0.01	0.05	12.27	0.12	0.02	0.00	0.01	86.7
5-12b	#66	0.21	0.22	16.02	37.25	17.39	0.03	9.69	0.03	0.00	0.29	1.20	0.03	0.09	11.27	0.05	0.06	0.00	0.08	95.1
5-12b	#67	0.20	0.24	15.94	37.41	17.39	0.02	9.81	0.02	0.00	0.30	1.25	0.06	0.10	11.34	0.07	0.04	0.00	0.10	96.0
5-12b	#68	0.21	0.19	15.77	37.06	17.39	0.02	9.79	0.00	0.00	0.26	1.25	0.02	0.06	11.49	0.08	0.10	0.00	0.08	95.1
5-12b	#69	0.01	0.00	23.65	26.76	17.39	0.00	0.00	0.04	0.01	0.04	0.08	0.04	0.11	12.79	0.04	0.07	0.00	0.02	86.7
5-12b	#70	0.02	0.00	23.86	26.41	17.39	0.00	0.02	0.00	0.02	0.05	0.11	0.00	0.09	12.53	0.09	0.05	0.00	0.00	87.0
5-12b	#71	2.12	0.00	9.04	37.15	17.39	0.00	0.02	0.03	0.88	0.00	0.47	0.05	0.01	3.57	0.05	0.04	0.00	0.03	86.0
5-12b	#72	2.15	0.00	8.46	37.35	17.39	0.02	0.03	0.00	0.73	0.01	0.65	0.05	0.05	4.36	0.07	0.02	0.00	0.00	86.9
5-12b	#73	1.94	0.00	9.35	36.89	17.39	0.00	0.06	0.03	1.26	0.00	0.60	0.02	0.03	2.98	0.07	0.02	0.00	0.03	86.5
5-12b	#74	0.19	0.20	16.16	37.35	17.39	0.00	9.84	0.06	0.00	0.25	1.11	0.07	0.05	10.78	0.08	0.03	0.00	0.09	95.1
5-12b	#75	0.14	0.20	16.06	37.69	17.39	0.00	10.01	0.00	0.00	0.25	1.09	0.03	0.05	10.76	0.11	0.00	0.00	0.02	95.5
5-12b	#76	0.19	0.18	16.21	37.96	17.39	0.02	9.99	0.00	0.00	0.29	1.14	0.05	0.08	10.77	0.10	0.08	0.00	0.09	96.0
5-12b	#77	0.63	0.00	2.12	47.13	17.39	0.05	10.83	0.00	0.00	0.03	0.59	0.01	0.05	0.81	0.03	0.00	0.00	0.25	94.6
5-12b	#78	0.60	0.00	2.09	46.94	17.39	0.03	10.85	0.00	0.00	0.01	0.56	0.00	0.00	0.88	0.02	0.00	0.00	0.27	94.2
5-12b	#79	0.80	0.00	1.24	45.57	17.39	0.00	10.61	0.01	0.00	0.01	0.83	0.04	0.02	0.79	0.04	0.02	0.00	0.28	94.5
5-12b	#80	0.21	0.14	16.31	37.81	17.39	0.00	9.82	0.03	0.00	0.28	1.40	0.03	0.05	10.61	0.06	0.05	0.00	0.09	95.4
5-12b	#81	0.20	0.17	16.30	37.38	17.39	0.06	9.79	0.00	0.00	0.27	1.22	0.05	0.04	10.86	0.07	0.04	0.00	0.11	95.2
5-12b	#82	0.25	0.16	16.32	37.41	17.39	0.03	9.88	0.01	0.00	0.24	1.33	0.00	0.03	10.36	0.07	0.05	0.00	0.14	95.1

Detection limit=0.01%

APPENDIX B

APPENDIX B3: Electron microprobe data

	Zap	Na2O	F	MgO	SiO2	Al2O3	SO3	K2O	P2O5	CaO	Cl	TiO2	Cr2O3	MnO	FeO	CoO	NiO	SrO	BaO	Total
5-3	#1	0.07	0.39	10.96	36.63	17.39	0.04	10.22	0.00	0.00	0.25	2.63	0.02	0.12	18.47	0.05	0.04	0.00	0.15	95.8
5-3	#2	0.11	0.43	10.86	36.21	17.39	0.04	10.20	0.01	0.00	0.27	2.67	0.03	0.07	18.47	0.05	0.02	0.00	0.10	95.4
5-3	#3	0.09	0.43	11.27	36.00	17.39	0.03	10.24	0.02	0.00	0.18	2.80	0.03	0.09	18.39	0.01	0.03	0.00	0.10	95.3
5-3	#4	0.11	0.42	11.60	35.74	17.39	0.05	9.80	0.03	0.00	0.20	2.49	0.02	0.09	17.99	0.03	0.00	0.00	0.08	94.6
5-3	#5	0.12	0.37	11.05	36.21	17.39	0.00	10.27	0.02	0.00	0.21	2.89	0.02	0.09	17.83	0.09	0.02	0.00	0.05	94.7
5-3	#6	0.27	0.00	1.56	45.12	17.39	0.00	11.25	0.01	0.00	0.00	1.29	0.00	0.00	5.61	0.02	0.00	0.00	0.06	94.1
5-3	#7	0.20	0.00	1.81	45.41	17.39	0.07	11.43	0.01	0.00	0.00	0.57	0.00	0.05	5.28	0.02	0.04	0.00	0.03	93.3
5-3	#8	0.15	0.34	10.95	35.91	17.39	0.03	10.09	0.02	0.00	0.24	2.74	0.02	0.13	18.20	0.00	0.04	0.00	0.06	94.7
5-3	#9	0.11	0.32	10.96	35.99	17.39	0.05	10.08	0.02	0.00	0.22	2.69	0.00	0.11	18.23	0.06	0.07	0.00	0.08	94.8
5-3	#10	0.12	0.43	11.17	35.53	17.39	0.03	10.17	0.00	0.00	0.23	2.64	0.02	0.11	18.01	0.05	0.02	0.00	0.08	94.1
5-3	#11	0.12	0.32	10.81	36.14	17.39	0.01	9.96	0.00	0.00	0.25	2.72	0.00	0.13	18.18	0.04	0.05	0.00	0.07	94.5
5-3	#12	0.20	0.00	1.83	45.47	17.39	0.02	11.59	0.00	0.00	0.02	0.98	0.02	0.03	5.47	0.00	0.00	0.00	0.04	93.6
5-3	#13	0.19	0.00	1.78	45.29	17.39	0.00	11.53	0.00	0.00	0.01	1.48	0.01	0.00	5.31	0.02	0.01	0.00	0.07	92.9
5-3	#14	0.67	0.00	0.00	63.29	17.39	0.02	16.46	0.00	0.00	0.00	0.02	0.00	0.00	0.00	0.00	0.00	0.00	0.14	98.8
5-3	#15	0.03	0.40	11.41	36.21	17.39	0.00	10.22	0.00	0.01	0.19	2.59	0.03	0.11	17.74	0.02	0.00	0.00	0.03	94.7
5-3	#16	0.05	0.39	11.34	36.03	17.39	0.00	10.29	0.00	0.00	0.21	2.41	0.05	0.08	17.90	0.02	0.00	0.00	0.06	94.7
5-3	#17	0.08	0.37	11.25	36.18	17.39	0.00	10.31	0.01	0.00	0.20	2.56	0.07	0.17	17.89	0.06	0.03	0.00	0.10	95.0
5-3	#18	0.06	0.40	11.10	36.05	17.39	0.02	10.26	0.00	0.00	0.20	2.53	0.07	0.17	17.96	0.06	0.06	0.00	0.05	94.9
5-3	#19	0.46	0.00	0.00	63.53	17.39	0.02	16.58	0.00	0.00	0.00	0.03	0.01	0.01	0.03	0.00	0.02	0.00	0.22	99.0
5-3	#20	0.04	0.37	11.29	36.29	17.39	0.02	10.21	0.02	0.00	0.20	2.63	0.06	0.14	18.20	0.05	0.05	0.00	0.09	95.6
5-3	#21	0.07	0.39	11.24	36.28	17.39	0.01	10.20	0.03	0.00	0.19	2.70	0.03	0.11	18.45	0.05	0.00	0.00	0.09	95.5
5-3	#22	0.08	0.35	11.17	35.99	17.39	0.00	9.93	0.00	0.00	0.20	2.56	0.07	0.15	17.93	0.02	0.07	0.00	0.10	94.1
5-3	#23	0.11	0.36	11.25	36.08	17.39	0.03	10.11	0.00	0.00	0.17	2.54	0.10	0.18	17.67	0.02	0.01	0.00	0.06	94.1
5-3	#24	0.08	0.40	11.25	36.44	17.39	0.04	10.25	0.00	0.00	0.22	2.52	0.04	0.08	18.01	0.00	0.03	0.00	0.04	95.4
5-3	#25	0.09	0.40	11.23	36.36	17.39	0.02	10.11	0.01	0.03	0.20	2.51	0.05	0.15	18.04	0.07	0.00	0.00	0.05	95.1
5-3	#26	0.77	0.00	0.00	63.70	17.39	0.04	16.09	0.00	0.00	0.01	0.02	0.04	0.00	0.09	0.00	0.00	0.00	0.22	99.3
5-3	#27	0.25	0.00	1.71	45.35	17.39	0.00	11.33	0.00	0.00	0.00	1.05	0.10	0.00	5.25	0.02	0.00	0.00	0.10	94.0
5-3	#28	0.10	0.40	11.63	36.45	17.39	0.06	10.33	0.02	0.00	0.18	2.38	0.00	0.15	17.68	0.11	0.04	0.00	0.08	95.8
5-3	#29	0.09	0.41	11.55	36.51	17.39	0.00	10.27	0.00	0.00	0.18	2.46	0.12	0.14	17.76	0.00	0.01	0.00	0.01	95.4
5-3	#30	0.59	0.00	0.00	64.34	17.39	0.00	16.59	0.04	0.00	0.00	0.04	0.04	0.00	0.06	0.00	0.00	0.00	0.22	100.3
5-3	#31	0.29	0.00	1.73	45.59	17.39	0.03	11.29	0.03	0.00	0.05	1.12	0.05	0.02	5.09	0.00	0.01	0.00	0.07	93.7
5-3	#32	0.83	0.00	0.00	64.19	17.39	0.01	16.15	0.00	0.00	0.00	0.00	0.02	0.00	0.05	0.03	0.00	0.00	0.24	100.0
5-3	#33	0.71	0.00	0.00	64.45	17.39	0.00	16.68	0.00	0.00	0.00	0.00	0.02	0.00	0.14	0.00	0.00	0.00	0.30	100.8
5-3	#34	0.09	0.41	11.43	36.47	17.39	0.04	10.32	0.07	0.00	0.20	2.46	0.01	0.14	17.85	0.07	0.00	0.00	0.06	95.5
5-5	#35	0.26	0.00	1.84	45.63	17.39	0.02	11.24	0.00	0.00	0.01	1.00	0.08	0.00	4.24	0.00	0.00	0.00	0.21	93.6
5-5	#36	0.25	0.00	1.94	45.80	17.39	0.02	11.07	0.02	0.00	0.03	0.87	0.08	0.02	4.37	0.02	0.01	0.00	0.19	93.1
5-5	#37	0.29	0.00	1.98	45.71	17.39	0.03	11.30	0.00	0.00	0.01	1.15	0.08	0.00	4.27	0.00	0.00	0.00	0.18	93.3
5-5	#38	0.12	0.18	12.76	36.53	17.39	0.05	10.25	0.00	0.00	0.14	2.17	0.06	0.10	15.49	0.05	0.00	0.00	0.12	94.1
5-5	#39	0.13	0.20	12.77	36.31	17.39	0.02	10.18	0.03	0.00	0.14	2.17	0.04	0.12	15.29	0.04	0.05	0.00	0.13	93.7
5-5	#40	0.11	0.19	12.78	36.36	17.39	0.06	10.19	0.00	0.00	0.16	2.13	0.07	0.10	15.54	0.03	0.00	0.00	0.13	93.7
5-5	#41	0.14	0.12	12.83	36.76	17.39	0.00	10.07	0.05	0.00	0.15	2.05	0.09	0.10	15.73	0.02	0.01	0.00	0.17	94.4
5-5	#42	0.09	0.16	12.91	36.67	17.39	0.01	10.21	0.00	0.01	0.19	2.15	0.13	0.07	15.60	0.00	0.01	0.00	0.06	94.3
5-5	#43	0.42	0.08	12.82	36.17	17.39	0.07	10.21	0.02	0.03	0.23	2.09	0.05	0.13	15.74	0.06	0.05	0.00	0.12	94.1
5-5	#44	0.12	0.35	12.96	37.01	17.39	0.03	10.31	0.01	0.00	0.19	2.17	0.05	0.14	15.91	0.05	0.00	0.00	0.08	95.4
5-5	#45	0.12	0.29	13.13	36.51	17.39	0.04	10.36	0.01	0.00	0.17	2.13	0.04	0.08	16.00	0.07	0.04	0.00	0.07	95.4
5-5	#46	0.08	0.31	12.91	36.34	17.39	0.00	10.20	0.02	0.01	0.14	2.19	0.02	0.08	15.83	0.03	0.01	0.00	0.10	94.4
5-5	#47	0.11	0.31	13.07	37.33	17.39	0.02	10.27	0.00	0.00	0.18	2.13	0.10	0.05	15.50	0.05	0.04	0.00	0.14	95.3
5-5	#48	0.10	0.27	13.69	37.44	17.39	0.03	10.14	0.03	0.01	0.11	1.79	0.05	0.08	15.41	0.00	0.03	0.00	0.09	95.8
5-5	#49	0.28	0.00	1.79	45.98	17.39	0.03	11.26	0.00	0.00	0.00	0.58	0.05	0.00	4.49	0.02	0.04	0.00	0.17	94.2
5-5	#50	0.29	0.00	2.09	46.21	17.39	0.12	11.37	0.02	0.00	0.02	0.64	0.05	0.00	4.26	0.00	0.04	0.00	0.18	94.4
5-2b	#51	0.42	0.00	1.87	45.28	17.39	0.09	11.30	0.03	0.03	0.01	0.63	0.03	0.03	5.23	0.02	0.03	0.00	0.24	94.6
5-2b	#52	0.26	0.00	1.81	45.95	17.39	0.00	11.28	0.03	0.00	0.01	0.79	0.00	0.03	4.82	0.00	0.01	0.00	0.25	94.5
5-2b	#53	0.54	0.00	0.00	63.06	17.39	0.04	16.48	0.03	0.00	0.02	0.00	0.03	0.00	0.04	0.01	0.02	0.00	0.39	98.9
5-2b	#54	0.04	0.48	11.65	36.47	17.39	0.05	10.22	0.01	0.00	0.20	2.29	0.05	0.11	17.69	0.00	0.03	0.00	0.04	95.8
1-13	#1	0.23	0.20	17.47	37.18	17.39	0.02	9.82	0.07	0.00	0.16	1.05	0.00	0.08	8.00	0.13	0.06	0.00	0.11	93.3
1-13	#2	0.21	0.23	17.94	37.44	17.39	0.00	9.82	0.05	0.00	0.19	1.09	0.00	0.06	8.13	0.09	0.03	0.00	0.11	94.0
1-13	#3	0.16	0.21	17.92	37.54	17.39	0.02	10.01	0.01	0.00	0.22	1.00	0.00	0.07	7.99	0.09	0.01	0.00	0.10	93.9
1-13	#4	0.71	0.00	1.22	44.69	17.39	0.01	10.55	0.01	0.00	0.00	0.73	0.04	0.01	0.55	0.02	0.02	0.00	0.27	92.6
1-13	#5	0.74	0.00	1.74	46.16	17.39	0.00	10.54	0.00	0.00	0.01	0.56	0.00	0.03	0.54	0.03	0.00	0.00	0.25	93.2
1-13	#6	0.62	0.00	1.73	43.86	17.39	0.66	9.72	0.01	0.40	0.03	0.84	0.06	0.02	1.87	0.01	0.00	0.00	0.24	92.9
1-13	#7	0.24	0.15	17.41	36.71	17.39	0.00	9.88	0.00	0.00	0.20	0.86	0.06	0.08	8.03	0.09	0.03	0.00	0.09	92.6
1-13	#8	0.70	0.00	1.64	45.37	17.39	0.05	10.62	0.01	0.00	0.00	0.81	0.06	0.00	0.70	0.06	0.03	0.00	0.30	92.9
1-13	#9	0.73	0.00	1.49	45.93	17.39	0.05	10.59	0.01	0.00	0.00	0.75	0.05	0.01	0.54	0.00	0.00	0.00	0.22	93.4
1-13	#10	0.82	0.00	1.12	45.06	17.39	0.04	10.60	0.00	0.00	0.00	0.78	0.06	0.02	0.53	0.01	0.00	0.00	0.28	93.7
1-13	#11	0.74	0.00	1.01	44.83	17.39	0.00	10.31	0.02	0.00	0.00	0.73	0.00	0.01	0.54	0.01	0.01	0.00	0.30	92.9
1-13	#12	0.76	0.00	1.75	44.31	17.39	0.00	10.43	0.00	0.00	0.04	0.72	0.00	0.00	0.90	0.03	0.03	0.00	0.25	92.9
1-13	#13	0.81	0.00	1.28	45.06	17.39	0.03	10.54	0.00	0.00	0.00	0.67	0.04	0.01	0.52	0.01	0.00	0.00	0.30	93.5
1-13	#14	0.81	0.00	1.20	44.26	17.39	0.05	10.50	0.00	0.00	0.00	0.65	0.01	0.00	0.65	0.00	0.00	0.00	0.26	92.3
1-13	#15	0.29	0.17	17.81	36.92	17.39	0.00	9.75	0.00	0.00	0.17	1.01	0.00	0.06	7.91	0.15	0.01	0.00	0.06	92.9
1-13	#16	0.25	0.14	17.90	37.68	17.39	0.00	9.87	0.00	0.00	0.18	1.06	0.03	0.06	7.63	0.12	0.00	0.00	0.03	93.7
1-13	#17	0.16	0.20	17.76	37.55	17.39	0.02	9.82	0.02	0.00	0.26	0.98	0.00	0.07	8.27	0.11	0.00	0.00	0.07	93.8
1-13	#18	0.31	0.10	15.96	38.08	17.39	0.00	9.94	0.00	0.00	0.21	0.93	0.03	0.11	7.53	0.11	0.00	0.00	0.11	93.9
1-13	#19	0.22	0.10	15.64	37.45	17.39	0.00	8.63	0.00	0.04	0.16	0.76	0.00	0.09	7.94	0.13	0.06	0.00	0.02	92.0
1-13	#20	0.28	0.17	17.68	37.36	17.39	0.00	9.85	0.00	0.00	0.18	0.96	0.00	0.06	8.09	0.09	0.03	0.00	0.09	93.7
1-13	#21	0.27	0.16	17.94	37.17	17.39	0.00	9.68	0.00	0.00	0.17	0.64	0.03	0.05	7.80	0.14	0.00	0.00	0.05	93.2
1-13	#22	0.27	0.19	17.01	37.00	17.39	0.00	9.40	0.00	0.02	0.22	0.78	0.00	0.04	7.93	0.11	0.00	0.00	0.08	91.8
1-13	#23	0.82	0.00	0.35	29.74	17.39	0.03	0.15	0.00	12.51	0.00	0.12	0.03	0.02	1.10	0.00	0.01	0.00	0.01	92.6
1-13	#24	0.69	0.00	1.41	45.42	17.39	0.00	10.53	0.00	0.00	0.00	0.79	0.07	0.00	0.49	0.00	0.00	0.00	0.22	93.0
1-13	#25	1.10	0.00	0.31	30.54	17.39	0.02	0.25	0.00	12.02	0.00	0.14	0.01	0.02	0.25	0.00	0.06	0.00	0.02	92.0
1-13	#26	0.79	0.00	1.55	46.12	17.39	0.02	10.45	0.00	0.00	0.02	0.78	0.01	0.03	0.50	0.05	0.00	0.00	0.26	93.9
1-13	#27	0.73	0.00	1.36	44.90	17.39	0.06	10.49	0.00	0.00	0.00	0.89	0.03	0.00	0.52	0.00	0.00	0.00	0.32	92.7

Detection limit=0.01%

APPENDIX B

APPENDIX B3: Electron microprobe data

	Zap	Na2O	F	MgO	SiO2	Al2O3	SO3	K2O	P2O5	CaO	Cl	TiO2	Cr2O3	MnO	FeO	CoO	NiO	SrO	BaO	Total
5-11	#1	5.38	0.00	0.00	53.51	17.39	0.02	0.04	0.06	11.28	0.01	0.00	0.01	0.00	0.05	0.02	0.00	0.00	0.00	99.0
5-11	#2	5.52	0.00	0.00	53.54	17.39	0.00	0.08	0.01	11.51	0.00	0.02	0.01	0.00	0.09	0.04	0.03	0.00	0.03	99.8
5-11	#3	0.20	0.19	12.76	35.99	17.39	0.04	9.76	0.02	0.00	0.28	1.78	0.10	0.11	14.93	0.09	0.03	0.00	0.12	95.0
5-11	#4	0.69	0.00	1.15	45.84	17.39	0.07	10.51	0.00	0.00	0.00	0.48	0.05	0.00	1.25	0.00	0.00	0.00	0.25	94.5
5-11	#5	0.26	0.21	12.65	35.96	17.39	0.01	9.66	0.00	0.00	0.29	2.01	0.09	0.13	15.14	0.11	0.00	0.00	0.14	94.9
5-11	#6	0.23	0.23	12.55	35.99	17.39	0.01	9.66	0.00	0.01	0.30	2.01	0.03	0.14	15.09	0.16	0.00	0.00	0.07	94.8
5-11	#7	5.86	0.00	0.00	54.38	17.39	0.02	0.06	0.04	10.56	0.01	0.00	0.00	0.00	0.13	0.00	0.00	0.00	0.04	99.0
5-11	#8	5.74	0.00	0.00	54.00	17.39	0.05	0.03	0.04	10.71	0.00	0.01	0.03	0.01	0.09	0.04	0.01	0.00	0.01	98.5
5-11	#9	5.96	0.00	0.00	54.47	17.39	0.03	0.03	0.04	10.71	0.00	0.01	0.00	0.00	0.05	0.00	0.06	0.00	0.03	99.5
5-11	#10	4.81	0.00	0.00	52.71	17.39	0.00	0.06	0.04	12.49	0.00	0.00	0.02	0.00	0.10	0.00	0.03	0.00	0.04	100.1
5-11	#11	0.26	0.25	12.92	35.73	17.39	0.00	9.62	0.00	0.00	0.24	1.39	0.06	0.05	15.19	0.13	0.06	0.00	0.08	94.7
5-11	#12	0.71	0.00	1.17	45.79	17.39	0.04	10.43	0.00	0.00	0.03	0.20	0.04	0.04	1.42	0.00	0.00	0.00	0.25	94.6
5-11	#13	0.26	0.22	12.64	36.11	17.39	0.02	9.53	0.03	0.03	0.28	1.63	0.00	0.12	14.76	0.15	0.02	0.00	0.05	94.1
5-11	#14	0.23	0.21	12.63	35.95	17.39	0.03	9.59	0.06	0.00	0.28	1.58	0.06	0.14	14.69	0.19	0.01	0.00	0.06	94.0
5-11	#15	0.24	0.25	12.49	36.48	17.39	0.00	9.34	0.00	0.00	0.28	1.64	0.04	0.16	14.78	0.18	0.02	0.00	0.12	93.9
5-11	#16	0.28	0.21	12.65	36.04	17.39	0.02	9.48	0.05	0.00	0.30	1.64	0.06	0.15	15.57	0.16	0.03	0.00	0.13	95.2
5-11	#17	0.05	0.03	3.96	37.14	17.39	0.01	0.01	0.07	6.60	0.02	0.06	0.00	2.26	27.78	0.11	0.03	0.00	0.03	99.8
5-11	#18	0.05	0.08	3.80	36.90	17.39	0.00	0.00	0.05	6.53	0.01	0.07	0.00	2.27	27.56	0.05	0.00	0.00	0.04	98.7
5-11	#19	0.00	0.05	4.47	37.00	17.39	0.02	0.01	0.00	6.62	0.00	0.07	0.00	1.35	27.99	0.11	0.04	0.00	0.01	99.4
5-11	#20	0.02	0.05	4.56	36.93	17.39	0.00	0.01	0.07	6.40	0.01	0.05	0.01	1.32	28.08	0.08	0.00	0.00	0.00	99.0
5-11	#21	0.66	0.00	1.08	46.08	17.39	0.00	10.36	0.01	0.00	0.00	0.41	0.04	0.01	1.15	0.05	0.00	0.00	0.30	94.6
5-11	#22	0.26	0.24	12.18	36.20	17.39	0.00	9.76	0.02	0.00	0.27	1.84	0.05	0.18	15.35	0.18	0.00	0.00	0.12	95.3
5-11	#23	0.02	0.07	4.35	37.17	17.39	0.01	0.02	0.03	5.31	0.00	0.10	0.02	1.65	28.91	0.06	0.00	0.00	0.00	98.8
5-11	#24	0.04	0.04	4.46	37.33	17.39	0.01	0.01	0.00	5.51	0.00	0.04	0.06	1.63	28.71	0.07	0.02	0.00	0.03	99.4
5-11	#25	0.05	0.09	4.44	37.39	17.39	0.00	0.00	0.00	5.24	0.00	0.03	0.00	1.40	28.96	0.03	0.00	0.00	0.02	99.2
5-11	#26	0.02	0.07	4.40	37.51	17.39	0.00	0.01	0.00	5.32	0.00	0.07	0.00	1.23	29.42	0.05	0.04	0.00	0.00	99.7
5-11	#27	0.63	0.00	1.37	46.40	17.39	0.04	10.73	0.00	0.00	0.01	0.44	0.06	0.00	1.11	0.00	0.01	0.00	0.26	94.8
5-11	#28	0.21	0.25	13.79	36.62	17.39	0.04	9.64	0.00	0.00	0.25	1.31	0.02	0.13	14.03	0.18	0.07	0.00	0.12	95.3
5-11	#29	0.61	0.00	1.36	46.16	17.39	0.00	10.36	0.00	0.00	0.00	0.16	0.02	0.00	1.09	0.01	0.00	0.00	0.26	94.4
5-11	#30	0.01	0.00	20.28	26.62	17.39	0.29	0.25	0.01	0.03	0.07	0.13	0.05	0.18	16.66	0.32	0.02	0.00	0.00	86.7
5-11	#31	0.12	0.27	13.10	34.61	17.39	0.02	8.35	0.03	0.07	0.24	0.77	0.06	0.15	16.03	0.39	0.01	0.00	0.04	92.3
5-11	#32	0.12	0.27	13.69	34.91	17.39	0.04	8.73	0.00	0.04	0.24	0.73	0.07	0.19	15.14	0.18	0.00	0.00	0.09	92.8
5-11	#33	0.12	0.22	13.81	34.58	17.39	0.04	8.59	0.00	0.03	0.23	0.75	0.05	0.13	15.35	0.21	0.00	0.00	0.10	92.9
5-7	#34	0.29	0.27	14.96	37.17	17.39	0.04	9.43	0.03	0.00	0.18	1.35	0.02	0.01	12.36	0.29	0.05	0.00	0.08	95.6
5-7	#35	0.31	0.31	14.82	37.32	17.39	0.00	9.50	0.00	0.00	0.17	1.44	0.02	0.04	11.81	0.31	0.00	0.00	0.13	95.1
5-7	#36	0.93	0.00	1.02	45.36	17.39	0.05	10.00	0.01	0.00	0.03	0.79	0.00	0.03	0.64	0.00	0.00	0.00	0.22	93.4
5-7	#37	0.99	0.00	0.89	45.10	17.39	0.01	10.20	0.06	0.00	0.00	0.59	0.00	0.00	0.67	0.06	0.02	0.00	0.17	93.7
5-7	#38	0.03	0.00	23.31	26.57	17.39	0.00	0.00	0.04	0.03	0.02	0.04	0.02	0.05	12.86	0.36	0.05	0.00	0.07	87.1
5-7	#39	0.02	0.00	23.09	26.33	17.39	0.00	0.00	0.03	0.00	0.02	0.06	0.04	0.07	12.82	0.41	0.04	0.00	0.00	86.3
5-7	#40	0.05	0.00	22.66	26.68	17.39	0.00	0.05	0.01	0.05	0.04	0.13	0.02	0.08	12.81	0.39	0.05	0.00	0.00	86.1
5-7	#41	1.03	0.00	0.94	44.97	17.39	0.03	9.99	0.00	0.00	0.00	0.47	0.02	0.02	0.60	0.02	0.01	0.00	0.18	93.3
5-7	#42	0.34	0.29	16.00	37.80	17.39	0.03	9.42	0.00	0.00	0.19	1.39	0.00	0.00	10.51	0.27	0.06	0.00	0.06	94.5
5-7	#43	0.28	0.29	15.63	36.46	17.39	0.01	9.41	0.00	0.00	0.16	1.14	0.00	0.06	10.82	0.28	0.05	0.00	0.06	93.1
5-7	#44	0.32	0.26	15.84	36.48	17.39	0.00	9.34	0.02	0.00	0.21	1.23	0.01	0.02	10.48	0.30	0.04	0.00	0.11	93.2
5-7	#45	0.28	0.38	15.95	37.59	17.39	0.03	9.31	0.00	0.00	0.18	1.28	0.01	0.04	10.19	0.25	0.05	0.00	0.08	93.2
5-7	#46	0.82	0.00	1.55	46.21	17.39	0.01	10.15	0.02	0.00	0.00	0.32	0.00	0.03	0.82	0.00	0.03	0.00	0.21	93.4
5-7	#47	1.08	0.00	0.99	44.95	17.39	0.03	10.28	0.08	0.00	0.05	0.40	0.02	0.03	0.62	0.00	0.00	0.00	0.24	93.8
5-7	#48	0.24	0.34	15.97	37.46	17.39	0.00	9.68	0.00	0.02	0.21	0.60	0.00	0.04	10.53	0.28	0.05	0.00	0.04	94.6
5-7	#49	1.08	0.00	0.93	45.54	17.39	0.02	10.08	0.05	0.00	0.00	0.44	0.00	0.01	0.64	0.02	0.03	0.00	0.23	94.4
5-7	#50	0.25	0.34	15.80	37.50	17.39	0.00	9.66	0.00	0.00	0.18	0.68	0.03	0.03	10.92	0.39	0.00	0.00	0.09	95.1
5-7	#51	1.06	0.00	0.99	46.21	17.39	0.03	10.31	0.01	0.00	0.04	0.19	0.01	0.00	0.65	0.06	0.04	0.00	0.15	95.8

Detection limit=0.01%

APPENDIX B

APPENDIX B4: Corrected sulphur isotope data for laser and conventional S-line analysis

Chimiwungo

Eq-Chi-062		Type	Depth	Sulphide	$\delta^{34}S$ raw	$\delta^{34}S$ corrected
1-13	UOS	S-LINE	138.05	CP(PY)	13.9	13.9
1-13	UOS	S-LINE	138.05	CP(PY)	15.7	15.7
1-13	UOS	LASER	138.05	CP	12.7	
1-15	UOS	S-LINE	140.65	CP(PY)	3.8	3.8
1-15	UOS	S-LINE	140.65	CP(PY)	4.6	4.6
1-26	OS	S-LINE	178.95	PO(CP)	16.3	16.3
1-26	OS	LASER	178.95	CP(PY)	16.2	16.2
1-26	OS	LASER	178.95	CP(PY)	16.4	16.4
1-27	OS	S-LINE	183.80	PO(CP)	13.4	13.4
1-28	OS	S-LINE	189.33	BN(CP)	18.5	18.5
1-30	OS	S-LINE	202.86	PO(CP)	2.6	2.6
1-30	OS	S-LINE	202.86	CP	2.3	2.3
1-32	OS	S-LINE	222.52	CP	15.2	15.2
1-33	OS	S-LINE	228.68	CP(PY)	10.0	10.0
1-36	OS	S-LINE	244.34	PO(CP)	12.8	12.8
1-43	LOS	S-LINE	281.37	CP	6.9	6.9

Eq-Chi-062		Type	Depth	Sulphide	$\delta^{34}S$ raw	$\delta^{34}S$ corrected
2-16	UOS	S-LINE	105.40	CP	12.6	12.6
2-16	UOS	S-LINE	105.40	CP	12.6	12.6
2-17	UOS	S-LINE	107.40	CP	3.0	3.0
2-20	OS	S-LINE	155.05	CP	16.5	16.5
2-20	OS	S-LINE	155.05	PY	16.6	16.6
2-5	LOS	S-LINE	259.36	CP	8.3	8.3

APPENDIX B

APPENDIX B4: Corrected sulphur isotope data for laser and conventional S-line analysis

Malundwe

Eq-Mal-094		Type	Depth	Sulphide	$\delta^{34}S$ raw	$\delta^{34}S$ corrected
5-7	OS	S-LINE	82.63	BN(CP)	9.4	9.4
5-7	OS	S-LINE	82.63	BN	10.0	10.0
5-7	OS	S-LINE	82.63	CP	9.6	9.6
5-7	OS	LASER	82.63	BN(CP)	9.7	10.0
5-7	OS	LASER	82.63	CP(BN)	9.8	9.8
5-8	OS	S-LINE	84.42	BN(CP)	9.0	9.0
5-8	OS	LASER	84.42	BN(CP)	7.0	7.3
5-8	OS	LASER	84.42	CP(BN)	5.6	5.6
5-8	OS	LASER	84.42	CP(BN)	7.0	7.0
5-9	OS	LASER	85.15	BN(CP)	14.0	14.3
5-10	OS	S-LINE	90.44	CP(BN)	15.2	15.2
5-12	OS	S-LINE	95.84	CP(BN)	10.3	10.3

Eq-Mal-094		Type	Depth	Sulphide	$\delta^{34}S$ raw	$\delta^{34}S$ corrected
4-3	OS	S-LINE	94.82	BN(CP)	11.7	11.7
4-3	OS	S-LINE	94.82	BN(CP)	12.4	12.4
4-5	OS	S-LINE	96.64	BN(CP)	11.6	11.6
4-6	OS	S-LINE		CP	9.6	9.6
4-8	OS	S-LINE	103.75	BN(CP)	7.3	7.3

Eq-Mal-094		Type	Depth	Sulphide	$\delta^{34}S$ raw	$\delta^{34}S$ corrected
3-3	OS	S-LINE	90.88	CP(BN)	8.0	8.0
3-5	OS	S-LINE	95.15	CP(BN)	8.1	8.1

Background

Eq-Mal-094		Type	Depth	Sulphide	$\delta^{34}S$ raw	$\delta^{34}S$ corrected
7-10	BG	S-LINE	221.70	PY	6.2	6.2
7-10	BG	S-LINE	221.70	PY	5.8	5.8
7-11	BG	S-LINE	223.46	PY	3.9	3.9
7-11	BG	LASER	223.46	PY	3.9	3.9
7-11	BG	LASER	223.46	PY	4.2	4.2

APPENDIX B

APPENDIX B4: Calculated correction factor for laser analysed sulphur isotopes

Correction Factors

	1	2	3	4	7
Mineral	**Sample**	**Line No.**	**δ34S (Conv.) ‰**	**δ34S (Laser) ‰**	**Correction Factor (‰)**
Bornite	M5-7	LS6819		9.7	0.3
BN(CP)	M5-7	SA11394	10		
	M5-8	LS6826		7.0	inhomogeneous
	M5-8	LS6827		5.6	
	M5-8	SA11364	9.1		
Chalcopyrite	M5-7	LS6820		9.8	0
CP(BN)	M5-7	SA11395	9.6		
Chalcopyrite	C1-13	LS6829		12.7	inhomogeneous
CP(PY)	C1-13	SA11370	13.9		
	C1-13	SA11397	15.70		
Pyrite	M7-11	LS6816		3.8	0
PY	M7-11	LS6817		4.1	
	M7-11	SA11368	3.9		

Inhomogeneous samples can not be used